The Dissertation Committee for Andrew R. Dick Certifies that this is the approved version of the following dissertation:

Design and Development of Base-Catalyzed Materials for Microelectronics Applications

Committee:

Carlton Grant Willson, Supervisor

Christopher Ellison, Co-Supervisor

Benny Freeman

Chris Mack

Paul Ho

Design and Development of Base-Catalyzed Materials for Microelectronics Applications

by

Andrew R. Dick, B.S.

Dissertation

Presented to the Faculty of the Graduate School of

The University of Texas at Austin

in Partial Fulfillment

of the Requirements

for the Degree of

Doctor of Philosophy

The University of Texas at Austin

August 2016

Dedication

To my parents

Acknowledgements

I am grateful to all of the many people who have aided me in my graduate studies at UT. Without all of their help, I surely would not be where I am today.

Firstly, I would like to thank my advisor, Dr. C. Grant Willson. His guidance has allowed me to explore many different projects and become a better scientist. I would also like to thank both Donna Martin and Kathleen Sparks for fighting the bureaucracy and allowing me to focus on research.

Many group members, past and present, require acknowledgement for their support as well. When I first joined the Willson group, I was put on the pitch division project. Ryan Mesch was very helpful in introducing me to the project and providing guidance throughout my tenure at UT. His synthetic suggestions were also immensely helpful for the Unzip and new PBG projects. I am also grateful for my collaborators on the directly patternable dielectrics project: Colin Hayes, Philip Liu and in particular William Bell for attempting to pattern many of the materials I synthesized. I also must thank Brennan Mueller, Jared Schwartz, and Prof. Paul Kohl of Georgia Tech and Brandon Rawlings of Intel for their measurements of the mechanical and dielectric properties of our patternable dielectrics. I have also been fortunate to work with Xiaohan Wang and Seung Ryul Na and learn everything there is to learn about graphene from them.

Additionally, I have always been able to bounce ideas off of Michael Maher, Greg Blachut, Austin Lane, Chris Bates, William Durand and Benjamin Cassidy. Ryan Deschner also helped me keep the ancient CPE SEM functioning. During my time here, I was also able to work with two talented undergraduates, Brendan Luke and Erin Maines,

and a visiting high school student, William Wang. I wish them only the best in all their future endeavors.

The large number of visiting scientists throughout my time here has also been both helpful and enjoyable. Masahiro Okazaki was a great friend and became a fellow barbeque enthusiast during his stay here. Yuji Hagiwara was a magnificent chemist that could synthesize any of our crazy PBG ideas. Takanori Kawakami, though we only overlapped briefly, showed me how to do basic PROLITH simulations. Kazanori Mori helped me synthesize some of the more exotic monomers for the Unzip project. I was also fortunate enough to share an office and enlightening conversations with Takehiro Seshimo and Kensuke Matsuzawa.

I would also like to thank the Ellison group members, as I occupied their lab quite frequently running countless IRs. In particular, special thanks goes to Reika Katsumata for her advice and help with keeping the SEM running and Chae Bin Kim for his suggestions of PBGs and spin-coating solvents.

I am also much indebted to the Turro group at Columbia University. Their insights in photochemistry have allowed for our successes in the pitchdivision, Unzip, and amidine PBG projects. Specifically, thank you to Yougjun Li, Steffan Jockusch, and Prof. Nicholas Turro.

Finally, I would like to thank my committee members: Chris Ellison, Benny Freeman, Chris Mack, and Paul Ho for their advice and guidance. Their expertise in polymers and photolithography has helped me to better focus my graduate work.

Design and Development of Base-Catalyzed Materials for Microelectronics Applications

Andrew R. Dick, PhD.

The University of Texas at Austin, 2016

Supervisor: Carlton Grant Willson

Co-Supervisor: Christopher Ellison

Most lithographic processes in the microelectronics industry rely on the use of processes catalyzed by photochemically generated acids. The generation of organic bases photochemically is much less common, but allows for design of new resolution enhancement techniques and packaging materials.

The microelectronics industry has been able to continue its path toward smaller transistors for several decades, but recently 157 nm and EUV lithography processes have faced delays. Alternative strategies such as double patterning are now required to keep the pace of scaling and they greatly increase manufacturing costs. This dissertation discusses a resolution enhancement technique termed pitchdivision designed to extend 193 nm lithography. This process depends on addition of a photobase generator (PBG) to commercial photoresists that enables printing of both positive and negative features, effectively doubling resolution. Using PBGs that require two separate photochemical events to generate base allows for improved image quality over standard PBGs.

The use of PBGs in photosensitive polyimide packaging materials is also detailed. In packaging of integrated circuits, there is a need for an insulating material having low dielectric constant that provides support for the wires connecting the silicon chip to the

circuit board. Aromatic polyimides meet many of the integration requirements, and can be patterned using PBGs in a base-catalyzed process. However, the UV absorbance of such materials is too high for thick films. The fluorinated polyimide pyromellitic dianhydride-co-2,2'-bis(trifluoromethyl)benzidine (PMDA-TFMB) was therefore auditioned for this use. PMDA-TFMB was printed using 365 nm lithography using near-UV PBGs and achieved resolution as small as 2.5 μm. This material was found to have a dielectric constant around 3.0, and a coefficient of thermal expansion of 6 ppm/K.

Further work on the system sought to improve both material properties and lithographic patterning. The use of alternative monomers was explored. New PBGs capable of producing stronger amidine bases were also synthesized and used to cure PMDA-TFMB.

Finally, the discovery of new catalysts for low temperature curing of polyimides is described. These materials include organic and inorganic salts that allow for the complete curing of polyimides below 200°C. The material properties of films cured with these catalysts are described.

Table of Contents

List of Tables

List of Figures

Chapter 1: Introduction to Photolithography

BACKGROUND

The first electronic general purpose computer was developed by the US Army during World War II. This device was known as the Electronic Numerical Integrator and Computer (ENIAC) and was originally created to calculate artillery firing tables.[1] The ENIAC was extremely costly and required constant maintenance, but the advantages over mechanical computers were clear. A skilled person with a desk calculator could calculate a 60 second ballistic trajectory in about 20 hours. ENIAC could do the same calculation in 30 seconds.[1] The real advantage to ENIAC, however, was that it was reprogrammable. This allowed it to solve problems far beyond ballistics calculations, including problems in aerodynamics, weather prediction, and reservoir simulations.[2] It was even used in the first simulation work to determine the feasibility of thermonuclear weapons.[3]

Despite the improvements over previous mechanical devices, there were significant issues with the ENIAC. Weighing in at 30 tons and spread over 1800 square feet, the device consisted of 17,000 vacuum tubes, 7,000 diodes, 70,000 resistors and 10,000 capacitors all soldered together by hand.[4] ENIAC consumed an enormous 150 kW of electricity while running and cost the equivalent of $7 million dollars after adjusting for inflation.[5] Additionally, ENIAC was constantly experiencing vacuum tube failures and rarely was able to operate for more than 100 hours a week.[6]

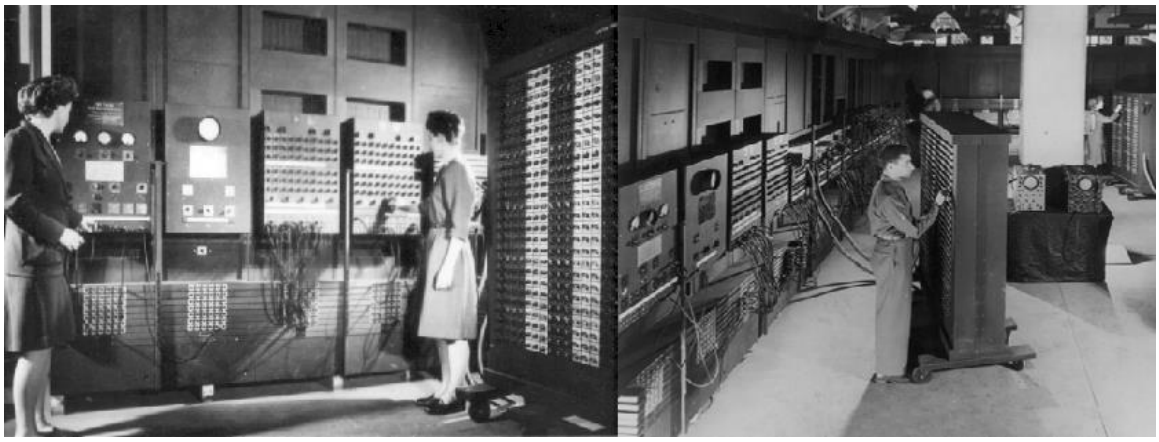

Figure 1.1: Photographs of the ENIAC (US Army Photographs)

The major improvement between the ENIAC and modern computers is the replacement of vacuum tubes with more reliable and energy efficient transistors. William Shockley, Walter Brattain, and John Bardeen of Bell Labs invented the transistor in 1947. Instead of using commonly available metal sulfide based semiconductors, they explored materials such as single crystal silicon. However, at this time silicon could not be produced in sufficient purity, so the silicon devices gave poor results.

Shockley, Brattain, and Bardeen then began to explore using higher purity germanium as a semiconductor material to develop the first transistor.[7-9] A transistor works as an electronic valve that controls the flow of electricity in a circuit. Figure 1.2 shows a picture of the first transistor built by Bell Labs. In this device current flows from the left wire and out the right wire. The triangular material connecting the wires is made of semiconducting germanium. By applying a voltage on the top wire, the germanium becomes more conducting and allows current to flow through the germanium from left to right. These transistors could be made much smaller than vacuum tubes, required significantly less energy to operate, and were much less prone to failure. These properties

allowed the design of increasingly complex circuits presenting new challenges. For their efforts, Shockley, Brattain, and Bardeen received the Nobel Prize in Physics in 1956.

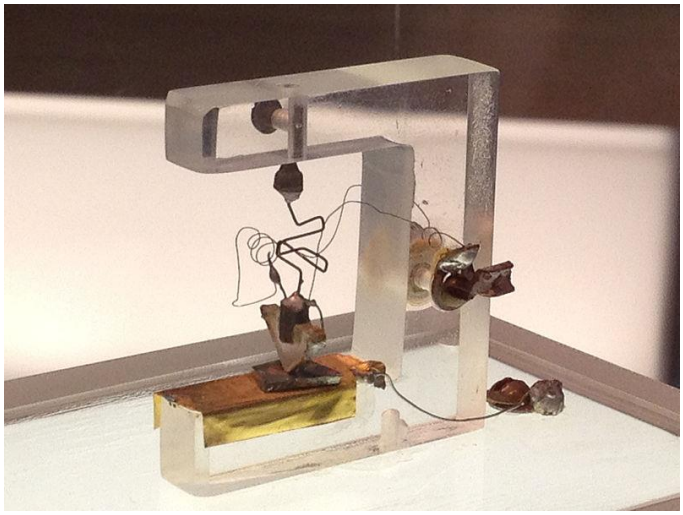

Figure 1.2: The first transistor developed by Bell Labs[10]

While transistors solved the problems associated with vacuum tubes, circuits still remained quite large as they consisted of a set of components such transistors, capacitors, and resistors manually soldered together. These large devices were difficult to mass produce and were therefore expensive and unreliable. The next step was developing a platform to combine all the discrete elements of a circuit into one *integrated* circuit. The invention of the integrated circuit (IC) occurred in 1958 and was separately discovered by two different researchers. Robert Noyce of Fairchild Semiconductor was awarded a patent, but Jack Kilby of Texas Instruments was the first to demonstrate a working device. It was not until 2000 that Kilby was awarded the Nobel Prize in Physics.

Kilby's original device consisted of transistor, capacitor, and resistor components all on a single piece of germanium. His idea came from the high costs associated with the

Micro-Module program used at the time by Texas Instruments (TI).[11] He later described his motivation:

> *The cost analysis gave me my first insight into the cost structure of a semiconductor house. The numbers were high — very high — and I felt it likely that I would be assigned to work on a proposal for the micro module program when vacation was over unless I came up with a good idea very quickly. In my discouraged mood, I began to feel that the only thing a semiconductor house could make in a cost-effective way was a semiconductor. Further thought led me to the conclusion that semiconductors were all that were really required — that resistors and capacitors, in particular, could be made from the same material as the active devices. I also realized that, since all of the components could be made of a single material, they could also be made in situ, interconnected to form a complete circuit.*

There were limitations with Kilby's initial design, however. Though TI quickly commercialized the IC as the Type 502 IC, connections were formed manually using easily damaged gold wires. Fairchild Semiconductor corrected this problem by using vapor-deposited aluminum and isolating these connections with mechanically strong silicon dioxide.[12] Fairchild marketed the first circuits using this fabrication technique in 1960 and this Al conductor/SiO_2 insulator structure remained the industry standard until the early 2000s.[13]

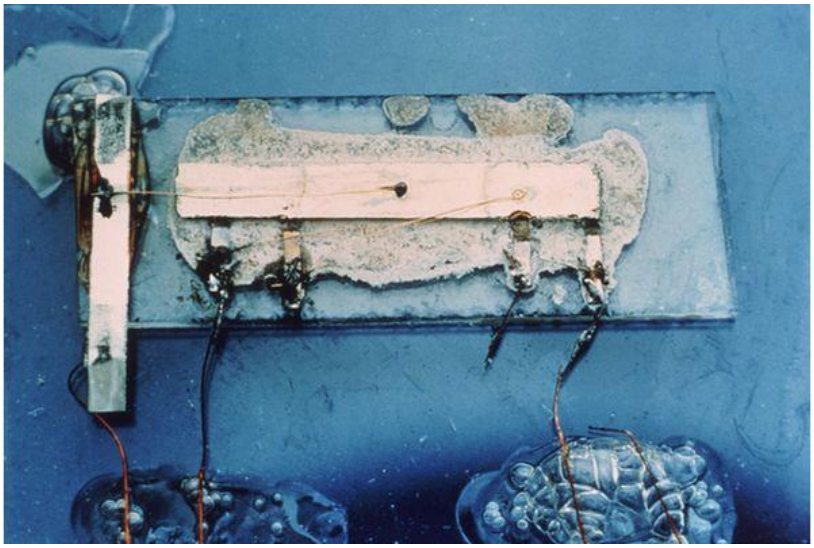

Figure 1.3: The original integrated circuit designed by Jack Kilby (Courtesy of Texas Instruments)

The development of the improved integrated circuit by Fairchild led to the continued decreasing size of circuits. In 1965 Gordon Moore of Fairchild Semiconductor observed that the number of transistors in an integrated circuit was doubling annually.[14] At this time period, devices were still quite large with no fundamental physical limits to shrinking device size in the near term. Moore believed that the trend would continue, driven by a purely economic force. The cost to produce one patterned wafer of chips was largely fixed; increasing transistor density would allow for chips half the size (and cost) or with twice the computing power (at the same cost) of the previous generation. The initial trend was a bit optimistic, but Moore amended this observation in 1975 to transistor density doubling every two years.[15] The trend has since become known as Moore's Law and is not so much a physical law as an economic truth for the microelectronics industry that has continued to this day.

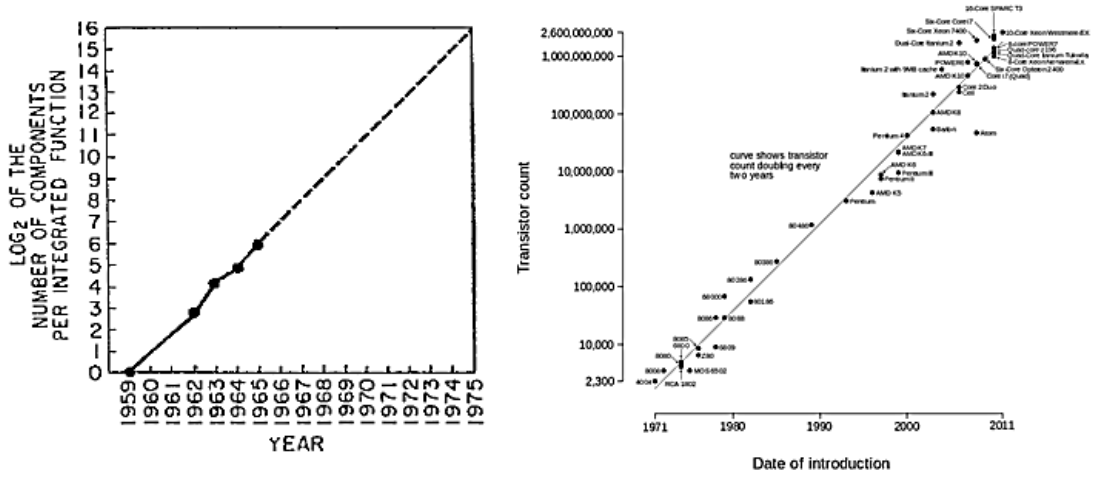

Figure 1.4: Processor transistor counts approximately doubling each year following Moore's Law. Moore's initial paper (left)[14] and data from 1971-2011 (right).[16] Copyright 1998, IEEE

PHOTOLITHOGRAPHY

The ability to keep pace with Moore's Law is largely due to the ability to define features on semiconductors in a process called photolithography. From its Greek roots, photolithography literally means to write in stone with light, which in truth is not a bad description of the process. In this process light is passed through a photomask consisting of a binary design of transparent and opaque regions. The transmitted light then strikes a substrate (e.g. a silicon wafer) coated with a photosensitive polymeric material called the photoresist. Photoresist is so called because it is both photosensitive and resists etching.

A chemical reaction then occurs in the exposed regions that changes the solubility. The exposed wafer is then submerged in a developer solution which selectively dissolves either the exposed (positive tone) or unexposed (negative tone) regions (Figure 1.5).

After development the wafer is then etched. Areas still covered in photoresist resist the etching and remain unaffected. However, in the areas where the resist developed away, the etchant is able to attack the underlying substrate. This results in the transfer of the pattern from the photomask into the desired substrate. Finally, after the pattern has been etched to a desired depth, the excess photoresist is stripped away. Conductors, insulators or semiconductors can then be added to etched areas to build IC components. This entire process is then repeated up to 40 times in order to create all the necessary layers for a functioning device.[17]

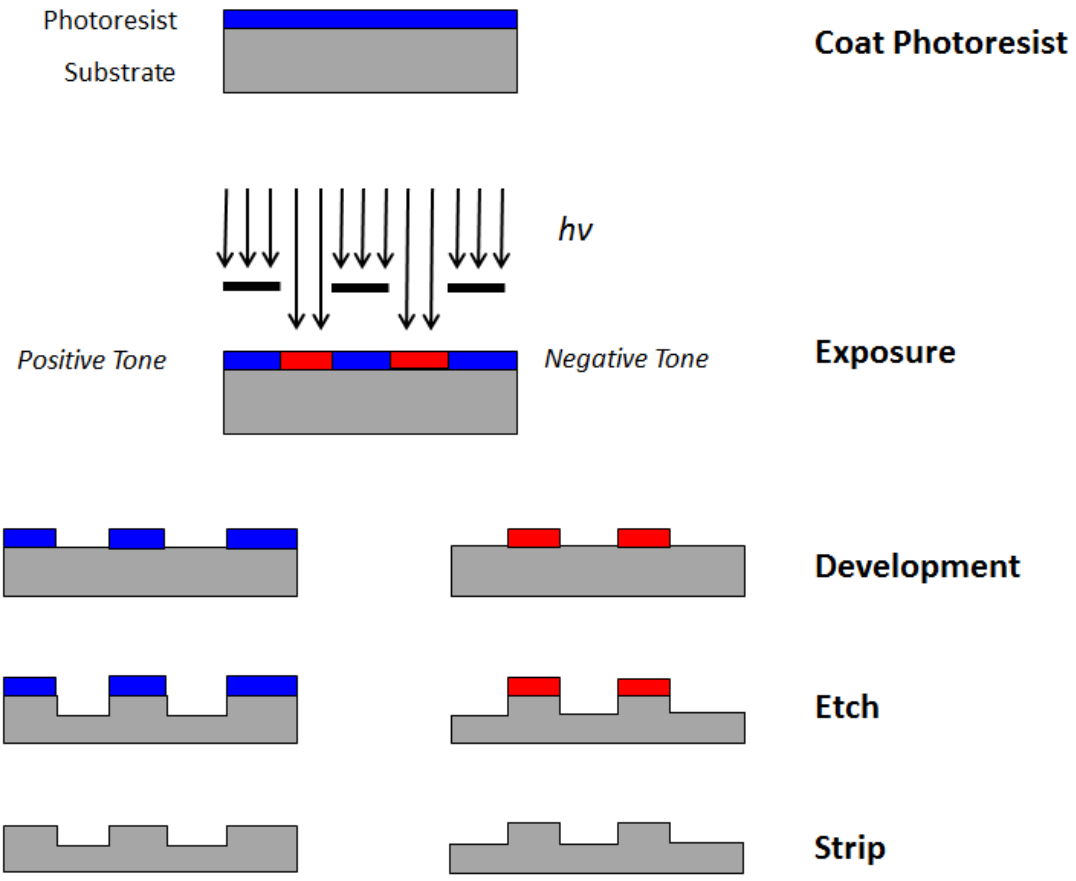

Figure 1.5: Schematic of the photolithographic process

LITHOGRAPHIC RESOLUTION

In photolithography, resolution is the smallest feature that can be patterned repeatedly and with acceptable quality.[17] Further, the quality of the lithography is very dependent on the structure being printed. Essentially, the resolution is the smallest feature that can be printed that maximizes profits for the fab. This resolution, R, is defined by the Rayleigh resolution criterion:

$$R = k_1 \frac{\lambda}{NA} \tag{1.1}$$

where λ is the wavelength of light used for the exposure, NA is the numerical aperture of the optics, and k_1 is a lumped parameter describing everything else about the process such as the use of optical proximity correction, phase-shift masks, off-axis illumination, etc.

From equation 1.1, it is clear that smaller images could be printed if k_1 and the exposure wavelength were decreased, or if the numerical aperture was increased. For repeating patterns, the k_1 parameter has a fundamental limit of 0.25, though modern methods print at around 0.3-0.4, down from early values close to 1.0. The numerical aperture (NA) is the product of the index of refraction and the sine of the capture angle of light passing through the lens system. The NA of the lens has also changed substantially since the early exposure tools used; the earliest exposure tools operated at NA around 0.28 while current tools operate at about 1.35. Figure 1.6 shows the lens stack of a modern exposure tool. The current theoretical NA limit using 193 nm immersion lithography is 1.44, which is the index of refraction of the immersion fluid (water). However, even higher index immersion fluids are still an area of research, though they have not been implemented due to purification and degradation challenges.[18] The final parameter, wavelength, will be discussed as it relates to resist chemistry below.

Figure 1.6: Photograph of a modern exposure tool with the lens stack visible.[18] Copyright 2009, Annual Reviews.

EARLY PHOTORESISTS

The changing requirements of a photoresist have led to the creation of many different resist chemistries since the 1950s. At their core, these materials must be both photosensitive and etch resist.

The first photoresists were developed in the early 1950s and based on negative tone poly(vinylcinnamates).[19-20] However, these materials had poor adhesion and were quickly replaced. The first commercially successful photoresists were produced by Kodak and sold as Kodak Thin Film Resist (KTFR). These resists consisted of partially cyclized polyisoprene and a bis(aryl azide) crosslinker. During exposure (typically g-line, 436 nm) the aryl azide groups decompose to form reactive nitrenes (Figure 1.7). These

reactive species can then insert into the double bonds of the isoprene polymer forming aziridine bonds. As the bis(aryl azide) can form two nitrenes, it acts as a crosslinker and creates a negative tone resist.

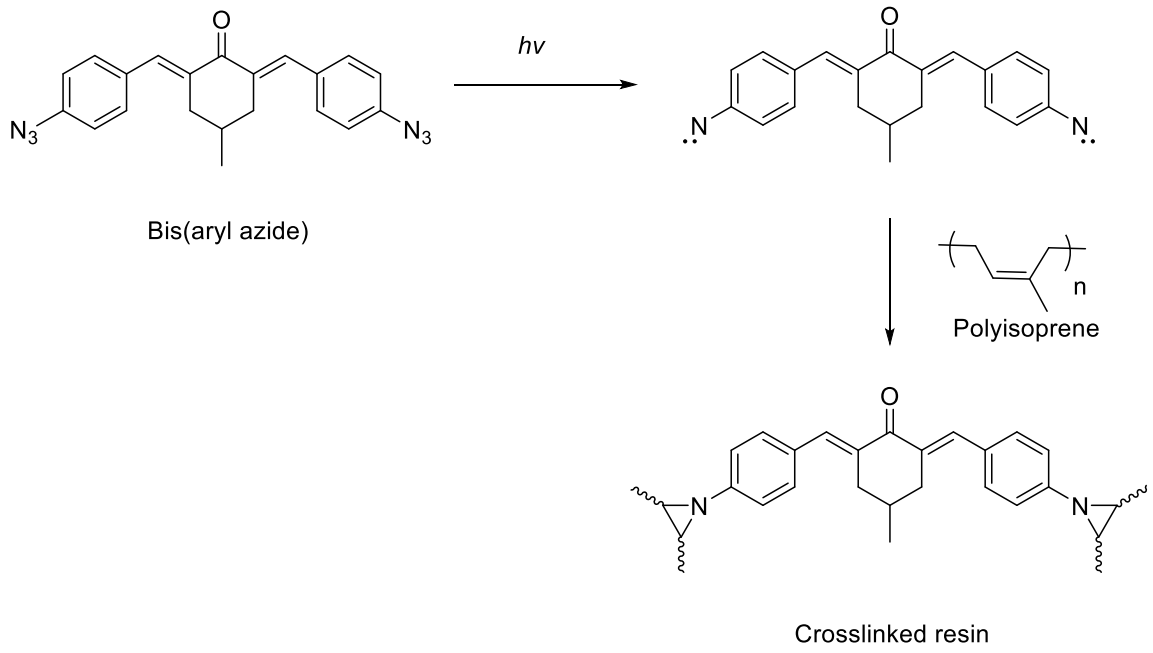

Figure 1.7: Mechanism of imaging in bis(aryl azide)/polyisoprene resists

KTFR photoresist was the standard resist in the industry until the 1970s where feature sizes became less than 3 microns. The use of crosslinking in this resist began to create problems when narrower and narrower lines were printed. The solubility switching in this resist comes from the increase in molecular weight upon crosslinking. While the crosslinked areas prevent dissolution in the developer, they are still swelled by the developer. As the thin lines must expand but still remain adhered to the surface, a characteristic snaking pattern is observed in lines subjected to swelling (Figure 1.8).

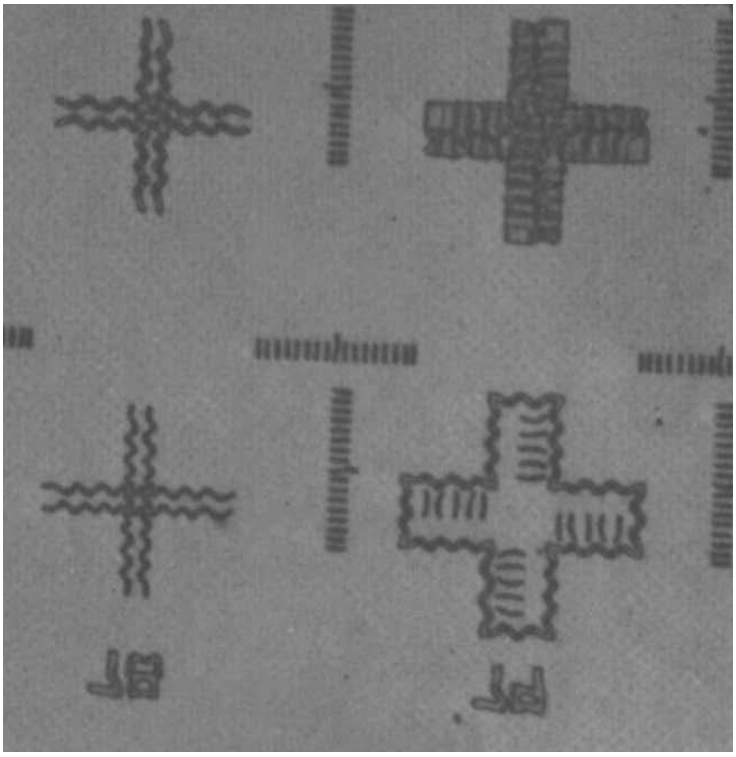

Figure 1.8: Snaking observed due to swelling in negative tone resist features.[21] Reprinted with permission from Willson et al. Copyright 1983 American Chemical Society.

Also among the earliest resists were those based on novolac resin containing a diazonaphthoquinone (DNQ) additive (Figure 1.9). Novolac is a phenol-formaldehyde resin that resists etching in large part due to the aromatic groups present in the polymer. The acidic phenols are also retained in the final polymer structure, making the resin extremely soluble in aqueous base solutions such as tetramethylammonium hydroxide (TMAH). The addition of Lewis basic DNQ to the resin creates a network of hydrogen bonding that greatly reduces the solubility of the resin. At high enough loadings, the novolac becomes insoluble in TMAH. When exposed to UV light, DNQ undergoes a Wolff rearrangement that gives off nitrogen and forms a highly reactive ketene. Adventitious water present in the resin then attacks the ketene to form a carboxylic

acid.[22] The resulting carboxylic acid, being acidic, is soluble in aqueous base developer and results in a solubility switch in the areas exposed to light.[23] This makes novolac based resins positive tone resists and solves the swelling problem present in the negative tone crosslinking resists.

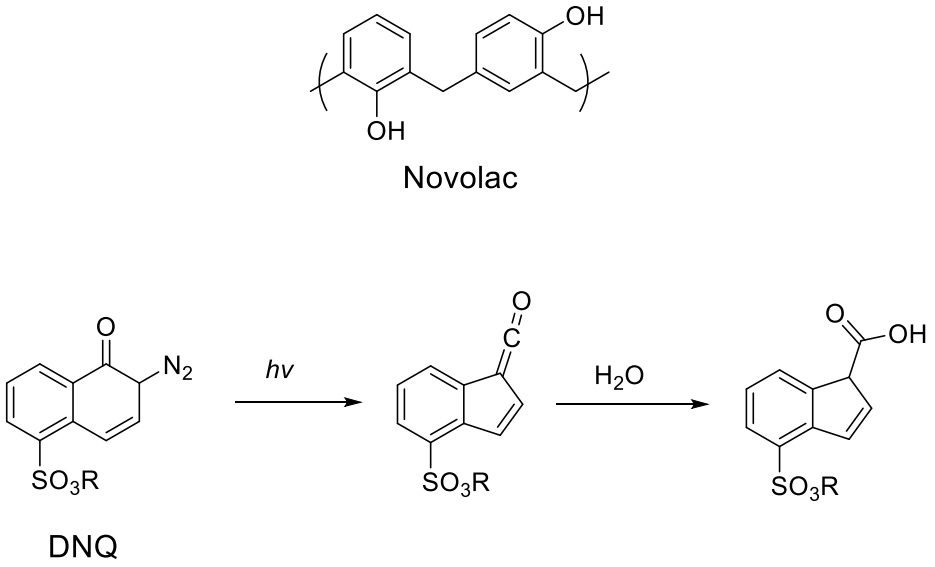

Figure 1.9: DNQ/novolac photoresist chemistry

DNQ/novolac was the standard photoresist used for manufacturing until the late 1980s. The standard light source at the time was a mercury arc lamp. Over time the industry decreased the wavelength used for patterning from g-line (436 nm) to i-line (365 nm), corresponding to bright peaks in the mercury emission spectrum (Figure 1.10). Printing at i-line instead of g-line decreased the minimum feature size possible by about 20%, according to Rayleigh's criterion. However, decreasing wavelength further became a challenge. As can be seen in the figure, the next logical wavelength would be around 300 nm (mid UV). However, novolac is strongly absorbent at this wavelength, but considerably less so around 250 nm. A characteristic emission peak exists at 254 nm, so

the industry desired to pattern next generation devices at this wavelength. However, as can be seen in Figure 1.10, only a small number of 254 nm photons are generated relative to the much brighter wavelengths used previously. Patterning would require infeasibly long exposures using novolac based resists. However, the great etch resistance, aqueous base development, and relatively low cost allowed novolac resists to continue to be used in lower resolution applications.

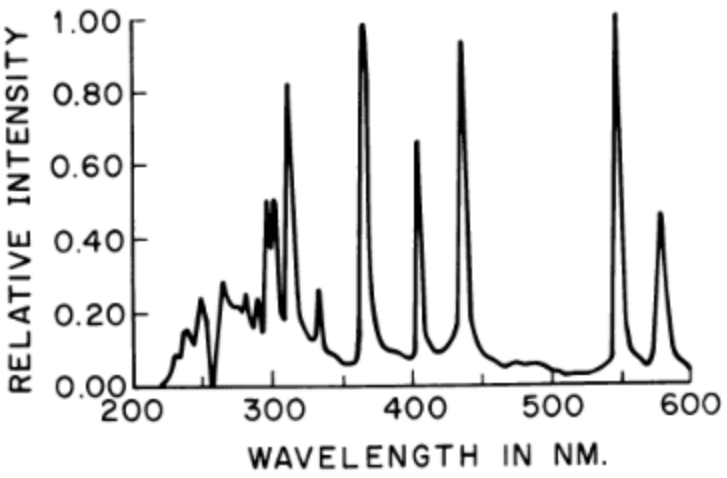

Figure 1.10: Emission spectrum of a high pressure mercury arc lamp. Reprinted with permission from Thompson et al.[24] Copyright 1983 American Chemical Society.

CHEMICALLY AMPLIFIED PHOTORESISTS

The shift toward deep ultraviolet (DUV, such as 254 nm) wavelengths suffered from both a weak exposure source and the very high optical densities of novolac resin, DNQ, and DNQ photoproducts. The low source power meant that many fewer photons would be available for photochemical reactions. In the early resists the source was bright enough that one photon could initiate one reaction and the resist could still be printed in a reasonable amount of time. However, this was not the case for DUV where one photon

would have to trigger a series of chemical reactions if the resist were to be commercially viable. This concept is called chemical amplification and was already used in some negative tone resists based on radical crosslinking. However, the industry had just recently shifted away from the KTFR negative tone resists and was opposed to revisiting them due to their aforementioned swelling issues.

Considerable work at IBM in the 1980s was devoted to developing chemically amplified resists (CAR). Initially, the work focused on depolymerization of polyacetals, but the most promising work was based on protected poly(4-hydroxystyrene) (PHOST).[25] Originally unprotected PHOST was developed as a replacement to novolac, mostly due to its decreased absorbance at 254 nm. However, DNQ is not an effective dissolution inhibitor for PHOST, so the contrast in these resists was too low for commercial applications.[21] Grant Willson, Jean Frechet, and Hiroshi Ito of IBM protected the PHOST polymer as its t-butoxycarbonyl (t-BOC) ester. This made the polymer no longer soluble in aqueous base. However, in the presence of acid the t-BOC group is cleaved catalytically into isobutylene and carbon dioxide (Figure 1.11). The PHOST, containing an acidic phenol, is soluble in aqueous base. Upon addition of a photoacid generator such as aryl sulfonium or iodonim salts,[26] poly(t-BOC styrene) functions as a chemically amplified positive tone photoresist. The IBM resist was extremely sensitive to DUV radiation, having a sensitivity around 1 mJ/cm^2. For comparison, this is about 100 times more sensitive than the DNQ resists.[21] The only major complication with this resist was ironically due to its extreme sensitivity. Airborne amine contamination from other steps in the photolithographic process quenched the generated acid and caused the CARs not to print.[27] Eventually this was solved through the use of carbon filters to absorb airborne contaminants.

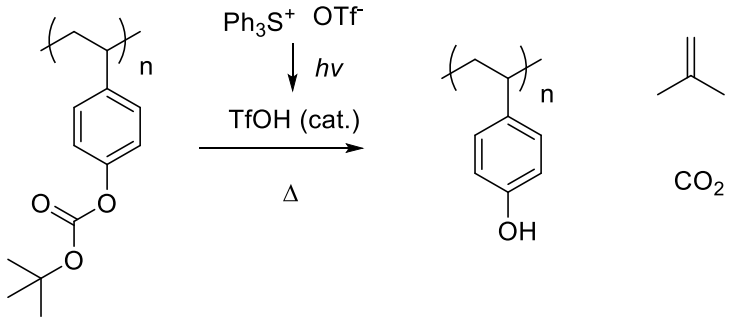

Figure 1.11: Acid catalyzed cleavage of poly(t-BOC styrene)

In an effort to further decrease feature size, the industry again sought a smaller wavelength for patterning. The next wavelength was 193 nm, generated from an ArF excimer laser. With the adaption of CARs, bright KrF excimer lasers (248 nm) replaced mercury lamps for DUV lithography.[28] However, the implementation of 193 nm lithography brought a new set of challenges. Photoresists had long obtained their etch resistance from the use of aromatic groups. However, at 193 nm, aromatic groups are too highly absorbent to be used. This required that aliphatic materials be used in order to reduce optical density. Unfortunately, aliphatic polymers also tend to have much lower etch resistance. A notable exception to this is cycloaliphatic monomers, and in particular monomers containing adamantyl groups.[29] These units are typically incorporated as pendent methacrylate esters as these monomers can still be radically polymerized like styrene derivatives but generate much more UV-transparent polymers. The structure of a generic 193 nm photoresist is shown in Figure 1.12. The use of multiple different monomers allows for the simultaneous achievement of high photosensitivity and etch resistance.

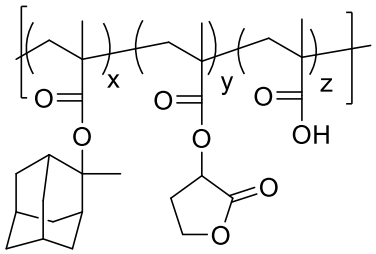

Figure 1.12: Typical example of a 193 nm photoresist based on a methacrylate terpolymer.

ArF has been used in manufacturing since 2001. Adoption of immersion lithography by placing a fluid between the photoresist and the final lens further reduced the feature sizes of printed images by increasing the numerical aperture. However, the industry has been struggling to decrease the exposure wavelength further. Much effort was expended on developing F_2 excimer laser (157 nm) lithography, but difficulties in creating photoresists, lenses and immersion fluids ultimately led to the abandonment of this wavelength.[30] Currently, extreme-ultraviolet lithography (EUV) is being explored, but faces many of the same problems. This has led to research in alternative technologies such as nanoimprint lithography and directed self-assembly. The reader is directed to several dissertations from our group for further discussion on these topics.[31-33] However, the industry has currently been forced to use multiple patterning schemes to continue shrinking features printed using ArF as no feasible alternative has emerged.

MULTIPLE PATTERNING

Unfortunately for the microelectronics industry, the limit of 193 nm immersion lithography was about a 40 nm half pitch, achieved in 2009. This corresponded to a k_1 value of about 0.3 and numerical aperture of 1.35. Further improvements to these parameters were impractical as they were near their fundamental limits. Combined with

the failures at implementing 157 nm and EUV wavelengths, the industry was limited to printing 40 nm features with no clear route toward smaller features, unlike in all previous generations.

The solution adopted by the industry is termed double patterning lithography (DPL). The Rayleigh criterion (Equation 1.1) only applies to the full pitch of dense features, and not the actual size of the features themselves. This means that it is entirely feasible to print features smaller than 40 nm if the full pitch remains 80 nm or above. One could imagine the most straightforward way of double patterning would be to merely expose a line space pattern with the linewidth a third of the spaces, then move the mask over and expose a second image (Figure 1.13). While this method is conceptually easy to understand, it does not actually work in practice. The "unexposed" regions are not actually unexposed. Due to diffraction, a sinusoidal aerial image is formed and the regions that are not printed just have less than the threshold dose for dissolution.[34] By performing a second exposure, some "unexposed" areas will have received enough dose to clear and the printed image will not be the desired line and space pattern.

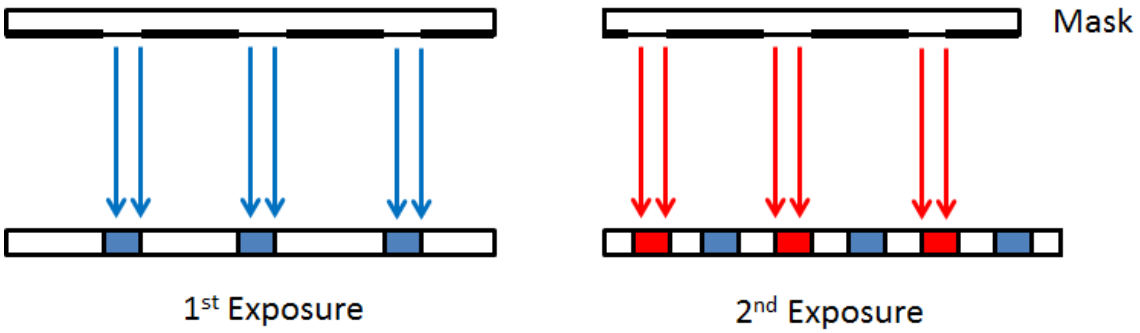

Figure 1.13: Simplified illustration of double exposure lithography

As basic double exposure lithography cannot be used to increase resolution, various double patterning techniques containing intermediate etch steps have been developed. Recently the industry developed a process called litho-freeze-litho-etch (LFLE) for the 32 nm node, though it was never used in manufacturing.[35] Today, self-aligned double patterning (SADP) and litho-etch-litho-etch (LELE) are the currently used methods for double patterning the 14 nm node.[36] Dual tone development[37] (DTD) and directed self-assembly (DSA) have also been proposed as alternative methods, but neither has been implemented.[33, 38]

The process flow for SADP is shown in Figure 1.14. In this process, a photoresist is patterned normally at twice the pitch of the desired features. A spacer material (such as SiO_2) is then deposited conformally over the patterned photoresist. An anisotropic etch step is then performed to leave only the spacer material on the sidewalls of the resist. The resist is then stripped, and the spacer pattern etched into the underlying substrate. Removing the remaining spacer material leaves the final doubled image.

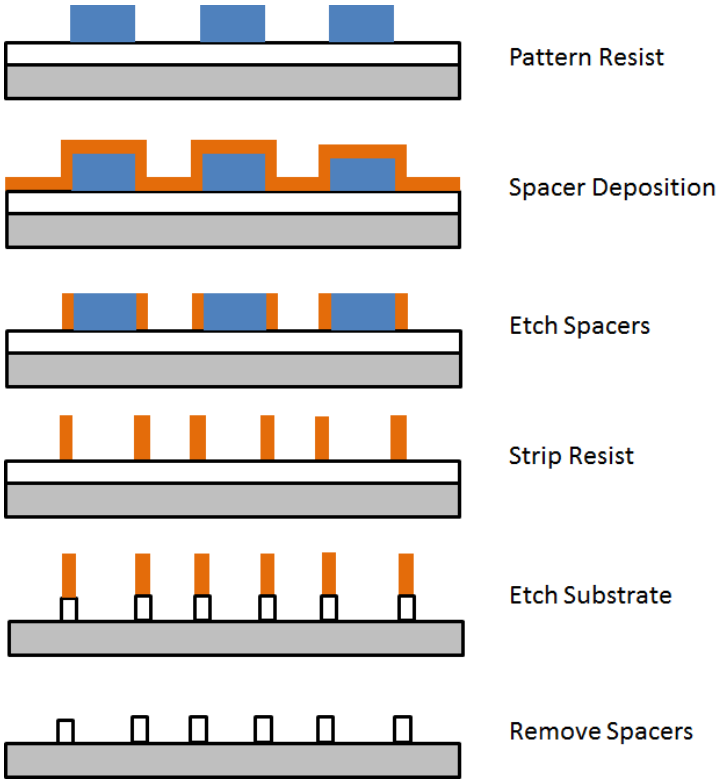

Figure 1.14: Process flow of self-aligned doubling patterning (SADP)

This process has the advantage of only requiring one lithography step to generate the pattern (though a second lithography step is required to trim the ends). Additionally, the process is self-aligned due to the use of the resist sidewalls as templates for the spacers. However, the entire process still requires an additional deposition step and an anisotropic etch step to create the desired pattern, making it considerably more expensive than a standard lithography step.

INTERCONNECT DELAY

The speed of computers is affected by both the speed of the transistors as well as the interconnects between them. Until recently, the total delay of the circuit was

dominated by that of the gate delay of the transistors (Figure 1.15). However, transistors have gotten much smaller in recent generations and the rapidly increasing number of transistors on each chip has vastly increased the amount of wiring required to connect them. Packing more wires closer together requires that the wires be smaller, which in turn decreases cross-sectional area and electrical conductance. The increased interconnect density also results in increased capacitance between wires as the wires are closer together. The time delay in an RC circuit is simply the product of resistance and capacitance, so increasing the density of increasingly less conductive wires results in a large increase in the interconnect delay.

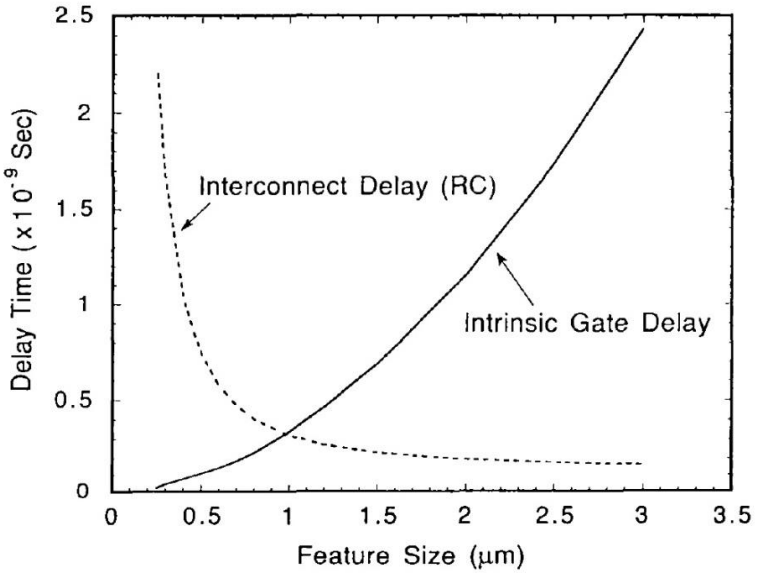

Figure 1.15: Effect of scaling on gate and interconnect delays.[39] Copyright 1994, MRS

Much of the interconnect delay can be reduced by methods such as increasing the number of metallization layers in a device. Indeed, the number of metallization layers has rapidly increased as the feature size has decreased below the 350 nm node.[40] However, around this time (late 1990s) the industry switched from the standard Al/SiO_2 structure

used since the early 1960s. Copper metallization was chosen instead as it has considerably lower resistivity than aluminum (17 vs. 27 nΩ*m). However, implementation of Cu metallization was quite difficult and required a completely new process. Unlike Al that could be coated then selectively etched to form wires, Cu had to be electroplated in pre-patterned trenches to generate wires. This process is called the Dual Damascene Process and is currently used for all Cu metallization steps.

New dielectric materials were also considered to replace SiO_2. Silicon dioxide has a relatively modest dielectric constant around 4.0, depending upon the deposition method. The dielectric constant describes how well a material shields the effects of electric fields generated by charges compared to vacuum. More importantly, the dielectric constant of the insulator material is also directly proportional to the capacitance of a circuit. SiO_2 is actually quite good as a dielectric material as it is mechanically very strong and also thermally stable. Alternatively, IBM originally used polyimides for the interlayer dielectric in the 1980s, though this was mostly due to lower costs and good planarizability, and not for their lower dielectric constants.[40] However, even the moderate dielectric constant of SiO_2 was becoming too high for the sub-micron nodes. The first lower dielectric constant material ("low k") was a fluorinated version of silicon dioxide, lowering the dielectric constant to about 3.8 at the cost of some mechanical stability.[41] The strategy for decreasing the dielectric constant further has focused on a continued incorporation of fluorine and carbon containing materials to break up the silicon-oxygen bonds in SiO_2, as well as adding porosity to the material. Currently, interlayer dielectrics have a dielectric constant around 2.2. While it may be possible to decrease this value further, there is a general trend of decreasing mechanical strength with decreasing the dielectric constant.[40] Further decreases may not be practical from a device reliability perspective.

DISSERTATION STRUCTURE

The purpose of this chapter is give the reader background information on the microelectronics industry and especially the photolithographic process. The remainder of this document focuses on utilizing photolithography to pattern both new materials as well as modify the output of existing processes.

Chapter 2 focuses of the development of an alternative method to double patterning that functions by modifying ArF resists to print both positive and negative tone images, effectively doubling the number of features printed. This method is termed pitchdivision and it can reduce the k_1 value below the fundamental limit of 0.25. Whereas doubling patterning methods require additional tools, this method can be used with existing process equipment.

Chapter 3 focuses on the development of a base catalyzed photosensitive polyimide (PSPI) system for use as a packaging dielectric material. A photobase generator creates organic bases upon exposure, which acts as curing catalysts for the system. The cured material is no longer soluble in developer, resulting in a negative tone chemically amplified photoresist. Chapter 4 describes the search for new resist materials to improve both patterning and material properties of these PSPI resists.

Chapter 5 details the discovery of new catalysts for the low temperature curing of polyimides, which should allow for easier integration of PSPI into devices. Finally, Chapter 6 discusses the development of photobase generators capable of producing stronger amidine and guanidine bases in order to improve contrast in the PSPI system.

Chapter 2: Pitch Division Lithography using Two-Stage Photobase Generators

In chapter 1, the current industrial method of double patterning lithography (DPL) was introduced. The self-aligned double patterning (SADP) method achieves doubling of resolution but it also essentially doubles the number of lithography steps required for patterning, greatly increasing the cost of production. This chapter introduces a chemical solution to lowering the Rayleigh constant to values as small as 0.125 in a process termed pitchdivision. Much of this work was developed in our lab by Drs. Xinyu Gu and Ryan Mesch.[42-43] The main advantage of pitchdivision over SADP is that, in theory, no new equipment or processing steps would be required to print features with half the pitch in a standard chemically amplified resist. That is, 22 nm grating features could be printed using a standard 45 nm single patterning processes, or sub-10 nm features could be printed without needing quadruple patterning.

INTRODUCTION TO PITCH DIVISION LITHOGRAPHY

The continued lack of a bright EUV source has forced the microelectronics industry to adopt a double patterning strategy in order to achieve the resolution required for the 22 and 14 nm nodes. While ASML (essentially the only EUV tool maker) continues to promise that EUV tools will be production-ready soon,[44] self-aligned quadruple patterning (SAQP) will likely be required in case this goal is not met.[45] The desire to avoid even more patterning steps has resulted in a renewed interest in chemical methods for density-doubling lithography.

While a standard chemically amplified photoresist (CAR) divides the aerial image into two parts, a density doubling resist divides the image into three parts. Figure 2.1

shows an illustration of this process where instead one threshold exposure dose, there are now two. As is the case with a standard positive tone resist, upon reaching the positive threshold (E_0) the resist becomes soluble in developer. However, with further exposure a second, negative threshold (E_n) appears.

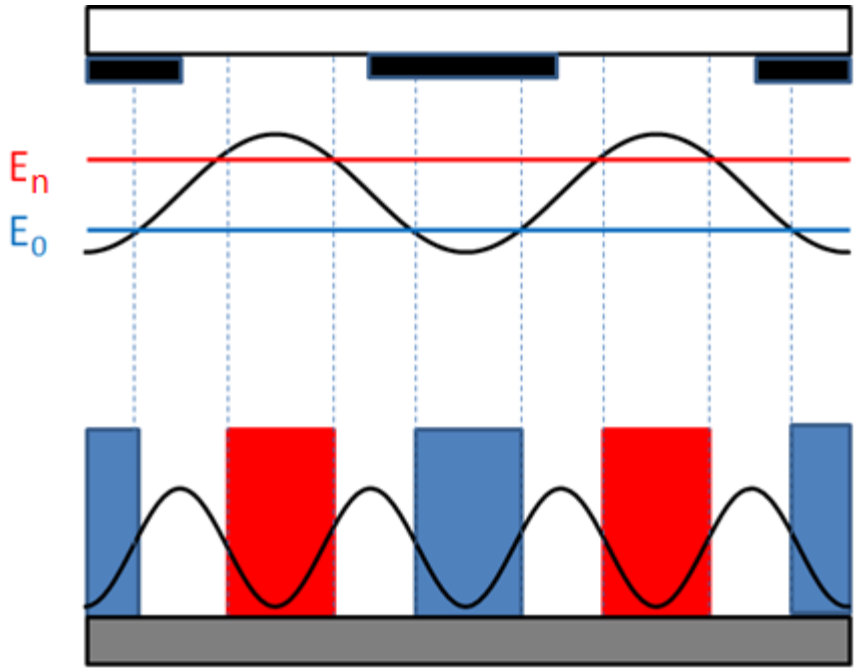

Figure 2.1: Illustration of density doubling lithography utilizing two exposure dose thresholds

IBM filed the first patent for this type of photoresist in 1996.[46] Their material was a positive tone photoresist consisting of methoxypropene protected poly(hydroxystyrene) and triphenylsulfonium triflate photoacid generator to which an acid sensitive crosslinking agent such as tetramethoxymethyl glycoluril (Powderlink™) was added. At low exposure dose the material behaves as a regular positive tone photoresist; however, larger doses begin to crosslink the polymer matrix enough so that it is no longer soluble

in aqueous base developer.[47] The scheme is shown in below in Figure 2.2. An SEM micrograph of frequency doubled isolated lines is shown in Figure 2.3.

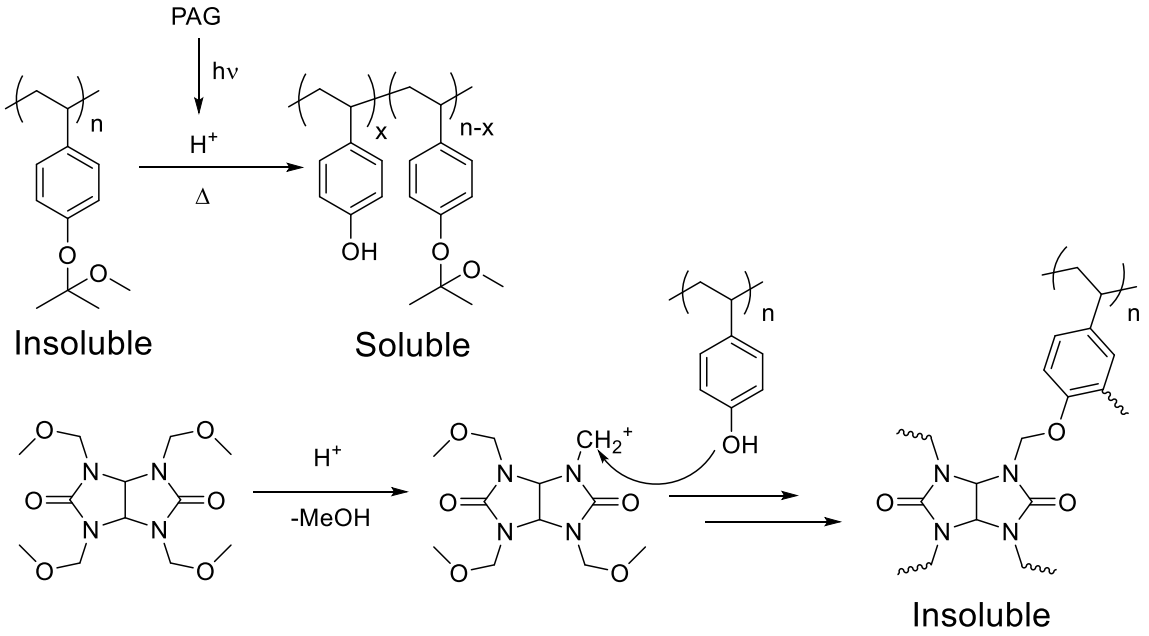

Figure 2.2: Solubility switching chemistry used in IBM frequency doubling resist

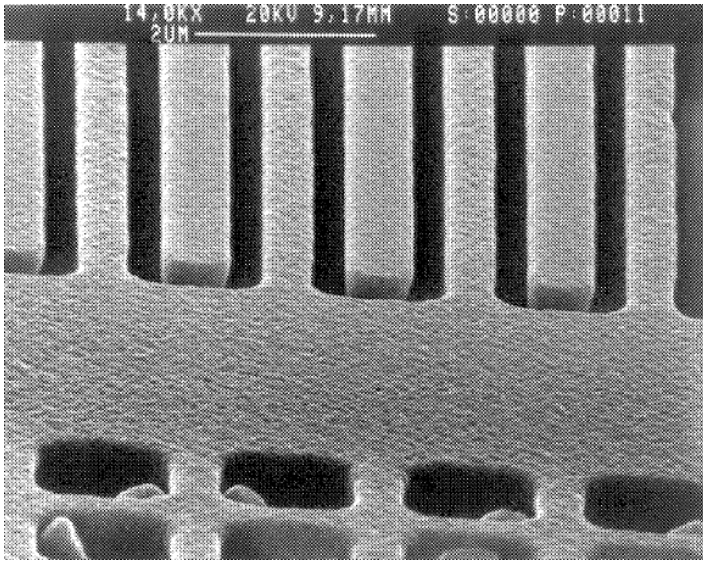

Figure 2.3: SEM micrograph of patterned IBM crosslinking type frequency doubling photoresist. Original pitch is 2 μm.[46]

A very similar approach was reported by Fedynyshyn at MIT Lincoln Labs,[48] who used a copolymer of ethyl adamantyl (EAdMA), hydroxy adamantyl (HAdMA), and γ-butyrolactonyl methacrylates (GBLMA) and a PAG as the photoresist. The methacrylates are deprotected upon exposure and subsquent acid generation to form a positive tone resist during TMAH development. At higher exposures doses the hydroxyl groups of the HAdMA and ring opened GBLMA begin to form esters with the deprotected acids and crosslink the polymer matrix, as shown in Figure 2.4. The major improvement in this system over the IBM system comes from the decreased UV absorption of the aliphatic monomers; the styrenic system is much too absorbant for imaging at 193 nm.

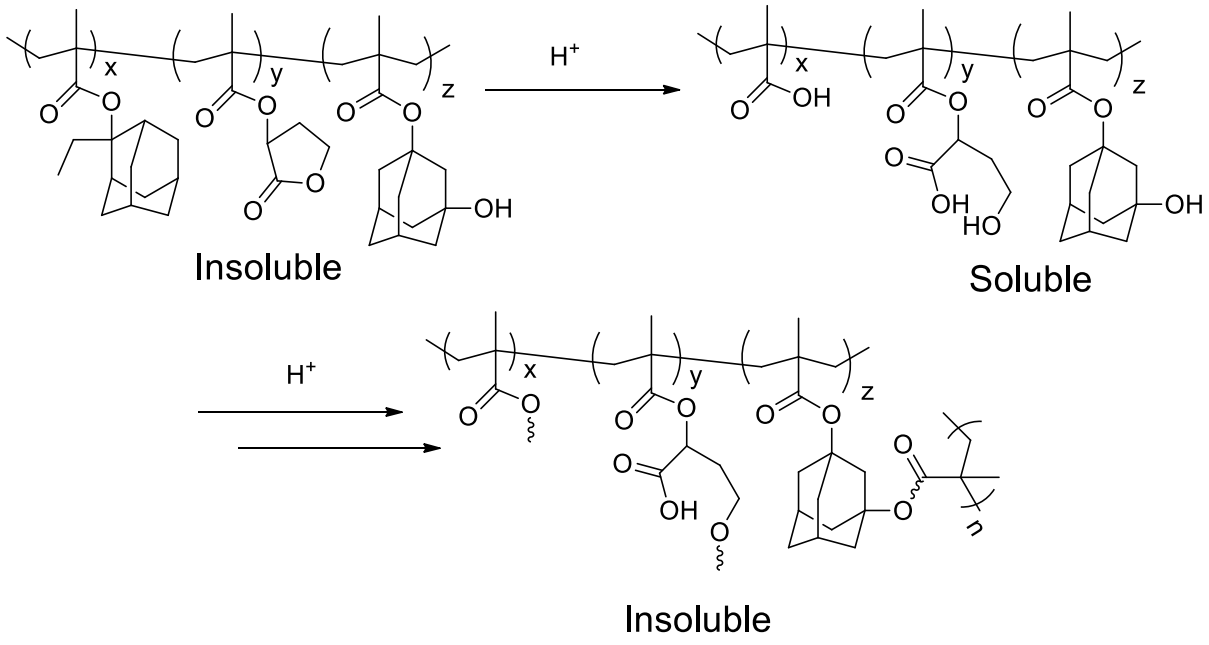

Figure 2.4: Solubility switching chemistry used in MIT multi-tone resist formulations

While both crosslinking systems are able to generate images for larger pitches, performance at smaller pitches is greatly diminished. This is due to the use of crosslinking to generate the negative tone image. The crosslinked films are no longer soluble in developer, but they are still greatly swelled by it. This causes the printed lines to bow out and manifest as high line-edge roughness and even bridging defects at smaller pitches.

A multiple solvent development method for frequency doubling has also been proposed known as dual-tone development (DTD).[37] As originally developed by Asano, this method uses PAG and tert-butoxycarbonyl protected poly(hydroxystyrene). The photogenerated acid cleaves the protecting group to generate the hydroxystyrene, which

is soluble in TMAH developer. The film is then rinsed and developed in organic solvent, dissolving the low dose areas where the polymer is still mostly protected, but leaving the partially deprotected, and now reasonably polar, middle dose region. Figure 2.5 shows that precise dose control is required for the DTD system.

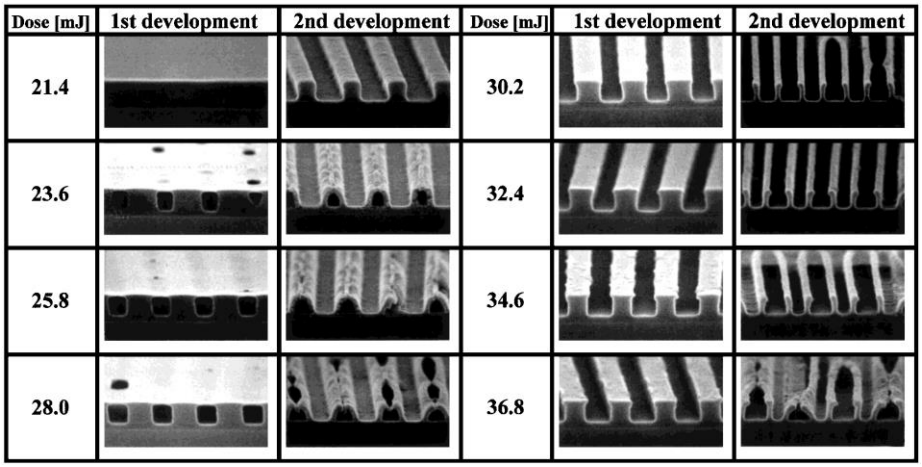

Figure 2.5: DTD using a t-BOC styrene resist. Diluted TMAH solution is used in the 1st development, followed by a 2nd organic development to generate the frequency doubled pattern in resist. Copyright 1999 The Japan Society of Applied Physics[37]

While the DTD method appears favorable as it uses no additional processes or tools other than one organic development step, implementation is a challenge. Fonseca et al. at Tokyo Electron and IMEC have worked to optimize the process.[49,50] Their work has found that a flood exposure and subsquent bake is needed after the initial postive tone development. While adding acid indiscriminately may seem counterintuitive, some acid and base still remain in the film after postive tone development. By carefully controlling the amount of acid, base, and flood exposure, the deprotection gradient can be maximized, resulting in lower LER and the ability to print at smaller pitches. Fonseca et

al. also found that flood exposure allows for the critical dimension (CD) control that earlier works lacked as the positive tone trench CD is largely independent of flood exposure dose, while the negative trench CD is an extremely strong function of flood exposure dose. This allows for an easily adjustable method to guarentee the desired evenly spaced lines and space pattern. However, even with optimization, the method still suffers from acid gradient problems leading to poor line edge roughness. Further work has shown that adding a second patterned exposure after positive tone development can improve image fidelty and reduce LER, though this would require an additional alignment step and would therefore offer no major advantage over self aligned double patterning.[49]

Recently Hori et al. of TOK have modified the DTD process with several new coating steps after the initial patterning.[51] In this pattern split process (PSP) a polymer containing dissolved sulfonic acid is first coated onto the patterned photoresist and then a polymer with dissolved base is coated on top of the acid layer. During baking both acid and base are able to diffuse into the photoresist, allowing for greater contrast than was possible during the flood exposure in DTD. The use of the base layer prevents the deprotection in the top of the resist film so that only the side walls are deprotected and the entire film does not dissolve.

The first pitchdivision resists were demonstrated in our lab by adding photobase generator to standard ArF photoresists.[52] This alters the net acid as a function of dose profile of the resist, creating a nearly parabolic net acid profile rather than the first order kinetics observed in a standard resist (Figure 2.6). In this process, the photoresist

performs as a standard positive tone resist in the low exposure dose region. Further exposure generates more base and the acid begins to be neutralized, decreasing the net acid in the film. Figure 2.6b shows the threshold response of the resist. The solubility of deprotected resists in TMAH tends to be highly non-linear, so even small changes in net acid create large differences in film retention. As the pitchdivision resist crosses this threshold twice for every feature in the mask, the pitch of the printed image should be halved.

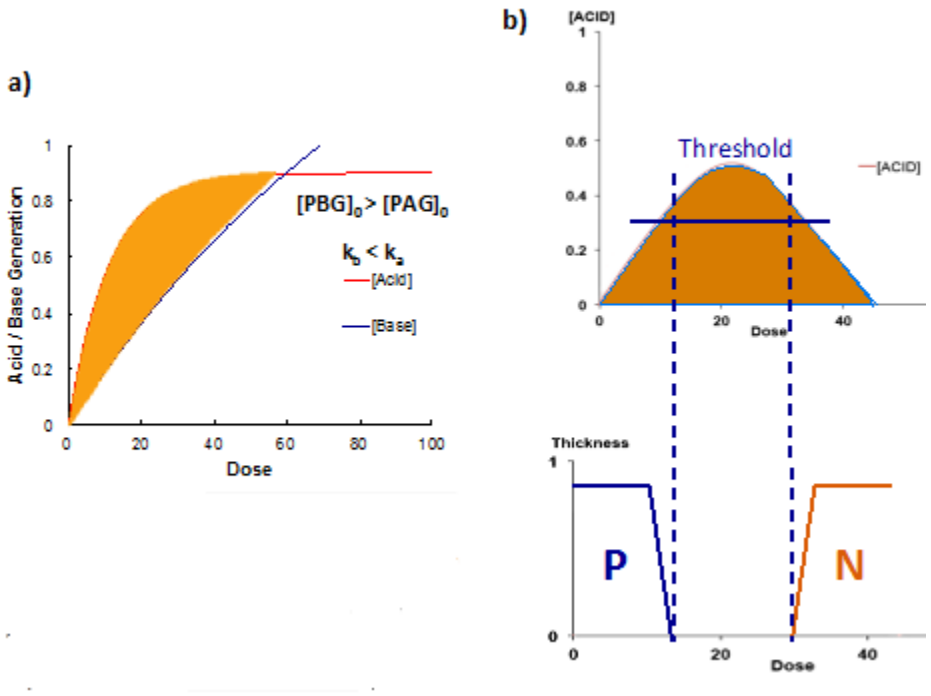

Figure 2.6: a) Net acid profile for resist containing higher PBG loading than PAG with slower base generation kinetics. b) Generation of positive and negative tone features due to parabolic net acid profile (Adapted from Ref 43)

Commonly used PAGs and PBGs both follow first order kinetics with respect to dose, as shown in equation 2.1:

$$C = C_0(1 - e^{-kE}) \quad (2.1)$$

where C_o is the initial concentration of photoactive compound, C is the concentration of photogenerated acid (or base) as a function of the exposure dose, and k is the photolysis rate consant.[53]

In order to create this parabolic net acid curve, a higher stoichiometric loading of PBG relative to PAG is required. Additionally, the rate constant of base generation needs to be lower than that of the acid generation in the PAG.[42] That is, the product of quantum efficiency and fractional light absorbance of the PBG at the exposure wavelength must be less than that of the PAG. Typically the PAGs employed in commercial resists are based on triaryl sulfonium perfluorosulfonate salts (e.g. triphenylsulfonium nonaflate, TPS Nf). Fortunately, upon exposure to deep UV light these salts generate super acids (pKa < -10) with high quantum efficiency (0.3-0.5).[54] Even relatively weak bases such as amines will effectively quench these acids. In the case of the often slower base generation, at low exposure doses equation 2.1 approaches:

$$B = PBG_0 * k_b * E \quad (2.2)$$

where B is the base concentration, PBG_0 is the initial concentration of photobase generator, and k_b is the photolysis rate constant of the PBG.

Modeling of these systems was performed by Dr. Xinyu Gu in a version of PROLITH software modified to have a photogenerated base quencher input.[42] We found that there are two new system parameters that affect the performance of these resists, which we called the contrast and the E-factor. In a typical exposure of a dense line/space pattern at the resolution limit of the lens, the aerial image looks like the curve in Figure 2.7. This is true regardless of the type of resist used. The figure shows the minimum and

maximum intensities (I_{min} and I_{max}, respectively) at the wafer surface as well as the previously defined E_o and E_n values that correspond to solubility switching thresholds. The contrast and E-factor are defined as:

$$contrast = \frac{I_{max} - I_{min}}{I_{max} + I_{min}} \tag{2.3}$$

$$Efactor = \frac{E_n - E_0}{E_n + E_o} \tag{2.4}$$

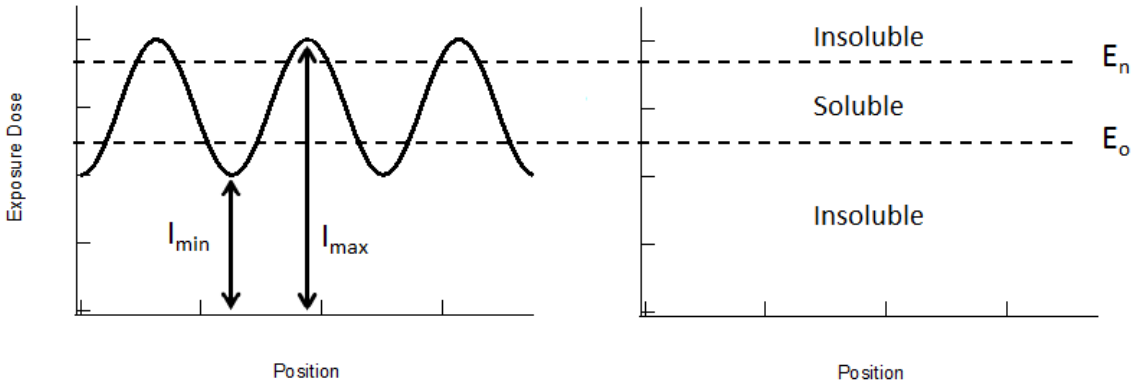

Figure 2.7: Typical aerial image profile indicating important parameters of E-factor and contrast

The contrast parameter relates to the shape of the aerial image. This shape is a function of the exposure wavelength and pitch size, as well as other factors such as the type of illumination and the use of phase shift masks. In general these parameters are difficult to adjust, making the contrast essentially a constant for a given exposure tool near the resolution limit. The E-factor, however, can be more easily changed. It describes the spatial relationship between E_0 and E_n. Both values are functions of PBG loading, post exposure bake (PEB) temperature, and PBG quantum efficiency. For the pitch division process to work, both E_0 and E_n must lie within the dose span of the aerial

image, as shown in Figure 2.8. From the figure it is clear that higher contrast is preferable as this increases the process latitude.[55] It is also evident are that the E-factor must be smaller than the contrast and that the E-factor must be carefully controlled to generate the desired equal sized lines and spaces pattern. For a high contrast aerial image (0.6-0.9), the E-factor needs to be around 0.5-0.6.[42] Much more in depth simulation work on the topic has been performed by Dr. Xinyu Gu, and the reader is directed to his dissertation for further reading on the topic.[42]

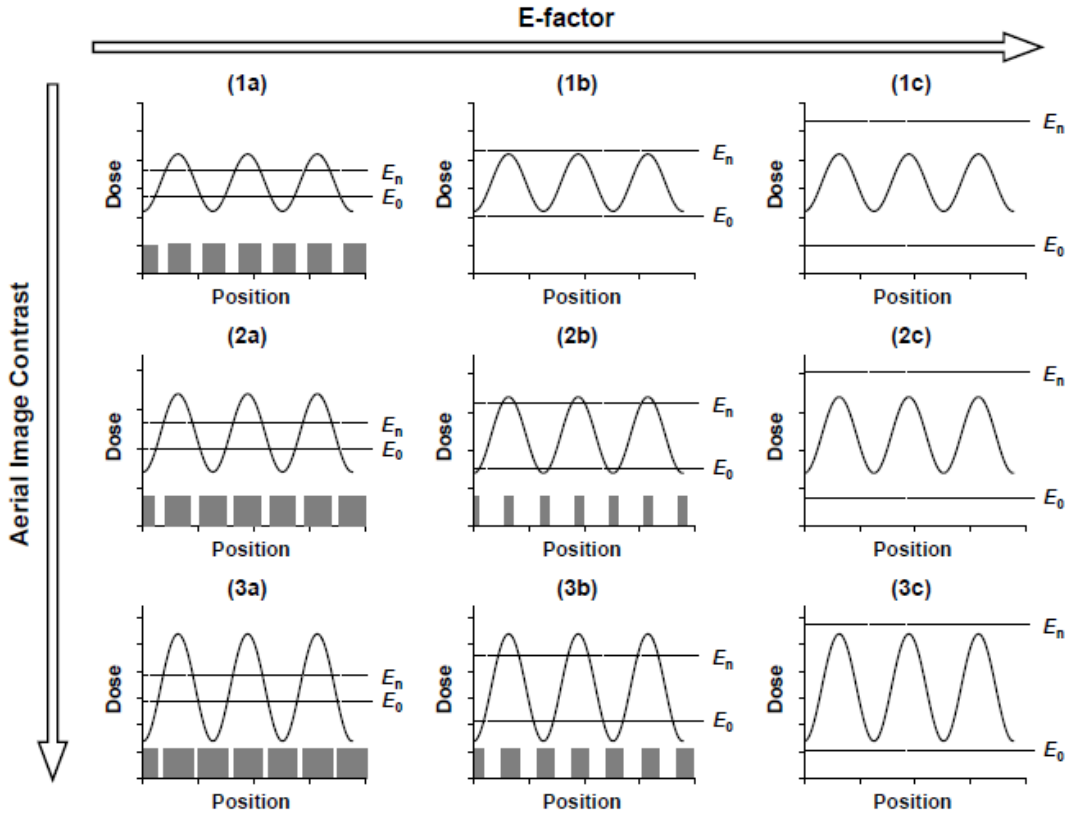

Figure 2.8: Illustration of resist profiles after development as functions of contrast and threshold response. (Adapted from Ref 42)

Modifying the threshold values to achieve the correct E-factor is the key to achieving pitchdivision. The shape of the net acid curves is only a function of two

variables: the initial PBG/PAG loading and the ratio of rate constants, k_a/k_b. At minimum, both of these ratios must be greater than 1 for the modification of a standard positive tone resist. If $k_a < k_b$, or even a similar value, all of the photogenerated acid is immediately quenched and the resist will never reach E_0. Figure 2.9 shows the net acid profiles for k_a/k_b ratios of 1.5 and 3.0 using the linear approximation for base generation. In the case of 1.5, very little net acid is present in the film, so no image will be formed. Finally, if $PAG_0 > PBG_0$, then all of the acid at the higher exposure doses will not be quenched and no E_n will be observed.

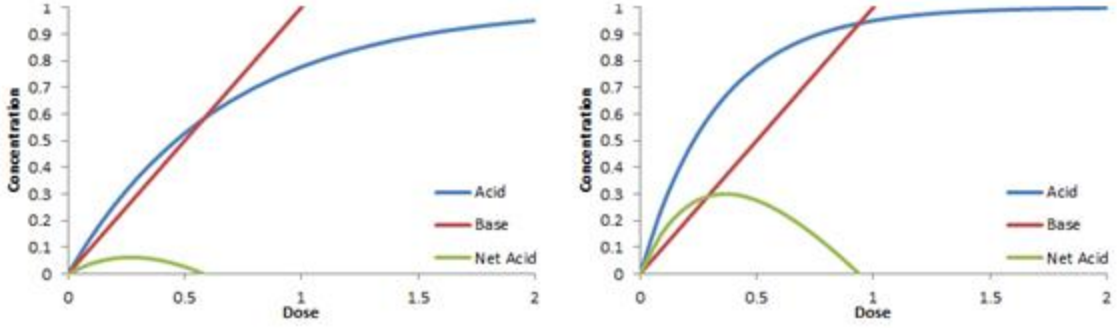

Figure 2.9: Effect of k_b on net acid profiles for $k_a/k_b = 1.5$ (left) and 3.0 (right)

In the case where k_b is much smaller than k_a, base is not generated quickly enough to quench the acid. This leads to increasingly shallow curves in the net acid profile and results in significant problems with line edge roughness (LER), especially in the negative tone image.[42] The effective base generation rate can be increased simply by the addition of more PBG. However, this approach is not ideal as high loadings lead to increased optical density and degraded dissolution performance.

Finally, the pitch halving aspect of pitchdivision can result in printed images that are quite different than the image printed using a standard resist (Figure 2.10). Many of these problems are also encountered using SADP and SAQP, however.[56-57] The industry solution for this problem has been to print only mono-directional dense line/space

patterns and then perform a trim step with a separate exposure to remove loops at the ends of patterns. This loop behavior is clearly visible in Figure 2.3 and a similar trim step would be required for pitchdivision resists.

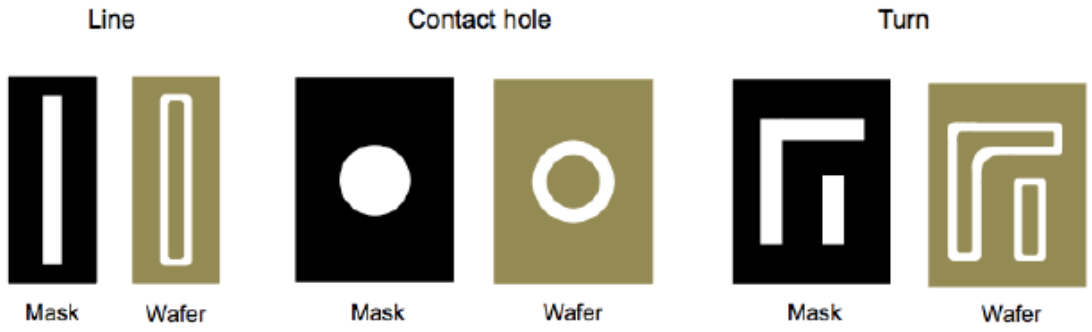

Figure 2.10: Illustration of printed pitchdivision images using conventional mask patterns. (Adapted from Ref 42)

PITCHDIVISION USING ONE-STAGE PHOTOBASE GENERATORS

Photobase generators were originally developed as a way to protect organic amines during synthesis.[58] The advantage over other protecting groups is that these light sensitive groups are often cleaved selectively under mild conditions. Additionally, the use of light as a deprotection reagent provides an orthogonal method for complex molecules that would otherwise require many more protection/deprotection reactions. Historically, PAGs have been more common in the microelectronics industry, due to the ability to generate super acids at high quantum efficiency.[26, 54] PBGs have been much less common in the industry, though in the 1990s IBM reported patterning polyimide films using PBGs.[59-60] More recently a review has been written on available PBGs.[61] Further details

about our improvements to the base-catalyzed polyimide patterning system can be found in Chapter 3. More information about PBGs can be found in Chapter 6.

While many different PBGs have been proposed for pitchdivision lithography, work in our group focused primarily on the carbamates shown in Figure 2.11. The most widely explored photo-labile protecting group (PPG) is the 2-nitrobenzyl group (ONB). This group is thermally stable to near 200°C, strongly absorbent in the deep UV, and has a moderate quantum efficiency.[62-63] As such, it was one of the first PBG chosen for use in photoresists.[64-65] This type of photobase is further detailed in Chapter 6, and work on the other photobases below is the subject of the dissertation of Dr. Ryan Mesch.[43] For the purposes of this dissertation, only the results obtained using ONB will be discussed.

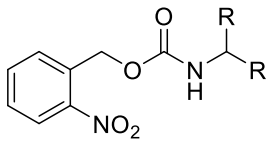

2-Nitrobenzyl carbamate (ONB)

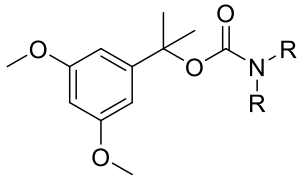

3,5-Dimethoxybenzyl carbamate

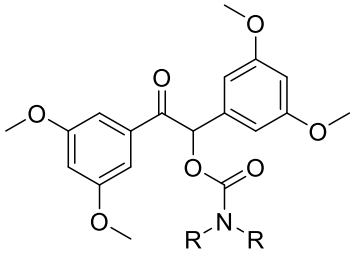

3,3',5,5' Tetramethoxybenzoin carbamate

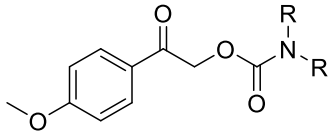

4-Methoxyacetophenone carbamate

Figure 2.11: PBGs explored for use in pitchdivision experiments

ONB based PBGs were found to give the sharpest contrast at the threshold values when added to commercial resists.[43] Initial experiments also showed the importance of

specific base selection. Only primary and secondary amines were available for use with these chromophores. Using a primary amine generates a primary amide upon addition of the PPG. Primary amides have an acidic hydrogen that can render the compound unstable at high temperatures, making them unsuitable for the processes requiring a post exposure bake step.[66-68] Previous results from our group also showed the strong correlation between catalyst steric hindrance and diffusion rate, leading to the use of di-substituted amines to limit diffusion and blur.[69] From a safety and convenience point of view, commercially available diethyl and diisopropyl carbamoyl chlorides were used to prepare the first pitchdivision PBGs.[42] However, the volatility of the generated bases was immediately observed to be an issue. Diethylamine and diisopropylamine have boiling points of 55°C and 85°C, respectively. The standard, commercial positive tone chemically amplified resists used in the experiments required post exposure bake temperatures in excess of 110°C. The resulting contrast curves using PBGs based on these amines had very shallow slopes at E_n. Increasing the PBG loading even further did not solve the problem and lead to films not completely clearing upon exposure.[43] Using heavier cyclohexylamine and dicyclohexylamine analogs, however, resulted in much steeper thresholds. Figure 2.12 shows the contrast curve for the best pitchdivision PBG found, 2-nitrobenzyl dicyclohexylcarbamate (ONB-DCHC).

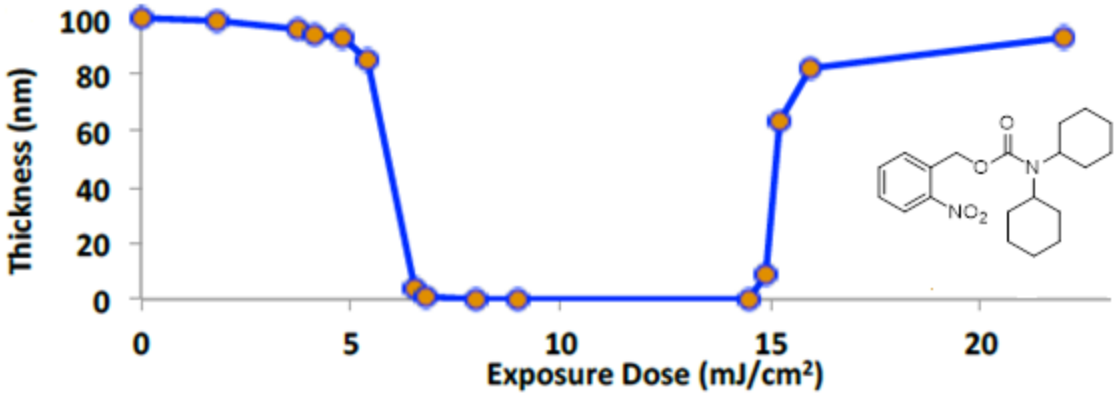

Figure 2.12: Contrast curve for commercial resist with ONB-DCHC. (Adapted from Ref 43)

Initial imaging experiments were performed at Intel by Robert Bristol using a commercial resist/ ONB-DCHC formulation. These initial experiments were performed using an interferometric tool as the light source. This tool is commonly used in lithographic research as it generates a nearly perfect sinusoidal intensity function as the aerial image regardless of the numerical aperture (NA). This perfect sine wave results in the maximum obtainable amount of contrast and allows for printing even at k values approaching 0.25. The resist used in this experiment was modified with base quencher to adjust the E-factor to generate equal lines and spaces. Figure 2.13 shows the first printed images using pitchdivision on a 220 nm half-pitch mask at NA = 0.22 and k = 0.25.[52] The process worked and generated a 110 nm half-pitch printed pattern.

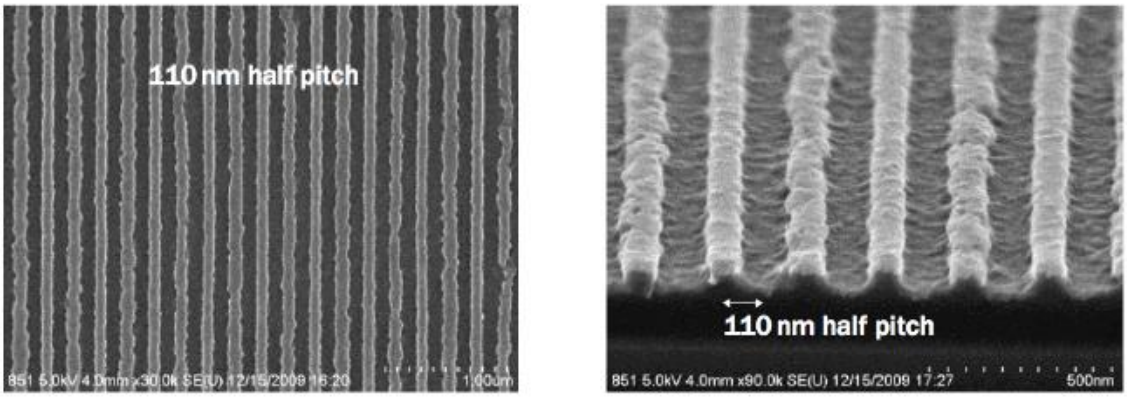

Figure 2.13: SEM micrographs of 110 nm half pitch lines and spaces printed using a 220 nm mask. (From Ref 42)

Smaller pitches were also attempted at Intel including a 90 nm half pitch mask in order to create a 45 nm L/S pattern (Figure 2.14). While the 45 nm pattern was generated, there is a noticeable decline in image quality. The line edge roughness (LER) in this image is unacceptable for commercial applications. Upon closer inspection, every other line appears to be particularly rough. This is even easier to see in the cross sectional SEM in Figure 2.13. As pitchdivision resists create a pattern of alternating positive and tone lines, one tone was clearly printing worse than the other. The higher LER tone was hypothesized to be the negative tone from the simple kinetic models (Figure 2.9). Further work performed by Xinyu Gu in collaboration with JSR corporation and IMEC confirmed that this was the case by using a 9 line array mask.[42] This generates an aerial image that is not perfectly sinusoidal and has significant deviations at the outer lines, allowing for positive identification of both tones due to their vastly differing thicknesses. However, additional simulation work showed that this is only true for printing 1:1 line to space images. Using very large doses actually generates low LER negative tone lines and high LER positive tone lines.[42] The reader is directed to the dissertation of Xinyu Gu for further discussion on simulations of the effect of critical dimension on LER.[42] Further

discussion in this dissertation will solely focus on printing equal line and space patterns where the negative tone will always have a larger LER.

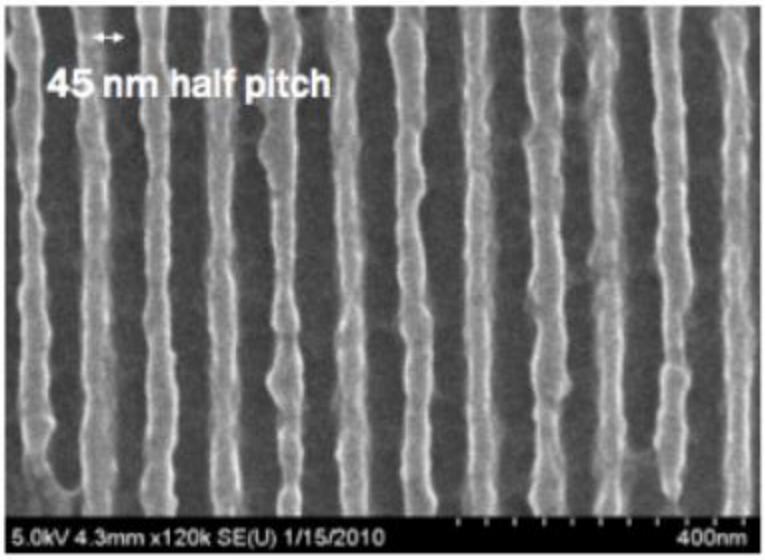

Figure 2.14: SEM micrograph of 45 nm half pitch printed using 90 nm mask. (From Ref 42)

TWO-STAGE PHOTOBASE GENERATORS

Many different methods were attempted to reduce LER in both the positive and negative tone images. Yongjin Cho from Cheil Chemical Company (a commercial supplier of electronic materials) experimented with a polymer bound PBG to try to reduce base diffusion.[70] While the contrast curve became much steeper at the E_n threshold, images printed at the same E-factor for both free PBG and polymer bound PBGs still experienced considerable LER. Another method has been to merely increase the [PBG]/[PAG] ratio.[42] This results in a larger gradient at E_n, though at significant cost. The overall net acid profile becomes smaller, and the addition of large amounts of PBG greatly increases the optical density of the film and adversely affects resist dissolution.

Additional PBG will also further increase the LER of the positive tone as the generated base is immediately quenching the acid in the low dose region.

Modeling by Gu showed that the acid gradient in the positive tone is only about a third of the that in the native resist.[42] In order to decrease the LER in the low dose region during pitchdivision, it was proposed that a method of delaying base generation was required. This would allow the positive tone image to function normally and not immediately begin to be quenched by base. Additionally, this non-linear base generation should accelerate at higher doses and improve the negative tone image as well.[43] To create this effect, we imaged a two-stage photobase generator where two separate and sequential photochemical reactions are required. This is shown below. Note that this is different from so-called two photon absorption where a molecule absorbs two photons at the same time, increasing the molecule's energy by the sum of the two photon energies.[71]

$$\text{Latent PBG} \xrightarrow[k_{b1}]{h\nu} \text{PBG} \xrightarrow[k_{b2}]{h\nu} \text{Base}$$

Figure 2.15 shows a how the net acid gradients can be increased by using a 2-stage PBG. The slope at the positive tone threshold is basically unchanged from the native resist, even at 10.5 equivalents of PBG to PAG. This is also a significantly higher loading than used for the 1-stage PBG, showing that delayed base generation can be used to improve the negative tone acid gradient without damaging the positive tone image. As shown in the figure, the rate constants of the 2-stage PBG to 1-stage PBG and 1-stage PBG to base where set to be the same (i.e. $k_{b1} = k_{b2}$). This ensures the maximum deviation from first order behavior. In the case where these rate constants are vastly different, the rate of base generation essentially becomes first order with the rate being that of the slower reaction. For example, if $k_{b2} >> k_{b1}$, as soon as PBG is generated, it is

immediately consumed; the end result is the same as using a less quantum efficient 1-stage PBG.

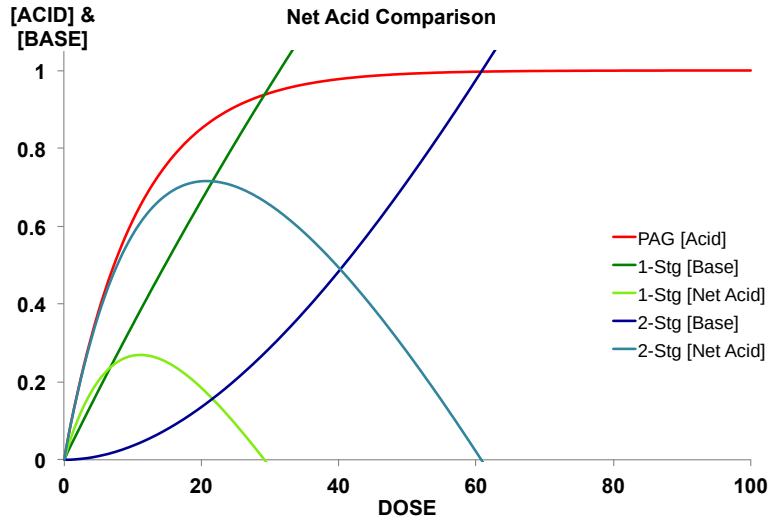

Figure 2.15: Comparison of net acid produced with a 1-stage PBG (Green) and a 2-stage PBG (Blue). (k_{b1}=0.008, k_{b2}=0.008, k_a=0.095, 1-Stage [PBG]/[PAG]=4.5 2-Stage [PBG]/[PAG]=10.5)

While the use of a 2-stage PBGs for pitchdivision sounds great in theory, there was very little precedent for preparing one.[72] Despite this, there has been considerable interest in their use in lithography.[34, 73-76] Work in our group has focused on developing 2-stage PBGs that function based on different mechanisms. These included modifying the benzoin and acetophenone PBGs in Figure 2.11 with phenacyl ether protecting groups, designing a photo-aromatizing PBG, and preparing a symmetrical 2-nitrobenzyl bis-carbamate.[77-78] While the phenacyl protected 2-stage benzoin PBG functioned as a PBG, the k_{b1} value (phenacyl deprotection) was much lower than k_{b2}, resulting in similar contrast curves and nearly indistinguishable SEM results. The photo-aromatizing PBG

suffered from the same issue.[77-78] The reader is directed to the thesis of Ryan Mesch for a complete discussion on synthesis and printing using these ineffective PBGs.[43]

When designing a PBG with the same rate of photolysis for each step, we believed that using the same photochemical reaction for each step should give very similar rates. To test this, a 2-stage ONB carbamate (ONB2-CHA) was prepared by Ryan Mesch (Figure 2.16). The idea with this compound is that either ONB group could be cleaved to form the standard 1-stage PBG (in this case ONB cyclohexylcarbamate (ONB-CHA)).

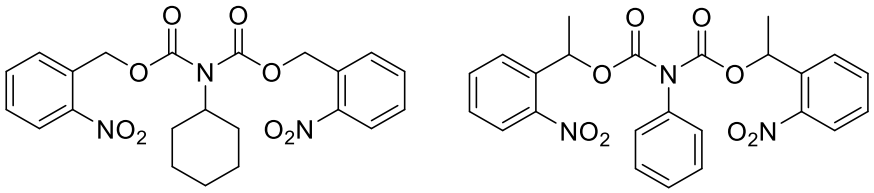

Figure 2.16: Symmetrical 2-stage PBGs based on ONB protecting group

The major challenge with the 2-stage PBGs is the difficulty in quantifying base production. While the corresponding PAGs have been quantified relatively easily by our group previously[54], base quantification proved much more difficult. In many of the systems, radical recombination resulted in a large variety of products, making techniques such as HPLC, GCMS, and ion chromatography ineffective. Figure 2.17 shows the photoproducts of two ONB based PBGs. The standard version, ONB-CHA, generates cyclohexylamine and 2-nitrosobenzaldehyde upon exposure.[79-80] However, the aldehyde is sufficiently electrophilic to quickly react with the generated cyclohexylamine to form imines as well as cyclic indazolones.[81-82]

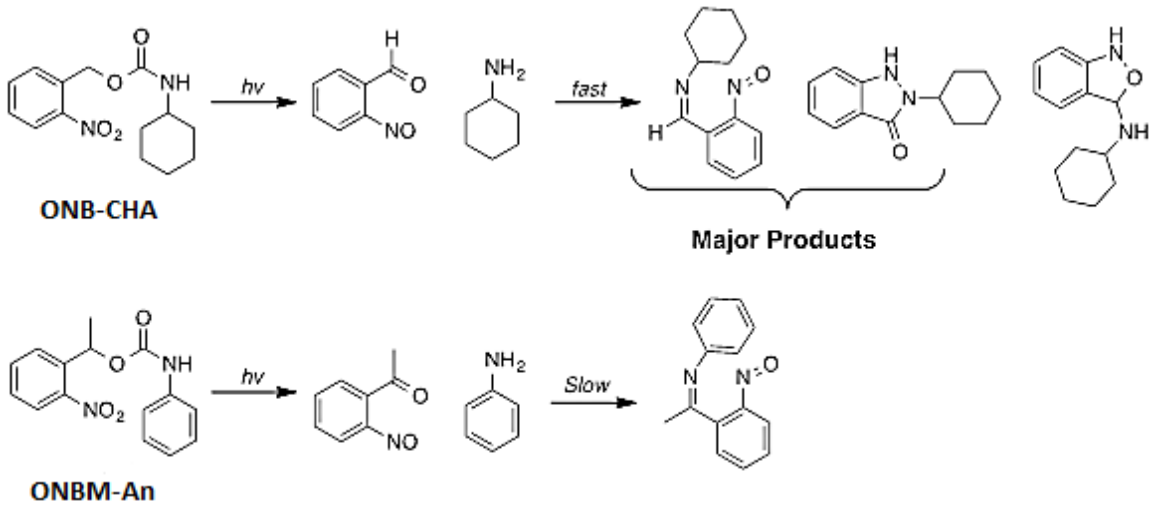

Figure 2.17: Photoproducts of 1-stage ONB based PBGs

In order to reduce recombination, the ONBM-An PBG was synthesized. This PBG generates the weaker and less nucleophilic base aniline, as well as the much less electrophilic 2-nitrosoacetophenone. Imine formation is greatly reduced and the aniline is not destroyed. Using aniline as the base is also beneficial as it is UV active and can be observed by HPLC using a UV detector. Using cyclohexylamine based PBGs required isocratic runs and index of refraction monitoring, which we found to be insufficiently sensitive for quantification.

First HPLC calibration curves were created for both aniline and ONBM-An. Figure 2.18 shows the calibration curve for aniline detecting at 254 nm. A similar curve for the 1 stage carbamate was also obtained, though at 275 nm as it was much more absorbent than aniline. Initial testing on the compound was performed in a quartz NMR tube in Ar purged acetonitrile (Figure 2.19). The NMR tube was exposed to 254 nm light using a Rayonet photochemical reactor. The initial results for this PBG showed that the reaction was much cleaner than that of ONB-CHA, as the sum of the concentrations of starting material and generated base remained constant throughout the exposure. In fact,

this is even true after 1 hour of exposure and conversion approaching 85%. This methylated variation could therefore be used as a spectacular protecting group for amines.

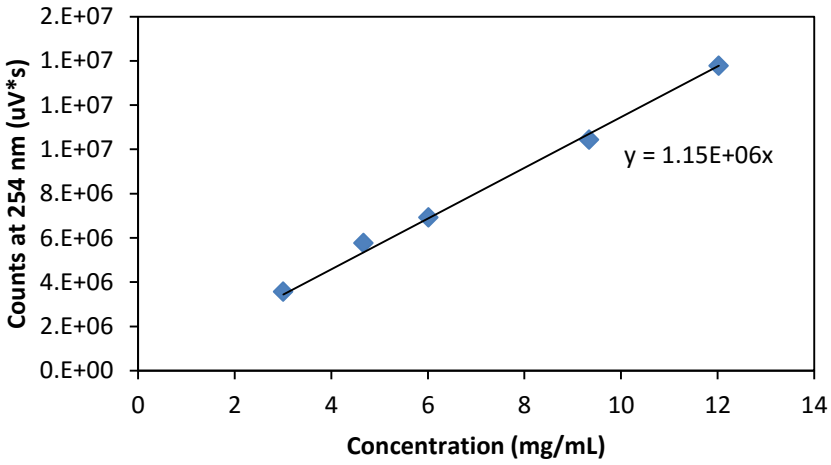

Figure 2.18: HPLC calibration curve for aniline at 254 nm

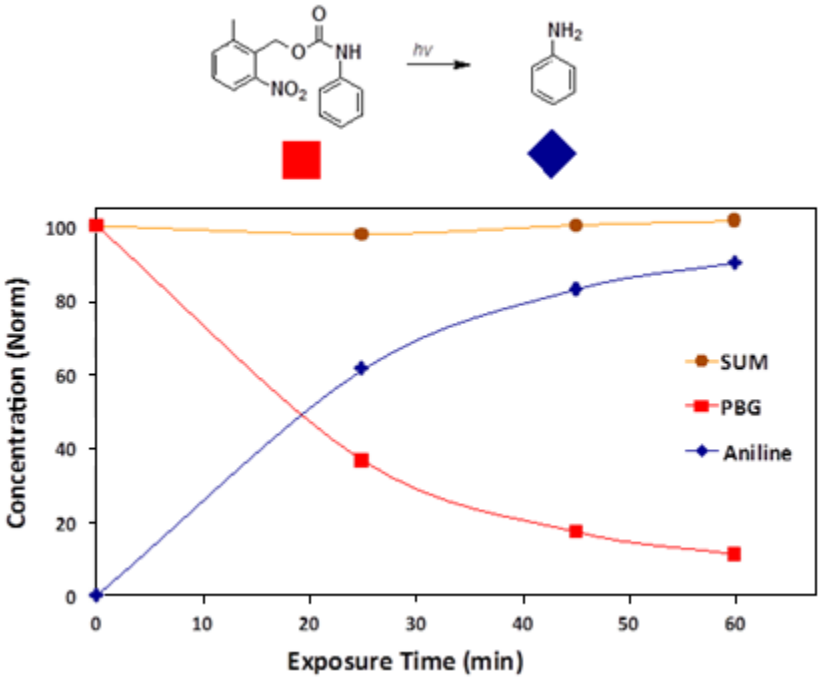

Figure 2.19: Initial 254 nm exposure of ONBM-An showing clean reaction

As the preliminary results for ONBM-An base generation appeared promising, the 2-stage version ONB2M-An was also prepared by Ryan Mesch. Both 1 and 2-stage methylated PBGs were sent to Yongjun Li and Steffen Jockusch at Columbia University for quantum efficiency measurements. Figure 2.20 shows the HPLC analysis of acetonitrile solutions of each compound irradiated at 254 nm. The lack of by-products is consistent with the results at UT. Additionally, the use of an in-line ESI detector allowed for the new peak formed at 4.9 minutes to be positively identified as 2-nitrosoacetophenone. The quantum yields for both PBGs were calculated using valerophenone as an actinometer.[78] Valerophenone undergoes an efficient Norrish type II upon UV exposure with a quantum yield of Φ = 1.0 in acetonitrile (consumption of valerophenone)[83], allowing for convenient calculation of photon flux by GC. The quantum yields at 254 nm were found to be Φ = 0.21 (ONBM-An) and Φ = 0.12 (ONB2M-An). This gives only a factor of 1.75 difference between the stages, so we expected to observe the desired delay in base generation. Figure 2.21 shows that this is the case. A significant delay is present in the low exposure dose region.

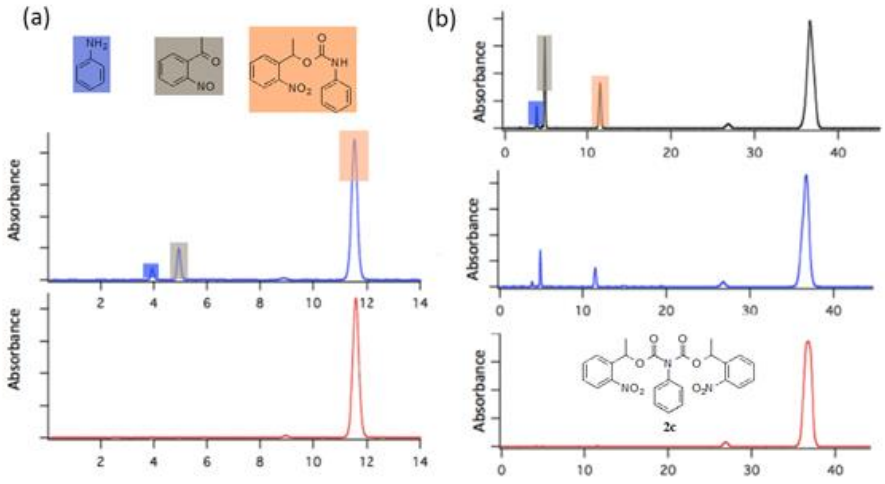

Figure 2.20: HPLC analysis of 1 (a) and 2 (b) stage methylated aniline ONB carbamates in acetonitrile irradiated at 254 nm. Analyte detection at 288 nm.

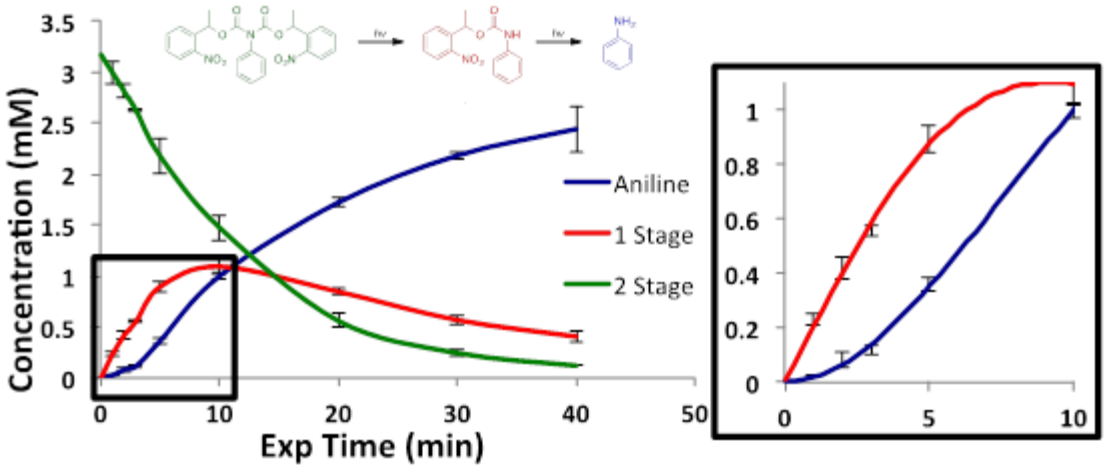

Figure 2.21: HPLC analysis of ONB2M-An irradiated at 254 nm in acetonitrile. Analyte detection at 230 and 275 nm.

The methylated aniline PBG experiments showed that these compounds do result in a delayed base generation, so the next step was to incorporate them into a chemically amplified resist for patterning. The main goal of these studies would be to determine if the LER is decreased using the 2-stage PBG. For this purpose, the aniline based PBGs were not used as aniline is aromatic and would considerably increase the optical density of the resist, especially at the higher loadings used for 2-stage PBGs. Instead, ONB-CHA and ONB2-CHA were chosen. While these PBGs will both generate imines or indazolones during exposure, these nitrogenous species should still be sufficiently basic enough to quench the photo-generated super acid.

Comparing the LER from 1 and 2 stage PBG formulations is actually quite difficult due to many factors affecting the process. These include PBG loading, PEB temperature, optical density, and differing kinetics.[55] In order to print a 1:1 line and space pattern, the conditions required are quite different for the 1 and 2 stage PBGs. Therefore we decided that printing at constant E-factor would be the best way to compare LER and

line width roughness (LWR).[55] This ensures that equal line and space patterns will be compared. Images were printed using a 193 nm interferometric tool built by IBM.[84] As previously described, this type of source generates a perfectly sinusoidal aerial image and offers the maximum obtainable contrast. Commercial TOK TARF Pi6 001ME was used as the base resist and formulations were prepared to obtain an E-factor between 0.55 and 0.60 at a PEB temperature between 100-110°C. The results of printing 100 nm half-pitch images using a 200 nm half-pitch aerial image are shown in Figure 2.22.

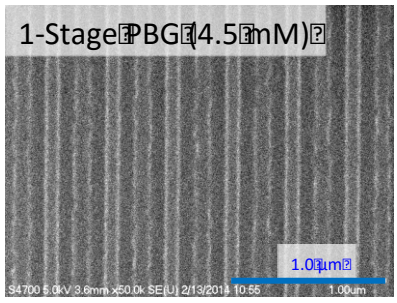

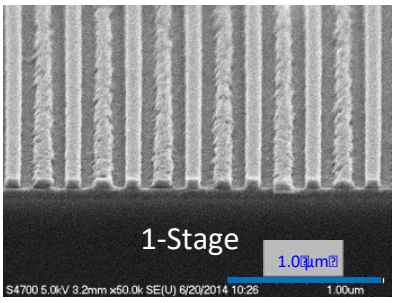

PEB=109ºC E_{op}=16 mJ

	CD	LWR	LER
P	103	12	9
N	113	44	23

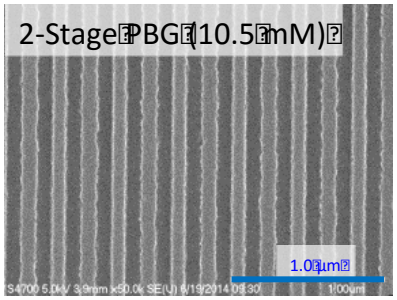

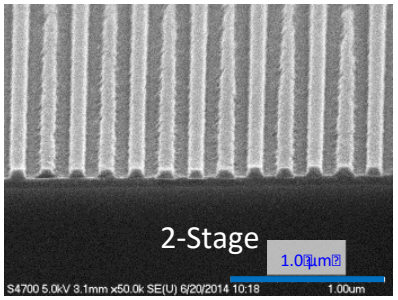

PEB=100ºC E_{op}=10.9 mJ

	CD	LWR	LER
P	100	9	6
N	110	17	12

Figure 2.22: SEM micrographs comparing pitchdivision results using 1 and 2 stage ONB-CHA PBGs in commercial photoresist. CD, LER, and LWR measurements obtained from SuMMIT software.

Visual inspection of the SEM micrographs clearly shows that the quality of the negative tone line is vastly improved in the case of the 2-stage PBG. The LWR and LER

were measured using SuMMIT software. For the native resist, these values were 12 nm and 8 nm for lines measured to be 202 nm. These values are very close to those measured for the positive tone for both of the PBGs. Interestingly the positive tone is even sharper using the 2-stage resist than in the native resist. However, the negative tone improvement is really where the improvement is for the 2-stage PBG over the 1-stage. There is about a factor of 2 decrease in LWR and LER moving from the 1-stage formulation to the 2-stage formulation. The negative tone roughness values are actually only slightly higher than the native resist. The z-axis roughness is also greatly decreased in the negative tone images, which would be important during image transfer into the underlying substrate. These results clearly show that this 2-stage PBG allows for greatly improved image quality when compared to the 1-stage PBG.

CONCLUSIONS

The first photobase generator utilizing two sequential photoreactions having similar rate constants was developed. We were able to quantify base generation by modifying the traditional 2-nitrobenzyl photosensitive protecting group with a methylated benzyl position and using the less nucleophilic base aniline. This slowed down the recombination reaction observed in the standard PBGs and allowed for quantification by HPLC. The predicted delay in base generation was observed by HPLC. In agreement with modeling, images printed using an interferometric tool showed that the positive LWR and LER of 2-stage pitchdivision formulations are very similar to those of the native resist. While the LWR and LER of the negative were higher than the native resist, they were still a factor of two lower than in the 1-stage PBG formulation. These results

show that non-linear base generation is possible and that it can be used to greatly improve image fidelity in pitchdivision resists.

EXPERIMENTAL

General Methods

All PBGs were synthesized by Dr. Ryan Mesch.[43] ARC 29S was donated by Brewer Scientific and ArF resist TARF Pi6 001ME generously was donated by TOK America. HPLC grade acetonitrile (Fisher) was used without further purification. Hot plates open to air were used to bake photoresists. UV exposures were performed at 193 nm using an IBM custom interferometric tool. Exposed resists were developed in 2.38% TMAH solution for 1 min.

HPLC for Base Quantification

HPLC for base quantification was performed on a Waters 600 series instrument equipped with a photodiode array. The injection volume was 20 μL. A gradient of 20:80 to 100:0 MeCN:water in 14 minutes at 2.0 mL/min was used as the mobile phase. A reverse-phase C_{18} column (4.6 x 150 mm, 5 μm particle size) was used as the stationary phase. The column was maintained at 50°C during runs, and the system was equilibrated for at least 10 minutes between runs. Aniline was detected at 230 nm and 1 and 2 stage methylated aniline PBGs at 275 nm due to their much higher absorption compared to aniline. A calibration curve of at least 5 points was generated for each species.

PBG samples were dissolved in HPLC grade MeCN and charged into quartz NMR tubes. The samples were degassed by bubbling argon through them. The solutions were then exposed to 254 nm light in a Rayonet photochemical reactor. Periodically

aliquots (~50 μL) were taken and injected into the HPLC. The experiment was repeated three times for both the 1 and 2 stage methylated aniline PBGs and the error bars represent the standard deviation of the three trials. The raw data are located in the appendices.

The HPLC at Columbia was equipped with an ESI mass detector and was used for quantum yield determination, as well as positive identification of the 2-nitrosoacetophenone by-product.

Quantum Yield Measurements

Valerophenone with a quantum yield of 1.0 (loss of valerophenone in acetonitrile solutions) was used as actinometer for quantum yield measurements.[78] The loss of valerophenone was quantified by gas chromatography (GC) equipped with a flame ionization detector and a capillary column (Cp-Sil 5 CB low bleed/MS, 0.05 mm × 25 m, 0.25 μm particle size) at Columbia University. A calibration curve for each compound was generated with five points, and the linear range of the detector was determined. In a typical quantum yield measurement, the absorbances of sample and the standard in acetonitrile solutions were matched at the irradiation wavelength. Two milliliters of the sample or standard solution was deoxygenated (argon bubbling) and irradiated in sealed 1 × 1 cm Suprasil quartz cells under stirring with a magnetic stirring bar using a low-pressure Hg lamp emitting at 254 or 300 nm as light source. Aliquots of the solution (15 μL) at different irradiation times were withdrawn from the photolysis cell for GC and HPLC analysis and quantified by calibration curves for each compound being analyzed.

The conversions in these photoreactions were kept below 30% to minimize interference from secondary products.

Chapter 3: Photosensitive Polyimide for Microelectronics Packaging

INTEGRATED CIRCUIT PACKAGING[1]

Photolithography, as described in Chapter 1, is used to produce patterned wafers. The end product coming from many chip manufacturers is a full wafer containing many individual chips (Figure 3.1). After the lithography processes, the full wafers are typically sent to a separate packaging company.[85] The wafers are cut into individual chips. In the industry a chip is often referred to as a *die* due to the *dicing* step used to separate the *dies*. By itself, the die is quite fragile and the delicate structures are exposed to the environment. Something is required to seal and protect the die. This encapsulation device is called the "package" and it allows for the die to operate in ambient conditions. Indeed, some packages have even been designed to tolerate extreme conditions such as high temperature and high radiation environments.

[1] This chapter contains figures and data previously published in:

Dick, A. R.; Bell, W. K.; Luke, B.; Maines, E.; Mueller, B.; Rawlings, B.; Kohl, P. A.; Grant Willson, C., High aspect ratio patterning of photosensitive polyimide with low thermal expansion coefficient and low dielectric constant. *JM3* **2016,** *15* (3), 033503-033503.

The work of the author primarily focused on materials synthesis including both photobase generators and dielectric polymers. Additionally the author also performed UV and IR spectroscopy studies, Dill parameter determinations, and PROLITH modeling.

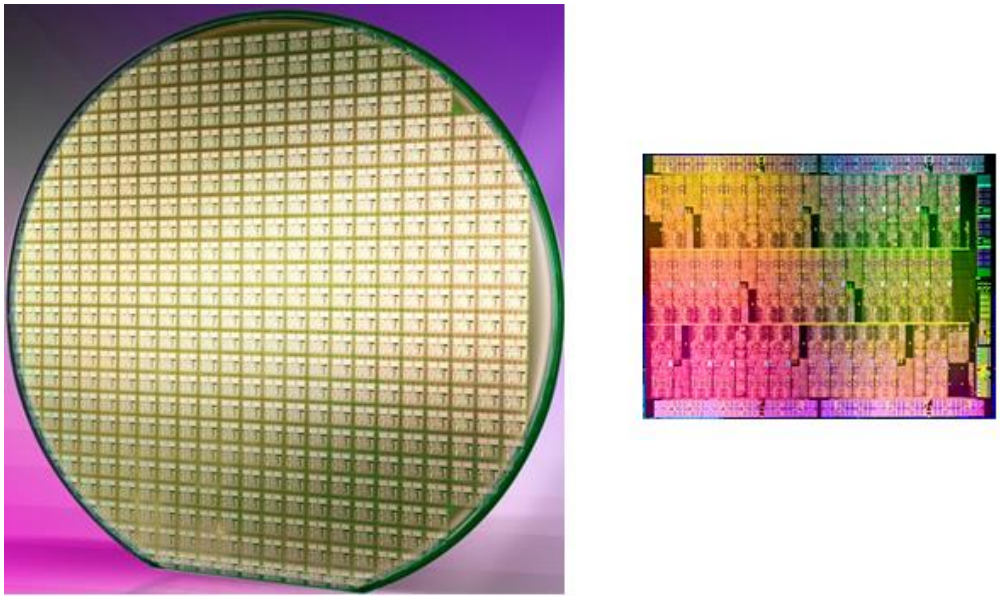

Figure 3.1: Patterned full wafer (left) and a single die (right).[86-87] (Courtesy of Intel)

While the primary purpose of the package is to protect the die, there are two other main considerations. First and foremost is that electrical signals have to come into and out of the die, so electrical connectivity is required. This is most relevant in applications such as state-of-the-art high-end microprocessors where a high density of input/output (I/O) connections is desirable. The larger number of connections maximizes bandwidth between the chip and the board, allowing for faster communication. The other major consideration is the amount of heat generated by modern chips; temperatures in high-performance devices can reach 100°C during normal operation. The push toward chip stacking and other 3-D architectures further compounds this heat problem. The package must be able to effectively dissipate all of this waste heat so that the device is not damaged. Historically, innovation in the package design has been fairly neglected compared with die. However, these issues mean that the package actually has a measurable influence on device cost, performance, and reliability.

The first packages developed were based on ceramic flatpacks and were favored by the military and aerospace industries due to the ability to hermetically seal the circuits. These designs remained popular in those industries even well after the adoption of plastic packages. The industry quickly moved toward dual in-line packaging (DIP) and this method became the first commercially successful option. This packaging was developed at Fairchild Semiconductor in the 1960s initially as a ceramic material but later versions adopted a cheaper and easier to mass produce epoxy based version. As shown in Figure 3.2, the DIP is a rectangular plastic device that encapsulates the chip and has its pins arranged in two lines. The pins are connected to the chip by a series of small wires in a process called wire bonding. The packages for the first Intel chip, Intel 4004, relied on this technology. This device contained only 16 I/O pins to connect 2,300 transistors, ran at a meager 740 kHz, and was patterned using 10 micron lithography.[88]

Figure 3.2: Dual Inline Package containing 16 I/O pins. The silicon die is located between the two plastic shells.[89]

Due to the ever increasing number of transistors per device predicted by Moore's law, more I/O pins were required to adequately service the larger chips. The initial

solution was to continue with the DIP scheme, just adding additional pins such as the 40 pin DIP used in Intel's second generation 8008 device.[88] However, industry standards set the spacing between pins to 0.1 inches, meaning that adding more pins resulted in substantially larger packages. Eventually this bulky solution became limited to 64 pins by the end of the 1970s for processors such as the Motorola 68000.[90-91]

Eventually small-outline packages (SOP) and then plastic quad flat packs (PQFP) became popular as they decreased pin spacing and began to use all four edges of the chip. These wire-bonding type schemes are still used to connect some chips to their packages. However, unlike in early chips that use of wire bonds for connections, wire-bonding is now only used where the I/O density requirements are low. The limitation of this method is that wiring is only possible along the perimeter of the chip (Figure 3.3). Improvements in packaging have focused on addressing this problem by enabling the entire surface area of the chip to be wired in a process called flip-chip interconnection. This method was originally developed by IBM for use in its mainframe applications.[92] In this process, bonding pads are placed over the entire surface of the die and they are connected to the package by solder joints. In addition to greatly improving the I/O density available, the short and abundant connections also allow for much improved heat dissipation over wire bonding.

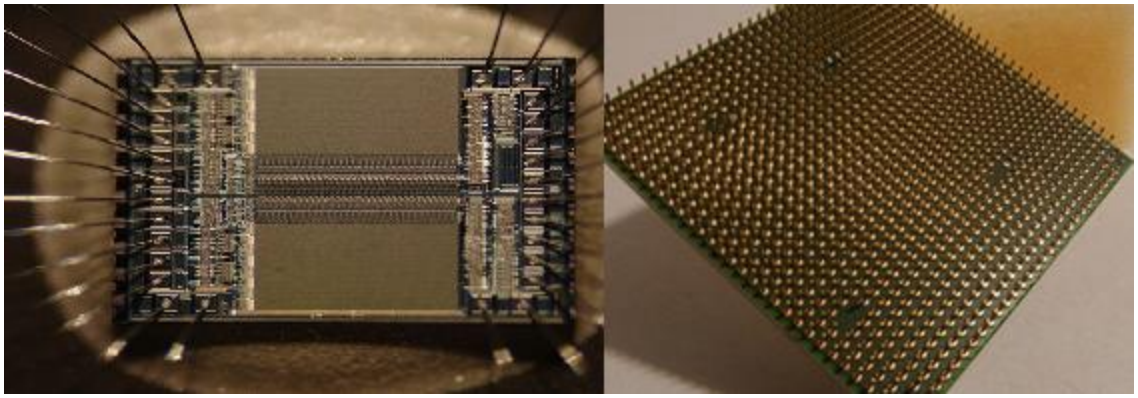

Figure 3.3: Wire-bonding of a chip (left) and pin grid array used in flip-chip packaging (right)[93-94]

After its introduction by IBM, flip-chip has developed into three major types of arrays for connections. These are the pin grid array (PGA), land grid array (LGA), and ball grid array (BGA). PGA was used extensively in early packaging when DIP became unwieldly. It consists of an array of pins on the chip side that connect to sockets on the package side. This method retains the same 0.1 inch pin spacing as DIP and was replaced by Intel and Advanced Micro Devices (AMD) in the early 2000s in favor of LGA.[95] LGA is essentially PGA reversed; the pins are located on the package side. In LGA packaging there is also option of directly soldering the chip to the board rather than having package side sockets. BGA is very similar to socket-free LGA. In BGA solder balls are attached to bonding pads on the chip side and heated to reflow and form electrical connections. This is in contrast to LGA which uses flat contacts for soldering rather than solder balls. BGA offers the advantages of the smallest possible connections currently available for the highest I/O density. The shorter connections also improve heat conduction and provide lower inductance. However, the major difficulty with BGA is that the connections are not mechanically compliant. Solder ball connections cannot bend and

flex like other connections, so thermal stresses generated after solder reflow due to coefficient of thermal expansion mismatch can cause joint failures.

Today, flip-chip packages are produced in a process called sequential build-up (SBU). This process was first developed by IBM, but has become the industry standard after adoption by Intel.[92] The process begins by using FR-4 as the "core." The main purpose of the core is to provide a rigid substrate for the electrical connections for the chip and redistribute power and signals. FR-4 is a fiberglass reinforced epoxy resin and is the green part of printed circuit boards. Copper foil is then laminated on both sides of the board to produce a "copperclad laminate." The copper foil is then subtractively patterned to form the desired circuit. The separate layers are then connected by drilling through the board and electroplating copper to form vias that connect layer to layer. Modern high end devices require cores that consist of multiple FR-4 and copper layers.

A schematic of a typical package using flip chip ball grid array (FCBGA) is shown in Figure 3.4. In addition to the rigid core "build-up" layers are also present. These are much thinner layers (< 20 μm) and are located on either side of the core. These layers are built *sequentially* on top of each other in the SBU process. As in the core, the build-up layers consist of copper and an insulator, however without any fiberglass present. These layers are patterned using either conventional photolithography and subsequent etching or in a direct laser drilling process.[96] Neither method is without its drawbacks, however. Photo-patterning requires a separate photoresist and a series of subsequent processing steps (recall Chapter 1). Direct patterning by laser drilling has the advantage of being a one step process. However, it is extremely energy intensive and tends to damage more sensitive organic dielectrics, leading to lower quality features than when using a separate photoresist.[97] The feature size available from laser drilling also tends to be larger than that achievable by photolithography. To improve on this process, it would

be desirable to have a photosensitive material that could be used as the dielectric in the build-up layers. This would offer the advantage of improved feature quality while removing many of the processing steps. The goal of this project is to create a photo-patternable material for use in these build-up layers.

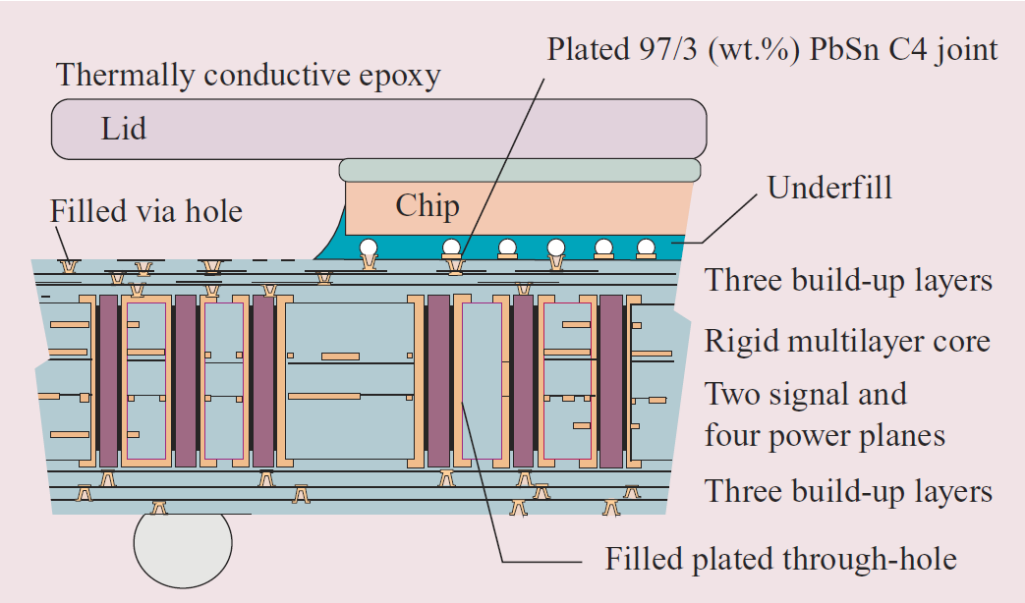

Figure 3.4: Schematic of Ball Grid Array package showing build-up layers and rigid core.[92] (Copyright 2005, IBM)

PHOTOSENSITIVE POLYIMIDE

The material of choice for this application is aromatic polyimide due to its unique combination of material properties. Polyimides (PI) were used in the 1980s as interlayer dielectrics due to their lower dielectric constant than SiO_2, good planarization, and relatively low cost.[40] Additionally, PI have also been used to form stress-buffer layers between the chip and the rest of the package in order to reduce the stress on the chip and improve reliability.[98-99]

The PI of pyromellitic dianhydride-co-oxydianiline (PMDA-ODA), known by its DuPont tradename, Kapton®, is so commonly used that it has become essentially synonymous with polyimide. Aromatic polyimides tend to have low coefficients of thermal expansion and high thermal stability, usually in excess of 400°C. Typically these materials also have low dielectric constants, reasonable etch resistance, as well as excellent resistance to organic solvents and good hydrolytic stability.

The insolubility of most polyimides does, however, complicate processing. This requires that a soluble polyimide precursor be used and then cured to imidize the material. Poly(amic acids) (PAA) produced from the polycondensation of a dianhydride with a diamine are by far the most common precursors. (Figure 3.5) Poly(amic esters) can also be used, and are created from the condensation of a diamine and a diester diacid chloride monomer. In the case of aromatic monomers, even the precursor polymers tend to only be soluble in amide solvents such as dimethylformamide, and n-methylpyrrolidone. After a solution of the precursor is coated onto the substrate of choice, the material is cured at high temperature (>300°C) to ring close the polymer to the imide form.[100] Dehydrating agents such as acetic anhydride/pyridine can also be used to chemically cure the PI at reduced temperatures.[101]

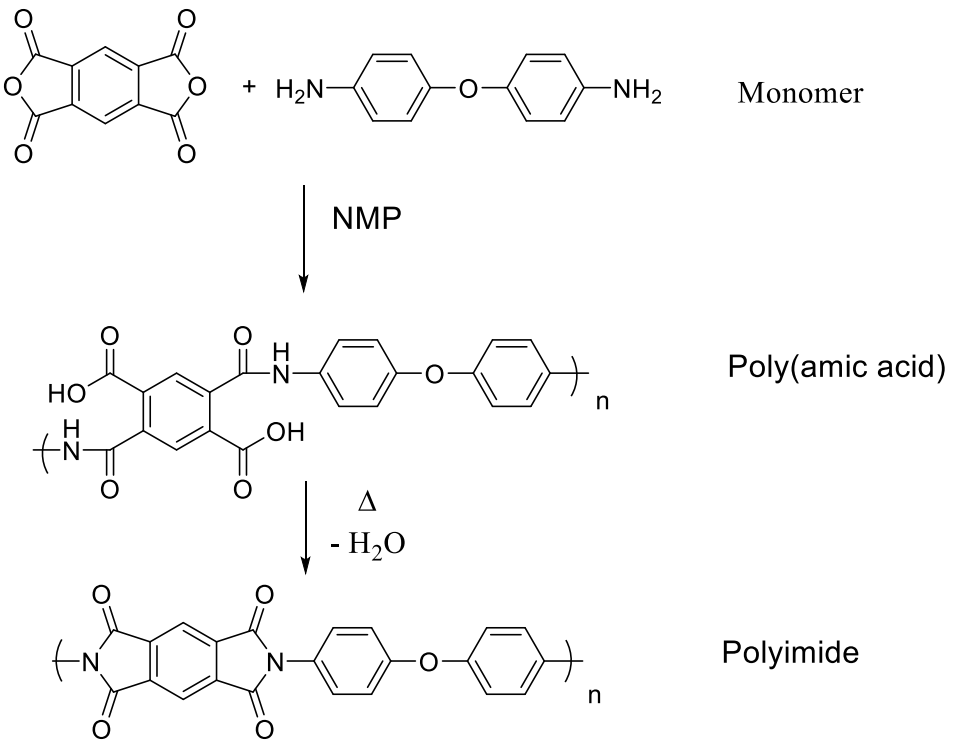

Figure 3.5: Synthesis of PMDA-ODA. Poly(amic acids) are equilibrium mixtures of isomers.

For use in microelectronics devices, the polyimides must be patterned, typically using a separate photoresist. This is performed by first coating the desired substrate in an adhesion promoter so that the polyimide will be chemically bound to the surface. The precursor polymer, usually, poly(amic acid) is then coated on top of the adhesion promoter and baked to drive off excess solvent. After subsequent high temperature thermal curing, the material is dehydrated to form insoluble polyimide. A photoresist is then coated on top of the fully cured polyimide, exposed to light through a mask and developed. The image is than etched into the underlying polyimide layer. Finally the resist is striped. Additionally, depending on the exact process and photoresists used,

multiple baking steps and a full thermal cure are required at different stages in the process.

In order to simplify the patterning process, photosensitive polyimides (PSPI) have received considerable attention. These materials act as a combination of polyimide and photoresist. The process for these materials consists of coating the PSPI onto the desired substrate, exposing the PSPI to light through a mask, developing the PSPI and then a final thermal cure. The reduction in processing steps can be clearly seen in Figure 3.6. The process removes the need for a separate photoresist as well as a potentially damaging etch step. A few reviews have been written on the large variety of PSPI[102-103] that have been reported, so this thesis will only highlight the major differences in the schemes employed for patterning. The reader is directed to these comprehensive reviews for further reading.

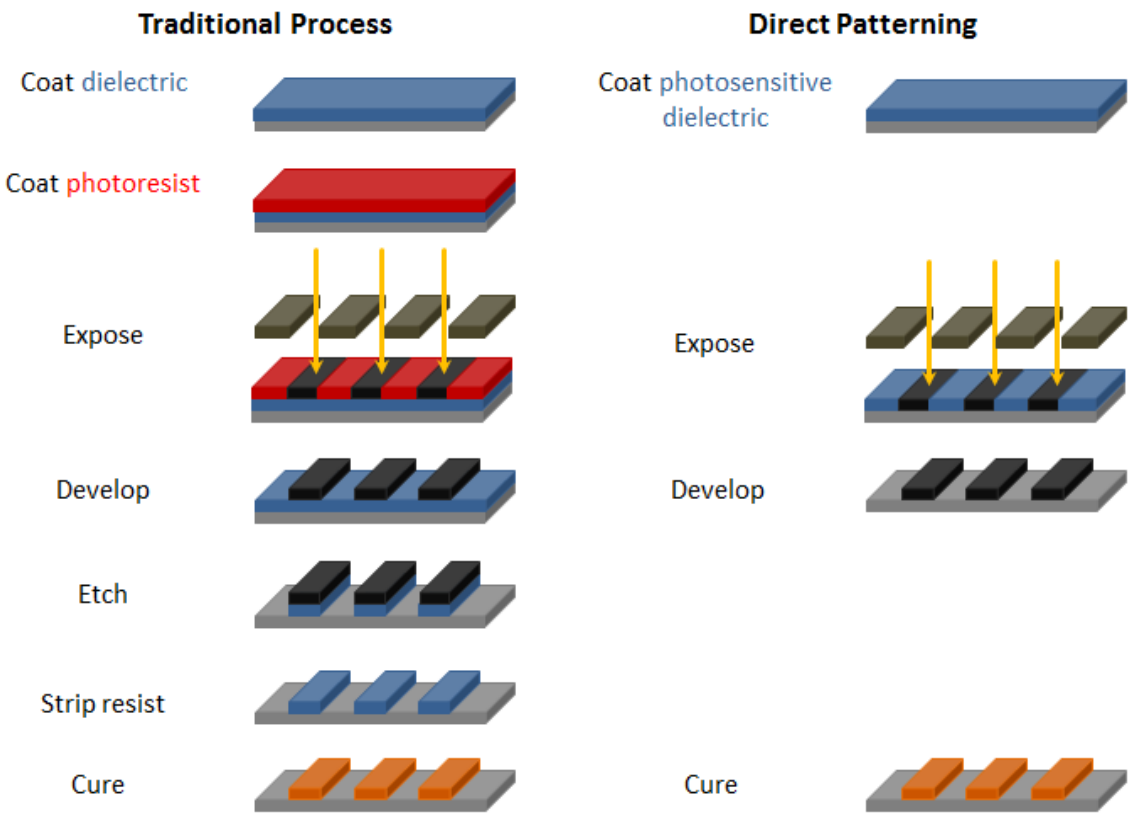

Figure 3.6: Comparison of (negative tone) traditional and direct dielectric patterning

POSITIVE TONE PHOTOSENSITIVE POLYIMIDE

Many positive tone photosensitive polyimides have been devised. Positive tone PSPI designs are not typically chemically amplified and usually involve the addition of diazonaphthoquinone (DNQ) derivatives to act as a dissolution inhibitor for poly(amic acids), poly(hydroxyimides), or poly(isoimides).[104-107] In a typical example[105], a poly(amic acid) copolymer of pyromellitic dianhydride (PMDA), biphenyl tetracarboxylic dianhydride (BPDA), and 2,2' bis(trifluoromethyl)benzidine (TFMB) is patterned using 2,3,4-tris(1-oxo-2-diazonaphthoquinon-4-ylsulfonyloxy)benzophenone (D4SB, Figure 3.7). The benzophenone derivative is essentially a benzophenone molecule with three pendant DNQ groups; the function is basically the same as in non-

chemically amplified DNQ-novolac resists. Ortho-nitrobenzyl protected poly(hydroxyimides) have also been developed, though with very low sensitivity ($D_{0.5}$ > 5J/cm^2).[108]

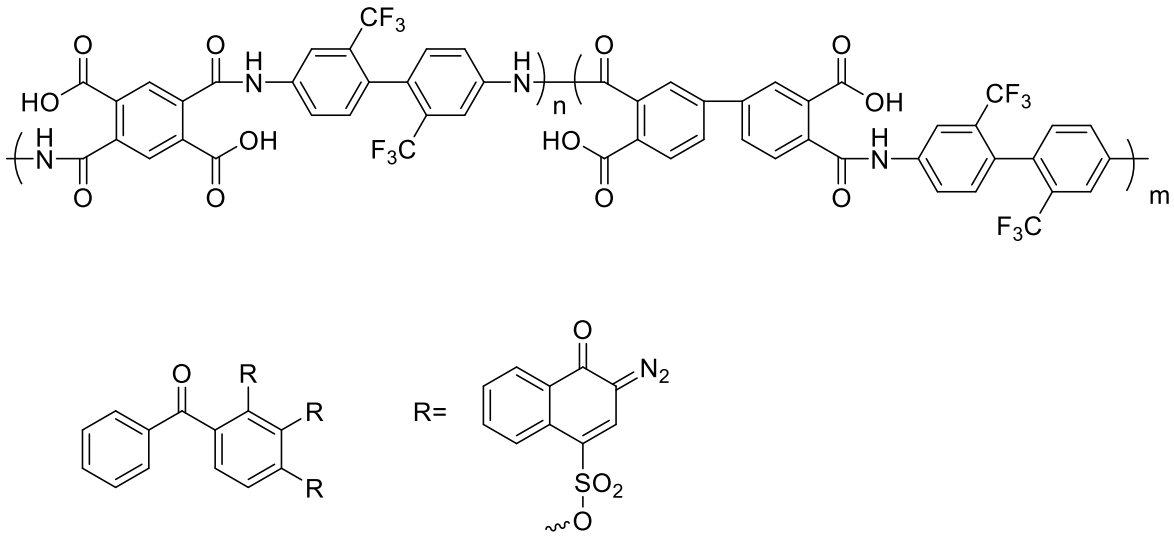

Figure 3.7: Example of DNQ based positive tone PSPI

NEGATIVE TONE PHOTOSENSITIVE POLYIMIDE

Negative working PSPI is much more common than its positive tone counterpart. The first practical PSPI was developed by Rubner et al. at Siemens. This material was a negative tone PSPI and based on the crosslinking of pendant 2-hydroxyethylmethacrylate esters by a photo-radical generator.[109] (Figure 3.8) A competing method developed by Yoda et al. of Toray relies on the addition of tertiary amine methacrylates to form salts with a poly(amic acid).[110] Similarly, a photo-radical generator is also used to crosslink ionically bound methacrylate esters. (Figure 3.9)

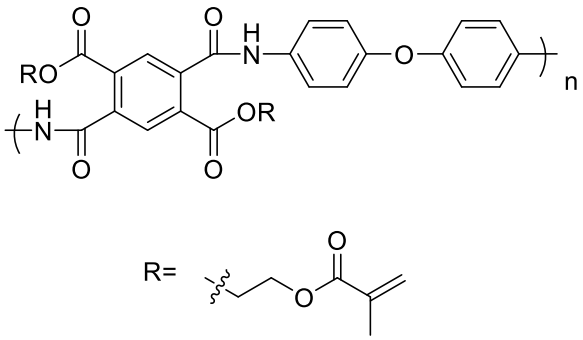

Figure 3.8: Siemens methacrylate ester based negative tone PSPI

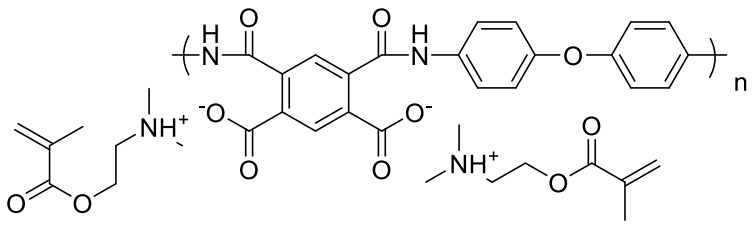

Figure 3.9: Toray methacrylate salt based negative tone PSPI

The Siemens and Toray type PSPI are used in the same way (Figure 3.10). The precursor material is first spin-coated onto the desired substrate and soft baked to remove residual solvent. The material is then exposed to light to initiate crosslinking. The unexposed regions can then be developed away. A final thermal cure is then performed to convert the material into polyimide. While these materials have been extensively used in the microelectronics industry, they have many drawbacks. Perhaps the most problematic is the cure shrinkage exhibited by these systems. During the final thermal curing the methacrylate sidechains are volatilized as the chains ring close to the imide form, causing the films to shrink around 50%.[60] This extreme shrinkage tends to cause significant

sidewall slopes in the fully cured material (Figure 3.11),[111] as well as voids due to the volatilized crosslinkers.[112] Commercial materials using these schemes are typically Kapton based, which are strongly colored and therefore require high exposure doses, on the order of multiple J/cm^2. Photogenerated radicals are also quenched by atmospheric oxygen, further degrading crosslinking efficiency and increasing the required dose.

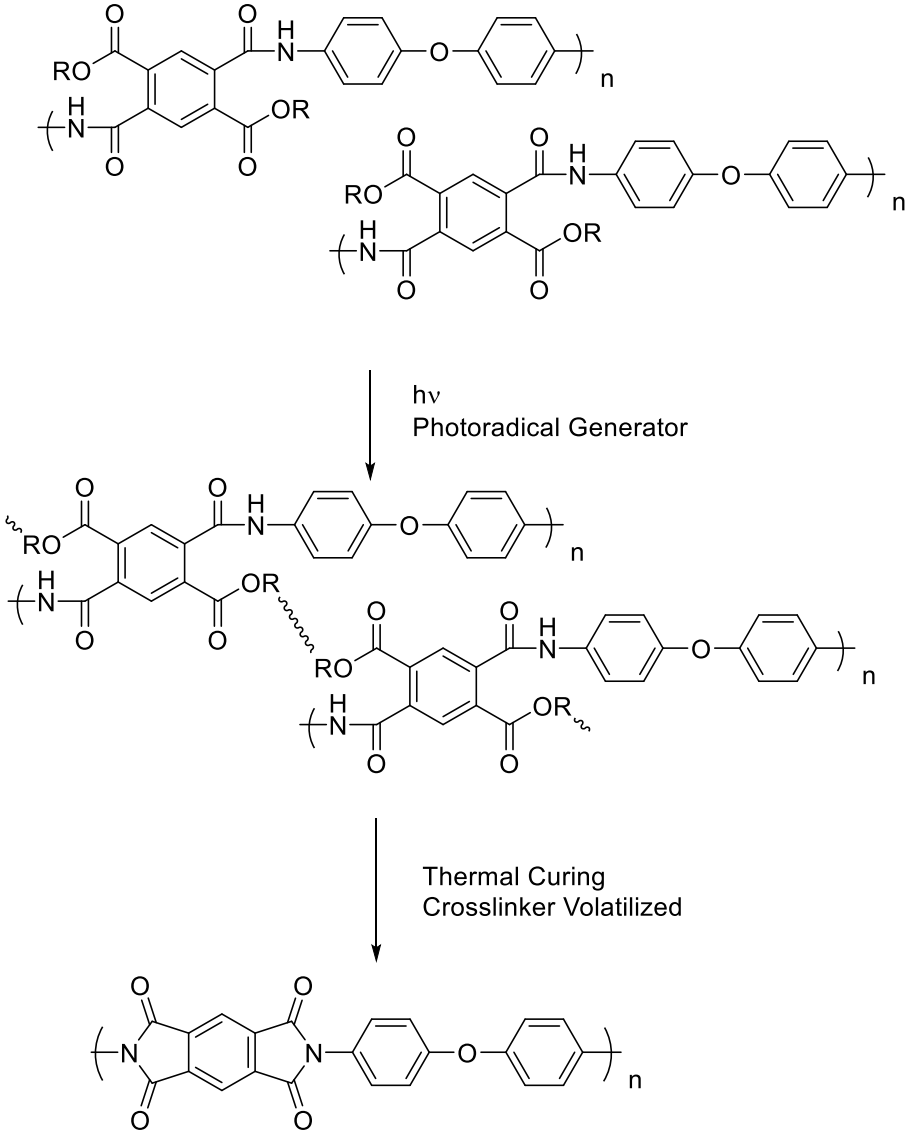

Figure 3.10: Imaging scheme for traditional crosslinking negative tone PSPI

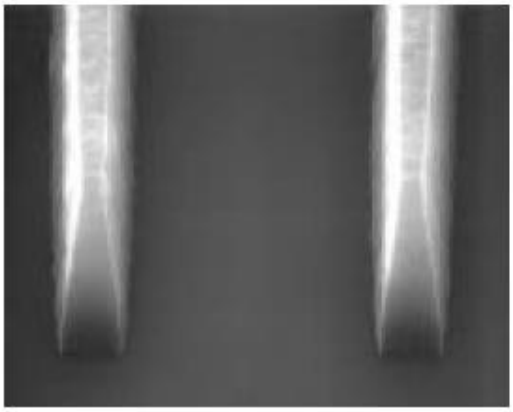

Figure 3.11: Commercial negative tone PSPI showing significant sidewall sloping (Copyright 1996 Society of Photo Optical Instrumentation Engineers)[111]

A different crosslinking approached based on benzophenone and thioxanthone based dianhydrides has also been reported.[113-114] In these systems the ketone carbonyl is excited to a triplet state upon UV exposure, according to classical photochemistry (Figure 3.12).[115] The excited triplet then can abstract a hydrogen atom from a nearby hydrogen donor, such as a benzylic hydrogen, to create two radical species. The photogenerated radicals can then react to form a new bond, crosslinking the material. While the chemistry of the reaction is well known, the efficiency is low and even further decreased in the solid state.

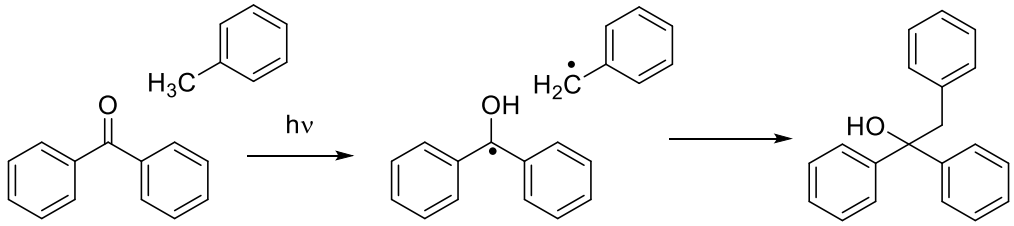

Figure 3.12: Photo-crosslinking mechanism in benzophenone

CHEMICALLY AMPLIFIED PSPI

Finally, both negative and positive tone chemically amplified PSPI have also been reported. The positive tone variations typically consist of a photoacid generator and either t-butoxycarbonyl or tetrahydropyranyl protected fluorinated poly(hydroxyimide).[116-117] These positive tone designs allow for high aspect ratio and high resolution printing. The use of flexible fluorinated monomers offers low dielectric constants and improved optical transparency but sacrifices much of the desirable aromatic PI properties in order to gain improved patterning capabilities.

Much of the chemically amplified negative tone work was developed by IBM in the 1990s, and the remainder of the chapter will be dedicated to their approach. While workers at IBM were coating PI precursors onto substrates containing a chromium coated copper under-layer and then baking to fully cure the PI, it was noticed that there were areas where the PI film came in contact with the copper due to defects in the chromium. At first IBM believed that copper must be hindering the curing of the PI films, but it was eventually discovered that trace amounts of methylamine in the NMP casting solvent were actually catalyzing the imidization reaction.[118] In areas exposed to copper, the methylamine complexes with the copper and does not act as a curing catalyst.

During the early 1990s, work at IBM also focused on solving other problems encountered with poly(amic acid) solutions.[119] As shown in Figure 3.13, the monomers are in equilibrium with the PAA. This creates viscosity changes that can be quite dramatic and problematic for processes such as dilution and heating.[120] The solutions are also unstable on storage.[121] Slowly the polymer will begin to lose water and imidize, causing an increase in viscosity and eventually becoming a gel. Even stored in a freezer, these materials only tend to last for months at the longest. The viscosity of PAA solutions is also very high and the solubility low relative to many other common polymers due to

the polyelectrolyte effect from the carboxylic acid groups on the polymer. Together these characteristics make viscosity dependent processes such as spin-coating difficult, especially for thick films (> ~1 μm) requiring high solids loading.

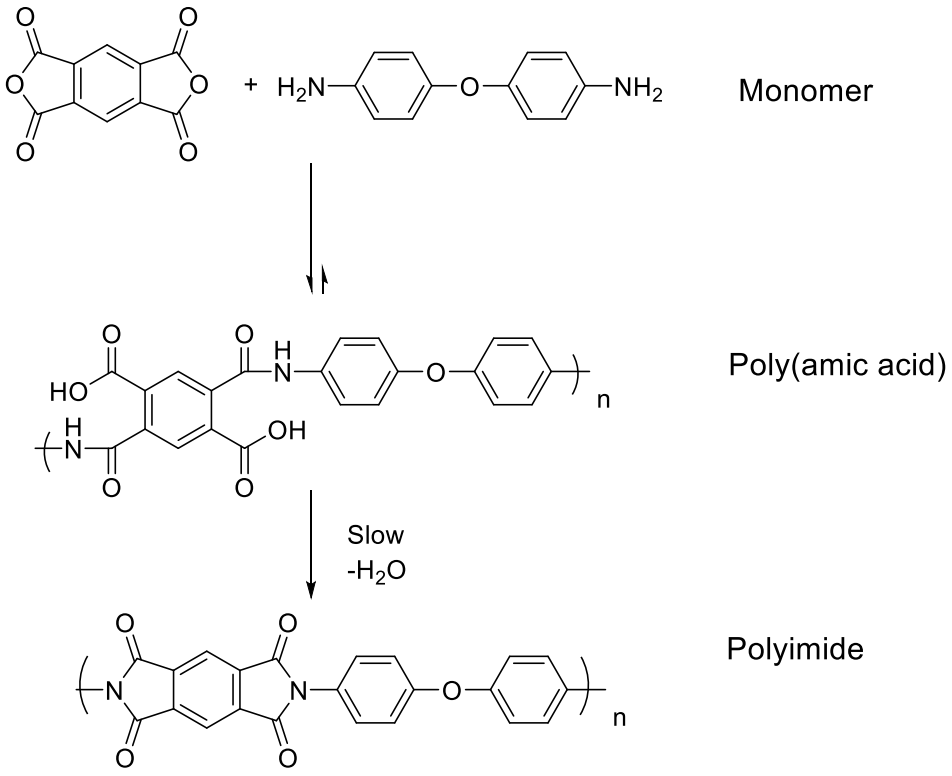

Figure 3.13: Poly(amic acids) are in equilibrium with monomer and slowly imidize upon storage to insoluble gels

These problems with PAA led IBM to investigate the use of poly(amic esters) (PAE) to replace PAA in their processes. While these materials can be prepared by methods such as a reaction of the deprotonated PAA with an alkyl halide or amide acetals, these methods tend to cause a large amount of imidization as well.[122] A better route involves the reaction of the dianhydride monomer with an alcohol follow by chlorination to form a diester diacid chloride.[119, 123] Reaction of the diacid chloride

monomer with an aromatic diamine in presence of pyridine gives the ester polymer (Figure 3.14). We found this method to work well even in the case of poorly nucleophilic diamines and no imidization was observed in the polymer by IR spectroscopy.

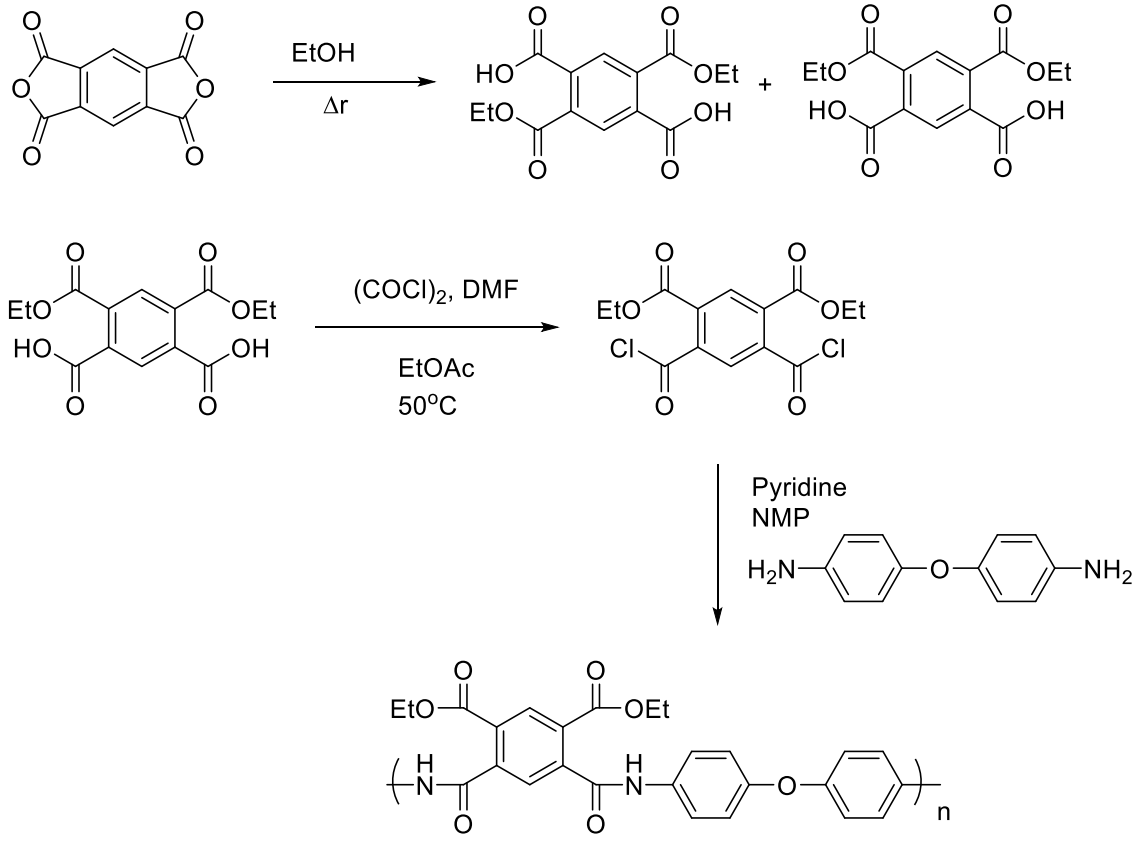

Figure 3.14: Synthesis of meta diethyl ester of PMDA-ODA polymer

Previous work at IBM showed that model compounds of polyimide precursors have imidization temperatures that depend greatly on the presence of base.[124] While poly(amic esters) require temperatures above 300°C for complete curing, the onset of curing is around 170°C. Addition of alkyl amine bases catalyze the curing and allow for imidization around 120-150°C. Further work showed that the imidization appears to follow general base catalysis, with the strong amidine base 1,8-diazabicyclo[5.4.0]undec-7-ene (DBU) being orders of magnitude faster than other tertiary amine bases such as

triethylamine. Nucleophilicity and hydrogen bonding of the amine appear to be less important.[125] It was also found that the ester polymers are stable to pyridine indefinitely, meaning that it is a sufficiently weak enough base to be used as a proton scavenger during polymerization. The proposed mechanism is shown below in Figure 3.15.

Figure 3.15: Proposed base catalyzed imidization mechanism[125]

As the imidization reaction is base catalyzed and the solubility of cured PI is negligible, IBM immediately identified this system as a chemically amplified photoresist. Adding photobase generator to a PAE resulted in a chemically amplified negative tone resist.[59-60, 126] These resists function by the generation of an amine base during UV exposure. Subsequent post exposure bake below ~170°C causes imidization to occur only in the exposed regions. The partially imidized regions are no longer soluble in organic solvents, allowing for unexposed regions to be developed away selectively. This system is preferable to the Rubner and Toray type systems for a variety of reasons. In the base catalyzed system the solubility switching and curing reactions are the same. This means that basically any polyimide precursor can be made patternable by the addition of photobase generator. The lack of methacrylate crosslinkers or dissolution inhibitors is also advantageous as these situations lead to higher cure shrinkage and/or degraded material properties if they are retained in cured films.

The main challenge of this system is due to the large absorbance of most PI films even out into the visible range. Early systems using PMDA-ODA required sensitizers and

even then were only able to print images about 5 μm thick.[60] While this was likely satisfactory for the interlayer materials of the time, and extremely thick by the standards of modern photoresists, films tens of microns thick are required for packaging applications. As most of the PBGs known function in the near to deep UV, most of the work has been on improving the transparency of the PI precursor in the near UV region.[127-131] Typically this done by using aliphatic or flexible monomers, often at the cost of reduced contrast due to the fully cured PIs now being soluble. While more transparent films have been made, there are still few reports of patterning thick films.[132]

PACKAGING REQUIREMENTS

The requirement for connecting multiple chips into the same circuit requires either a true vertical 3D architecture complete with through silicon vias (TSVs) or an alternate structure with multiple chips on top of a silicon interposer. In the case of the interposer, fine wiring running at the packaging level is necessary to connect the chips, and this requires the use of some lithographic patterning scheme.[133]

The requirements for the packaging dielectric are quite different than the interlayer material; reduction of the dielectric constant (ε_r) is not the primary objective. The major push in this project is toward photo-patternable thick films, on the order of tens of microns compared to less than 100 nanometers in modern photoresists for advanced lithography while retaining desirable material properties in the films. In the case of packaging dielectrics, a large amount of seemingly conflicting material properties are required.

The dissipation factor (DF) relates to how a dielectric material dissipates the energy of electrical fields into heat and this should be kept to a minimum. The coefficient

of thermal expansion (CTE) is a measure of how much a material expands due to changes in temperature and must also be minimized. Water absorption is also important due to the relatively large amount of polar groups in PI relative to other engineering plastics, and is often not negligible. Absorbed water raises both the dielectric constant and dissipation factor. Finally, the material needs to be photopatternable for implementation in new 3D architectures and preferably use light of a wavelength currently used in the microelectronics industry. The specifications for these properties are listed in Table 3.1, along with the properties of PMDA-ODA, BPDA-PPD, and PMDA-TFMB. These PI are also drawn in Figure 3.16.

Material Property	Target	PMDA-ODA	BPDA-PPD	PMDA-TFMB
ε_r	< 3.0	~ 3.5	3.1	2.6
DF	< 0.01	0.002	0.002	-
CTE	< 30 ppm/K	20-40	3-8	-3
Water absorption	< 1%	3.5	1.4	1.9
Film thickness	15 μm	~ 4-5	-	-
Resolution	5 μm	5	-	-
Precursor color		brown	brown	colorless

Table 3.1: Project targets and material properties of select polyimides[134-139]

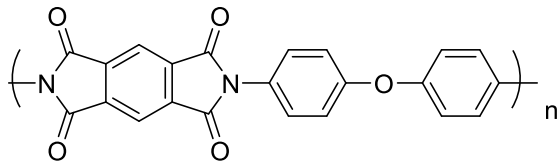

PMDA-ODA

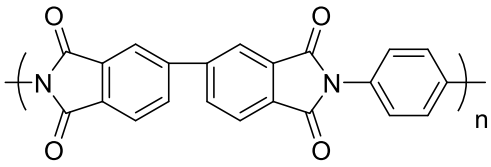

BPDA-PPD

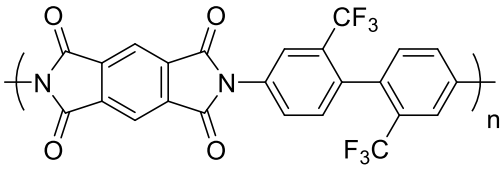

PMDA-TFMB

Figure 3.16: Structures of select polyimides

Understanding how structure affects the material properties in necessary for designing new PI that can meet the project targets. Many of the properties of PMDA-ODA (and by extension most other fully aromatic PI) can be traced back to the charge transfer complexes (CTCs) formed in the PI.[140-141] Aromatic imides also are also electron deficient and have been used in applications such as electron acceptors in photovoltaics.[142] When polymerized with electron rich diamines such as ODA, a polymer of alternating partial positive and partial negative charges is formed. This results in an intra-molecular charge transfer complex. Charge transfer is also inter-molecular especially in the case of pi stacking aromatic imides.[143] The most visible manifestation of the formation of the CTCs is the color of the aromatic polyimides. Rather than being colorless like most common plastics, PIs are typically dark yellow to brown. Here the absorption is due to the small bandgap between the occupied π orbital of the diamine and the unoccupied π* orbital of the imide ring.[140] The CTCs also result in much stronger

bonding between individual polymer chains relative to most other polymers. These strong intermolecular interactions result in a material having excellent mechanical properties[137] and being impervious to solvents.

DIELECTRIC CONSTANT

For a dielectric, the most characteristic property is the dielectric constant, ε_r. Also known as the relative permittivity, this property is the ratio of the permittivity of a material to that of vacuum permittivity, ε_o:

$$\varepsilon_r(\omega) = \frac{\varepsilon(\omega)}{\varepsilon_0} \tag{3.1}$$

where the dielectric constant is a function of frequency (ω). This property relates to how the polarization of a material is affected by an external electrical field. High dielectric constant materials more effectively shield the fields generated by nearby wires. In a circuit the time delay relates to how long electrical signals take to travel and is a measure of the speed of the circuit; for an RC circuit, the time delay is simply the product of resistance and capacitance. As two adjacent wires separated by dielectric material function as a capacitor, minimizing the dielectric constant is required to maintain circuit speed as the line spacing decreases. A quantitative relationship of the relative permittivity to characteristics of matter is given by the Debye equation:

$$\frac{\varepsilon_r - 1}{\varepsilon_r + 2} = \frac{N}{3\varepsilon_0}\left(\alpha_e + \alpha_d + \frac{\mu^2}{3k_bT}\right) \tag{3.2}$$

where N is the number of molecules per volume, α_e is the electronic polarizability, and α_d is the distortion polarizability.[144] The $\mu^2/3k_bT$ term represents the contribution due to permanent dipoles where μ is the orientation polarizability, k_b is the Boltzmann constant and T is the temperature. How these different components affect the overall dielectric constant are shown is Figure 3.17.

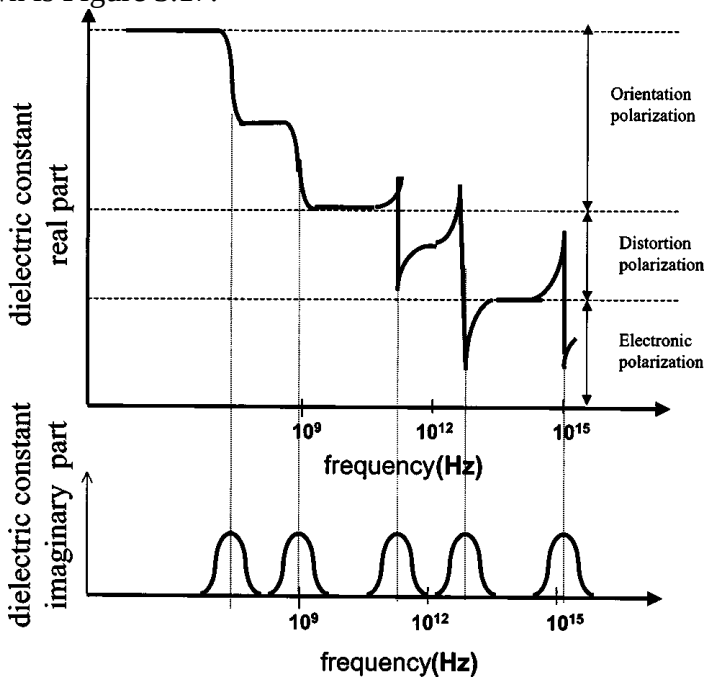

Figure 3.17: Frequency dependence of real and imaginary parts of the dielectric constant[144] (Copyright 2003, AIP Publishing)

As seen in Figure 3.17, the Debye equation shows that there are only certain frequency ranges over which each of the component polarizabilities is a critical factor. For example, for frequencies above ~10^{14} Hz (visible light) only electrons are light enough to be efficiently polarized and only the electronic polarization (α_e) term is important. At these frequencies the dielectric constant is simply related to the index of refraction (n) by Maxwell's identity:

$$\varepsilon_\infty = n^2 \qquad (3.3)$$

Today, most electronic devices operate in the GHz range, meaning that all terms in the Debye equation are important and all must be taken into account when choosing a dielectric material.

Reducing N, the number of molecules per volume, is a common method of reducing dielectric constant in interlayer materials.[40-41] Typically this is done by the use of porogens in inorganic materials or structural modifications such has bulky groups to interrupt packing. The poor packing increases free volume, lowering density and ε_r in polymers.[145-147] However, these approaches also tend to weaken the materials, which can be quite detrimental for the package's primary task of protecting the chip.

The polarizability and dipole strength factors are also important at the frequencies in modern devices and need to be minimized. A set of common bonds encountered in organic materials along with their polarizabilities and bond strengths are shown in Table 3.2. From the table it is clear that double and triple bonds are very polarizable, leading to increased dielectric constant. Therefore, while conjugation increases bond strength, in general π bonds need to be avoided in favor of less polarizable σ bonds. Also noteworthy is that C-F bonds, the strongest single bonds known, are quite polar though not very polarizable. This is a result of fluorine being the most electronegative element and causing most of the electrons density in the bond to be tightly bound to the fluorine. Symmetrical incorporation of C-F bonds can therefore give materials with low polarizability and without a net dipole, generating materials with very low dielectric constants. However, indiscriminate fluorination can actually increase the dielectric constant.[148]

Bond	Polarizability ($Å^3$)	Bond energy (Kcal/mol)	Bond Dipole (D)
C-C	0.531	83	0
C-F	0.555	116	1.4
C-O	0.584	84	0.7
C-H	0.652	99	0.3
O-H	0.706	102	1.5
C=O	1.02	176	2.3
C=C	1.643	146	0
C≡C	2.036	200	0
C≡N	2.239	213	3.5

Table 3.2: Polarizability, bond enthalpies, and dipoles of common organic bonds[41, 149-151]

Additionally, the dielectric constant has both real and imaginary parts:

$$\varepsilon_r(\omega) = \varepsilon_r'(\omega) - i\varepsilon_r''(\omega) \tag{3.4}$$

Where ε_r' is the real part and ε_r'' is the imaginary part. The real part describes how well a dielectric material shields electrical charges and the imaginary part describes how efficiently the material dissipates electrical fields into heat. Often dielectric loss is described as the loss tangent (tan δ), formed by the ratio of the real to imaginary parts. This ratio can also be referred to as the dissipation factor (DF).

$$\tan\delta = DF = \varepsilon_r''(\omega)/\ \varepsilon_r'(\omega) \tag{3.5}$$

Much of the dielectric loss is due to interaction of the oscillating field with ionic and polar species present and these groups should be avoided. The dissipation factor

should be as low as possible, with most commercial materials having values below 0.01.[138-139, 152-156]

The water absorption requirements are related to the effect of water on dielectric constant, in addition to potential electrochemical corrosion issues. Water has a dielectric constant of around 80 at room temperature and a dissipation factor of 0.157 at 3 GHz.[157-158] This means that even modest water absorption in a film can result in large and detrimental effects on the dielectric properties.

From a dielectric constant point of view, fluoropolymers such as Teflon or Viton are among the best nonporous materials known, with dielectric constants around 2.0.[41, 159] Fluorinated materials also tend to have low water absorption.[40] However, solubility, processibility, and thermal stability issues along with a coefficient of thermal expansion around 130 ppm/K completely rule out pure fluorocarbon polymers as useful dielectric materials.[41]

COEFFICIENT OF THERMAL EXPANSION

The use of polymeric materials as dielectrics is mainly hindered by their coefficient of thermal expansion (CTE). While organic polymers tend to have lower dielectric constants and less complex deposition requirements than nonporous inorganic materials, polymers also have among the largest CTEs of any solid materials, typically on the order of 100 ppm/K.[160] This poses a significant problem in device integration, particularly during the solder reflow step when the CTE mismatch introduces strain on the thousands of electrical connections that are made to the substrate. Figure 3.18 is a cartoon that shows the (exaggerated) effect of the low CTEs of the silicon chip (3 ppm/K), the packaging substrate (~14 ppm/K), and the copper metallization (17 ppm/K)

with a high CTE dielectric (blue) during the solder reflow step. As the figure shows, the effect is seen after the package cools to ambient conditions. The stress generated in a film on a substrate due to CTE mismatch can be described as:

$$\sigma = E_f \Delta T (\alpha_f - \alpha_s) \tag{3.6}$$

where E_f is the Young's modulus of the film, ΔT is the change in temperature, α_f is the CTE of the film, and α_s is the CTE of the substrate.[161] This means that the greater the CTE mismatch, the larger the stresses formed upon cooling, and the more likely the device will fail. Recently, the transition to lead free solders has exacerbated this problem, as reflow temperatures around 250°C are required for the new solders instead of about 200°C for SnPb solders.[162] If CTE mismatch is large enough, warpage, via delamination, solder joint failure, and even cracking of the die can occur.

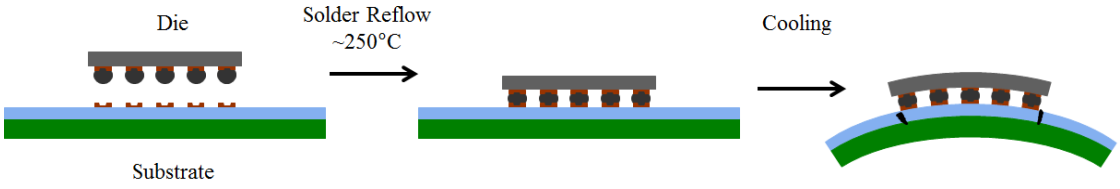

Figure 3.18: Cartoon of effect of CTE mismatch during solder reflow step

Preventing these failure modes requires a close matching of CTE between all the materials used. The silicon die, copper metallization, and FR4 (glass-reinforced epoxy resin) substrate all have low CTEs and great effort has been made to optimize these materials. Therefore the build-up dielectric must have a similar, low dielectric constant and a CTE less than ~30 ppm/K for implementation.[139]

DIELECTRIC PATTERNING REQUIREMENTS

Lithography requirements at the packaging level are much different than in interlayer dielectrics. In the build-up layer of the package, the copper vias are typically not smaller than 5-10 μm, but each layer thickness is 10-20 μm.[111, 139, 163] For this project, the requirement is 5 μm dense line/space patterns in a 15 μm thick film (aspect ratio = 3.0). Finally, the patterning should be compatible with the installed base of standard exposure tools used in industry, meaning that the patterning wavelength should be no longer than 365 nm (mercury i-line). While the pitch requirements are orders of magnitude larger than those of the smallest interconnects, the aspect ratio is challenging. The extremely thick films present depth of focus and optical density challenges.

The initial work on this project focused on repeating the patterning of the poly(amic ethyl ester) of PMDA-ODA initially reported by IBM.[59] The initial work was performed at UT by William Bell on the para diethyl ester of PMDA-ODA (pPMDA-ODA-EE) using an ortho-nitro carbamate photobase generator (Figure 3.19).[68] The system contained a 15 wt% loading of a PBG that only works in the deep UV. The material worked in a proof of concept experiment to print 5 μm L/S patterns, but the optical density of the resin is so high that thicker films are opaque. Even 5 μm thick films require very high imaging doses.

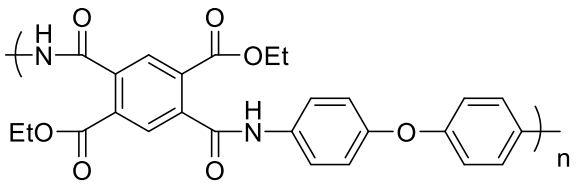

pPMDA-ODA-EE

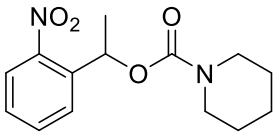

ONB PBG

Figure 3.19: Initial proof of concept PSPI system

PATTERNING WITH NVOC PHOTOBASE GENERATOR

In order to print films at the required thicknesses, the resin must be much less optically absorbent than PMDA-ODA. As shown in the PI comparison table (Table 3.1), solutions of PMDA-TFMB are colorless and the fully cured material has properties close to the specifications. As discussed earlier, PIs often charge transfer complexes between the electron poor dianhydride and the electron rich diamine that increase the optical density in the UV.[140] However, the structure of PMDA-TFMB and its precursors are such that formation of CTCs is inhibited by both steric and electronic effects. Compared with ODA, TFMB has extremely electron withdrawing trifluoromethyl groups instead of an electron donating oxygen linkage. The decrease in electron density weakens the charge transfer effect. The structure of the TFMB monomer also appears to hinder complex formation. The trifluoromethyl groups on each ring cause TFMB to take on a twisted configuration that cannot effectively complex with PMDA. A comparison of the UV absorbance of PMDA-ODA and PMDA-TFMB ethyl ester PAEs (PMDA-ODA-EE and PMDA-TFMB-EE, respectively) is shown in Figure 3.20. At the proposed patterning wavelength of 365 nm, PMDA-ODA-EE has an absorbance of about 0.3 μm^{-1}, effectively limiting patterning to a few microns at the very most.[59] In comparison, PMDA-TFMB-EE has an absorbance of about 0.05 μm^{-1}, which should allow for printing of much thicker films.

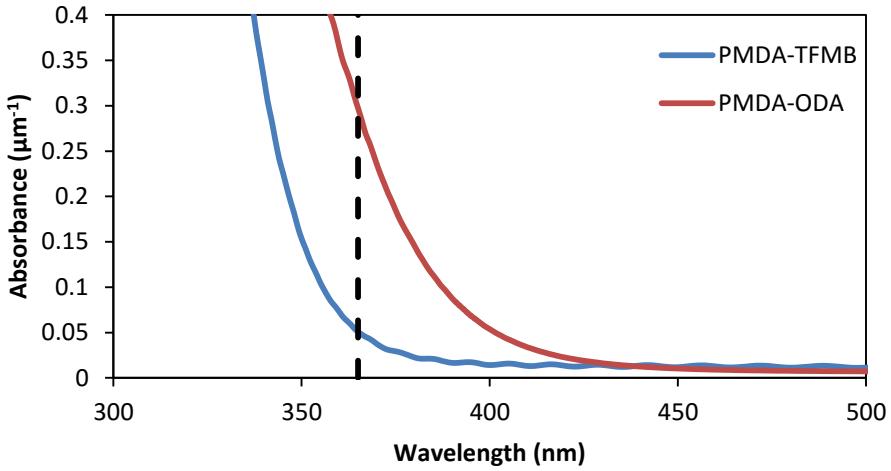

Figure 3.20: UV-Vis spectra of poly(amic ethyl esters) of PMDA-ODA and PMDA-TFMB. The proposed exposure wavelength (365 nm) is shown in black.

Unfortunately, when printing pPMDA-TFMB-EE with the i-line active photobase NVOC piperidine (Figure 3.21), patterning was satisfactory, but the films produced were rough and grainy.[68] This effect was even more pronounced when attempting to spin coat multiple micron thick films onto silicon wafers. After coating, the films were white, opaque, and rough. Likely, this is due to lyotropic behavior due to the rigid para linkages and the inflexible TFMB monomer.[164-165]

However, PAEs can be produced as the pure meta isomer or a mixture of isomers as well (recall Figure 3.14). The precursor PMDA diethyl dicarboxylic acids can be fractionally crystallized from ethyl acetate to obtain nearly pure isomers after one recrystallization. Unlike in the case of PAA were the material is an equilibrium mixture of isomers, the PAEs retain the isomeric purity of the starting diacid chloride. The para isomer tends to form much more rigid polymers than the meta isomer and this results in much higher viscosities (~2-3x) at the same degree of polymerization and concentration, even for flexible diamines such as ODA (pPMDA-ODA-EE, Figure 3.21).[119] The

solubility of polymers produced exclusively from the para isomer with rigid diamines also tend to be quite poor.[166] The meta isomer generates much less viscous and more soluble polymers in the case of rigid diamines and as the final cured polyimide is the same[167], using the meta isomer offers a convenient method to improve the processibility of thick films and avoid the liquid crystalline behavior.

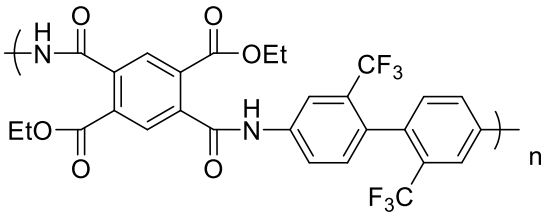

pPMDA-TFMB-EE

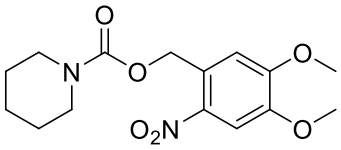

NVOC piperidine

Figure 3.21: pPMDA-TFMB-EE and NVOC piperidine photobase

The PMDA-TFMB meta diethyl ester (mPMDA-TFMB-EE) has vastly improved solubility in the casting solvent compared to the para isomer. Whereas the para isomer could be formulated in concentrations up to about 15 wt%, the meta isomer was soluble up to about 35 wt%. Spincoating this material produced smooth films that did not scatter light like the para isomer. Additionally, the improved solubility allowed for generation of much thicker films (up to about 20 μm uncured) to be cast.

We were able to print 2.5 μm line/space patterns in relatively thin 1.5μm films at 1500 mJ/cm^2 i-line for 5% NVOC piperidine loadings and developing with mixtures of NMP in methanol. The sidewall profiles are also quite vertical, in comparison to the sloped walls produced by commercial acrylate-based PSPI. (Figure 3.22)

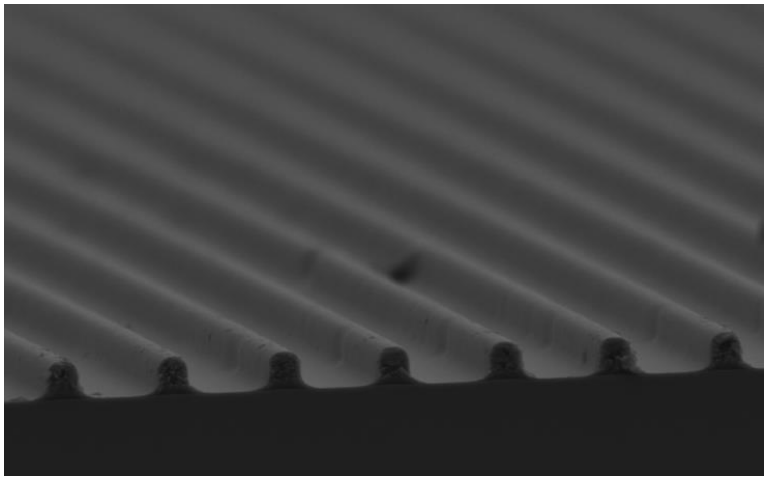

Figure 3.22: Fully cured 2.5 μm L/S pattern in 1.5 μm thick mPMDA-TFMB-EE printed with NVOC piperidine PBG.

QUANTIFYING RESIST PERFORMANCE AND CALCULATING IMIDIZATION BY IR SPECTROSCOPY

PSPIs function as photoresists, so their performance can be analyzed using methods developed for traditional photoresists. Contrast curves for the 5% NVOC piperidine/ mPMDA-TFMB-EE system were prepared using films 1-2 μm thick, and are shown in Figure 3.23. The three most important parameters from a resist contrast curve are D_0, the maximum dose that still causes the film to clear; D_{100}, the minimum dose required to retain the entire film; and the contrast, defined as:

$$\gamma = \left(\log_{10} \frac{D_{100}}{D_0}\right)^{-1} \tag{3.7}$$

At low exposure doses (< 200 mJ/cm^2) the films were completely developed away, while doses larger than 900 mJ/cm^2 were sufficient for patterning. Intermediate values, however, experience considerable swelling during development, causing

significant roughness and producing films that are thicker than the initial film thicknesses. Baking at 150°C gave a contrast of about 2.0, while the contrast at 170°C was about 1.4. Also unusual compared to standard crosslinking type negative tone resists is the noticeable loss in film thickness after development. As the resist material goes from the amic ester form to the polyimide, ethanol is generated and diffuses out of the film, resulting in cure shrinkage. However, this process generates far less shrinkage than in the Rubner type systems.

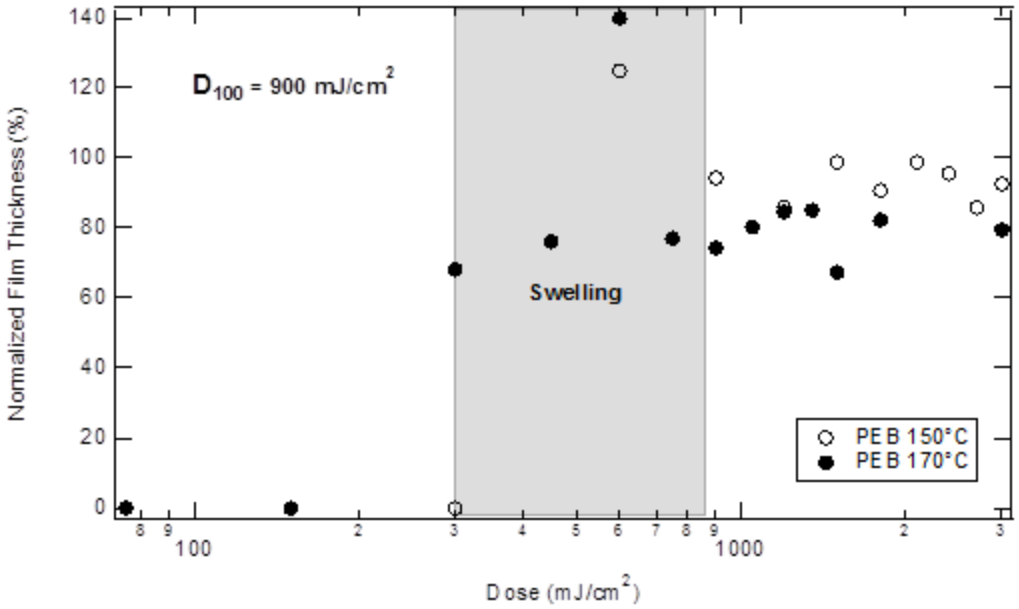

Figure 3.23: Contrast curves for 5% NVOC piperidine/mPMDA-TFMB-EE for post exposure bake temperatures of 150°C and 170°C for 10 minutes

The imidization reaction reaches higher conversion with increasing temperature due to both reaction kinetics and base diffusion. Thus, thinner films remain after the 170°C post exposure bake compared to the 150°C bake. However, even after a 10 minute bake at 170°C, the imidization is incomplete and further shrinkage occurs during a final cure step. Contrast likely could be improved by post exposure baking at a higher

temperature to further enhance the base catalyzed reaction and diffusion, so the amount of imidization was quantified by infrared spectroscopy. As shown in Figure 3.24, there are three characteristic peaks in the IR that can be used to track the degree of imidization. The small band that appears at 1783 cm^{-1} is due to the asymmetric carbonyl stretch of the newly formed cyclic imide. Also prominent is the stretch at about 1360 cm^{-1}, which corresponds to the C-N stretch between the imide nitrogen and the aromatic carbon. During the imidization process the peak at 1491 cm^{-1} which corresponds to the C-C aromatic stretches does not change. While the C-N stretch is often used in the quantification of the other polyimides as it is the largest peak in the spectrum,[131] the trifluoromethyl groups from TFMB overlap with this peak, making quantification difficult and requiring use of the carbonyl stretch instead. As there is no initial peak for the imide carbonyl, the degree of imidization can be calculated as:

$$\text{Imidization} = (A_{1783}/ A_{1491})_{\text{sample}} / (A_{1783}/ A_{1491})_{\text{cure}} \quad (3.8)$$

Where imidization is the fractional conversion of the ester groups to imides, A_{1783} is the area of the C-O stretch of asymmetric stretch of the imide carbonyl and A_{1491} is the C-C aromatic stretch used as an internal standard. Subscript “sample” after the ratio refers to the polymer baked at each temperature for 10 minutes. “Cure” refers to the samples after complete curing.

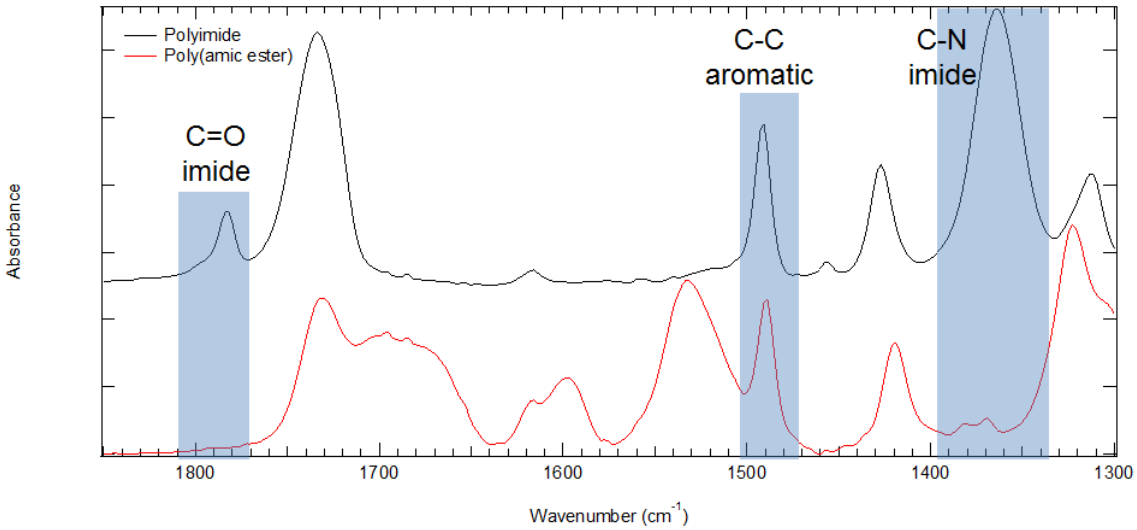

Figure 3.24: Infrared Spectra of mPMDA-TFMB-EE (red) and resulting PI (black) after curing. Relevant peaks are highlighted.

The degree of imidization in the 5% NVOC/ mPMDA-TFMB-EE resist was calculated by flood exposing films to 2 J/cm^2 i-line radiation and post exposure baking (PEB) at various temperatures for 10 minutes. The results show that significant background imidization occurs in samples heated to 170°C (Figure 3.25). This is the point where thermal decomposition of NVOC piperidine becomes important, and is the likely reason why the contrast of the resist is higher at 150°C than 170°C despite the fact that base catalysis is more effective at higher temperatures. Also noteworthy from this experiment is the relatively low amount of imidization in the film; only 10% of the ester groups are converted to imides. This is in stark contrast to the more flexible base catalyzed PSPI developed by IBM that achieved imidization as high as 80%.[59-60] However, this required a PBG loading of 20%. It is remarkable that the mPMDA-TFMB-EE films print with such a small amount of imidization.

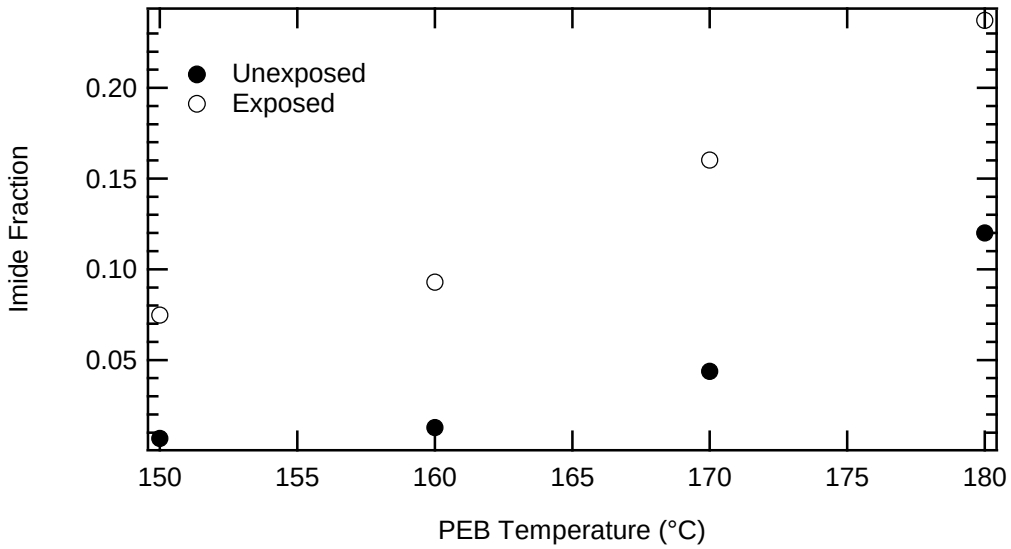

Figure 3.25: Effect of PEB temperature on imidization in 5% NVOC/mPMDA-TFMB-EE PSPI. Exposure dose: 2J/cm^2 i-line. PEB time: 10 min.

When attempting to print much thicker images, significant optical density problems began to appear. The absorbance of the NVOC piperidine photobase is quite large, and it does not photobleach at i-line.[68] To quantify and model resist performance a series of parameters called the Dill parameters (alternatively called the ABC parameters) are used.[168] These consist of the constants A, B, and C given by:

$$A = \frac{1}{D}\ln\left(\frac{T(\infty)}{T(0)}\right) \tag{3.9}$$

$$B = -\frac{1}{D}\ln\left(\frac{T(\infty)}{T_{12}}\right) \tag{3.10}$$

$$C = \frac{A+B}{A}\left(\frac{1}{1-T(0)}\right)\left(\frac{1}{T(0)}\right)\left(\frac{1}{T_{12}}\right)\left.\frac{dT}{dE}\right|_{E=0} \tag{3.11}$$

where D is the film thickness, T(x) is the transmittance of the film at dose x, T_{12} is the transmittance of the air-resist interface, and dT/dE at E=0 is the initial change in transmittance of the film per exposure dose.[169] The A and B values of the resist are the bleachable and non-bleachable absorption coefficients, respectively. The C value is the first order exposure constant describing how quickly the film reaches its final absorbance.

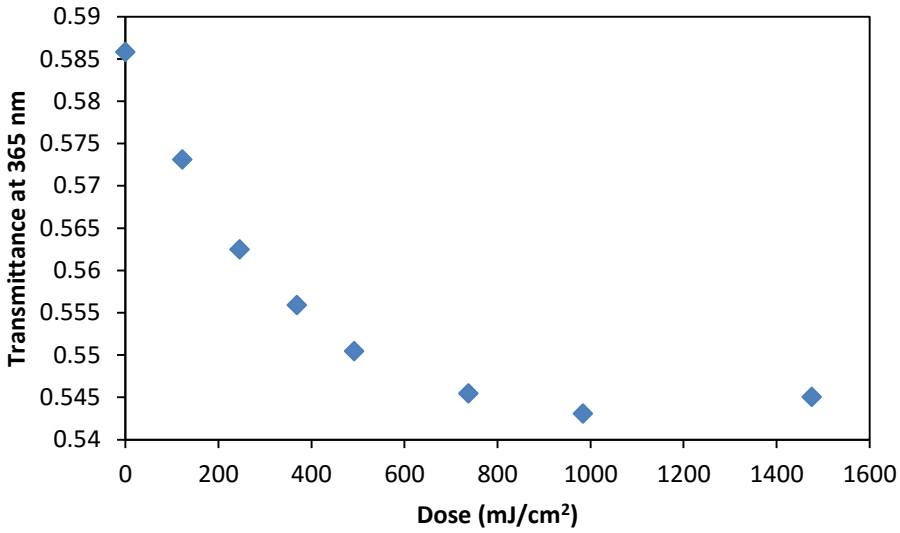

Figure 3.26: Transmittance as a function of exposure dose for 1.7 µm thick film of 5% NVOC piperidine in mPMDA-TFMB-EE

Figure 3.26 shows the transmittance at i-line as a function of exposure dose (i-line) for a 5% NVOC piperidine PBG in mPMDA-TFMB-EE film 1.74 µm thick. The Dill parameters for this resist and values for typical i-line resists are included in Table 3.3. As can be seen from the table, the Dill parameters for the NVOC piperidine/mPMDA-TFMB-EE system are vastly different from a typical i-line photoresist. The A value is negative, indicating that the resist actually becomes more absorbent at the exposure wavelength during exposure. This is particularly problematic

for patterning very thick films, especially combined with the relatively large B value. The B value is the portion of the film absorbance that does not change with exposure and is 0.3 μm^{-1}, meaning that patterning multiple micron thick films will fail due to the high optical density. The C value is also lower than a typical resist, indicating that the resist is not very photosensitive. This is likely due to the poor quantum efficiency of the NVOC photobase.[170-171]

Dill Parameter	NVOC PSPI	Typical i-line resist	Units
A	-0.042	0.9	μm^{-1}
B	0.30	0.05	μm^{-1}
C	0.0025	0.018	cm^2/mJ

Table 3.3: Dill parameters for a typical i-line resist[169] and NVOC/mPMDA-TFMB-EE resist

With the Dill parameters known, it is relatively straightforward to model the exposure of the resist in PROLITH software.[172] A simulation of the image in resist for a 5 μm line/space pattern in 1.5 and 15 μm thick films exposed with 365 nm light was performed, as shown in Figure 3.27. While the 1.5 μm film appears to print reasonably well with some slight undercutting, it is quite evident that the thicker film suffers from high optical density. This modeling predicts that very large doses would be required to print films thicker than about 5 μm, forcing a move toward less absorbent and more efficient PBGs for these PSPI.

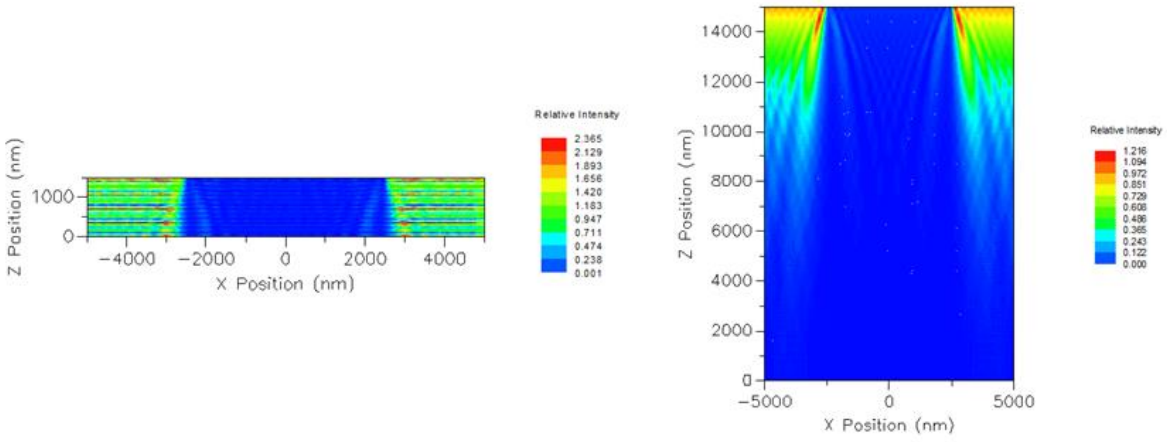

Figure 3.27: PROLITH image in resist simulations of NVOC/mPMDA-TFMB-EE resist exposure at i-line for 1.5 micron film (left) and 15 micron film (right)

Another major concern about the NVOC piperidine was the volatility of the piperidine base that is generated. Piperidine has a boiling point of 106°C, and as all post exposure baking has been performed at temperatures much above this, there was a concern that base may be evaporating out of the film and affecting the top surface of the film. Figure 3.28 shows SEM images of 15 μm and 20 μm full pitch L/S pattern in 12 μm thick 5% NVOC piperidine/mPMDA-TFMB. The material was printed on a mask aligner in hard contact mode using 2.1 J/cm^2 i-line radiation and baked for 10 minutes at 160°C before being developed with 30% NMP/methanol. A fibrous material at the top surface of the film became increasingly noticeable at smaller pitches. We attributed this material to piperidine coming out of the exposed areas of the film and imidizing the surface of the film.

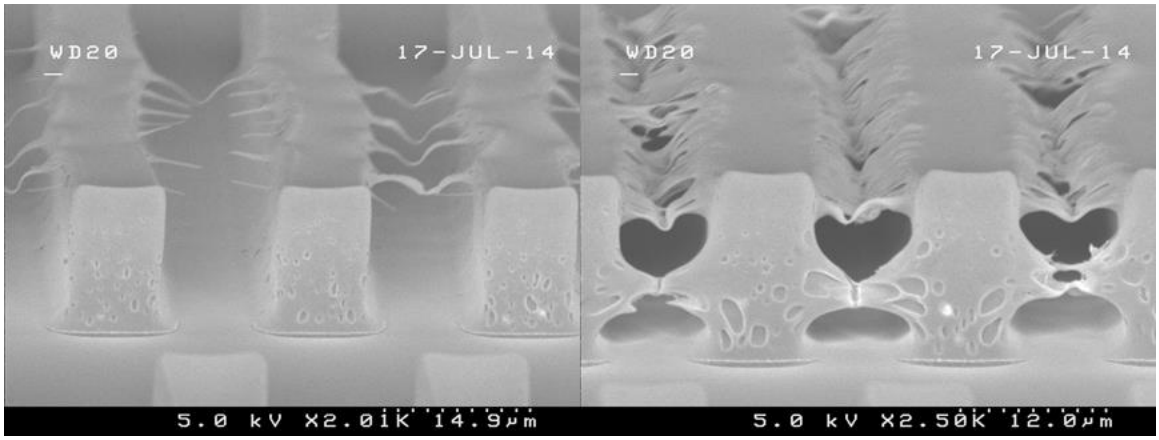

Figure 3.28: Surface defects in NVOC piperidine/mPMDA-TFMB-EE attributed to base volatility for 20 µm (left) and 15 µm (right) full pitch L/S patterns

CINNAMIDE PHOTOBASE GENERATORS

The low quantum efficiency, high optical density, and increase in optical density of NVOC upon exposure lead to the search for a new photobase generator. One of the more promising candidates was a series of cinnamide based PBGs that were originally developed as amine protecting groups for organic chemistry that could be cleaved with i-line exposure.[173] Work at Dai Nippon Printing showed that these materials could also print PAA, though loadings of 15 wt% PBG were required.[130, 132] Additionally, the films printed were much thinner and at larger pitch than what was required for this project.

Early studies of cinnamic acids showed that the cis form undergoes ring closure to the lactone and later kinetic data showed that the process follows general acid catalysis.[174] Figure 3.29 shows the mechanism for conversion of a trans cinnamide to the lactone and amine. The issue with this process and the reason it was not considered as the initial PBG candidate for this project is the requirement for acid; using a PBG that requires acid to work appears counterintuitive. In the case of the PAA work at Dai

Nippon Printing, this was not a problem as the matrix resin already contained large amounts of carboxylic acid and work by Ueda showed that NVOC PBGs can pattern PAAs.[127] It was also reported that unsubstituted cinnamide PBGs are not very efficient compared to 4-alkoxy derivatives[132], so initial testing was performed with (E)-3-(2-hydroxy-4-methoxyphenyl)-1-(piperidin-1-yl)prop-2-en-1-one (**3.3a**, Figure 3.30).

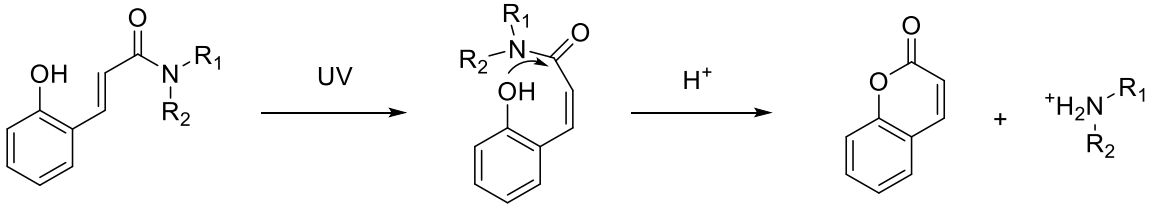

Figure 3.29: Mechanism for the ring closing lactonization of cinnamides

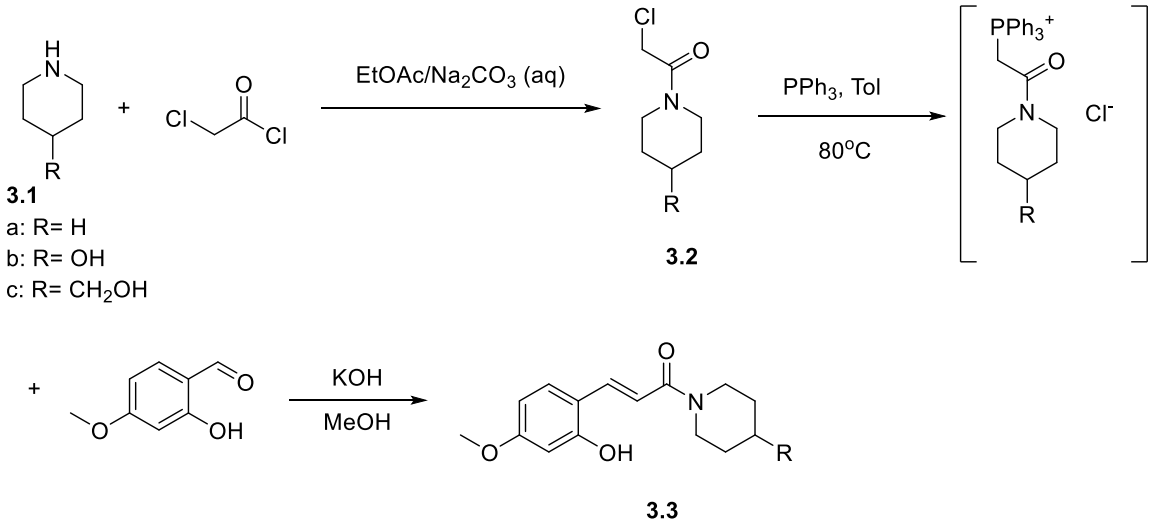

Figure 3.30: Synthesis of cinnamide type photobase generators

The initial testing of the cinnamide piperidine PBG was to determine if it could function in the solid state without any acid in the film. Films containing a 5% loading of

PBG to polymer were cast on silicon and exposed to 365 nm light in the same manner as the NVOC testing. However, no visible changes occurred in the films and the resist would not develop using the NMP/methanol developer. To test the requirement of acid to produce images, dilute solutions of the PBG in THF containing no acid and containing 1% acetic acid were exposed broadband UV light in quartz cuvettes and changes monitored by UV-Vis spectroscopy (Figure 3.31). The concentrations used were 97 μM and 96 μM, respectively. While the reaction in either case requires roughly the same exposure dose to reach completion, the UV spectrum is very different in the case where acid is present. In both cases exposure initially causes an isomerization from the trans to cis form. However, the ring closing lactonization appears to be slow or non-existent in the absence of acid and is not observed on the time scale of the experiment (~10 minutes). It is interesting that the lactone formed has a similar extinction coefficient to that of the starting material, in comparison to the cis isomer formed in the pure THF exposure. The newly formed lactone ring has some aromatic character and appears to retain much of the conjugation of the initial trans cinnamide. This is in contrast to the cis cinnamide, which is sterically hindered and not in conjugation, resulting in a dramatic reduction in extinction coefficient.

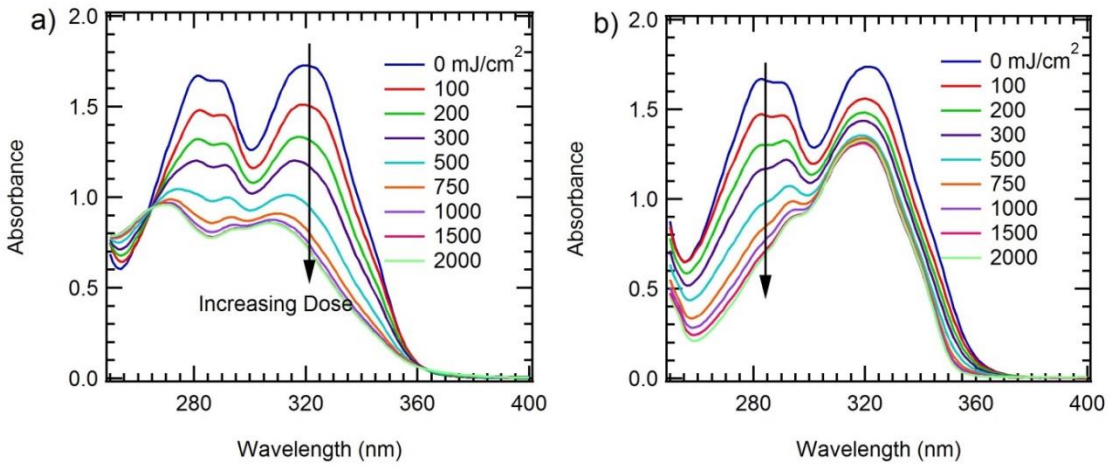

Figure 3.31: UV-Vis spectra of **3.3a** exposed to UV light. a) in THF b) in 1% acetic acid/THF

This new class of cinnamide PBG also allowed for easier implementation of less volatile piperidine derivatives than in NVOC PBGs. As shown in Figure 3.30, these PBGs were synthesized in multi-step process involving reaction of the base with chloroacetyl chloride to form an amide, refluxing the alkyl chloride with triphenylphosphine and then reacting with 2-hydroxy-4-methoxy benzaldehyde in a Wittig reaction. 4-Hydroxypiperidine and 4-piperidnylmethanol were particularly attractive bases as they both have boiling points above 200°C while having similar basicity and the low steric hindrance of piperidine. These materials have been reported in patents that describe a synthesis route that involves EDC coupling of a cinnamic acid with the desired amine,[175] the same method as the unsubstituted piperidine cinnamide PBGs.[130, 132] This method gives relatively poor, 30% yields for unsubstituted piperidine, and inclusion of hydroxyl substituents that greatly decrease volatility gave yields of 5-10%.[175]

The substituted piperidine cinnamide PBGs were tested for catalysis of imidization in films of mPMDA-TFMB-EE by IR spectroscopy. These films were cast

from 10% acetic acid in NMP and post apply baked (PAB) at 100°C for 10 minutes prior to exposure to 2 J/cm^2 i-line radiation. As shown in Figure 3.32, both **3.3b** and **3.3c** imidized PMDA-TFMB ester films better than unsubstituted **3.3a** at a constant 5wt% loading. We attribute this to the decreased volatility of generated base. The unexposed films performed essentially the same regardless of the cinnamide PBG used; there was very little imidization below 140°C, but imidization increased to over 10% at 160°C. The lower PEB temperatures for the cinnamide PBGs compared to NVOC are also noteworthy. Above about 140°C, trans cinnamides can isomerize and convert to the lactone, producing amine. Interestingly, the 4-hydroxypiperidine gave higher contrast than either the unsubstituted piperidine or the 4-piperidinyl methanol PBGs. This cannot be attributed to the very minor differences in molar concentration at constant 5wt% loading nor volatility as both bases are far below their boiling points. The smaller molecular size of hydroxypiperidine compared to piperidinyl methanol may explain the more efficient curing for **3.3b**. The curing process requires diffusion of the generated amine catalyst and this process is quickly inhibited as the polymer imidizes and the glass transition temperature (Tg) increases. The diffusion of molecules in polymers scales strongly with the size of the diffusing molecule, especially in the case of glassy polymers (T < Tg) where the free volume is much lower.

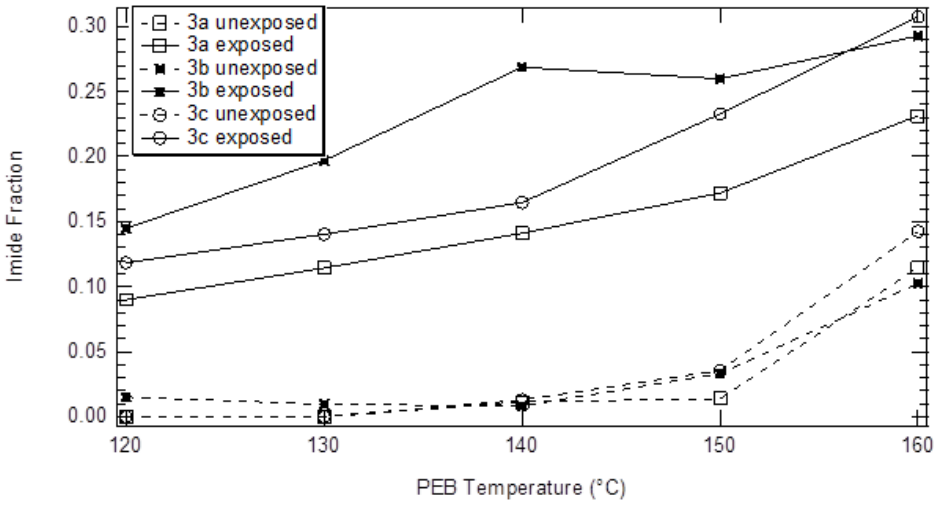

Figure 3.32: Comparison of various cinnamide PBGs effect on curing of mPMDA-TFMB-EE at 5% loading. Exposure dose was 2J/cm^2 i-line and PEB for 10 minutes.

The catalyst loading of **3.3b** was varied as shown in Figure 3.33. Only a minor difference is seen between the 5 and 10 wt% loadings but the 15 wt% loading performed significantly better. However, this amount of PBG causes noticeably more background imidization compared to both 5 and 10% loadings. It is also important to note the relatively small amount of imidization occurring in this system compared to other base-catalyzed ester systems.[60] The difference in imidization in the exposed and unexposed regions for this system is only about 15-20%. The lack of imidization compared with other PSPIs is likely due to the backbone rigidity of PMDA-TFMB compared to the more flexible polymers having decreased UV absorbance but larger CTE.

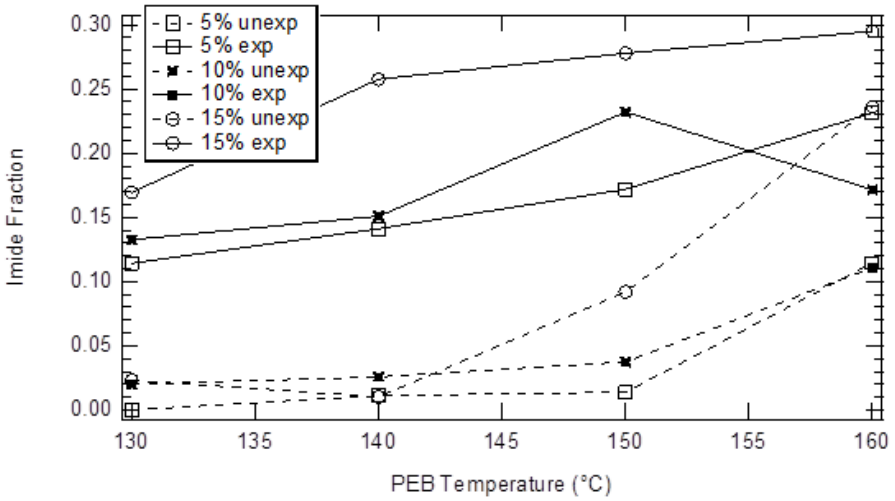

Figure 3.33: Comparison of curing for different loadings of **3.3b** in mPMDA-TFMB-EE. Exposure dose was 2J/cm^2 i-line and PEB time was 10 minutes.

As the piperidine cinnamide PBG has a very low absorbance at i-line (260 M^{-1} cm^{-1})[132] and photobleaches unlike the NVOC PBG, resist performance was predicted to be much improved. To quantify the performance, the Dill parameters of a 7.0 μm thick film of 5% piperidine cinnamide PBG in mPMDA-TFMB-EE were determined. A film was cast from 10% acetic acid in NMP onto a quartz disc and the transmittance measured as a function of i-line exposure dose (Figure 3.34). The striking difference between the curve in Figure 3.34 versus that of NVOC (recall Figure 3.26) is that transmittance at i-line increases upon exposure. The calculated Dill parameters are shown in Table 3.4 and compared with those calculated for the NVOC system. The photobleaching in the cinnamide system shows up as the positive A value. The B and C values are also closer to those of a standard i-line resist. While the non-bleachable absorbance is still large compared to an i-line resist, it is only about half that of the NVOC resist. The C value is about half the value of a typical i-line resist, meaning that the cinnamide resist requires a larger dose than commercial i-line resists, but it is still about three times larger than the

NVOC system. Taken together, these values mean that the cinnamide PBG should perform considerably better than the NVOC PBG, especially in thick film patterning.

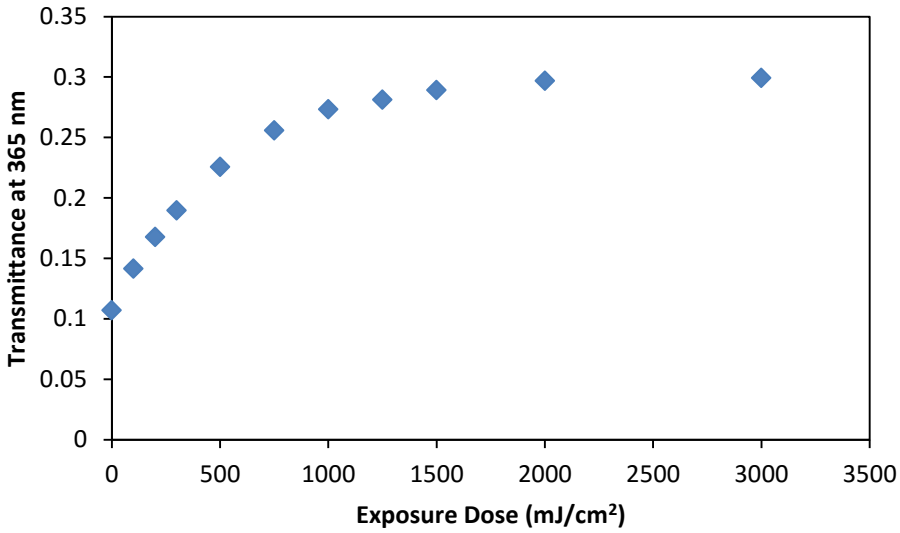

Figure 3.34: Transmittance as a function of i-line exposure dose for 7 µm thick films of 5% cinnamide PBG **3.3a** in mPMDA-TFMB-EE

Dill Parameter	NVOC PSPI	Cinnamide PSPI	Units
A	-0.042	0.15	μm^{-1}
B	0.30	0.16	μm^{-1}
C	0.0025	0.0082	cm^2/mJ

Table 3.4: Comparison of Dill parameters of NVOC and cinnamide PBG/PSPI systems

Thick films of cinnamide PBG in mPMDA-TFMB-EE were prepared similarly to those used in attempts at thick film patterning with NVOC piperidine (Figure 3.35).[68] Coatings were made from formulations containing 5wt% cinnamide PBG to mPMDA-TFMB-EE dissolved in 10:90 acetic acid:NMP. Thick films (20 µm) were then spin-coated onto wafers treated with anti-reflective coating. The material was then baked for

10 minutes at 100°C to remove most of the solvent before being exposed to 1200 mJ/cm^2 i-line light in hard contact mode on a mask aligner. The exposed film was then baked for 10 minutes at 130°C and developed in 1:3 NMP: methanol for 6 minutes. The film was then rinsed with methanol and fully cured in a vacuum oven at 350°C before being imaged. The final film thickness after curing was about 14 µm, representing a 30% cure shrinkage.

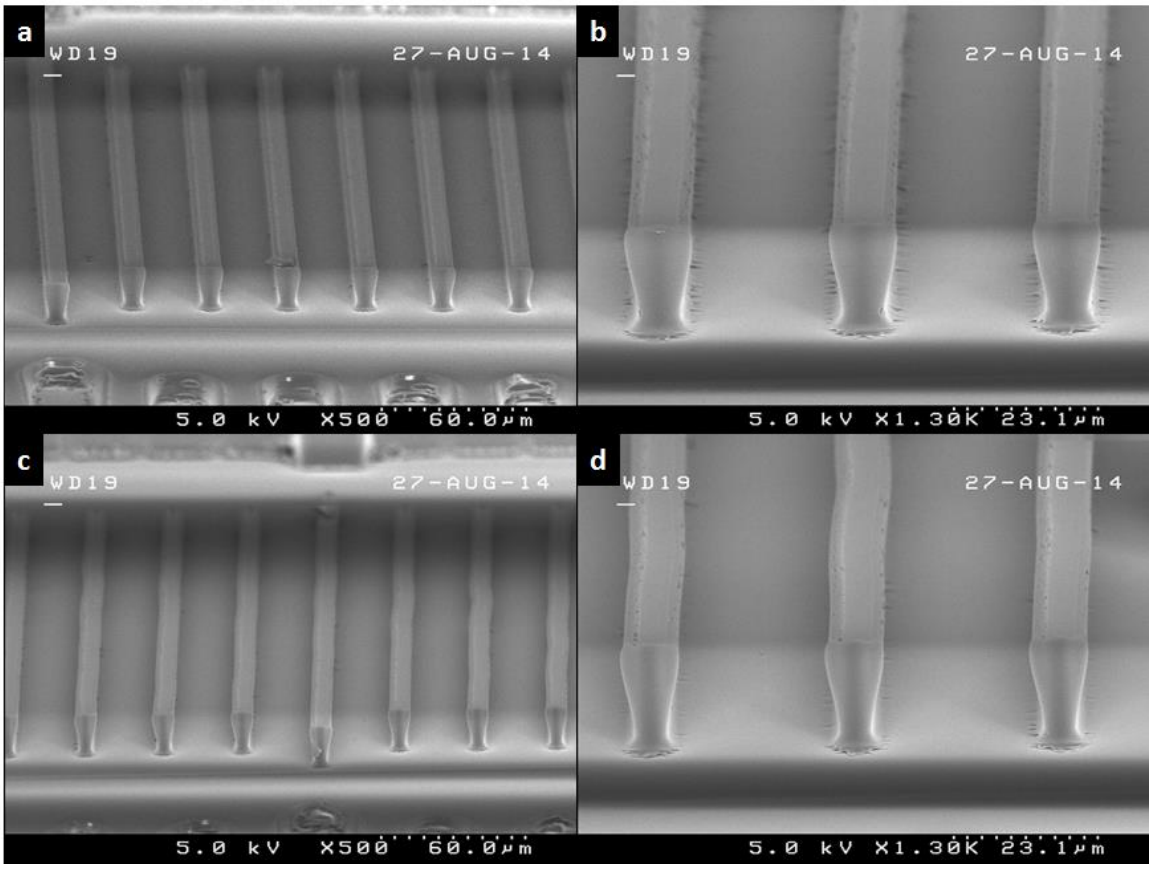

Figure 3.35: SEM micrographs of cured PMDA-TFMB printed using 5% cinnamide **3.3a**. Fully cured thickness is 14 µm. a) and b) 8 µm lines; c) and d) 6 µm lines

The images in Figure 3.35b and 3.35d clearly show a tapered profile with the lines thinning at the bottom of the film. Note that this is the opposite slope of that produced by

the Rubner resist design. This is quite typical of negative tone resists where the absorbance of the resist is large at the exposure wavelength. This behavior was also observed in the NVOC printing,[68] though the use of cinnamide PBG greatly improved image quality. Thick films of NVOC piperidine begin to delaminate from the surface at similar pitches, likely due to the more exaggerated tapered profile. The key advantage to this chemically amplified PSPI is clearly visible in the reduced cure shrinkage and ability to print high aspect ratio features that have mostly vertical sidewall profiles. However, at these thicknesses even the relatively low absorption from the mPMDA-TFMB-EE polymer is causing the tapered line profiles. An even less i-line absorbent polymer is needed. Alternatively, it may be possible to "tune" the side wall taper by trading for loss in post cure thickness by using longer (e.g. propyl or butyl) esters.

COEFFICIENT OF THERMAL EXPANSION

There are multiple methods for determination of the CTE of films. Among these thermomechanical analysis (TMA) and wafer deflection techniques are commonly used by the microelectronics industry. In TMA a free-standing film of material is maintained at constant tension while the temperature is cycled. This method measures the linear, in-plane CTE (α_{xy}) as:

$$\alpha_{xy} = \frac{1}{L}\frac{dL}{dT} \tag{3.12}$$

where L is the initial characteristic length (film thickness in this case) and T is the temperature. TMA analysis on PMDA-TFMB films was performed by Dr. Brandon Rawlings of Intel Corporation over the temperature range of 0-150°C (Figure 3.36). As can be seen in the figure, PMDA-TFMB has a very low in-plane CTE, about 6 ppm/K over this temperature range. This value is much lower than the project target of 30 ppm/K

and also even lower than the desired ITRS value of 12 ppm/K.[139] It is also significantly lower than Kapton polyimide (20-40 ppm/K).

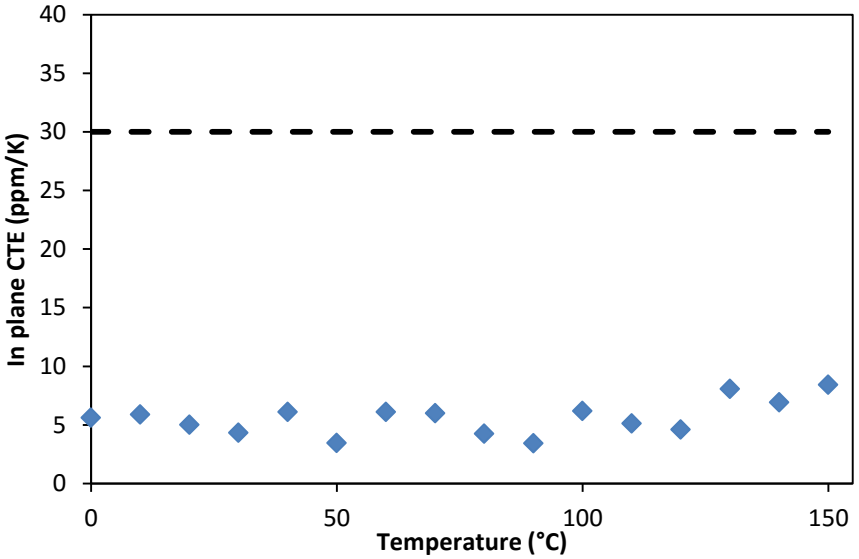

Figure 3.36: In plane CTE of PMDA-TFMB. The dotted line represents the project maximum allowable value.

To confirm these results, a wafer deflection experiment was performed at Georgia Tech by Dr. Mueller. In this experiment a wafer becomes bowed due to the differences in CTE between the film and the underlying substrate and the stress in the film measured as a function of temperature (Figure 3.37). The CTE is calculated as[176]:

$$\frac{d\sigma}{dT} = \left(\frac{E_f}{1-\gamma}\right)_{film} \left(CTE_{substrate} - CTE_{film}\right) \tag{3.13}$$

where dσ/dT is the change in stress with temperature and $E_f/(1-\gamma)$ is biaxial modulus of the film. For PMDA-TFMB, Dr. Mueller found $E_f/(1-\gamma)$ to be 5.12 GPa. The slope of Figure 3.37 is -0.0327 MPa/K, and the CTE of silicon is 2.6 ppm/K. This gives a CTE of PMDA-TFMB of 9.0 ppm/K, in excellent agreement with the TMA data.

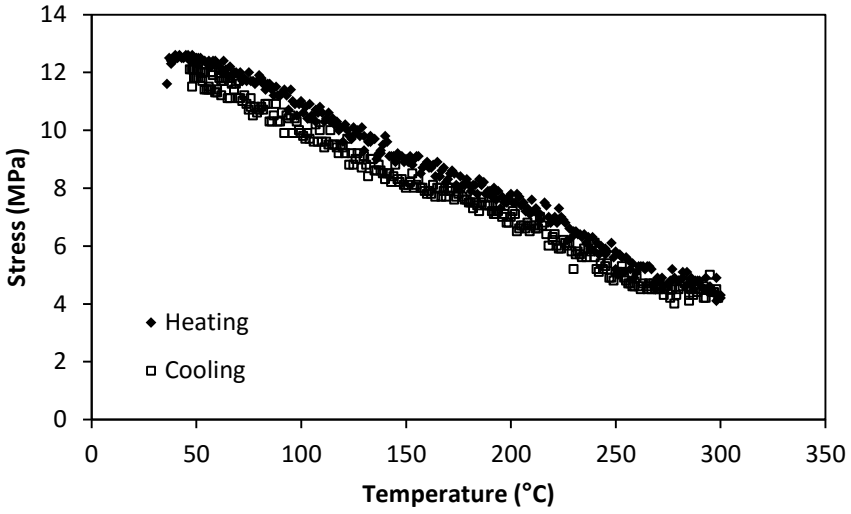

Figure 3.37: Stress versus temperature for 5.5 μm PMDA-TFMB film on silicon wafer

However, rigid aromatic PIs exhibit birefringence. The difference in the indices of refraction (Δn) of a material in different planes is the birefringence and this difference can reach up to 0.24 in extremely rigid PIs such as BPDA-PPD.[101, 135] In PIs the birefringence results from the rigid polymer chains orienting in the plane of the substrate, giving uniaxial anisotropy where the properties of the material are different in the in-plane and out-of-plane directions.[177-179] Low stress PIs, that is PI that have low CTEs, exploit of this anisotropy. Along the polymer backbone there is limited stretching available to individual bonds, and due to the in-plane orientation of rigid PI chains, the CTE in the plane is extremely low. However, the weak interaction from stacking chains results in the out-of-plane CTE values being very large.[180-182] Current ITRS goals for out-of-plane CTE of 40 ppm/K are less demanding than in-plane requirements, though large values could likely lead to via delaminations.[139] Dr. William Bell measured the z-axis CTE of PMDA-TFMB films by ellipsometry and found it to be 163 ppm/K over the temperature range 50-200°C, which is much larger than the requirement for

implementation in devices.[68] However, this requirement is based on the assumption of isotropic modulus. The modulus of PIs in the out-of-plane direction is much lower than in-plane, so stresses generated will also be lower for the same CTE.[182]

Typically dielectric packaging materials use a silica nanoparticle filler strategy to reduce the CTE, as silicon dioxide has a near zero CTE.[92] Another possibility is use of cubic zirconium tungstate, which actually has a negative CTE between -273°C and 777°C.[183-184] The CTE is isotropic and quite large for a ceramic at -7.2 ppm/K. This material has already been shown to lower CTE in PI composites.[185-187] However, the dielectric constant of ZrW_2O_8 is relatively large at about 10 and most of the films used large filler loadings.[188] Finally we are also considering the addition of boron nitride nanotubes (BNNTs) as the filler. Not only do these nanotubes have a low dielectric constant and very low CTE, but also are thermally conductive and could improve heat management in 3-D architectures.[189-191] However, experiments with this material are currently limited due to the high cost of BNNTs and the predicted large loadings required for significantly improved thermal conductivity. There is also some concern that long nanotubes could cause light scattering and adversely affect photo-patterning. Future work will focus primarily on BNNTs as filler material as our group has just recently demonstrated the ability to produce significant amounts of BNNTs by using carbon nanotubes as a sacrificial template.

DIELECTRIC PROPERTIES

Initial testing of the dielectric constant of PMDA-TFMB films was performed using ellipsometry in reflectance mode. Recall that for transparent materials the dielectric constant approaches the square of the refractive index for optical frequencies (THz).[144]

However, PIs tend to have polar groups and they absorb water, leading to dielectric constants at GHz and MHz frequencies being larger than those measured by optical methods. As modern electronic devices operate in GHz frequencies, other measurement techniques must also be used, though ellipsometry can be used for a quick and easy to perform estimate. Additionally, for many fluorinated PI the optical and GHz dielectric constants tend to be quite close.[146] A graph of the estimated dielectric constant (n^2) for cured PMDA-TFMB using a uniaxial model is shown in Figure 3.38. The anisotropy of the films is clearly visible in the about 0.4 difference between the n^2 values for the ordinary (in-plane) and extra-ordinary (out-of-plane) components. In the case of PMDA-TFMB the birefringence is about 0.14 at 633 nm, representing a particularly anisotropic polyimide. Also, at this wavelength both of the in-plane and out-of-plane values are less than 3.0, meaning that PMDA-TFMB should meet the project requirements. The value in the literature for this material of 2.6 is also different from the 2.37 out-of-plane value measured by ellipsometry.[134-135] However, the literature values were determined using parallel plate capacitors operating at 1 MHz, and should have a larger dielectric constant than optical frequencies.

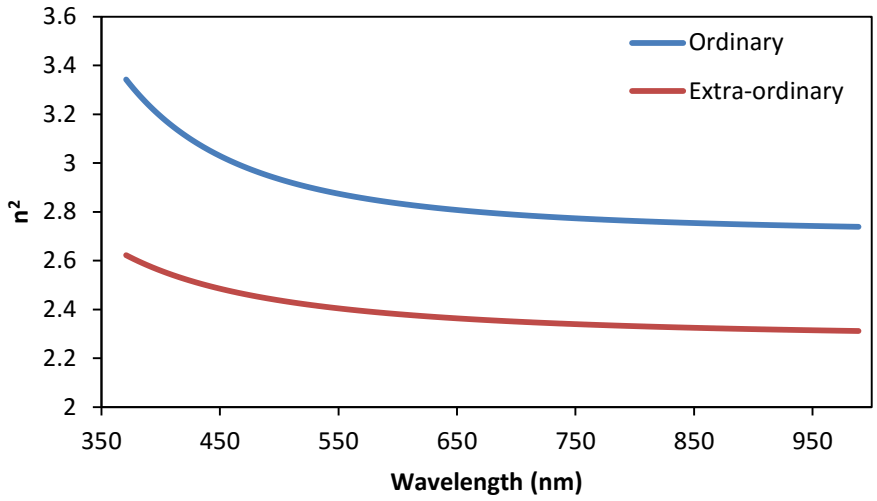

Figure 3.38: Estimate of the dielectric constant of PMDA-TFMB at optical wavelengths by ellipsometry

We currently do not have the ability to test the dielectric constant and dissipation factor of films at microwave frequencies, so materials were sent to Dr. Brennan Mueller at the Georgia Institute of Technology and Mr. Dave Zhang at Intel Corporation for measurement. At Georgia Tech, parallel plate capacitance measurements were performed at 200 kHz while Intel provided data at GHz range frequencies using a split-post dielectric resonator (SPDR).[192-194] By building a parallel-plate capacitor, the out-of-plane dielectric constant is measured, while SPDR gives the in-plane values. The results for the dielectric constant and dissipation factor are shown in Figure 3.39. Interestingly, the values obtained from the capacitor method are larger than those reported in literature.[134] PMDA-TFMB is known to have a water absorption around 2%[135], and the literature values for dielectric constant were obtained in 0% relative humidity after drying for two days. Dielectric constant measurements at Intel Corporation were performed under ambient conditions. However, as the packaging division of Intel is located in Chandler,

Arizona, the relative humidity was likely very low. The measurement of the lower in-plane dielectric constant may have hidden some the effects of water absorption as well.

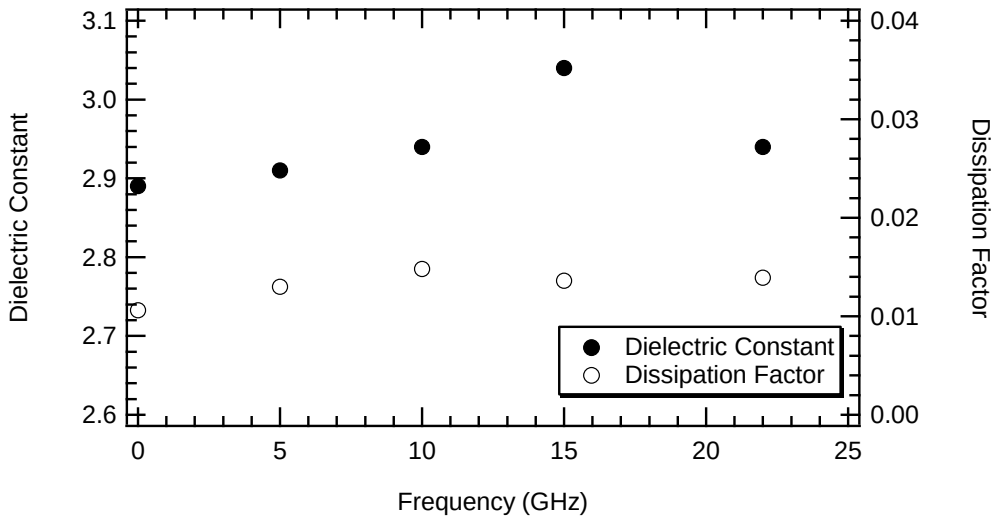

Figure 3.39: Dielectric properties of fully cured PMDA-TFMB

Water absorption was very evident for the films tested at Georgia Tech, however. Dr. Mueller noticed that immediately upon removing films from a vacuum oven following a dehydration bake, both the dielectric constant and dissipation factor began to quickly increase (Table 3.5). This allowed only a few measurements over the course of minutes before the dried film absorbed enough water to return to its original state.

Film Condition	Dielectric Constant	Dissipation Factor
Ambient storage	3.16 ± 0.05	0.0162 ± 0.0005
Dried (150°C in vacuum, 2h)	2.89 ± 0.04	0.0106 ± 0.0004

Table 3.5: Effect of drying on PMDA-TFMB in-plane electrical properties at 200 kHz

Overall, PMDA-TFMB appears to meet the dielectric requirement as it is below 3.0 in the GHz range in the plane. Undoubtedly, water absorption is the cause of discrepancy between literature values and those reported here. The dissipation factor is also slightly larger than the project goal of 0.01, though this is also likely due to water in film. Water exhibits very large dielectric loss at microwave frequencies, so even a small amount of water in the film will greatly increase the dissipation factor.[158] As the package is not hermetically sealed, a method of lowering water absorption is required. This has led us to the investigation of other rigid, lower water absorption PI that are discussed in later chapters.[101, 134-135]

CONCLUSIONS

A directly patternable polyimide based system was demonstrated. This system was able to provide patterned fluorinated poly(amic esters) using only a minimal amount of photobase generator to generate a negative-tone chemically amplified photoresist. Substituting PMDA-TFMB for PMDA-ODA improved film transparency and allowed for features as small as 2.5 μm to be resolved in thin films and features with an aspect ratio of 2.0 in 14 μm thick films. A summary of the project goals and our current progress using this system is shown below in Table 3.6. New, less water absorbent polymers are the topic of Chapter 4. In plane CTE measurements are well within the target, however, out of plane CTE is large. The reader is directed to the thesis of Dr. William Bell for a more through discussion of z-axis CTE.[68] Finally, the cure temperature requirement was not discussed in this chapter, but it is an important consideration for device integration. Our work using organic and inorganic salt catalysts to reduce the curing temperature of polyimide precursors is the subject of Chapter 5.

Material Property	Target	PMDA-TFMB
ε_r	< 3.0	3.0
DF	< 0.01	0.015
CTE	< 30 ppm/K	6
Water abs.	< 1%	2
Resolution	5 μm	2.5
Aspect ratio	3	2

Table 3.6: Summary of project goals and data obtained for PMDA-TFMB PSPI system. Green shading indicates that the target has been met. Yellow indicates values that are close to the specification and could be met with process optimization.

EXPERIMENTAL

General Methods

All solvents and regents were obtained from commercial sources and used as received, unless otherwise specified. ONB PBG, PMDA-TFMB para ethyl ester polymer, and PMDA-ODA para ethyl ester polymer were prepared by Dr. William Bell. DCM was distilled from CaH_2 while THF and DMF were purified by eluting through an alumina column solvent delivery system under argon. NMP was vacuum distilled from P_2O_5. TFMB monomer was purified by sublimation prior to use. Reactions were run in flame-dried glassware and under nitrogen atmosphere, expect where noted. ^{1}H and ^{13}C NMR spectra were obtained on a Varian Unity Plus 400 MHz instrument. Solvent proton peaks are used as the internal standard ($CDCl_3$ ^{1}H 7.26 ppm, ^{13}C 77.0 ppm; DMSO-d6 ^{1}H 2.49 ppm, ^{13}C 39.5 ppm). HRMS (CI) was performed on a VG analytical ZAB2-E instrument and HRMS (ESI) on an Ion Spec FT-ICR instrument. All MS data was obtained by ESI unless otherwise specified.

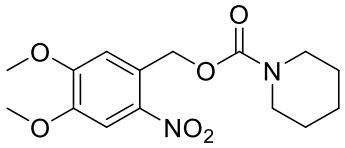

4,5-dimethoxy-2-nitrobenzyl piperidine-1-carboxylate (NVOC piperidine)

Prepared in a slight modification to literature procedure.[195] Nitroveratraldehyde (5.0g, 23.6 mmol, 1 eq) was reduced to the benzyl alcohol by addition of small portions of $NaBH_4$ (total: 1.5g, 2 eq) in 100 mL THF. After the reaction was complete by TLC, the solution was partitioned between sat. NH_4Cl(aq) and EtOAc. The organic phase was collected and the solvent removed in vacuo. to obtain 4.76g (94%) of nitrovertyl alcohol. The alcohol (1.5g, 7 mmol, 1 eq) was then dissolved in 40 mL THF and added dropwise to a 15% solution of phosgene in toluene (15.1mL, ~21 mmol, 3 eq) at 0°C overnight. The excess phosgene was then removed by flowing dry nitrogen over the solution and the rest of the solvent removed in vacuo to obtain 1.90g (98%) of the chloroformate. Finally, the crude chloroformate (500mg, 1.81 mmol) was dissolved in 5 mL DCM at 0°C and piperidine (0.43mL, 2.4 eq) was added dropwise. After completion of the reaction, the solution was washed with 1N HCL, then brine, dried over Na_2SO_4, filtered, and the solvent removed to obtain the title compound as a light yellow powder (0.500g, 87%). ^{1}H NMR ($CDCl_3$) δ 7.69 (s, 1H), 6.98 (s,1H), 5.52 (s, 2H), 3.96 (s, 3H), 3.95 (s, 3H), 3.47 (br s, 4H), 1.65-1.51 (m, 6H); ^{13}C NMR ($CDCl_3$) δ 154.6, 153.3, 148.0, 139.9, 128.5, 110.1, 108.2, 63.9, 56.4, 56.3, 45.0, 25.6, 24.3 HRMS (ESI) $[M+Na]^+$ calcd: 347.1214 found 347.1218

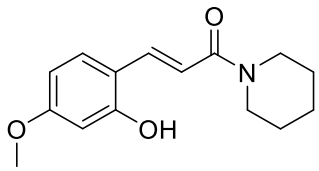

(E)-3-(2-hydroxy-4-methoxyphenyl)-1-(piperidin-1-yl)prop-2-en-1-one (3.3a)

Prepared according to literature procedure[130]. Recrystallized from ethanol to obtain a slightly yellow solid in 22% overall yield. ^{1}H NMR (DMSO) δ 10.17 (br s, 1H), 7.66 (d, 1H), 7.57 (d, 1H), 7.01 (d, 1H), 6.39 (m, 2H), 3.70 (s, 3H), 3.55 (m, 4H), 1.58 (m, 2H), 1.46 (br s, 4H); ^{13}C NMR (DMSO) δ 165.4, 161.7, 157.9, 137.1, 129.8, 115.6, 114.8, 106.1, 101.4, 55.5, 46.4, 43.0, 27.0, 25.9; HRMS (ESI) $[M+Na]^{+}$ calc: 284.1257 found 284.1257

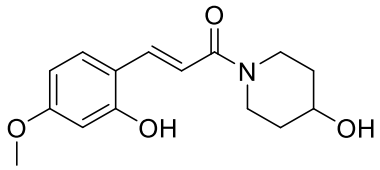

(E)-3-(2-hydroxy-4-methoxyphenyl)-1-(4-hydroxypiperidin-1-yl)prop-2-en-1-one (3.3b)

4-hydroxypiperidine (4.0g, 19.8 mmol, 1 eq) was dissolved in 150 mL of EtOAc and 75 mL of sat. aq. Na_2CO_3 was added to obtain a biphasic mixture. Chloroacetyl chloride (2.4mL, 29.6 mmol, 1.5 eq) was then added dropwise over 5 minutes. The reaction was complete after 4 hours by TLC. The organic layer was separated, dried with Na_2SO_4, and the solvent removed in vacuo to obtain **3.2b** as a slightly yellow oil (3.08g, 88%). **3.2b** was then heated to 80°C overnight with triphenylphosphine (4.55g, 17.3mmol, 1 eq) in 100 mL toluene. After cooling to room temperature, the solvent was decanted to obtain a slightly oily white solid that was placed in high vacuum to remove the remainder of the toluene. The salt (4.66g, 10.6 mmol) was diluted with methanol and then 2-hydroxy-4-

methoxybenzaldehyde (1.61g, 10.6 mmol, 1 eq) was added. Finally, 0.6g KOH (10.6 mmol, 1 eq) dissolved in 50 mL methanol was added to form a bright yellow solution. After consumption of the starting material as monitored by TLC, the solvent was removed in vacuo and the crude material purified by flash chromatography (5:95 MeOH/DCM) to obtain 0.93g (32%) of the title compound as an off white solid. ^{1}H NMR (DMSO) δ 10.06 (br s, 1H), 7.67 (d, 1H), 7.58 (d, 1H), 7.02 (d, 1H), 6.39 (m, 2H), 4.73 (br s, 1H), 4.00 (br s, 2H), 3.70 (s, 3H), 3.67 (m, 1H), 3.23 (br s, 1H), 3.05 (br s, 1H), 1.72 (br s, 2H), 1.28 (br s, 2H); ^{13}C NMR (DMSO) δ 165.6, 161.8, 158.0, 137.2, 129.8, 115.5, 114.7, 106.2, 101.5, 66.2, 55.5, 43.0, 35.5, 34.5; HRMS(ESI) $[M+Na]^{+}$ calcd: 300.1206 found 300.1208

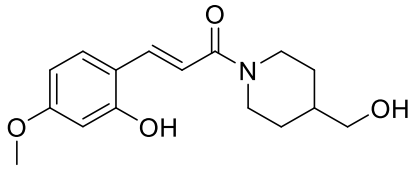

(E)-3-(2-hydroxy-4-methoxyphenyl)-1-(4-(hydroxymethyl)piperidin-1-yl)prop-2-en-1-one (3.3c)

Prepared as described for **3.3b** using 4-piperidinylmethanol in place of 4-hydroxypiperidine. Recovered white powder in 29% overall yield after chromatography (MeOH/DCM).; ^{1}H NMR (DMSO) δ 10.06 (br s, 1H), 7.67 (d, 1H), 7.58 (d, 1H), 7.01 (d, 1H), 6.40 (m, 2H), 4.47 (br s, 2H), 4.18 (br s, 1H), 3.70 (s, 3H), 3.24 (d, 2H), 2.99 (m, 1H), 2.57 (m, 1H), 1.62 (m, 3H), 1.00 (br s, 2H); ^{13}C NMR (DMSO) δ 165.5, 161.7, 158.0, 137.1, 129.8, 115.6, 114.9, 106.2, 101.4, 66.0, 55.5, 49.0, 30.1, 29.0; HRMS (ESI) $[M+Na]^{+}$ calcd. 314.1363 found 314.1361

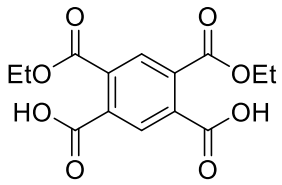

4,6-bis(ethoxycarbonyl)isophthalic acid

In a 1L round bottom flask, PMDA (100 g, 458 mmol) was refluxed overnight in 400 mL ethanol. The solvent was then removed in vacuo. to obtain a white powder. 425 mL of EtOAc was then added to the powder and the suspension was heated at 90°C for 30 minutes with vigorous stirring. The heating was stopped and the solution was stirred overnight. After filtering the precipitated, para-enriched isomer, the solvent from the mother liquor was removed, leaving a white solid containing 66.7g (46.3%) of 90:10 meta: para isomer mixture by NMR. The para isomer is symmetric and has only one aromatic peak at 7.98 ppm while the meta isomer has two aromatic peaks at 8.08 and 7.90 ppm. ^{1}H NMR (400 MHz, DMSO) δ 13.80 (br s, 2H), 8.08 (s, 1H), 7.90 (s, 1H), 4.30 (q, *J* = 7.1 Hz, 4H), 1.29 (t, *J* = 7.1 Hz, 6H). ^{13}C NMR (101 MHz, DMSO) δ 166.8, 166.3, 135.0, 134.1, 129.6, 128.3, 62.0, 13.9. HRMS $[M+Na]^{+}$ calcd. 333.0581 found 333.0585

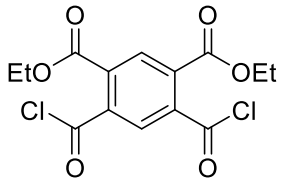

Diethyl 4,6 dichloroisophthalate

The meta-enriched isomer (10.0g, 32.2 mmol) was then dissolved in 125 mL ethyl acetate and a drop of DMF was added. The solution was then heated to 50°C and oxalyl chloride (8.3 mL, 97 mmol) was added dropwise over 10 minutes. After the bubbling had ceased, the solvent and excess oxalyl chloride were removed in vacuo. The crude diacid chloride

was then treated with activated charcoal and recrystallized twice from hexanes to obtain 8.50g (76%) of shiny, snow-white flakes of the title compound in a 95:5 meta: para ratio. ^{1}H NMR ($CDCl_3$) δ 8.38 (s, 1H), 7.93 (s, 1H), 4.45 (q, 4H), 1.42 (t, 6H); ^{13}C NMR ($CDCl_3$) δ 166.6, 163.7, 139.7, 132.1, 131.6, 126.8, 63.2, 13.8

PMDA-TFMB Ester Polymerization

Precursor poly(amic ester) was prepared using a slight modification of the literature procedure.[119] 2,2' Bis(trifluoromethyl)benzidine (TFMB, 1.50g, 4.69 mmol, 1 eq) was dissolved in 45 mL NMP then cooled to 0°C. A solution of **5** (1.63g, 4.69 mmol, 1 eq) in 7 mL THF was then added dropwise over 15 minutes. After the addition was complete, pyridine (0.75mL, 2 eq) was added dropwise and the reaction was stirred at room temperature overnight. The solution was precipitated into water, filtered, washed with water, methanol and ethyl acetate, and then dried at 50°C for 2 days in vacuo to obtain 2.79g of a white solid (97%).

Films and Exposures

Formulations were prepared by dissolving resist polymer and photobase in NMP for NVOC PBG or 10 wt% acetic acid in NMP for the cinnamide PBGs. The PBG loading was 5 wt%, and total solids loading was adjusted to 15-30 wt% to achieve varying film thicknesses. Silicon wafers were surface functionalized by coating them with neat (3-aminopropyl)triethoxysilane (APTES) and letting the neat APTES remain on the wafers for 1 minute prior to rinsing off the excess APTES with isopropanol. Then films were cast on the APTES coated wafers by spin-coating at 1500 rpm. Excess solvent was removed by a post apply bake at 100°C for 10 minutes. Patterned exposures were performed using a Suss MA6 near UV mask aligner. Exposed films were then baked on a

hot plate for 10 minutes at 130°C (cinnamide PBG) or 160°C (NVOC PBG). The films were then developed in a solution of 30% NMP in methanol. Final curing was performed at 350°C in a vacuum oven for 1 hour.

Degree of Imidization by IR Spectroscopy

Formulations were prepared using either a 5:95 cinnamide PBG:polymer in 10:90 AcOH:NMP solution or a 5:95 **4**:polymer solution in NMP; both at 10 wt% total solids. The solutions were spincoated (1500 rpm) onto APTES treated wafers and baked for 2 minutes at 100°C to obtain films approximately 800 nm thick. Half of the samples were exposed to 2 J/cm^2 of 365 nm filtered light from a Novocure 2100 spot curing system and then baked alongside unexposed samples at each temperature (120-170°C) for 10 minutes. All the films were then measured on a ThermoSci Nicolet 6700 FT-IR in transmission mode before being fully cured overnight at 350°C in a vacuum oven. No imidization was observed in samples after the post apply bake at 100°C. The degree of imidization was then calculated by:

$$\text{Imidization} = (A_{1783}/ A_{1491})_{\text{sample}} / (A_{1783}/ A_{1491})_{\text{cure}} \quad (1)$$

where imidization is the fractional conversion of the ester groups to imides, A_{1783} is the area of the C-O stretch of asymmetric stretch of the imide carbonyl and A_{1491} is the C-C aromatic stretch used as an internal standard in the study. Subscript “sample” after the ratio refers to the polymer baked at each temperature for 10 minutes. “Cure” refers to the samples after complete curing.

Measurements

Exposure doses were measured using a Coherent FieldMaxII-TO with PowerMax PM3 detector. Dielectric constant measurements at 200 kHz were performed by capacitance: a 450 nm film (after full cure at 350°C overnight) of PI was spincoated onto a 300 nm Al coated wafer containing 500 nm of thermal oxide. 300 nm Al was evaporated on top of the film through a mask to complete the capacitors. Split post dielectric resonance (SPDR) measurements were performed on free-standing films using a series of GHz range SPDR fixtures (Agilent/Keysight) with an Agilent N5277A analyzer. Coefficients of thermal expansion were obtained using both wafer bow and thermomechanical analysis methods. In the wafer bow method PI was cured on a Si wafer and the stress as a function of temperature was obtained using a Flexus F2320 and the CTE calculated as previously reported.[196] Thermomechanical analysis was performed on a TA Instruments Q400. UV-visible spectra of thin films on quartz were obtained using a ThermoSci Evolution 220 UV-visible spectrometer. Thin film thicknesses were obtained using a JA Woolam, Inc. VASE ellipsometer. Thicker films were measured using a Veeco Dektak profilometer. SEM micrographs were obtained using a Hitachi S-4500 SEM at 5kV accelerating voltage; Au/Pd was sputter coated on films prior to imaging to prevent charging.

Chapter 4: Alternatives to Base-Catalyzed PMDA-TFMB System

POSITIVE TONE PMDA-TFMB PSPI

The relatively low imidization contrast for the base catalyzed system along with the accompanying development issues lead us to consider a positive tone variant of PMDA-TFMB. The use of DNQ containing additives in PSPI was deemed unacceptable due to the high loading required (~30%) and the accompanying detrimental effect on both dielectric and CTE properties.[104-105] The requirement of using either PAA or pre-imidized polymers containing acidic groups was also undesirable for the same reasons, so only a chemically amplified scheme was considered. As discussed previously, this typically utilizes t-butyl or tetrahydropyranyl protected phenols or carboxylic acids. Protected hydroxyimides were ruled out due to the permanent phenol groups present in the material that would both absorb water and generate higher dielectric constant polymers. This left the PMDA-TFMB t-butyl ester polymer (mPMDA-TFMB-tBu)/ photoacid generator system as the only material that would likely satisfy the project goals (Figure 4.1).

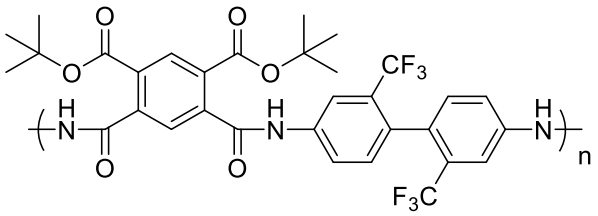

Figure 4.1: Proposed mPMDA-TFMB-tBu polymer for use as a positive tone PSPI

Polymers prepared from the di t-butyl ester of PMDA are quite rare and have been primarily investigated by AT&T Bell Laboratories.[197-200] Additionally, all of the materials were either polymers of ODA, methylene dianiline (MDA), or various derivatives of

ODA. All of these polymers were also prepared by use of phosphoryl condensing agents originally developed for peptide coupling (Figure 4.2).[201-203] These condensing agents work by first deprotonating a carboxylic acid to generate an anion which attacks the condensing agent, breaking the P-N bond and releasing the benzoxazolone derivative (Figure 4.3). The resulting mixed carboxylic-phosphoric anhydride is very reactive and will react with any available nucleophile. This can be either the desired reaction were the anhydride reacts with an amine to form the amide, or the undesired side-reaction in which it reacts with the benzoxazolone derivative. This side-reaction is typically much less favored, except in the case where the amine coupling partner is a particularly poor nucleophile.[201]

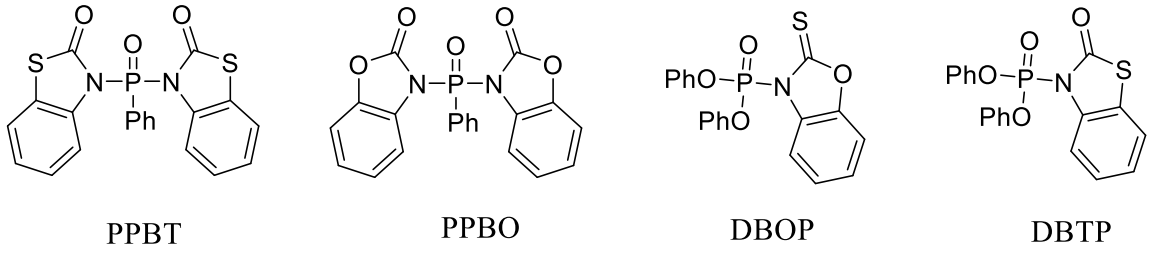

Figure 4.2: Phosphoryl condensing agents used amide and amic ester polymers

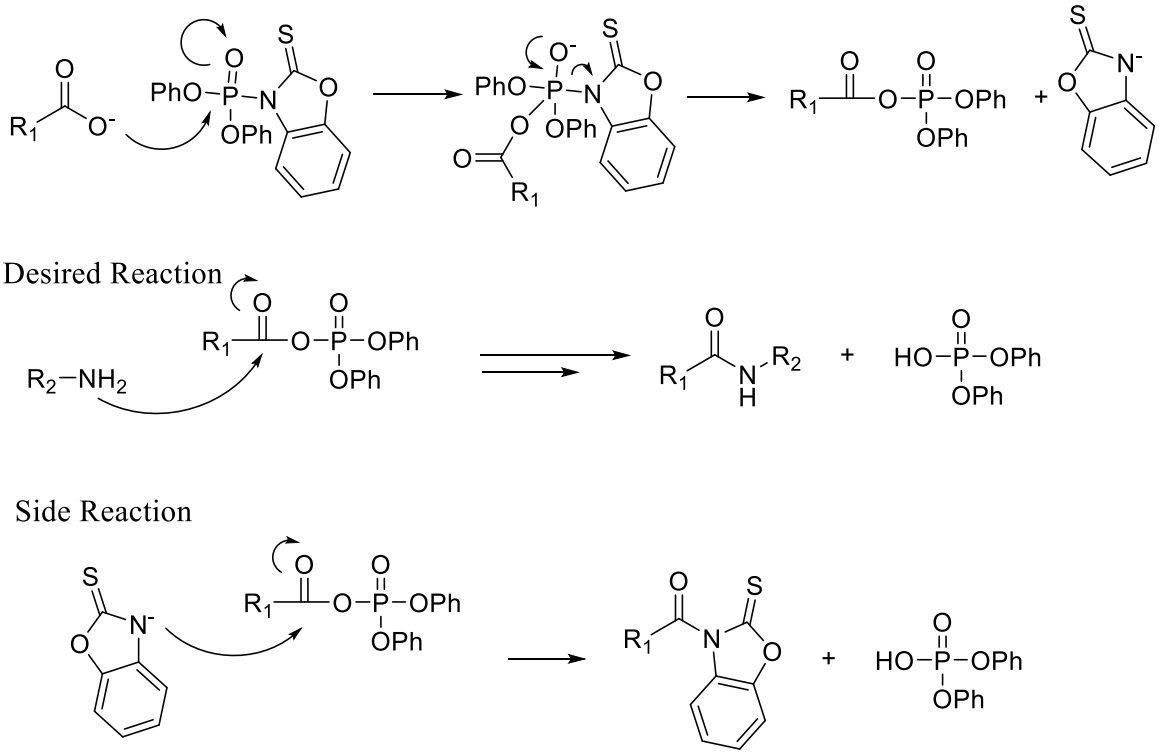

Figure 4.3: Mechanism of DBOP condensing agent

Despite the expected poor nucleophility of TFMB, there is one Japanese patent that claims to have produced an amic ester polymer containing TFMB using DBOP.[204] However, other groups have reported only moderate yields from coupling the analogous 3-trifluoromethyl aniline with carboxylic acids using similar condensing agents, and the formation of polymer would require essentially quantitate yields.[205]

We tried to condense PMDA t-butyl ester with TFMB in NMP using DBOP and TEA. However, there was no noticeable change in viscosity and nothing precipitated after pouring the reaction mixture into methanol. Other condensing agents including PPBT, PCl_3, EDC, carbonyl diimidazole and triphenyl phosphite were attempted, but no polymer was formed in any of these cases. To confirm that the condensation reaction worked,

PMDA-ODA t-butyl ester polymer (pPMDA-ODA-tBu) was prepared using DBOP in the method of Ueda.[199] The reaction became viscous and produced a bright yellow precipitate upon pouring into methanol.

The inability to form PMDA-TFMB ester polymers by condensing agents lead us back to considering a more activated acid chloride route. Originally we were concerned that the acid chloride route would be incompatible with t-butyl esters. T-butyl groups are cleaved by acid and hydrochloric acid would be produced during both the acid chloride and the polymer syntheses (Figure 4.4). While the HCl is neutralized by the pyridine in the polymerization, the HCl formed during preparation of the acid chloride was a major concern. Initial attempts to form the acid chloride in the same manner as the other alkyl esters[119] by reaction with oxalyl chloride in EtOAc at 50°C were unsuccessful. However, running the chlorination reaction at 0°C in THF and using the crude acid chloride product in the polymerization produced moderate molecular weight polymer (Mn = 12,900, DMF GPC, PS stds). Attempts to isolate the intermediate acid chloride by recrystallization prior to polymerization were unsuccessful and produced a white insoluble solid.

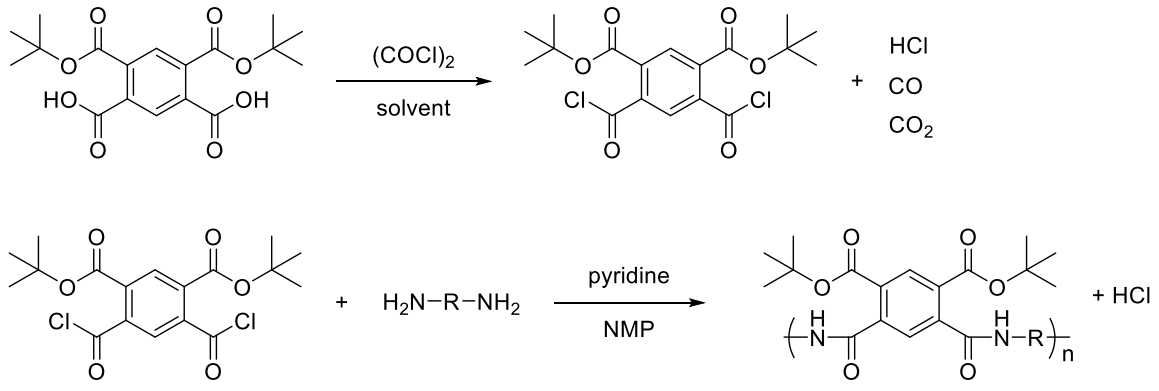

Figure 4.4: T-butyl PAE synthesis via acid chloride route

The polymer was tested as a photoresist by the addition of 5% triphenylsulfonium nonaflate PAG (TPS Nf) and casting a film from DMSO. The film was then divided into small samples and IR spectra obtained for after exposure to 3 J/cm^2 broadband UV radiation and baking at 140°C for 3 minutes as well as unexposed controls (Figure 4.5, red and orange traces). There was no noticeable difference between the spectra. The peak at just below 3000 wavenumbers represents the alkyl C-H stretches and there is no difference between unexposed, exposed, and as cast films. The polymer is still fully protected, even after exposure and subsequent PEB. This could be due to the presence of small amounts of NMP remaining in the polymer after synthesis or the DMSO solvent acting as a quencher. To test if the polymer is acid sensitive, one drop of pure trifluoroacetic acid was added on top of the film and it was baked at 140°C to determine if the t-butyl groups would cleave. The blue trace in Figure 4.5 shows that the t-butyl groups were removed, and that this material could work as a positive tone resist. Unfortunately, the only solvents able to dissolve PMDA-TFMB-tBu were either DMSO or amides, which are quenchers in this system.

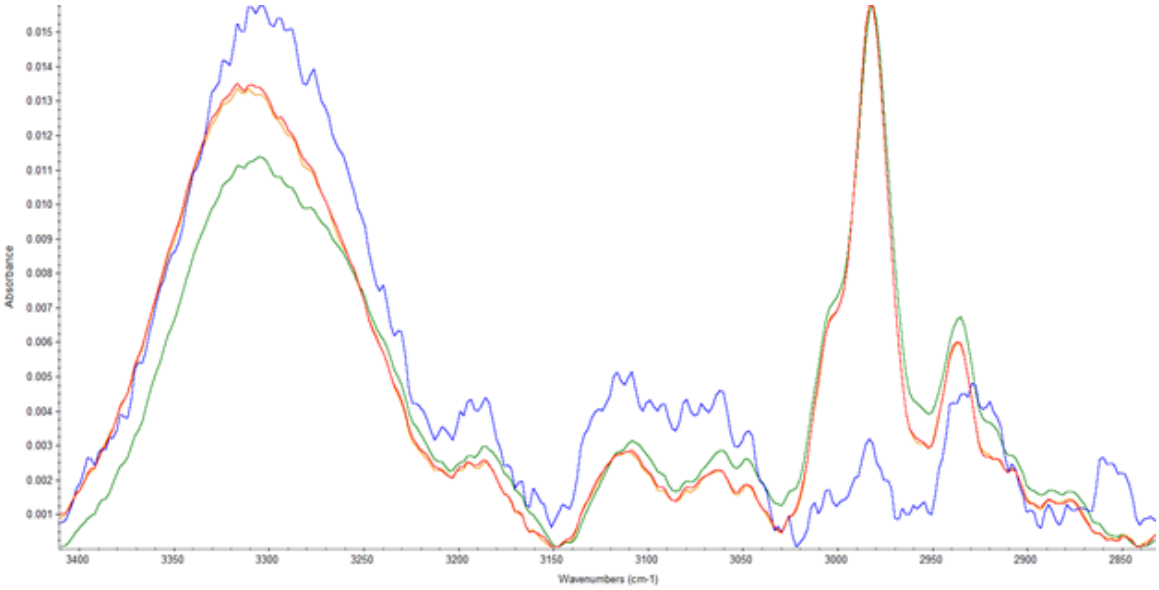

Figure 4.5: IR Spectra of mPMDA-TFMB-tBu ester with 5% TPS Nf PAG. Green) as cast. Orange) unexposed and baked at 140°C. Red) exposed to 3 J/cm^2 broadband UV and baked at 140°C. Blue) 1 drop TFA added and baked at 140°C

LOWER WATER ABSORPTION AND MORE TRANSPARENT POLYIMIDES

Many common polyimides and even some fluorinated polyimides have significant water absorption.[134-135, 148] Much of this water absorption can be traced back to the polar imide groups of the polymer. Water absorptions of around 1-4% are typical for most commercial PIs. In the mid-1990s it was found that replacing TFMB with TFMOB resulted in about 50% lower water absorption for the same dianhydride (Figure 4.6).[134] Using longer perfluorinated sidechains decreased water absorption and the dielectric constant further, but at significant increase in CTE.

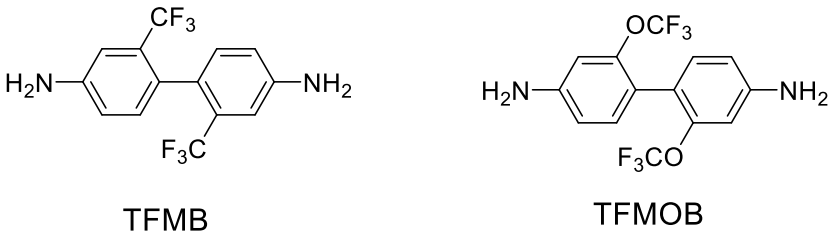

Figure 4.6: TFMB and TFMOB monomers

Initially TFMOB and other fluorinated ethers of benzidine were developed to improve the polmerizability of greatly electron deficient diamines.[134, 148] This is due to the considerably lower electron withdrawing power of the $–OCF_3$ group compared to $–CF_3$.[206] The $–OCF_3$ group is also remarkable in its incredible chemical and thermal stability, making it useable in high temperature polymers.[207] Indeed TFMOB was used as one of four monomers in the so-called fluorinated polyimide (FPI) developed as an interlayer dielectric from a collaboration between DuPont, Sematech, and UT-Austin.[41, 135, 208] However, there are a few downsides to incorporating TFMOB in the base catalyzed patterning scheme. TFMOB is significantly more expensive to produce and is not commercially available at present. Additionally, preparing this material on a lab scale is not safe due to the required use of pressurized anhydrous HF as the reaction solvent.

After obtaining a small amount of TFMOB from a Japanese supplier, it was polymerized with PMDA diethyl ester diacid chloride and the UV spectrum was compared to that of PMDA-TFMB and BPDA-TFMB ethyl ester PAEs (Figure 4.7). As shown in the figure, substitution of TFMOB for TFMB is quite detrimental to absorbance at 365 nm. An increase of about 40% is observed using PMDA as the dianhydride, ruling out incorporation of TFMOB for thick film patterning. The BPDA-TFMB UV spectrum is also shown in Figure 4.7. This polymer is reported to have a CTE of 20 ppm/K and water absorption of 1.3%, making it attractive for further study.[134] Unfortunately, BPDA-

TFMOB has a CTE that is too large for our purposes and was not considered for further testing, despite its low water absorption of 0.6%.

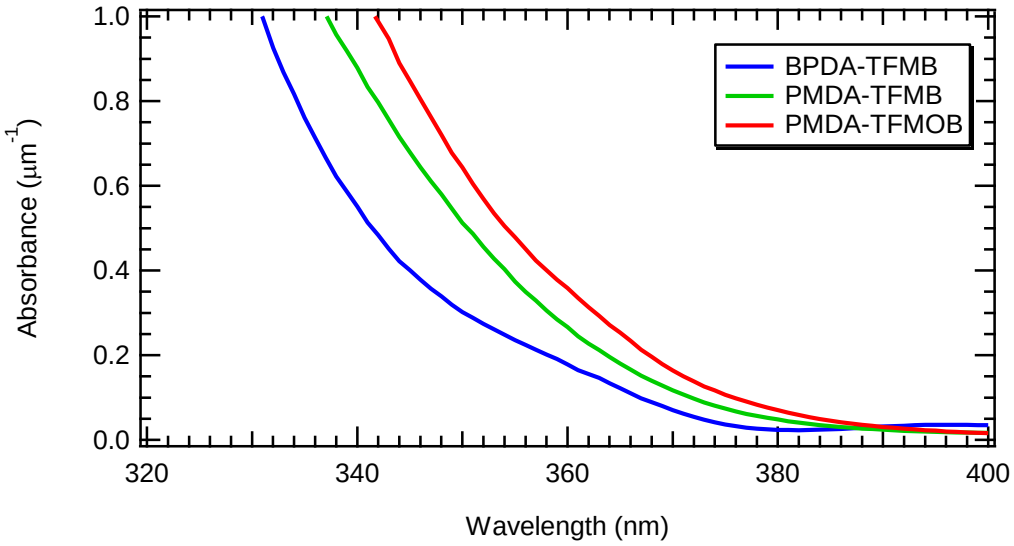

Figure 4.7: UV spectra of poly(amic ethyl esters) of TFMB and TFMOB

BPDA-TFMB ethyl ester was further investigated due to the significantly lower i-line absorbance than PMDA-TFMB. Like most other aromatic PIs, the absorbance in these system can also be traced back to charge transfer complexes. BPDA has two features that help to break up these CTCs. The biphenyl backbone of the polymer adds some flexibility and twists the backbone slightly, breaking up conjugation both intra- and inter-molecularly. The price is a moderate increase in the CTE. The UV transparency is aided by electronic effects as well. In PMDA a single aromatic ring has four very strongly electron withdrawing carbonyl groups attached, making the ring a particularly strong electron acceptor. Indeed, not many dianhydrides are known that are more electron deficient and rigid.[209] Instead BPDA only has two carbonyls groups on each ring,

significantly lowering the electron deficiency. As the biphenyl bond is rotatable, the conjugation between the two rings is limited.

Implementation of BPDA as PAEs is much more difficult than in PMDA due to purification issues. In the first step of making diester diacid chloride monomers, the dianhydride is refluxed in an alcohol to form a diester diacid, as shown previously in chapter 3. In the case of PMDA, only two distinct isomers are produced, and they are easily separable by fractional crystallization. However, for dianhydrides not having a plane of symmetry through the two anhydrides, three isomers form (Figure 4.8). The relative ratio of each isomer depends on the electron affinity of the bridging group between the two phthalic anhydride ends.[210] Electron withdrawing groups such as $–SO_2–$ favor attack on the para carbonyl whereas electron rich groups such as –O– result in more meta attack. In the case of BPDA, the directing effect only slightly favors meta attack, resulting in a ratio close to the 1:2:1 m,m: m,p: p,p ratio if there was no preference. As much of each isomer is present, selective crystallization is difficult, and unworkable in our hands for esters other than methyl version. Indeed the only literature report appears to be for the pure meta, meta isomer due to its lower solubility,[211] though isolation requires a series of recrystallizations to get the pure isomer. However, this isomer is less useful as it results in a rigid rod polymer due to polymerization occurring across the para acid chloride groups. Likely, polymerizations using TFMB would give the same rough films and light scattering observed in the case of para PMDA-TFMB ethyl ester polymer.

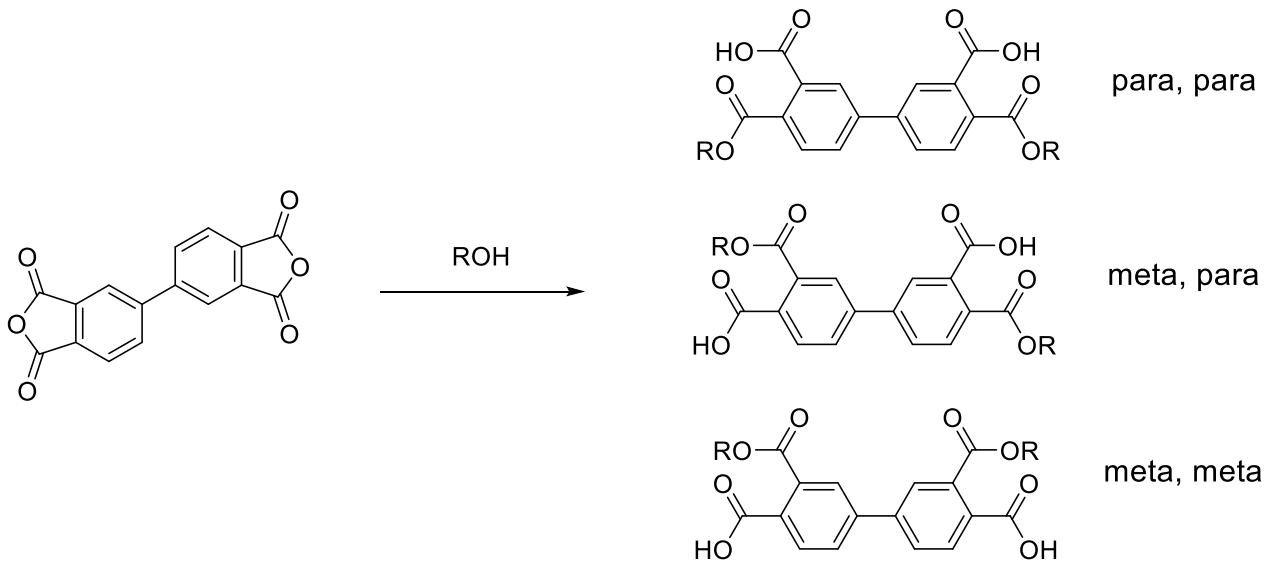

Figure 4.8: Isomers formed during reaction of BPDA and alcohols

The BPDA-ethyl ester isomer mixture was therefore used without purification to form the acid chloride in the same manner PMDA esters. However, after the reaction and subsequent treatment with activated carbon to remove colored impurities, only a slightly yellow oil could be obtained; no crystalline product was formed. The crude acid chloride mixture was then polymerized with TFMB to obtain fairly low molecular polymer (M_n~5 kDa) in only 23% yield. The extremely low yield is likely due to impure monomers. Much of the oligomeric material that formed was likely even lower molecular weight that did not precipitate into methanol. Casting thick films of this polymer also proved to be difficult. During organic development this low molecular weight material cracked badly (Figure 4.9). Work at IBM has shown that this cracking is due to solvent induced swelling at the top of the film.[212] As the diffusion of solvent to the bottom of thick films is slow, the top of the film expands much more than the bottom. This generates a

significant stress which is released as cracks in the film. The inability to develop thick films of BPDA-TFMB-EE led to the abandonment of this approach.

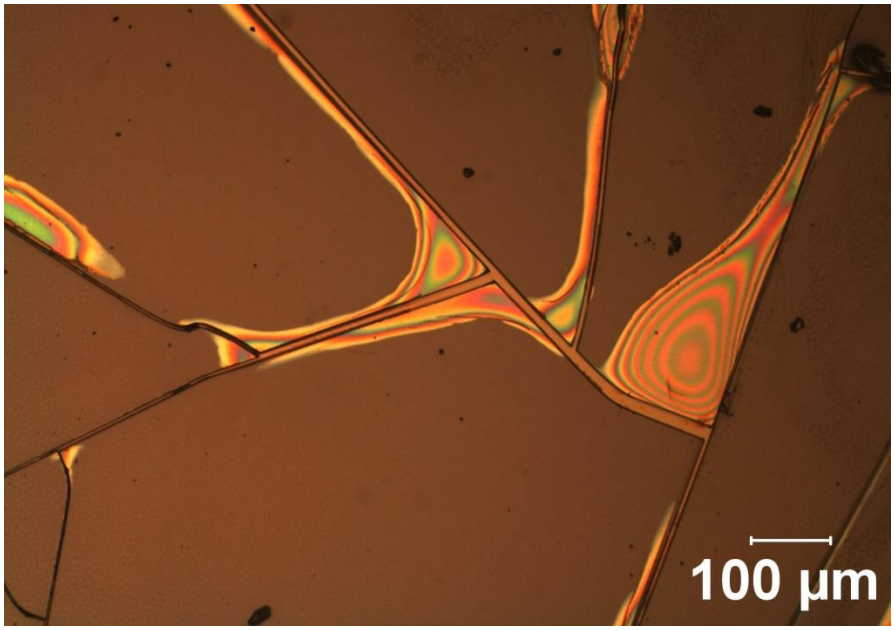

Figure 4.9: Cracks formed during development of low molecular weight 10 µm thick PAE film

CYCLOBUTANE DIANHYDRIDE POLYMERS

Aliphatic and cycloaliphatic monomers have been proposed as a way to obtain more transparent polyimides due to removal of charge transfer complexes.[213] Typically this is done by substituting either an aliphatic diamine or dianhydride, or both.[101, 214-222] While a variety of different non-aromatic monomers have been reported, most tend to suffer from high CTEs, low Tg and low thermal stability. Much of this can be attributed to the increased flexibility and non-planar nature of the polymer chains and the subsequent lack of alignment during curing. The only truly rigid cycloaliphatic low CTE

monomers available are 1,2,3,4-cyclobutanetetracarboxylic dianhydride (CBDA) and trans 1,4-cyclohexyldiamine (tCHDA).

The use of aliphatic monomers presents new challenges to preparing PIs. Alkyl amines such as tCHDA are much more basic than aromatic amines. When polymerized with many dianhydrides, carboxylic acid groups begin to form as the poly(amic acid) is produced. These alkyl amines are sufficiently basic that they form salts with the newly formed carboxylic acids and tend to form ionically crosslinked networks that precipitate out of solution.[215, 223] The reaction of cycloaliphatic dianhydrides with aromatic amines tends to have the opposite problem. The prototypical aliphatic dianhydride, bicyclo[2.2.2]oct-7-ene-2,3,5,6-tetracarboxylic dianhydride (BTA) has poor reactivity with many diamines and often leads to insufficiently low molecular weights for film forming.[220-221, 224] CBDA and its derivatives are actually fairly unique among non-aromatic dianhydrides in their ability to create high molecular weight polymers with aromatic diamines.[101, 223, 225] This is due to the large ring strain in CBDA compared with other alicyclic dianhydrides. The degree of polymerization using alicyclic dianhydrides scales with the degree of ring strain in the monomer.[226]

Our desire to substitute CBDA for PMDA in patterning was based on the remarkable material properties of CBDA-TFMB, which meet all the material requirements laid out in the project. The CTE is 20.7 ppm/K, water absorption is 0.39%, the dielectric constant at optical frequencies is 2.66 and the material is stable to 450°C.[101] The polymer is also completely insoluble in organic solvents and could supply development contrast in our patterning process. Most important, however, is the optical transparency of the films. Even the fully thermally cured material is completely colorless, as shown in Figure 4.10. The UV-Vis spectra of 25 μm films of CBDA-TFMB and a DuPont prototype polyimide for use in photovoltaics are shown in Figure 4.11 for

comparison.[227] The DuPont prototype film is slightly yellow and, due to its higher refractive index, transmits less light at optical wavelengths than CBDA-TFMB.

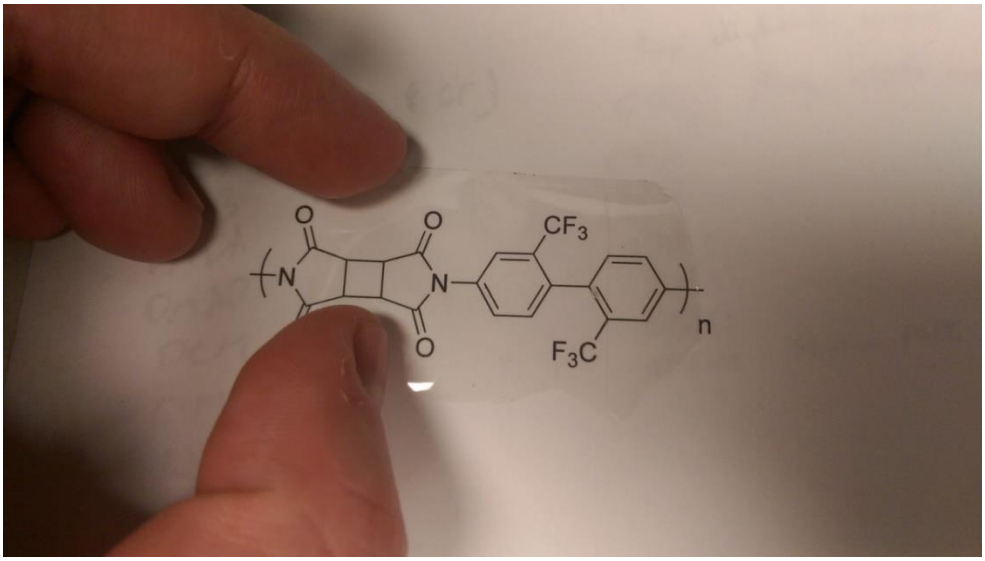

Figure 4.10: Free standing film of CBDA-TFMB on white background

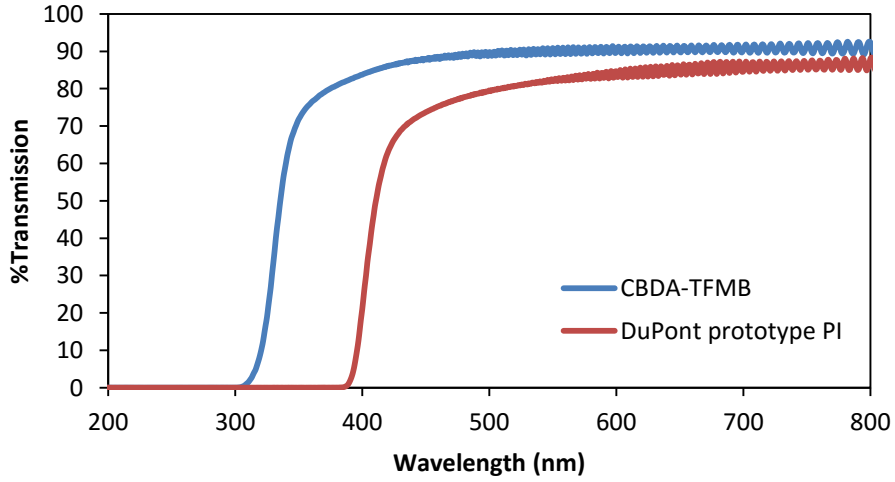

Figure 4.11: UV-Vis spectra of CBDA-TFMB and DuPont transparent PI

We first set out to simply replace CBDA for PMDA in the base catalyzed ethyl ester system. However, this was easier said than done. CBDA is only commercially

available from a few sources in small quantities and at very high prices considering the apparent simplicity of the monomer. For initial testing, a small batch was prepared by the dimerization of maleic anhydride, as shown in Figure 4.12. Researchers at Nissan Chemical Industries optimized the process as they were originally interested in new polymers for liquid crystal alignment layers.[214, 226] They also showed that by using EtOAc as the solvent, pure trans CBDA can be precipitated out of solution while the cis CBDA remained in solution. The trans form is more desirable as it gives more rigid polymers and, as the anhydride groups are on opposite sides of the cyclobutane ring, better polymerizability due to decreased steric interactions. Further references to CBDA will strictly refer to the trans isomer. Also noteworthy is that the [2+2] cycloaddition used to form the cyclobutane ring is reversible. UV light used in the reaction must be filtered to remove shorter wavelengths to suppress the electrocyclic ring-opening reverse reaction, and Pyrex glass effectively filters those wavelengths, giving much improved yields over quartz.[214] Indeed, the electrocyclic ring opening reaction has even been used to pattern CBDA containing polyimides as the polymer is cleaved by deep UV light.[225, 228] While we were able to synthesize CBDA at UT, the reaction is very long with our weak light sources and only generated a few grams of product after days of continuous UV exposure. Eventually, a collaboration with Nissan Chemical Industries provided us with large quantities of this valuable monomer.

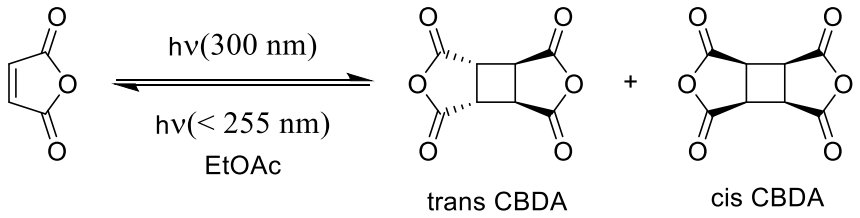

Figure 4.12: Synthesis of CBDA

Attempts to prepare the analogous ethyl ester monomer of trans CBDA were unsuccessful. When refluxed in an alcohol, a mixture of 3 products is produced: the 1,3 compound as well as both enantiomers of the 1,2 product (Figure 4.13). The resulting crude mixture could not be separated easily; attempted fractional crystallizations only resulted in oils. Polymerization of the crude acid chloride mixtures with TFMB resulted in low molecular polymers that were somewhat soluble in methanol. However, the separation of the dimethyl esters has been reported, so polymers of this material were prepared instead.[229]

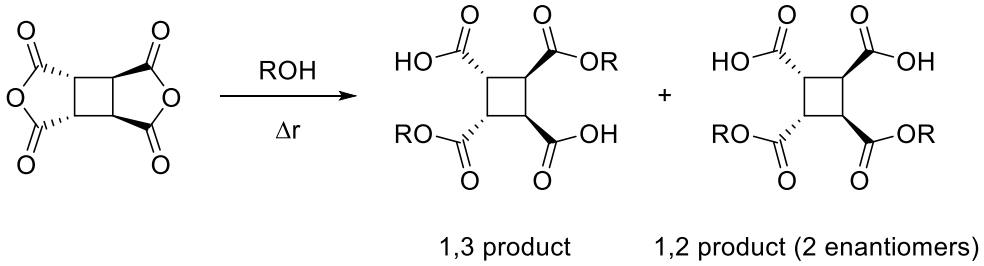

Figure 4.13: Isomeric products of CBDA alcoholysis

However, the dimethyl ester polymer of CBDA-TFMB (CBDA-TFMB-ME) was also soluble in MeOH and most other common solvents with the exceptions of water and hydrocarbons. The UV spectrum of a film of CBDA-TFMB-ME is shown in Figure 4.14, and it appears to be basically identical to the fully cured film meaning that CTCs have been eliminated in this system. This ester polymer is transparent down to about 340 nm, so there will not be optical density problems due to the matrix resin for photoresists utilizing this polymer. We attempted patterning of this material using a 5wt% NVOC piperidine PBG loading in CBDA-TFMB-ME using a 1.5 J/cm^2 broadband UV exposure and post exposure baking for 10 minutes at 160°C, similar conditions to PMDA-TFMB-EE printing. However, we were unable to find a developer for this system. All solutions

we attempted would either clear both exposed and unexposed regions, clear neither, or give scummy residues, likely due to significant swelling.

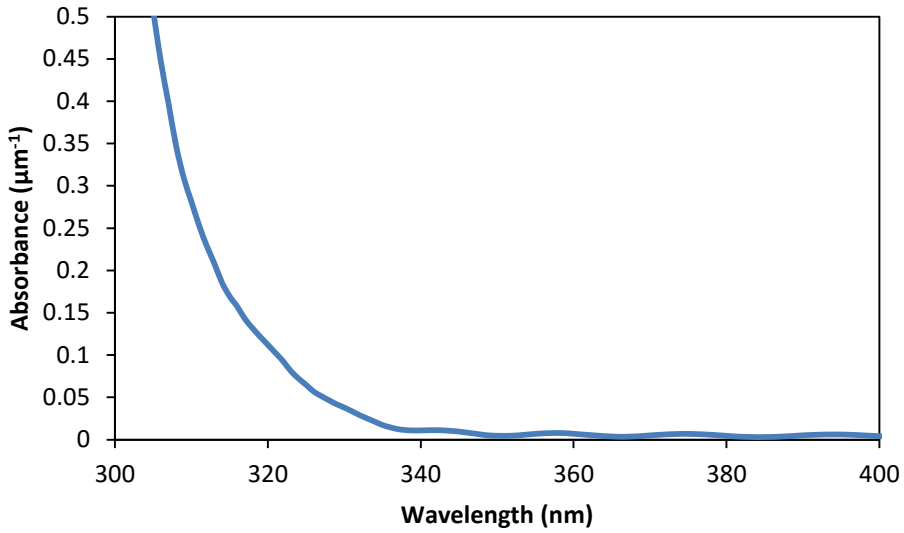

Figure 4.14: UV-Vis spectrum of CBDA-TFMB-ME

At first we thought the poor contrast was due to a poor solubility difference between the ester and imide forms. To confirm that the NVOC PBG was indeed imidizing the CBDA-TFMB-ME resist, we tracked the curing by IR spectroscopy (Figure 4.15). The bands of interest in this system lie at 1780 and 1370 cm^{-1}, and are shown magnified in Figure 4.16. These correspond to the imide carbonyl asymmetrical stretch and the C-N imide stretch, respectively. When comparing the exposed and unexposed films, there was no change upon UV exposure. There was also no noticeable imide carbonyl stretch nor C-N stretch whatsoever in the exposed films. While the imide carbonyl stretch is weak even in fully cure films (blue traces), the C-N stretch is quite prominent and shows that the NVOC PBG does not cause imidization in this system.

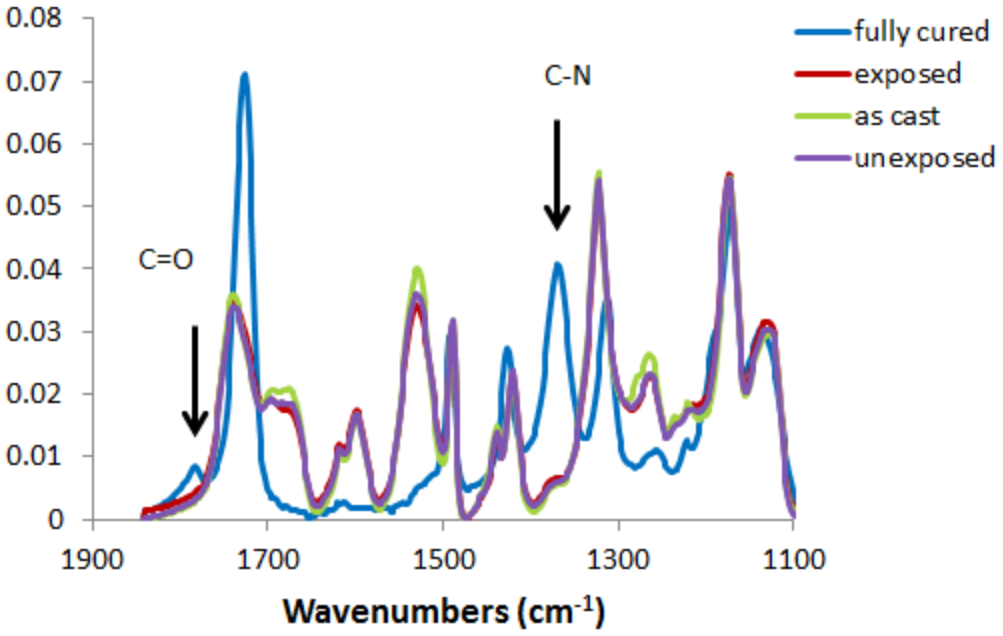

Figure 4.15: IR spectra of 5wt% NVOC PBG/CBDA-TFMB-ME system. Films were exposed to 1.5J/cm^2 broadband UV and PEB at 160°C for 10 min.

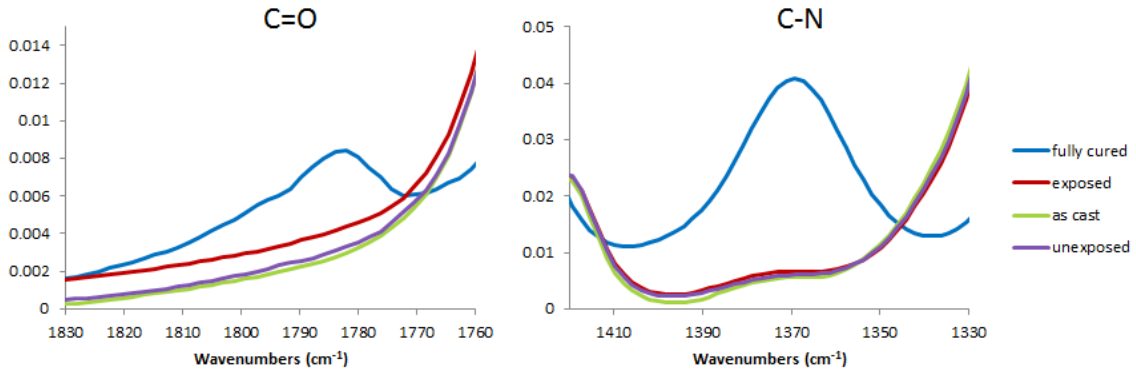

Figure 4.16: Magnified view of IR spectra of CBDA-TFMB-ME during patterning

As mentioned previously, CBDA polymers have been photo-patterned before, but only by the electrocylic ring opening reaction of the cyclobutane ring.[225, 230] Even preparing CBDA containing PAE is quite rare in the literature and almost exclusively as patents by Nissan Chemical Industries. Even then, their objective was for liquid crystal

alignment layers for improved storage stability over the PAA, and not as a method for patterning.[231-237] Also, unlike in the case of PMDA, there has been no equivalent kinetic study to measure the effect of amine bases on the imidization rate of amic ester model compounds.[124-125] To test the imidization model compounds **4.1a** and **4.1b** where prepared, as shown in Figure 4.17.

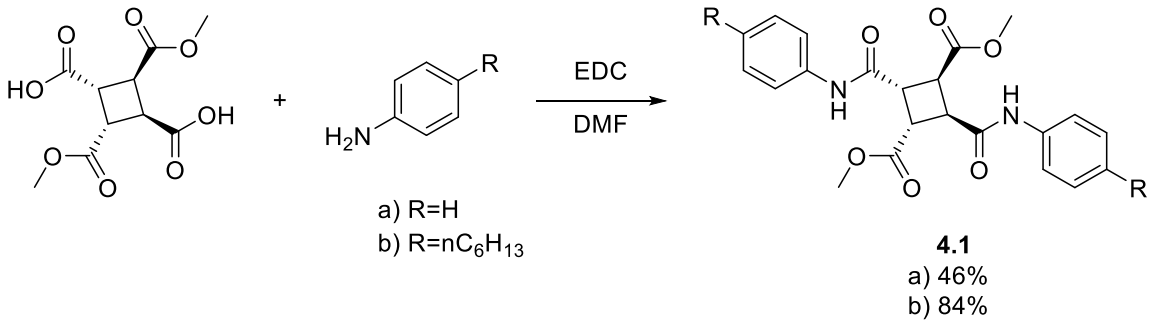

Figure 4.17: Synthesis of CBDA ester model compounds

EDC coupling was found to effectively couple both aniline and 4 n-hexylaniline to the CBDA diacid in moderate to good yields. The lower yield in the unsubstituted aniline version was likely caused by the relatively poor solubility of the intermediate mono-amide product, so a more soluble version with pendant hexyl groups was also prepared. From the base catalyzed mechanism (recall chapter 3), the reaction is assumed to be first order in both the CBDA diester diamide as well as the base.[125] However, since the reaction is catalytic in base, the base concentration remains constant and the overall reaction is pseudo-first order. ^{1}HNMR was chosen to monitor the reaction as the by-product methanol peak should not overlap with the starting material. DMSO-d6 was chosen as the solvent as it is a polar aprotic solvent like NMP or DMF, but is orders of magnitude less expensive than deuterated versions of those solvents. The unsubstituted aniline version was first tested with piperidine as the base (the amine generated in our

standard NVOC and cinnamide PBGs). The experiment was run at 15mg/mL of **4.1a** with 2 equivalents of piperidine. The reaction was quite slow and ^{1}HNMR spectra began to broaden considerably after a few hours, which was confirmed to be due to material precipitating out of solution. The hexyl version was also tried and found to remain in solution long enough to collect kinetic data (Figure 4.18). Figure 4.19 shows the plot of ln(concentration **4.1b**) vs. time. The straight line fit confirms that the reaction is pseudo-first order and gives the rate constant as 5.80×10^{-5} M^{-1} s^{-1}. This value is orders of magnitude slower than reported for n-butyl phthalamate with piperidine (1.8×10^{-3} M^{-1} s^{-1}).[125] It is likely that the imidization reaction is just too slow to print patterns in CBDA-TFMB-ME in only the few minutes allowed for baking, and thus this approach is not a viable solution for patterning. The experiment was also attempted using DBU instead of piperidine. However, the reaction proceeded too quickly and the insolubility of the resulting di-imide prevented quantitative data from being obtained. This means that a PBG generating an amidine or guanidine base may be able to photo-pattern thick CBDA-TFMB films. The search for such a suitable base generator is the subject of Chapter 6.

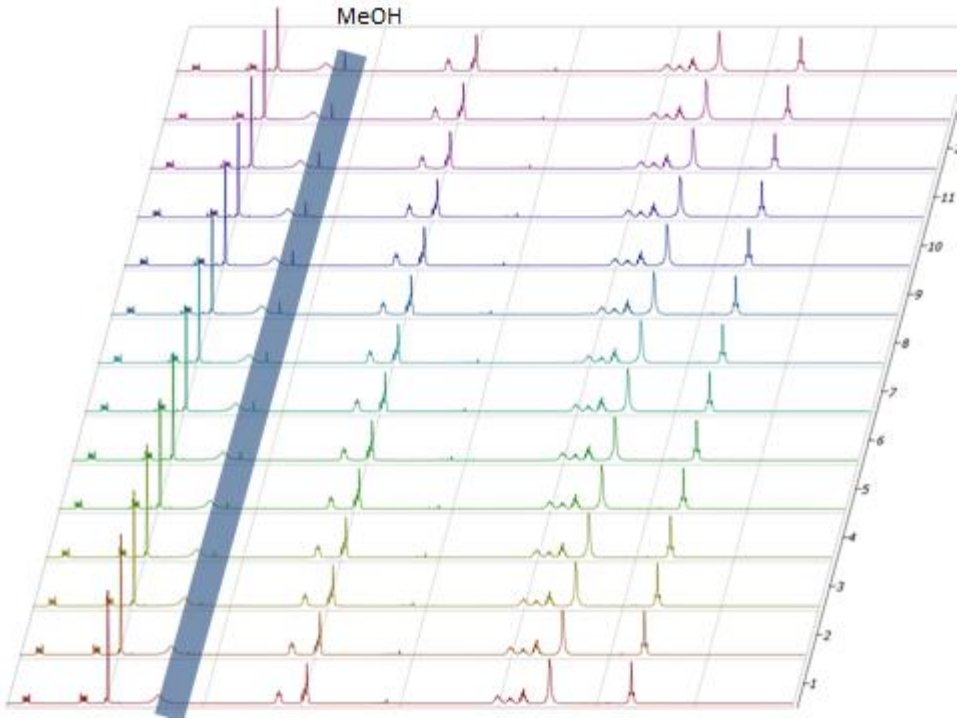

Figure 4.18: NMR spectra of **4.1b** reaction with piperidine in DMSO. The methanol peak formed is highlighted in blue.

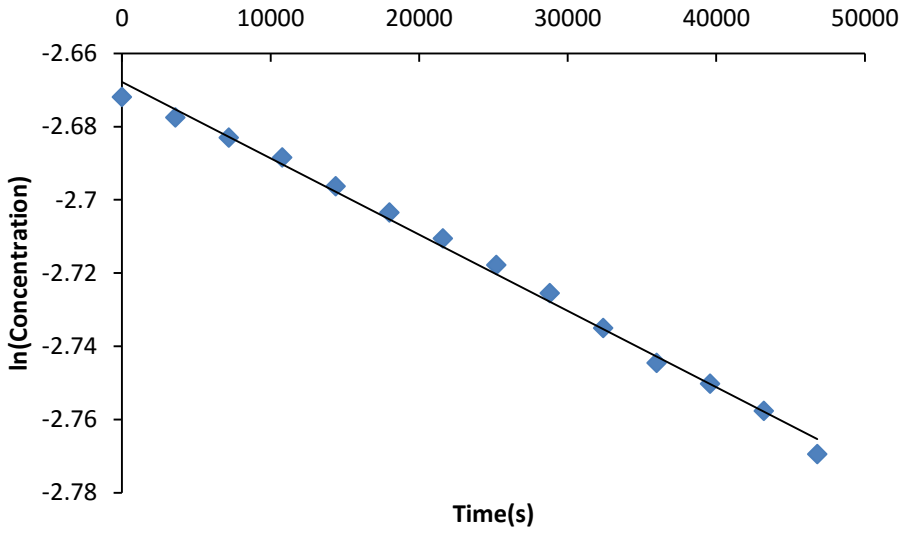

Figure 4.19: Kinetics of **4.1b** and piperidine in DMSO

POSITIVE TONE CBDA-TFMB

As the base catalyzed imidization reaction did not generate enough contrast for printing, other methods for patterning CBDA that relied on different mechanisms were considered.

The first new method considered was preparing a t-butyl ester CBDA polymer to act as a positive tone resist, analogous to our attempts at the PMDA version. While the PMDA-TFMB ester polymers did not print images, they did appear to be acid sensitive. Also, while those polymers were only soluble in amide solvents, the previously discussed CBDA methyl ester polymers were soluble in a wide range of organic solvents. We reasoned that if ran the polymerization in a non-amide solvent, there would not be trace amounts of weakly basic impurities affecting the acid catalyzed t-butyl ester cleavage.

While there are no reports of the t-butyl ester in the literature, it seemed reasonable that the ester could be prepared using CBDA and KOtBu similarly to the PMDA version (Figure 4.20).[197]

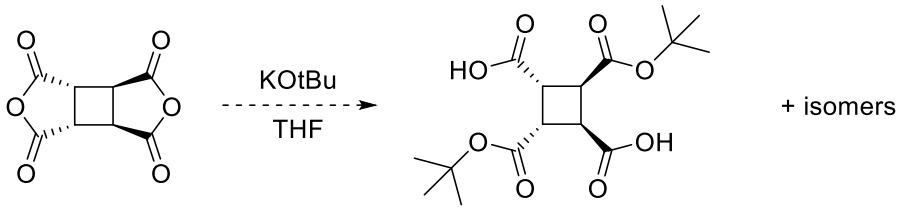

Figure 4.20: Proposed synthesis of CBDA t-Bu esters

However, a THF solution of KOtBu and CBDA just turned bright orange and did not produce a precipitate of the potassium salt. This may be due to the alpha protons present in CBDA that are not in aromatic anhydrides such as PMDA. The pKa of tBuOH in DMSO is 32.2 and that of the alpha proton on a simple ester is 29.5 (EtOAc).[238] The alpha protons in CBDA are likely to be even more acidic than this due to the more electron-withdrawing anhydride. Additionally, each alpha carbon is in the beta position

relative to two other carbonyls, likely further increasing acidity. As the pKa values are at least 3 units different, deprotonated CBDA should be the favored anion in a solution of KOtBu. Combined with the poor nucleophility of KOtBu, formation of the t-butyl ester did not occur. Simply refluxing CBDA in tBuOH for days resulted in no reaction. No reaction occurred using tBuOH and TEA in DCM either, which is useful for synthesizing other hard to prepare esters from anhydrides.[164]

A hexafluoroisopropyl ester derivative of CBDA was also considered with the idea being that a better leaving group could speed up the kinetics of base catalyzed imidization.[59, 125] We believe that we were able to prepare the ester by using TEA and hexafluoroisopropanol in methyl ethyl ketone. However, this ester is quite unstable and by NMR appeared to convert back to CBDA in a matter of days, rendering it unsuitable for use in polymers.

NEW RIGID FLUORINATED DIAMINES

Due to the problems encountered with the base catalyzed imidization reaction in CBDA, an aromatic dianhydride was considered again. However, the material must still be transparent to the exposure wavelength. While such PIs are reported in the literature, most are prepared from flexible dianhydrides and diamines or have meta linkages instead of para ones.[239] In general most tend to have large CTEs and water absorption just as large as traditional PIs. One method of lowering water absorption is to incorporate ester groups in so called poly(ester imides). The use of aromatic ester containing diamines also results in very low CTE when used with dianhydrides such as PMDA and BPDA.[240-242] One diamine in particular, (4-aminophenyl)-4′-aminobenzoate (APAB), forms polymers with properties very close to the required properties.[101, 241] While there are various reports

of alkyl derivatives of this monomer, there is no report in the literature of a fluorinated version.

As shown in figure 4.21, APAB is an asymmetrical diamine containing two different aromatic rings. The aminophenol side is much more electron rich than the aminobenzoate side. Additionally, each ring contains two unique places where fluorine could be added, for a total of four possible places for substitution. As one of the goals is high transparency, reduction of electron density on the electron rich phenol side was predicted to have a greater effect. On this ring the substitution can either be ortho or meta to the amino group. Work at IBM showed that there is a very large steric effect for trifluoromethyl groups on polymerizability in PAA systems.[148] Ortho trifluoromethyl substitution greatly hinders polymerizability and results in only oligomers while meta substitution still allows for viscous, high molecular weight solutions. Combining these ideas, it was hypothesized that 4-amino-2-(trifluoromethyl)phenyl 4-aminobenzoate (3FAPAB) and 4-amino-2,6-bis(trifluoromethyl)phenyl 4-aminobenzoate (6FAPAB) would form PI that are transparent, low CTE, low dielectric and low water absorption. The UV spectra of each of the compounds was then predicted using density functional theory (DFT) using Spartan software with the standard B3LYP/6-31G* model[243-246], and shown in Figure 4.21. The modeling predicts that both fluorinated APAB derivatives should have similar i-line absorbance to TFMB and will likely form transparent PIs, depending on the particular dianhydride utilized.

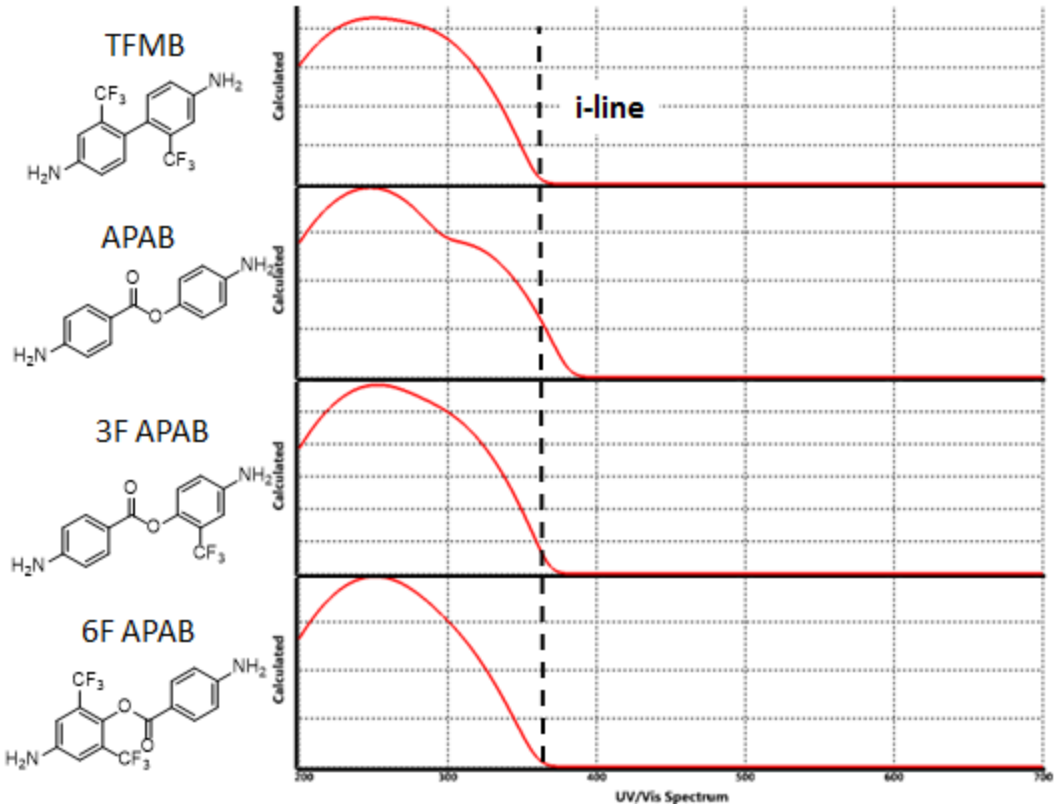

Figure 4.21: Predicted UV-Vis Spectra of APAB derivatives

The manufacture of APAB (**4.4a**) is straightforward and performed on large scale in industrial labs. A typical scheme employed is shown in Figure 4.22.[247] Other methods involve different activations of the carboxylic acid, but almost all perform a catalytic hydrogenation step to reduce the intermediate dinitro compound to the diamine.[248] Typical isolated yields of the diamine are about 75% after two steps.

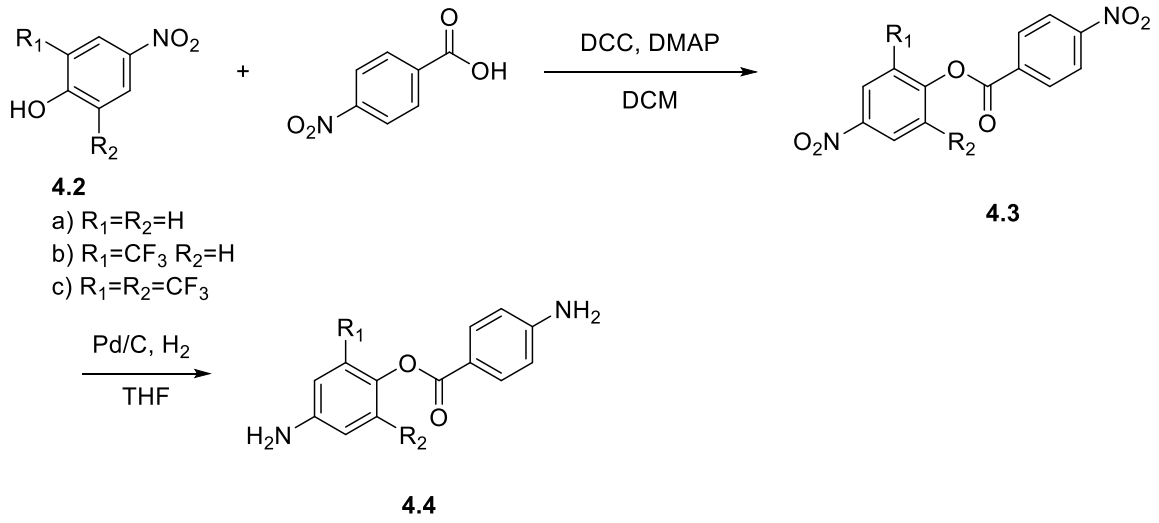

Figure 4.22: Commercial APAB synthesis route

A similar synthetic approach was envisioned for producing fluorinated APAB derivatives. However, 4-nitro-2,6-bis(trifluoromethyl)phenol (**4.2c**) is not even a known compound, though the methyl ether has been prepared.[249] While 4-nitro-2-trifluromethylphenol is available from a few sources, it is impractically expensive to use as a monomer. The simplest way reported of making the phenol involves Lewis acid catalyzed cleavage of the corresponding methyl ether. Simply refluxing the methyl ether in LiCl in DMF gives the deprotected phenol.[250-251] However, after attempting this reaction multiple times, the result always produced a black intractable tar with low yield of the phenol and a painful chromatographic separation. This led to the exploration of different synthetic routes.

Another method starts from inexpensive and widely available chlorobenzene as shown in Figure 4.23.[252-253] This route is quite attractive in that the starting material is inexpensive and the solvent and base are essentially free. When performing this reaction however, the 1:1 adduct of the product with DMSO appears to be the major product by

^{1}H NMR. Yields were also fairly poor at about 40% after distillation. These results are consistent with the literature where the both the free phenol and the adduct can form.[252] This adduct has an incredibly strong and unpleasant sulfur smell, and the reactivity was quite different than the unsubstituted 4-nitrophenol.

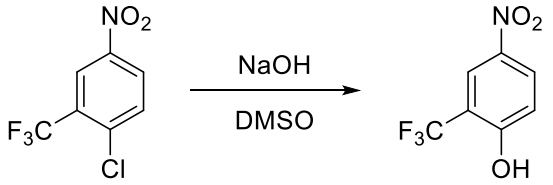

Figure 4.23: Nucleophilic aryl substitution route to 3FAPAB

The only reaction path that seemed to produce the deprotected phenol in high yield and not as a solvent adduct was refluxing the methyl ether in HBr/AcOH.[254] Here the HBr protonates the ether oxygen and the bromide attacks the methyl group, producing free phenol and gaseous methyl bromide as a side product. While the yield was not quantitative, no side products were detected by thin layer chromatography (TLC). Additionally, the starting material is not soluble in the reaction solvent at room temperature and precipitates out of solution, leaving the nearly pure phenol in solution which can be isolated in pure form by simple extraction.

For the acylation reaction to **4.3b**, the commercially available acid chloride 4-nitrobenzoyl chloride was used instead of activing the carboxylic acid in situ. Deprotonating **4.2b** with NaH in THF and then adding the benzoyl chloride gave **4.3b** in excellent yields.

The reduction of **4.3b** to **4.4b**, however, proved much more challenging. Using the same catalytic hydrogenation conditions as for in standard APAB[248] resulted in a

mixture of products by TLC. At first this was thought to just be the intermediate half-nitro, half amines generated. This was supported by the rapid consumption of starting material and all of the products staining with ninhydrin (a stain selective for amines). However, after a few hours the TLC no longer changed, and it is likely that some of the spots were hydrolysis products that were also eventually converted to amines. An older method for reducing aromatic nitro groups is $SnCl_2$, and this method was used to produce APAB in one of the earliest papers using the monomer.[255] However, this method used HCl as the solvent, and would likely hydrolyze **4.3b** as well. Instead 10 equivalents of $SnCl_2 \cdot 2H_2O$ in refluxing EtOH was used.[256] This modification is known to leave more sensitive groups such as aldehydes, ketones, halides, and benzyl and cyano groups intact.[256] The reaction completed in only 30 min with 93% yield. The retention factor was also different than the major product in the catalytic hydrogenation, confirming starting material degradation under catalytic hydrogenation conditions.

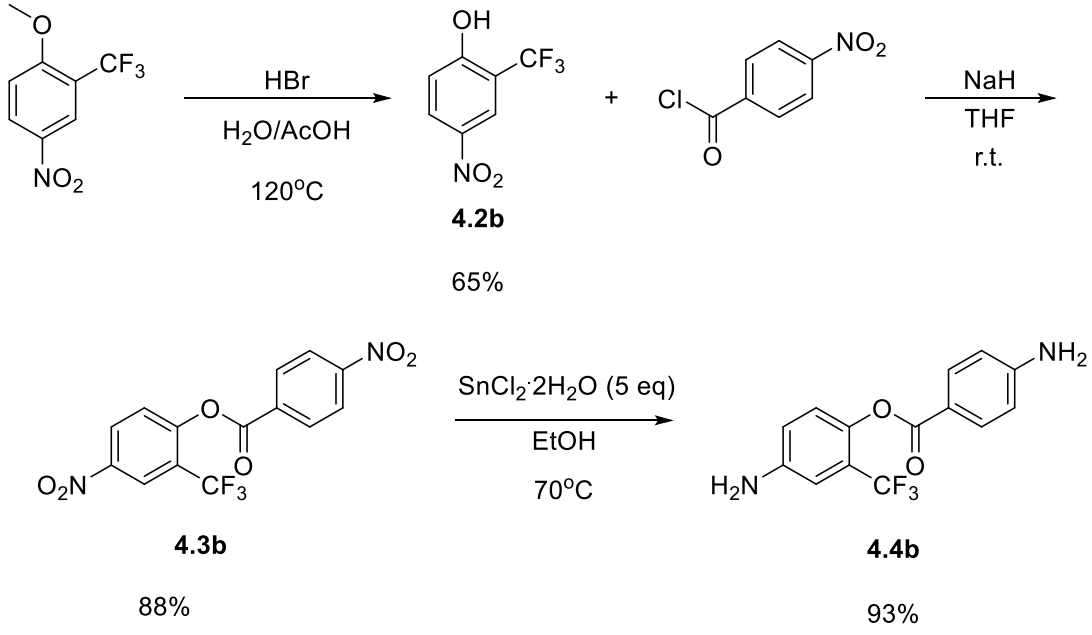

Figure 4.24: Synthesis scheme for 3FAPAB

As stated previously, a synthetic path to 6F-APAB was complicated by there being no literature reports of the synthesis of **4.4c**. However, various ethers have been prepared using metal alkoxides and halobenzenes in a manner similar to the NaOH/DMSO method used above for **1b**.[257-258] Reported yields for these reactions are much higher than in the mono trifluoromethyl version, likely due to the even greater electron deficiency of the system. However, this route would also require an ether deprotection and the analogous halobenzene starting material is not even commercially available. Another route to **4.2b** involving the direct hydroxylation of nitroarenes has been reported.[259-260] This method was not utilized for 3F-APAB due to the liquid ammonia and organic peroxides required, as many other routes were already published that required much milder conditions. However, this is not the case for compound **4.2c**. Reaction of 3,5 bis(trifluoromethyl)nitrobenzene with KOH and cumene hydroperoxide in liquid ammonia gave phenol **4.2c** in 63% yield after sublimation (Figure 4.25).

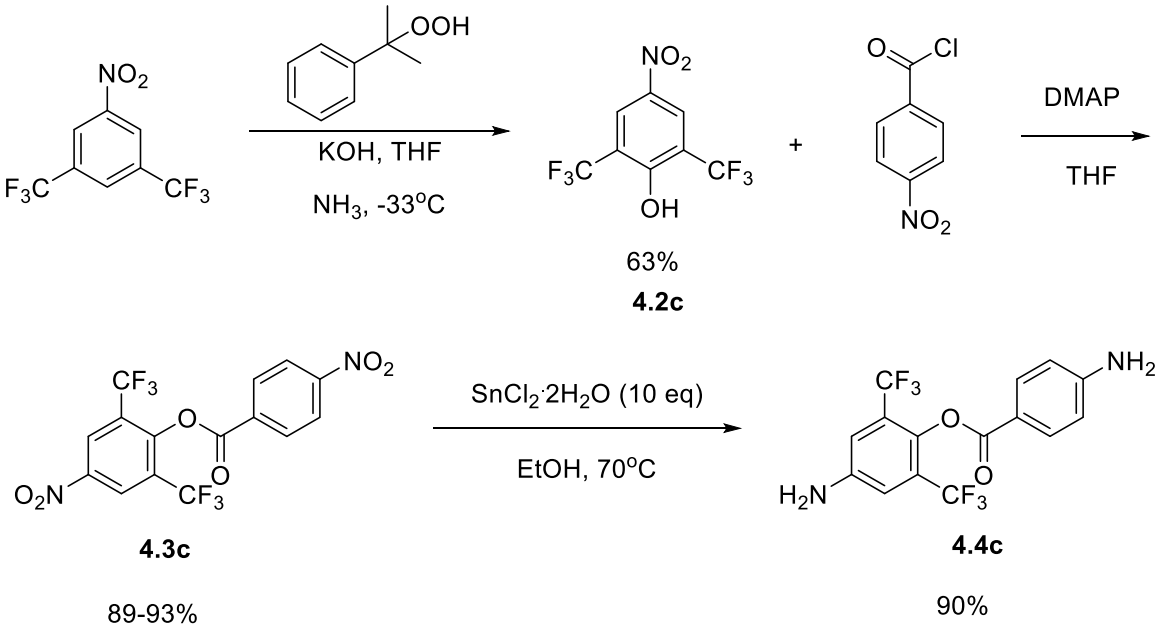

Figure 4.25: continued next page.

Figure 4.25: Synthesis scheme for 6FAPAB

Attempts to run a similar deprotonation and reaction with 4-nitrobenzoyl chloride on **4.2c** as in **4.2b** did not proceed to completion, even upon heating. This is likely due to a combination of both steric and electronic effects. The phenolate anion is sterically hindered by the ortho trifluoromethyl groups on either side. Additionally, nitro and trifluoromethyl groups are extremely electron withdrawing and result in this phenolate anion being a particularly weak nucleophile. However, reaction of **4.2c** with nitrobenzoyl chloride with one equivalent of DMAP as a catalyst gave **4.3c** in excellent yield in minutes in THF. Finally, the reduction to **4.4c** using $SnCl_2$ in EtOH also proceeded smoothly in 90% yield.

The polymerization of 3FAPAB with both CBDA and PMDA proceeded smoothly in both cases, giving viscous poly(amic acid) solutions in NMP. However, 6FAPAB was not very reactive toward either dianhydride and polymer solutions were about as viscous as NMP itself, even at high solids loadings. Whereas both 3FAPAB polymers spin-coated nicely to create thin transparent films, 6FAPAB polymers produced cloudy white films. These films were similar to the para PMDA-TFMB films discussed earlier and may also be due to the crystallinity of the precursor polymer. Upon curing at 350°C both CBDA-6FAPAB and PMDA-6FAPAB gave cloudy, slightly yellow, and very brittle films that disintegrated upon cooling. The corresponding 3FAPAB films were also slightly yellow, but much less brittle and remained films after curing. The UV-Vis spectra of the films, along with TFMB versions for comparison, is located in Figure 4.26.

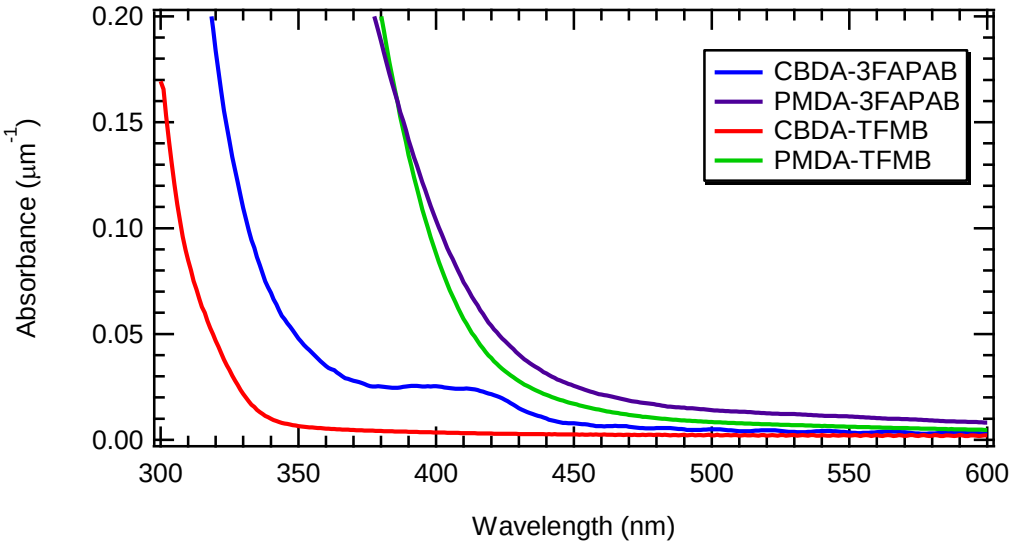

Figure 4.26: UV-Vis spectra of cured 3FAPAB and TFMB polymers

As can be seen from the UV-spectra, these new fluorinated polyimides still demonstrate significant charge transfer. The UV cutoff for PMDA-3FAPAB is essentially the same as PMDA-TFMB while the CBDA-3FAPAB polymer has significantly higher absorbance. Ultimately however, the ability to effectively pattern CBDA containing polyimides has eluded us and unfortunately these new monomers do not exhibit greatly improved material properties over PMDA-TFMB or CBDA-TFMB.

CONCLUSIONS

Four alternative methods to create PSPIs with improved performance over the mPMDA-TFMB-EE system were explored. These included a positive tone t-butyl ester polymer, BPDA based polymers, CBDA based polymers, and new fluorinated aminophenyl-aminobenzoate polymers. While the t-butyl polymers were found to be acid sensitive, attempts to pattern this polymer using PAGs was unsuccessful. BPDA polymers were found to have lower UV absorbance than PMDA based polymers.

However, these materials were much harder to purify and produced only low molecular weight polymers that cracked during organic development. CBDA based polymers had complete i-line transparency, even after curing. However, kinetic studies showed that these materials were not patternable using a PAE/PBG based approach. Finally, new fluorinated monomers were prepared based on their predicted UV transparency. While we were able to synthesize the monomers, the 6FAPAB monomer is thermally unstable and not very reactive toward polymerization. 3FAPAB had good reactivity with both PMDA and CBDA, but did not result in a markedly different UV spectrum compared to PMDA-TFMB.

Overall, despite exploring many alternative methods to improve on our mPMDA-TFMB-EE resin, we were unable to find a better platform. None of the materials tested exhibited both improved i-line transmittance and pattern-ability compared with the initial system.

EXPERIMENTAL

General Methods

All solvents and regents were obtained from commercial sources and used as received, unless otherwise specified. DCM was distilled from CaH_2 while THF and DMF were purified by eluting through an alumina column solvent delivery system under argon. NMP was vacuum distilled from P_2O_5. CBDA was donated by Nissan Chemical Company and was dried at 150°C in vacuum for 12 hours prior to use. TFMB monomer was purified by sublimation to remove colored impurities. TFMOB was supplied by Seika Wakayama. Reactions were run in flame-dried glassware and under nitrogen atmosphere, expect where noted. ^{1}H and ^{13}C NMR spectra were obtained on a Varian

Unity Plus 400 MHz instrument. Solvent proton peaks are used as the internal standard ($CDCl_3$ ^1H 7.26 ppm, ^{13}C 77.0 ppm; DMSO-d6 ^1H 2.49 ppm, ^{13}C 39.5 ppm). HRMS (CI) was performed on a VG analytical ZAB2-E instrument and HRMS (ESI) on an Ion Spec FT-ICR instrument. All MS data was obtained by ESI unless otherwise specified. IR spectroscopy was performed using a ThermoSci Nicolet 6700 FT-IR in transmission mode for films on double-side polished silicon wafers. UV-visible spectra of thin films on quartz were obtained using a ThermoSci Evolution 220 UV-visible spectrometer.

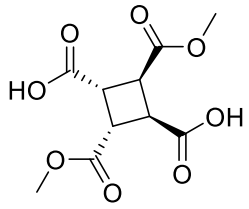

(1R, 2R, 3S, 4S)-2,4-bis(methoxycarbonyl)cyclobutane-1,3-dicarboxylic acid (DM-CBDA)[229]

CBDA (20.0g, 102 mmol) was refluxed overnight in 100 mL MeOH. After completion of the reaction, the solution was concentrated in vacuum to obtain a white sticky solid. The crude mixture of isomers was then recrystallized from 1:9 cyclohexane: EtOAc to obtain the 1,3 isomer as a white crystalline solid (9.89g, 37%). Mp 179-181°C. ^1H NMR (400 MHz, acetone) δ 3.72 (s, 4H), 3.66 (s, 6H). ^{13}C NMR (101 MHz, acetone) δ 172.2, 172.1, 52.3, 41.7, 41.4. HRMS $[M+Na]^+$ calc. 283.0424 found 283.0429

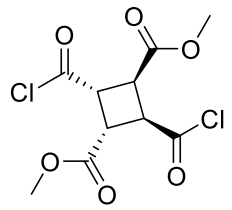

Dimethyl (1R, 2R, 3S, 4S)-2,4-bis(chlorocarbonyl)cyclobutane-1,3-dicarboxylate

In a 250 mL RBF with a condenser, DM-CBDA (9.81g, 37.7 mmol) was suspended in 100 mL of EtOAc. 5 drops of DMF were added and then oxalyl chloride (9.7 mL, 113.1 mmol, 3 eq) was added in small portions through the condenser. CAUTION! THE SOLUTION BUBBLES VIGOUROUSLY AND PRODUCES LARGE VOLUMES OF HCL, CO_2, AND CO! After bubbling ceased, all of the solid starting material dissolved and the solution became clear and colorless. The solution was concentrated to remove solvent and excess oxalyl chloride and recrystallized from hexanes (~600 mL) to obtain the product as white needles (8.42g, 75%) ^{1}H NMR (400 MHz, $CDCl_3$) δ 4.11 – 4.06 (m, 2H), 4.00 – 3.94 (m, 2H), 3.80 (s, 6H). ^{13}C NMR (101 MHz, $CDCl_3$) δ 171.2, 169.4, 53.3, 49.9, 42.7. HRMS $[M\text{-}Cl]^-$ calcd. 261.0166 found 261.0163

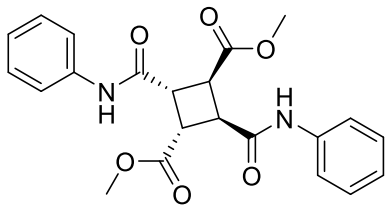

Dimethyl (1R, 2R, 3S, 4S)-2,4-bis(phenylcarbamoyl)cyclobutane-1,3-dicarboxylate (4.1a)

DM-CBDA, (0.623g, 2.39 mmol) and aniline (0.44 mL, 4.8 mmol) were dissolved in 10 mL DMF in a 50 mL RBF under nitrogen. EDC (0.918g, 4.8 mmol) was then added as a solid in one portion. The initially cloudy solution cleared to form a pale yellow solution. After stirring overnight the solution was poured into 200 mL of water, filtered, and

washed with water. The precipitated white solid was then dried in vacuum to obtain a white solid (0.452g, 46%). mp > 300°C. ^{1}H NMR (400 MHz, DMSO) δ 10.20 (s, 2H), 7.55 (d, *J* = 8.3 Hz, 4H), 7.29 (t, *J* = 7.8 Hz, 4H), 7.04 (t, *J* = 7.4 Hz, 2H), 3.93 (dd, *J* = 10.2, 6.6 Hz, 2H), 3.64 (dd, *J* = 9.9, 6.9 Hz, 2H), 3.49 (s, *J* = 4.7 Hz, 6H). ^{13}C NMR (101 MHz, DMSO) δ 171.6, 169.2, 139.3, 129.2, 123.9, 119.7, 52.2, 49.0, 42.9. HRMS $[M+Na]^{+}$ calcd. 433.1370 found 433.1372

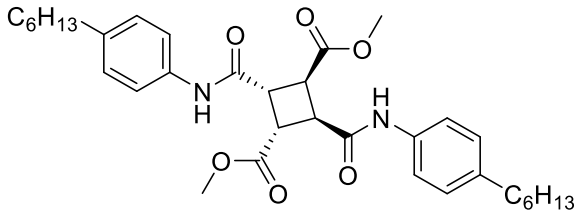

Dimethyl (1R, 2R, 3S, 4S)-2,4-bis((4-hexylphenyl)carbamoyl)cyclobutane-1,3-dicarboxylate (4.1b)

Prepared similarly to 4.1a in 84% yield as a white powder. Analytical samples were obtained by recrystallization from EtOAc:hexanes. mp > 300°C. ^{1}H NMR (400 MHz, DMSO) δ 10.10 (s, 2H), 7.45 – 7.42 (m, 4H), 7.09 (d, *J* = 8.5 Hz, 4H), 3.94 – 3.86 (m, 2H), 3.64 – 3.57 (m, 2H), 3.49 (s, *J* = 4.3 Hz, 4H), 1.55 – 1.46 (m, 4H), 1.24 (br, 12H), 0.87 – 0.78 (m, 6H). An additional peak for the benzylic protons overlaps with the solvent δ 2.50 (t, 4H). ^{13}C NMR (101 MHz, DMSO) δ 171.7, 169.0, 137.9, 137.0, 128.9, 119.8, 52.2, 42.9, 40.3, 35.0, 31.6, 31.4, 28.7, 22.5, 14.4. HRMS $[M+H]^{+}$ calcd. 579.3429 found 579.3430

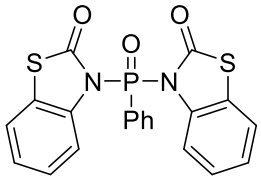

3,3'-(phenylphosphoryl)bis(benzo[d]thiazol-2(3H)-one) (PPBT)[201]

Benzo[d]thiazol-2(3H)-one (5.53 g, 30 mmol) was dissolved in 12 mL ACN in a 100 mL RBF. TEA (8.4 mL, 60 mmol) was added to the solution and it was cooled to 0°C. Phenylphosphonic dichloride (2.98 g, 15 mmol) in 12 mL of ACN was then added dropwise to the thiazolone solution. After complete addition, the reaction was stirred for 30 minutes. The precipitated white solid was filtered, washed with water and recrystallized from benzene. (2.82 g, 43%) mp 110-116°C. ^{1}H NMR (400 MHz, $CDCl_3$) δ 8.10 – 8.00 (m, 2H), 7.91 – 7.84 (m, 2H), 7.74 – 7.66 (m, 1H), 7.60 – 7.51 (m, 2H), 7.43 – 7.37 (m, 2H), 7.25 – 7.18 (m, 4H). HRMS $[M+Na]^+$ calcd. 446.9997 found 447.0002

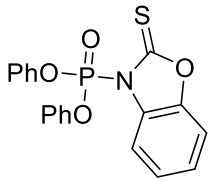

Diphenyl (2-thioxobenzo[d]oxazol-3(2H)-yl)phosphonate (DBOP)[202]

2-Benzoxazolethione (20.0g, 132 mmol) was suspended in 150 mL benzene in a 500 mL RBF with an addition funnel. TEA (18.5 mL, 132 mmol) was added slowly to form a dark solution. Diphenyl phosphorochloridate (27.4 mL, 132 mmol) was dissolved in 45 mL benzene and added to the addition funnel and added dropwise over 25 minutes. The precipitated salt was filtered and the filtrate concentrated in vacuum. The resulting black tar was recrystallized twice from hexanes to obtain slightly off-white crystals (30%). Mp 136-140°C. ^{1}H NMR (400 MHz, $CDCl_3$) δ 7.95 – 7.88 (m, 1H), 7.42 – 7.29 (m, 8H), 7.28 – 7.17 (m, 5H). ^{13}C NMR (101 MHz, $CDCl_3$) δ 180.4 (d), 149.6 (d), 147.7 (d), 132.1 (d),

130.2, 126.4, 125.6 (d), 120.4 (d), 115.0, 110.0. HRMS $[M+H]^+$ calcd. 384.0540 found 384.0444

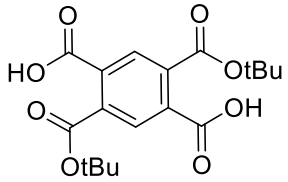

t-Butyl ester isomers of PMDA[197]

PMDA (40.0 g, 183 mmol) was dissolved in 800 mL THF in a 2L RBF with mechanical stirring. KOtBu (41.2 g, 367 mmol) was then added slowly with vigorous stirring to the PMDA solution. Stirring was continued overnight, and then the precipitated potassium salts were filtered and washed with THF. The precipitate was then dissolved in 1L of water and adjusted to pH 3 with HCl. The precipitated solid was then filtered and washed with water before being recrystallized from EtOH/water. The first crop yielded pure para isomer (25.0 g, 37%) and the second crop gave a mixture of about 80:20% meta:para isomer (8.2 g, 12%). HRMS $[M+Na]^+$ calcd. 389.1207 found 389.1203

2,5-bis(tert-butoxycarbonyl)terephthalic acid (para)

^{1}H NMR (400 MHz, DMSO) δ 13.73 (br s, 2H), 7.87 (s, 2H), 1.51 (s, 18H). ^{13}C NMR (101 MHz, DMSO) δ 167.1, 165.2, 135.1, 134.5, 128.6, 82.7, 27.5.

4,6-bis(tert-butoxycarbonyl)isophthalic acid (meta)

^{1}H NMR (400 MHz, DMSO) δ 13.73 (br s, 2H), 8.00 (s, 1H), 7.77 (s, 1H), 1.51 (s, 18H). ^{13}C NMR (101 MHz, DMSO) δ 167.0, 165.4, 135.8, 133.8, 129.2, 128.0, 82.7, 27.5.

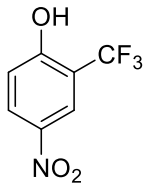

4-nitro-2-(trifluoromethyl)phenol (4.2b)[254]

A 500 mL RBF with reflux condenser was charged with 28.38 g (128.3 mmol) of 1-methoxy-4-nitro-2-(trifluoromethyl)benzene. 180 mL of 48% HBr and 90 mL of 30% HBr/AcOH was added. The solution was then refluxed at 120°C for 2 days. The solution was cooled to room temperature and quenched with water to precipitate unreacted starting material, which was filtered off. The aqueous solution was extracted five times with DCM, washed with brine, and then dried over $MgSO_4$, filtered and concentrated to obtain an off white crystalline solid. (17.36 g, 65%) Additionally, 7.94g (28%) of starting material was recovered. ^{1}H NMR (400 MHz, DMSO) δ 12.29 (s, 1H), 8.30 (dd, J = 9.1, 2.9 Hz, 1H), 8.24 (d, J = 2.8 Hz, 1H), 7.15 (d, J = 9.1 Hz, 1H); ^{13}C NMR (101 MHz, DMSO) δ 162.2, 139.1, 130.0, 123.6 (q, J = 5.4 Hz), 123.1 (q, J = 272.5 Hz), 118.1, 116.1 (q, J = 31.7 Hz); HRMS $[M+H]^+$ calcd. 208.0216 found 208.0216

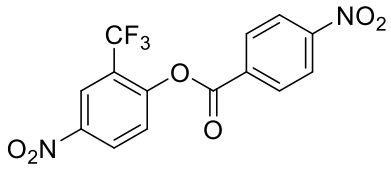

4-nitro-2-(trifluoromethyl)phenyl 4-nitrobenzoate (4.3b)

In a 250 mL RBF was added 5.00g (24.1 mmol) of **4.2b**. 150 mL of THF was added to obtain a pale yellow solution. NaH (1.01 g, 60% in mineral oil, 25.2 mmol) was added in 3 portions over 5 minutes. After gas evolution had ceased the solution was a clear brilliant yellow color. Solid 4-nitrobenzoyl chloride (4.48 g, 24.1 mmol) was then added in one portion and the solution quickly became pale and a precipitate began to form.

After 30 minutes the solvent was removed, the reaction was quenched with 100 mL of sat. aq. $NaHCO_3$ and extracted with DCM (3 X 100 mL). The DCM extracts were then washed with brine and dried over Na_2SO_4, filtered, and concentrated to obtain a slightly off-white solid. (88%) mp 107-108°C; ^{1}H NMR (400 MHz, DMSO) δ 8.70 (dd, *J* = 9.0, 2.8 Hz, 1H), 8.58 (d, *J* = 2.7 Hz, 1H), 8.49 – 8.42 (m, 2H), 8.39 – 8.33 (m, 2H), 8.06 (d, *J* = 9.0 Hz, 1H); ^{13}C NMR (101 MHz, DMSO) δ 162.4, 152.5, 151.5, 145.8, 133.3, 132.0, 130.0, 127.1, 124.8, 123.7, 123.4, 123.3, 122.9, 122.6, 121.0; HRMS (CI) $[M+H]^+$ calcd. 357.0334 found 357.0327

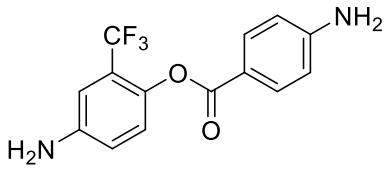

4-amino-2-(trifluoromethyl)phenyl 4-aminobenzoate (3FAPAB) (4.4c)

In 250 mL with reflux condenser, 4.88 g (13.7 mmol) **4.3b** and 30.9 g (137 mmol) $SnCl_2{\cdot}2H_2O$ were suspended in 54 mL EtOH. The mixture was heated to 70°C for 30 minutes. After the reaction was complete by TLC, the warm solution was poured into water and aq. NaOH was added until precipitated tin compounds were solubilized. The solution was then extracted three times with EtOAc, washed with brine, dried over Na_2SO_4, and concentrated to obtain a slight yellow powder. The powder was then recrystallized from EtOH to obtain slightly off white shiny flakes. (93%) R_f = 0.45 (50% EtOAc/hexanes); mp 186-188°C; ^{1}H NMR (400 MHz, DMSO) δ 7.76 – 7.66 (m, 2H), 7.02 (d, *J* = 8.8 Hz, 1H), 6.87 (d, *J* = 2.7 Hz, 1H), 6.80 (dd, *J* = 8.6, 2.6 Hz, 1H), 6.65 – 6.55 (m, 2H), 6.15 (s, 2H), 5.49 (s, 2H); ^{13}C NMR (101 MHz, DMSO) δ 165.1, 154.7,

147.2, 137.7, 132.3, 126.1, 125.2, 122.5, 122.2, 121.9, 118.1, 114.6, 113.2, 110.6; HRMS $[M+Na]^+$ calcd. 319.0665 found 319.0669

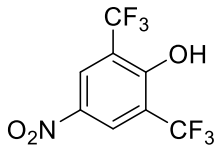

4-nitro-2,6-bis(trifluoromethyl)phenol (4.2c)

In a 3 neck 500 mL RBF with a dry ice/acetone cooled condenser and addition funnel was added 21.6 g (386 mmol) of powdered KOH. The flask and condenser were then cooled to -78°C using dry ice/acetone bath. Gaseous ammonia was then slowly flowed into the flask and condensed into about 130 mL of liquid. In a separate flask 10.0g (38.6 mmol) of 3,5-bis(trifluoromethyl)nitrobenzene, 8.10 g (42.5 mmol) of 80% cumene hydroperoxide and 39 mL of THF were thoroughly mixed before being added to the addition funnel. The dry ice bath was then removed and the nitrobenzene solution added dropwise to the liquid ammonia solution over 40 minutes. The solution immediately turned an orange color and a noticeable reflux began. After addition, the solution was stirred for an additional hour before 20.6 g (386 mmol) of solid NH_4Cl was added. The condenser was removed and the NH_3 evaporated. The solution was then acidified to pH 2 with 1N HCl and extracted with DCM (3x130 mL). The combined organic extracts were then washed with 0.5N NaOH (3x130 mL). The combined aqueous layers were acidified with HCl and again extracted with DCM, dried over Na2SO4, filtered, and concentrated to obtain a red-orange oil that solidified upon standing. The crude product was then purified by sublimation (0.8 torr, 60°C) to obtain a slightly yellow deliquescent solid. (6.73 g, 63%) mp 58-61°C; ^{1}H NMR (400 MHz, $CDCl_3$) δ 8.66 (s, 2H), 5.91 (br, 1H); ^{13}C

NMR (101 MHz, $CDCl_3$) δ 156.6, 140.3, 126.87, 126.8 (q J = 4.8 Hz), 123.4, 120.7, 119.9, 119.6; HRMS $[M-H]^-$ calcd. 273.9944 found 273.9951

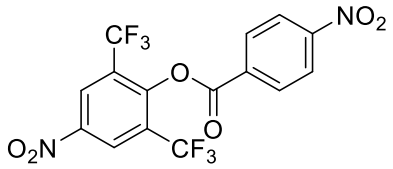

4-nitro-2,6-bis(trifluoromethyl)phenyl 4-nitrobenzoate (4.3c)

In a 250 mL RBF, 3.0 g (10.9 mmol) of **4.2c** and 1.33 g (10.9 mmol) of DMAP were dissolved in 60 mL THF. Solid 4-nitrobenzoyl chloride was then added (2.02 g, 10.9 mmol). The solution quickly changed from clear yellow to cloudy yellow. After a few minutes the solution color faded to slightly off-white. The reaction was then diluted with 300 mL of water and 150 mL of EtOAc. The organic layer was washed with brine, dried over MgSO4, filtered, and concentrated to obtain an off-white solid. (4.28 g, 93%) mp 101-102°C; ^{1}H NMR (400 MHz, $CDCl_3$) δ 8.85 (s, 2H), 8.44 – 8.40 (m, 2H), 8.39 – 8.34 (m, 2H); ^{13}C NMR (101 MHz, $CDCl_3$) δ 161.8, 151.6, 150.8, 145.5, 132.1, 131.8, 131.7, 127.9, 127.6, 126.7, 126.6, 124.2, 122.4, 119.7; HRMS (CI) $[M+H]^+$ calcd. 425.0209 found 425.0201

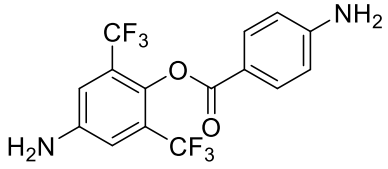

4-amino-2,6-bis(trifluoromethyl)phenyl 4-aminobenzoate (6FAPAB) (4.4c)

In a 100 mL RBF with reflux condenser was added **4.3c** (2.51 g, 5.91 mmol) of and 13.34 g (59.1 mmol) of $SnCl_2{\cdot}2H_2O$. EtOH (28 mL) was added and the suspension was heated at 70°C for 30 minutes. The solution was then poured into 100 mL of water and 150 mL

of EtOAc. The tin precipitate that formed was dissolved by addition of 2N NaOH. The organic layer was then washed with brine, dried over $MgSO_4$, filtered, and concentrated to obtain an oil. 20 mL of hexanes was added and the oil began to crystallize. The hexane was removed in vacuo to obtain a white solid (1.94 g, 90%) Analytical samples were obtained by recrystallization from benzene/hexanes. Mp 109-111°C (dec.); ^{1}H NMR (400 MHz, $CDCl_3$) δ 7.99 – 7.95 (m, 2H), 7.03 (s, 2H), 6.71 – 6.64 (m, 2H), 4.20 (s, 2H), 4.04 (s, 2H); ^{13}C NMR (101 MHz, $CDCl_3$) δ 165.2, 151.9, 144.7, 132.7, 126.2 (q, J = 31.5 Hz) 123.8, 121.1, 117.4, 115.7, 113.9; HRMS $[M+Na]^+$ calcd.= 387.0539 found= 387.0552

Polymer Synthesis General Procedure

BPDA-TFMB and CBDA-TFMB PAE polymers were prepared using the same method described for mPMDA-TFMB-EE in chapter 3, substituting BPDA and CBDA diester diacid chloride monomers for PMDA. However, the CBDA-TFMB-ME polymer was precipitated into water and not washed with methanol or ethyl acetate as this polymer was soluble in these solvents.

PAA Solutions

In a 25 mL RBF was added 600 mg (2.02 mmol) 3FAPAB. NMP (5.6 mL) was added to dissolve the diamine before CBDA (397 mg, 2.02 mmol) was added to form a 15% solids solution. The solution was then stirred overnight to obtain a very pale yellow viscous PAA solution.

CBDA-6FAPAB, PMDA-6FAPAB and PMDA-3FAPAB were prepared similarly as 15 wt% solutions in NMP.

CBDA Solution Phase Imidization Kinetics

4.1b (20.0 mg, 0.0346 mmol, 0.0691 mmol amic esters) was dissolved in 1.00 mL DMSO-d6. Piperidine (~1 eq) was added and the solution was quickly mixed and added to a NMR tube. The sample was run immediately on a Varian DirectDrive 600 NMR to obtain the ^{1}H NMR spectrum every hour for 13 hours. The two aromatic doublet peaks from the hexylaniline (δ 7.46, 7.11) were used as the internal standard to calculate the initial concentration of piperidine added. This was calculated to be 0.0359 M. The generated methanol peak (δ 3.17) was used to track the imidization, due to significant signal overlap in the aromatic region as imidization proceeded. The natural logarithm of the **4.1b** concentration was plotted versus time and slope of the line of best fit was -2.08 x 10^{-6}. Dividing by the base concentration gives the rate constant.

Chapter 5: Catalysts for Low Temperature Curing of Polyimides

INTRODUCTION

One of the major goals of the directly patternable dielectrics project was to define a process requiring a curing temperature below about 200°C that could be performed within one hour. During assembly of the package, the highest temperatures normally encountered are 200-250°C during the solder reflow step, and this process typically only lasts only a few minutes. Higher temperatures can be damaging for sensitive materials such as epoxy resins and underfill materials.[92] Even higher temperatures (>260°C) can potentially damage the die and cause the growth of intermetallic compounds.[261] With the development of chip stacking utilizing thinner chips, lower curing temperatures are desirable to limit stress from CTE mismatch between the package and the die. This temperature requirement is considerably lower than the 300-350°C cure temperature required for polyimides from poly(amic acid) or poly(amic ester) precursors, and the high cure temperature has been a major factor in the search for alternative materials (e.g. benzocyclobutane based dielectrics, cure temp ~250°C).[153-154]

Lowering the cure temperature of polyimides has been a topic of research for many years. Among the earliest methods explored was the radical crosslinking of pre-imidized materials containing diaminostilbene monomer[262] or bismaleimide oligomers[263] using organic peroxides and divinylbenzene based crosslinkers. Another successful method for creating a lower curing thermoset PI is the polymerization of monomer reactants approach (PMR) developed by NASA.[264-267] This scheme uses PI oligomers endcapped with norbornene units; the norbornene units undergo addition polymerization at temperatures around 260-300°C to create a crosslinked network.[268]

One of the more promising methods for low temperature curing of standard PAAs is variable frequency microwave (VFM) curing.[269-272] In this process the polyimide (or

many other uncured organic materials such as BCB) selectively interacts with microwaves, causing localized heating. Additionally, the microwaves increase rotation in the dipoles of the polymer, effectively lowering the activation energy for imidization.[269] This allows for curing of PI in the presence of epoxy based boards that would otherwise be destroyed during standard thermal curing.

Finally, low temperature curing has been performed on PI precursors using various amines, anilines, and phenols at 200°C, both in the solution phase[273-274] as well as in films.[125, 275-276] However, the solution process is only useful for soluble polyimides, which tend to be more flexible and lack many of the desirable properties required for microelectronics packaging. Therefore, the remainder of this chapter will focus on our efforts with amine based catalysts.

NEUTRAL AMINE CATALYSTS

It is well known that amines act as curing catalysts for poly(amic acids), poly(amic esters) and polyisoimides, all of which are precursors to polyimides.[125, 127, 275-276] In the case of PAAs, a 200°C curing temperature has been demonstrated in many systems by Ueda *et al*., utilizing both thermal and photobase generators (TBG and PBG, respectively).[127-129, 277-278] However, curing in PAE systems has been less successful. Most of the work in this area has either been performed by Volksen *et al.* at IBM or funded by IBM.[59-60, 124-126] The general findings are that secondary amines such as piperidine and piperazine perform better than primary amines for imidizing poly(amic alkyl esters), with tertiary amines being orders of magnitude slower. However, treating PMDA-ODA ethyl ester films at 200°C with secondary amines only resulted in moderate imidization (~45-60%).[124] What was noteworthy from this paper was that amidine bases

1,8-diazabicyclo[5.4.0]undec-7-ene (DBU) and 1,5-diazabicyclo(4.3.0)non-5-ene (DBN) completely cure PMDA-ODA-EE in 15 minutes (Figure 5.1). This DBU catalyst has even been used to fully cure PAA films for use as the gate insulator in organic transistors.[279] Resonance stabilization and ring strain make DBU about 100 times stronger of a base than alkyl amines.[280]

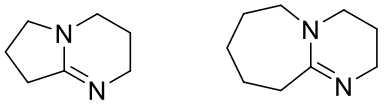

DBN DBU

Figure 5.1: Amidine bases DBN and DBU

Addition of DBU (and most non-tertiary alkyl amines) to PAE solutions results in rapid gelation at room temperature. Dr. William Bell was able to monitor the degree of imidization using IR spectroscopy in mPMDA-TFMB-EE films by adding DBU (1 wt% to polymer) to a NMP solution of mPMDA-TFMB-EE and quickly spincoating the material.[68] Figure 5.2 shows IR spectra of the 1 wt% DBU in mPMDA-TFMB-EE as cast film, as well as films baked at 200°C and 350°C for one hour. The as cast material has a very minor amount of imidization as indicated by the small peak in the carbonyl region. Heating to 200°C resulted in a significant increase in the imide carbonyl peak. By comparing the imide carbonyl stretch at 1780 cm^{-1} to the C=C aromatic stretch (1490 cm^{-1}) used as the internal standard, the degree of imidization could be calculated, assuming the 350°C bake for one hour (green trace) represented complete conversion. In this case, the 200°C cure resulted in 100% imidization.

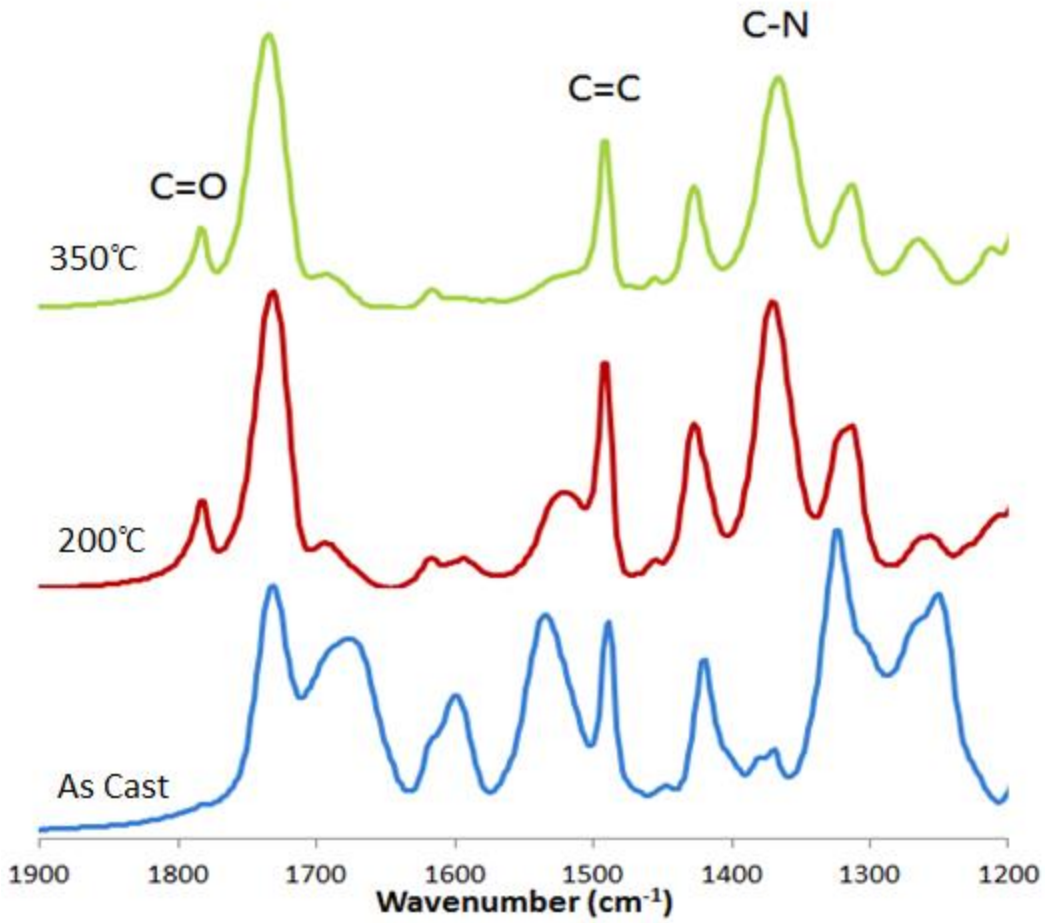

Figure 5.2: IR spectra of mPMDA-TFMB-EE film containing 1 wt% DBU. Blue: as cast, Red: 1 hour at 200°C, Green: 1 hour at 350°C (full cure)

AMIDINE SALTS

While even small amounts of DBU are effective at curing PMDA-TFMB-EE at 200°C, adding it directly to formulations is not possible due to the nearly instant gelation and complete lack of storage stability. There are reports of amidine PBGs based on salts of DBU or 1,5,7-Triazabicyclo[4.4.0]dec-5-ene (TBD) and a carboxylic acid.[281-286] Initial tests of latent amidine or guanidine bases focused on the salt of DBU and benzoic acid

(DBU benzoate) to ensure that these materials would be stable during storage. Unexpectedly this was not the case. Addition of DBU benzoate to mPMDA-TFMB-EE solutions quickly resulted in gelation, behavior similar to the addition of DBU itself. Unsurprisingly, this material also completely imidized films at 200°C in one hour.[68] The other common method for preparing amidine PBGs, by alkylation of sp^2 hybridized nitrogen to form a quaternary amine, was also considered. The model compound for this test was prepared by the alkylation of DBU with benzyl bromide (DBU BnBr) to form an organic soluble salt. Interestingly, there is one Japanese patent about using alkylated amidine tetraphenylborate salts as catalysts for epoxy curing.[287] This salt did not gel solutions of PMDA-TFMB-EE at room temperature, so films containing 5% DBU BnBr were heated for 15 minutes at various temperatures to determine the degree of imidization (Figure 5.3). While mPMDA-TFMB-EE does not begin to imidize until about 170°C without any additives, complete curing was achieved with a 5% DBU BnBr at about 210°C in 15 minutes.

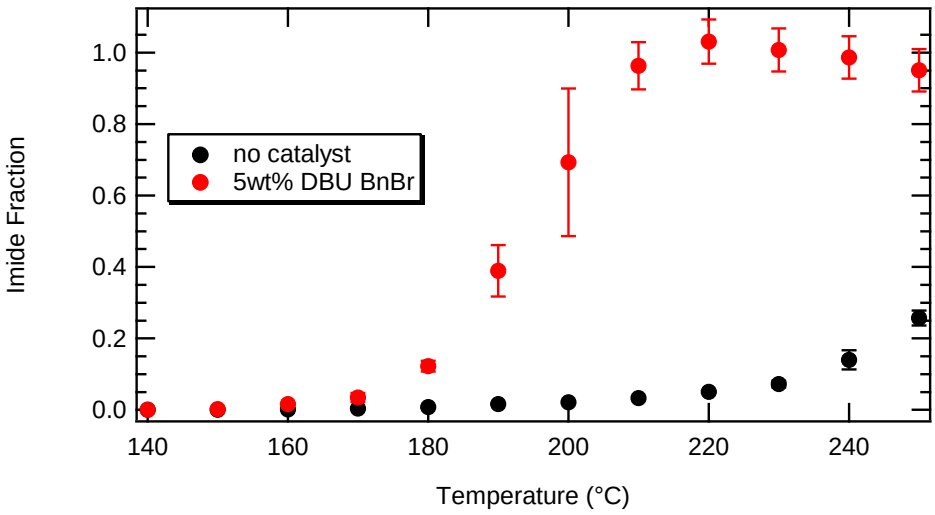

Figure 5.3: Imidization in mPMDA-TFMB-EE films after 15 minute cure at various temperatures

The large contrast observed in Figure 5.3 was thought to be due to de-alkylation by bromide ion substitution to regenerate free DBU base. Similar reactions are known to occur in standard quaternary alkyl ammonium salts such as tetra n-butylammonium bromide (TBAB, Figure 5.4).[288]

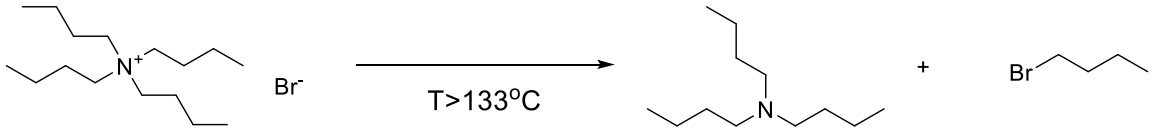

Figure 5.4: Entropy driven de-alkylation of TBAB

To confirm that de-alkylation was the mechanism for the low temperature curing, both thermogravimetric analysis (TGA) and differential scanning calorimetry (DSC) were performed on DBU BnBr (Figure 5.5). The thermal data collected, however, does not agree with this hypothesis. By TGA, DBU BnBr has no mass loss until nearly 300°C. The normal boiling point of benzyl bromide is 198°C[289], so if decomposition were taking place during the melting transition, significant mass loss should have occurred around 200°C. However, this did not occur and implies that DBU BnBr itself acts as a catalyst at elevated temperatures.

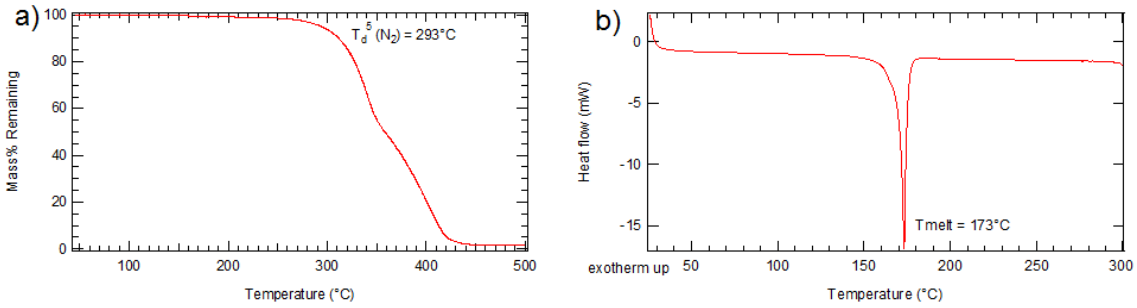

Figure 5.5: DBU BnBr thermal properties a) TGA b) DSC

This behavior in DBU BnBr is quite different from traditional thermal base generators. TBGs typically consist of amines protected as their tertiary-butoxycarbonyl (t-BOC) carbamates.[129, 277] When heated these compounds decompose into the free amine, carbon dioxide, and isobutene. There is also a class of TBGs that utilize hydroxylamide ring-closing to lactones that release free amine upon heating.[290-292] As was the case for NVOC and cinnamide type PBGs, these methods are unfortunately limited to primary and secondary amines. There have been a few reports of preparing various acylated DBN and DBU salts.[293-297] However, these materials are quite powerful acylating agents due to the free-base DBU leaving group. Any nucleophiles present in a solution containing these salts (e.g. water) would rapidly react to generate DBU and cause gelation, rendering such salts impractical as TBGs.

The low temperature imidization catalyzed by DBU BnBr led us to explore other alkylated amidine salts such as the salts of DBU and ethyl bromide (DBU EtBr) and DBN and benzyl bromide (DBN BnBr). These salts were added to mPMDA-TFMB-EE solutions as 5 wt% loadings to polymer and spin-coated to form films on silicon wafers. Films were then baked at various temperatures for 15 minutes, IR spectra were measured, and the degree of imidization calculated as discussed previously. From examination of Figure 5.6, it is clear that all three salts are very effective catalysts above 200°C, but will not imidize films at all below about 160°C. As both the NVOC and cinnamide PBGs used in the mPMDA-TFMB-EE patterning printed at these temperatures, the combination of DBU BnBr and PBG should enable low temperature curing of photo-patterned and developed films.

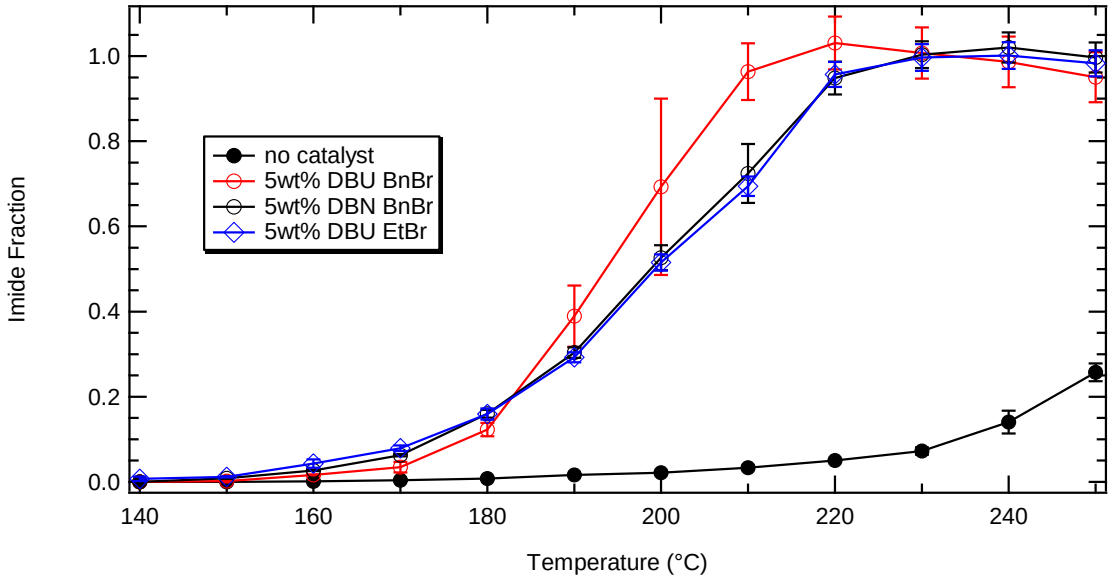

Figure 5.6: Effect of various alkylated amidine salts on curing of mPMDA-TFMB-EE

QUATERNARY ALKYL AMMONIUM SALTS

Quaternary ammonium salts such as TBAB decompose into tertiary amine and alkyl halides at elevated temperatures, as discussed previously.[288] It is also known that tertiary amines, while not as effective as primary or secondary amines, still work as imidization catalysts.[124-125] Combining these ideas, it seemed likely that quaternary ammonium salts should also work as imidization catalysts. Tetra n-butylammonium (TBA) salts were identified for testing as they are commercially available due to their use as phase transfer catalysts, and due to the lipophilic cation that makes them quite soluble in organic solvents. The fluoride, bromide, and iodide salts (TBAF, TBAB, and TBAI, respectively) were added as 5 wt% loadings in mPMDA-TFMB-EE and cured in the same manner as the amidine salts (Figure 5.7). Surprisingly, all of the halide salts performed similarly with complete curing around 230-240°C. This result was unexpected

as basic anions such as fluoride are known to be imidization catalysts.[124] TBAF was also unexpectedly stable in PAE solutions with a curing onset temperature nearly the same as the other salts explored. While TBAF did perform slightly better than the other TBA halide salts, all of TBA salts were less effective catalysts than the amidine salts.

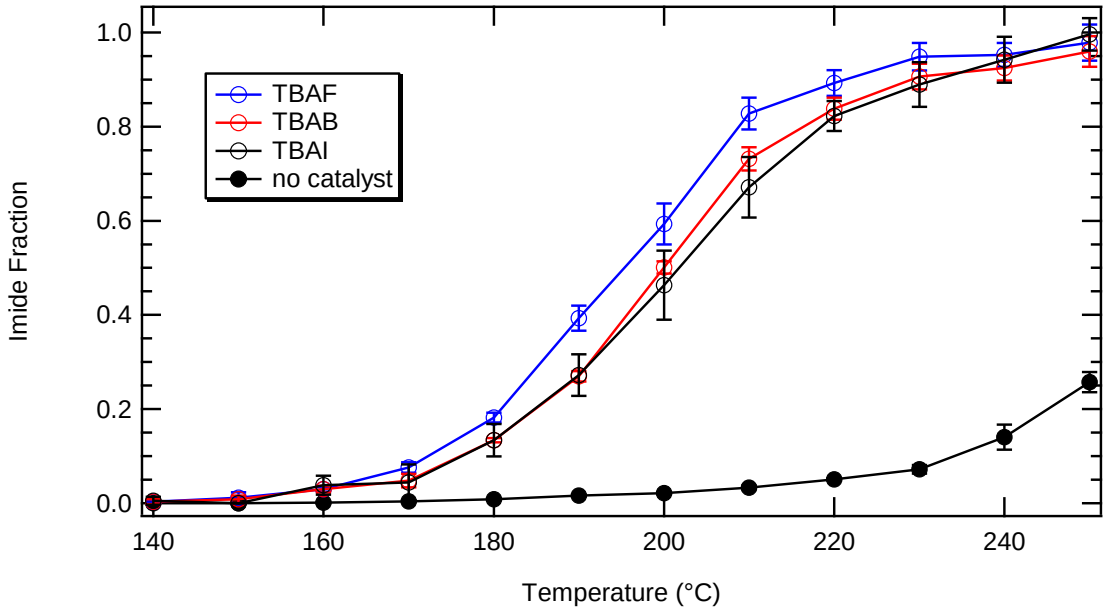

Figure 5.7: Effect of tetra n-butyl ammonium halide salts on mPMDA-TFMB-EE curing. Films were cured for 15 minutes.

As TBA halides are not stable toward de-alkylation at the curing temperatures of mPMDA-TFMB-EE, the imidization in the TBA halide salt systems possibly resulted from the in-situ generation of tri n-butylamine in the film. Many other TBA salts are available, and most are more thermally stable than the halides (Table 5.1). The values in the table represent a 5% mass loss as determined by TGA in nitrogen. The boiling point of tributylamine is just above 200°C, so the non-halide salts in the table are not generating the free amine below the 250°C curing temperature used in previous experiments.

TBA Salt	T_{dec} (°C)
Br	186
I	194
BF_4	348
PF_6	318
OTs	261
OTf	327

Table 5.1: Decomposition temperatures of various TBA salts determined by 5% mass loss on TGA in nitrogen

The more thermally stable TBA salts were also tested as 5 wt% loadings in mPMDA-TFMB-EE (Figure 5.8). Samples were again cured for 15 minutes at temperatures from 140-250°C. While the tetrafluoroborate (BF_4) and hexafluorophosphate (PF_6) salts performed about the same as the halides, these salts could not have degraded to the amine. This implies that some other unknown mechanism is responsible for the imidization. The other important finding is that not all of the TBA salts performed identically; tosylate (OTs) and triflate (OTf) salts were considerably less active catalysts. These salts did not completely cure mPMDA-TFMB-EE even at 250°C. The onset temperature for imidization with these additives also appears to be much higher than the other salts. The molecular weights for each of the salts is reasonably close (other than TBAF) due to the large TBA cation, so the effects from slight differences in molar concentrations should be minimal. BF_4, PF_6, and OTf anions are also considered non-coordinating anions due to their poor nucleophilicity and lack of interaction with their cation.[298] While it is reasonable that TBA OTf should be the least effective catalyst tested, it still causes much more imidization than the control without any salt. Together,

these data suggest that the cation may be responsible for some of the effect and that using sulfonate anions results in less active catalysts.

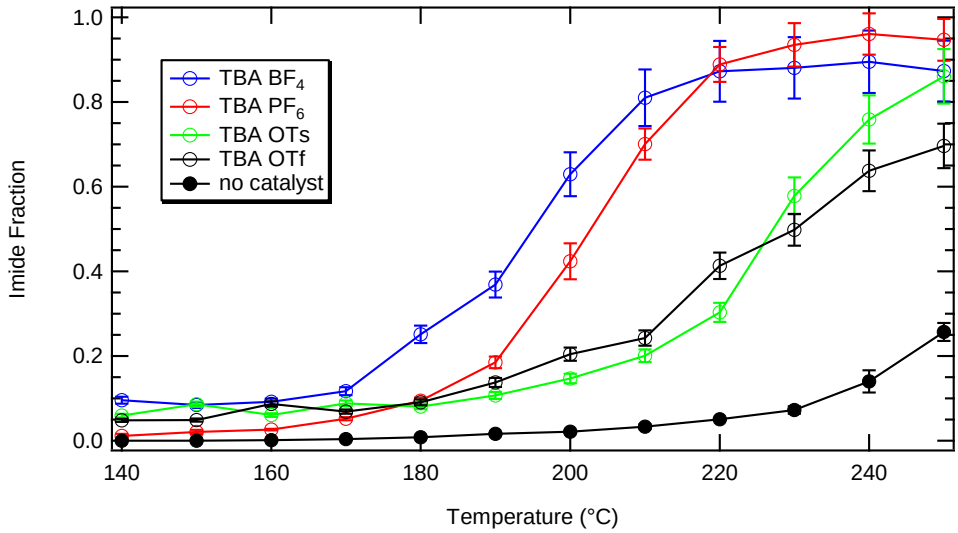

Figure 5.8: Effect of various TBA salts on imidization in mPMDA-TFMB-EE. Films were cured for 15 minutes

IONIC LIQUIDS

Due to the relatively low melting points (or decomposition points) of many of the catalysts explored, we believed that other ionic liquids with even lower melting points may improve low temperature curing. Common room temperature ionic liquids 1-butyl-3-methylimidazolium tetrafluoroborate (BMIM BF_4) and triethylsulfonium bis(triflimide) (Set_3 Tf_2) were chosen along with cetylpyridinium chloride (C_{16}Py Cl) for testing (Figure 5.9). Cetylpyridinium chloride melts at 77°C, which is low enough to be considered an ionic liquid. These ionic liquids were added to mPMDA-TFMB-EE solutions in NMP at the standard 5 wt% loading, and baked for 15 minutes at various temperatures in the same manner as the previous salts. The imidization response was then compared to the

representative TBAB and DBU BnBr salts (Figure 5.10). Several trends emerge from the graph. The cetylpyridinium chloride performs about the same as TBAB and suggests that unconjugated ammonium cations are less effective catalysts than the conjugated BMIM and benzyl DBU cations. The BMIM BF_4 is also the most effective catalyst out of the salts tested, though the onset of imidization is at a lower temperature than the other salts, which may lead to problems during the post exposure bake for the base-catalyzed PSPI system. Finally, the SEt_3 NTf_2 was the least effective catalyst for this system; no imidization occurred below 200°C. However, complete curing was obtained after 15 minutes at 250°C; the TBA triflate and tosylate salts, despite a lower onset temperature, were still not imidized completely at this temperature. Interestingly, SEt_3 NTf_2 begins to quickly degrade around this temperature, so the starting salt may not be the active catalyst. Further work with the more thermally stable $LiNTf_2$ (next section) also suggests that this may be the case.

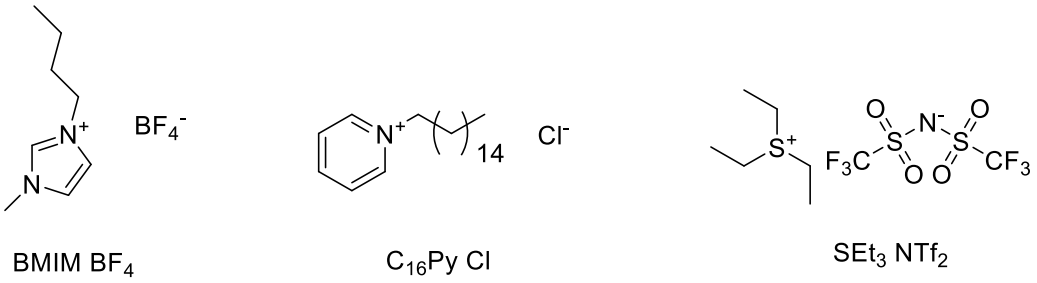

BMIM BF_4 $C_{16}Py$ Cl SEt_3 NTf_2

Figure 5.9: Ionic liquids explored for use as curing catalysts

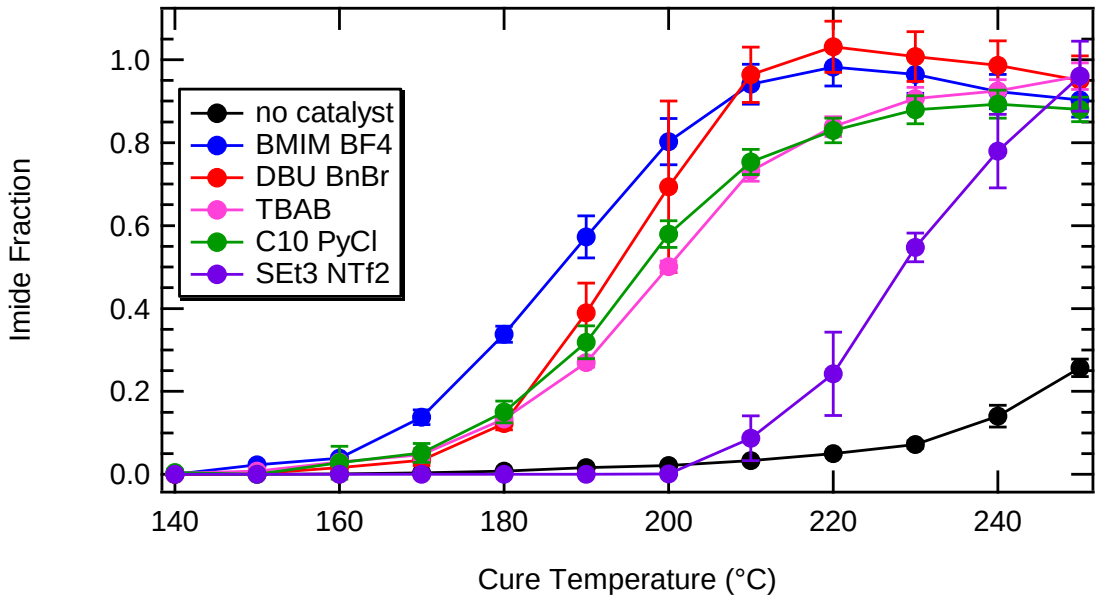

Figure 5.10: Comparison of the imidization of mPMDA-TFMB-EE using various types of salt catalysts. Films were cured for 15 minutes.

Lithium Salts

In our quest to better understand the cause of the catalysis of imidization by these salts, we attempted to find a salt that would not act as an imidization catalyst. As many lithium salts are soluble in the NMP casting solvent, we first tested a 5 wt% loading of lithium chloride in mPMDA-TFMB-EE (Figure 5.11, blue trace). Films were again cured for 15 minutes at various temperatures. Lithium chloride surprisingly caused some imidization in the film, reaching about 75% imidization at 250°C. The bromide and iodide salts were also tested and found to act as catalysts as well. In the case of the chloride and bromide salts the onset of imidization began around 180°C, which is about 20°C higher than that observed for the DBU and TBA halides. Lithium iodide, however, began to cause imidization at temperatures lower than 140°C. LiI is known to cleave

esters to their corresponding acids by a classical Sn2 reaction.[299-301] However, this typically requires refluxing in a basic solvent such as pyridine. Also, methyl esters are cleaved selectively in the presence of ethyl esters, suggesting that such a reaction would be quite slow, which is inconsistent with the extent of imidization observed. Other alkali halides were also used to cure mPMDA-TFMB-EE. Cesium chloride (green trace) was essentially inactive until 200°C and gave about 60% imidization at 250°C. Some of the reduced activity likely stems from the constant 5 wt% loading used throughout the trials; the constant weight loading results in a much lower molar concentration of the salt. Finally, we set out to test other alkali salts such as LiF and CsF to test the effect of the basic fluoride ion. However, neither of these salts was soluble in the NMP casting solvent. A comparison of all the alkali metal chlorides was also not possible due to the complete lack of solubility of sodium, potassium, and rubidium chloride.

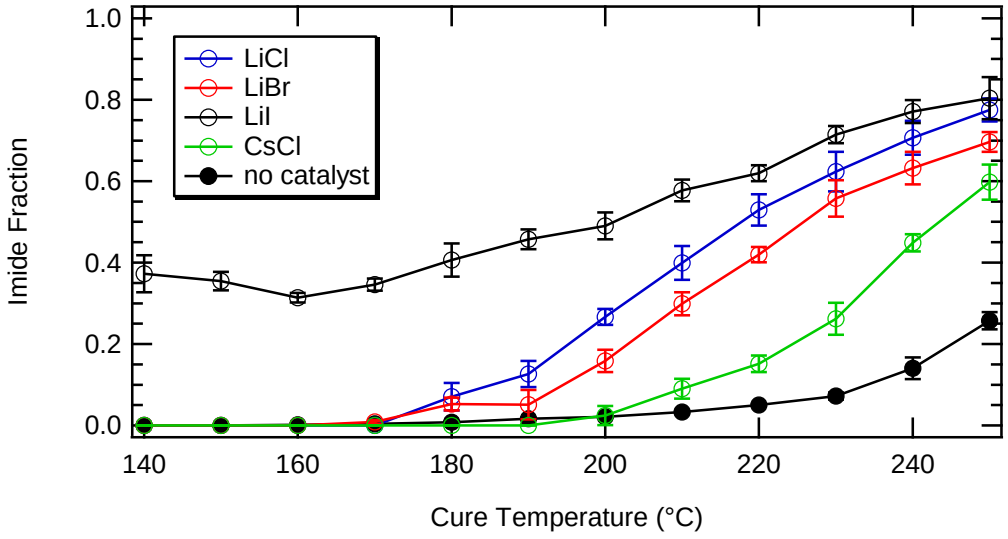

Figure 5.11: Effect of alkali metal halides on imidization of mPMDA-TFMB-EE. Films were cured for 15 minutes.

Other soluble lithium salts including the tetrafluoroborate, bistriflimide (NTf_2), acetate (OAc), and triflate were also explored at 5 wt% loading in mPMDA-TFMB-EE (Figure 5.12). $LiBF_4$ functioned similarly to both chloride and bromide salts, just as TBA BF_4 was about equally effective as TBA chloride and bromide. Lithium acetate substantially imidized the film at temperatures below 140°C, with a curing profile similar to that of the iodide salt. This is reasonable as acetate is a basic anion and is known to cure poly(amic esters).[124, 302] Typically this is performed using an additional dehydrating agent such as acetic anhydride, but these temperatures are likely high enough for effective dehydration without it. Finally, the triflate and bistriflimide are very poor catalysts as expected. The triflate causes more imidization than the salt-free case, though imidization appears to level off at about 30% around 230°C. The bistriflimide, an even weaker and more hindered base than triflate[303], is the only salt that we found to be completely ineffective at imidizing mPMDA-TFMB-EE.

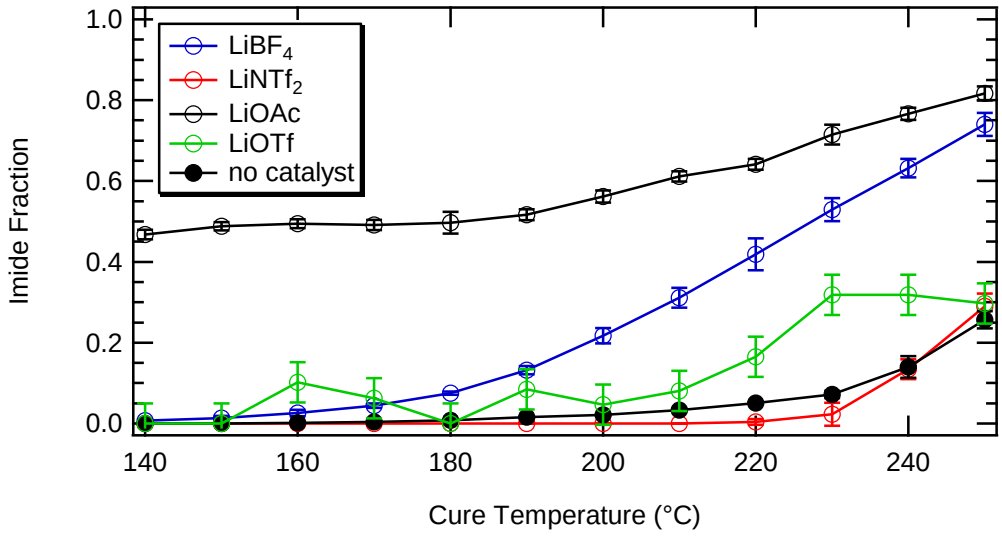

Figure 5.12: Effect of various lithium salts on imidization of mPMDA-TFMB-EE. Films were cured for 15 minutes.

From the lithium salt studies it is clear that even seemingly inert halide salts such as lithium chloride are moderately effective imidization catalysts. While they do not come close to fully curing PAEs at 200°C, considerably more imidization occurs than in the case of no additives in the PAE film. However, none of the lithium salts enabled complete curing of mPMDA-TFMB-EE at 250°C while almost every alkylated amidine and TBA salt that was tested did.

LEWIS ACIDS

Lithium salts, along with most other metal salts, are Lewis acids. Due to the very small size of the ion, lithium ions are among the hardest Lewis acidic ions known.[304] This led us to question if the observed imidization in the lithium salt systems was at least partially due to some Lewis acid catalyzed effect.

The standard mPMDA-TFMB-EE polymer with 5 wt% catalyst loading was again cured for 15 minutes at various cure temperatures. The initial experiment tested the effects of cerium chloride heptahydrate ($CeCl_3$), boron trifluoride diethyl etherate (BF_3), and the Bronsted acid p-toluenesulfonic acid monohydrate (TsOH, Figure 5.13). TsOH was chosen as it is a reasonably thermally stable and non-volatile strong acid that is a solid at room temperature for convenient weighing. Unlike many other strong acids, TsOH is also non-oxidizing, so only the effect of acid should be observed.[305] The degree of imidization was around 10-20% regardless of temperature and these salts may actually be inhibiting imidization at higher temperatures. Cerium chloride is a Lewis acid typically used in the Luche reduction,[306] though it has also been used in more traditional Lewis acid catalyzed reactions such as Friedel-Crafts alkylation.[307] $CeCl_3$ had an even smaller effect on imidization and was barely above the salt-free control. Boron

trifluoride, along with aluminum trichloride, are among strongest and most popular Lewis acid catalysts available. However, when added to mPMDA-TFMB-EE films, there was no difference at all between BF_3 containing films and the control.

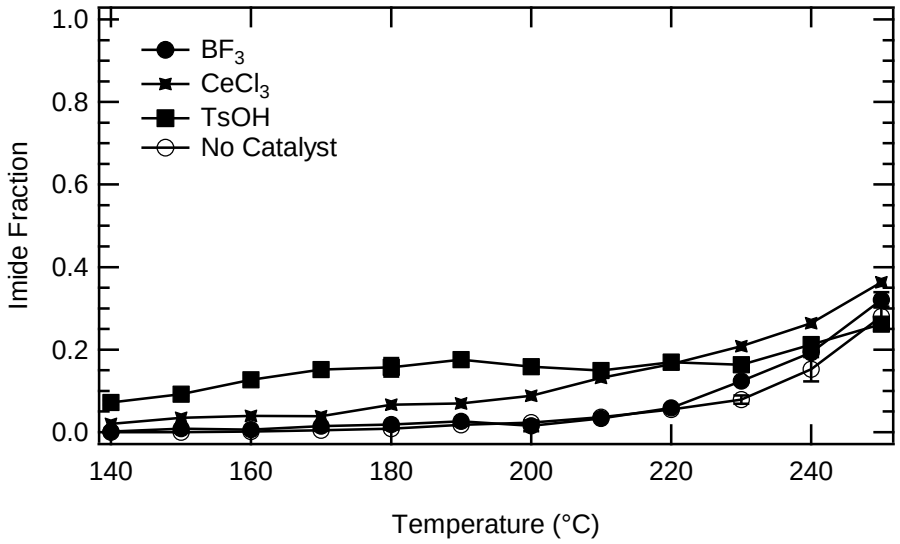

Figure 5.13: Effect of various acids on imidization of mPMDA-TFMB-EE. Films were cured for 15 minutes.

It is possible that multiple factors could be responsible for the complete lack of imidization using BF_3. BF_3 itself is a gas at room temperature, though the diethyl ether adduct used boils around 130°C. It is possible that all of the BF_3 just evaporated out of the film during baking. Another possible issue is the NMP casting solvent used. NMP is weakly basic and may form an adduct with the BF_3, reducing the acidity. Finally, BF_3 fumes strongly in air and is hydrolyzed readily.[308] Water in the solvent, polymer, or even air could destroy the BF_3 in the film.

To correct these shortcomings of BF_3, scandium triflate ($Sc(OTf)_3$) and ytterbium triflate ($Yb(OTf)_3$ were explored. Both compounds have found use as water stable Lewis acid catalysts that can actually be used as true catalysts rather than stoichiometrically.[309-

[310] These Lewis acids were also tested at a 5 wt% loading in mPMDA-TFMB-EE and baked in the same way as previous experiments. However, the IR spectra obtained was quite different than in all the previous experiments (Figure 5.14). The IR spectra using $Sc(OTf)_3$ are shown, but data for $Yb(OTf)_3$ were very similar. The film cured at 250°C has a noticeable peak around 1775 cm^{-1}, indicative of a carbonyl imide peak. However, the observed peak is much broader than those observed with other catalysts. There is also a nearly complete lack of change in the C-N imide stretch peak at 1370 cm^{-1}, suggesting that some reaction other than imidization is occurring. The ratio of carbonyl area to the aromatic C=C stretch is also very different than any of the previous salts explored. Normally this ratio is about 0.35 for fully cured films. However, in $Sc(OTf)_3$ the value was nearly 0.45, a very significant difference. The cause of this appears to be the C=C aromatic stretch used as the internal standard decreasing in intensity at complete curing at 350°C. This decrease should not occur as there are no volatile aromatic compounds in the formulations, and suggests that a reaction other than imidization is also occurring.

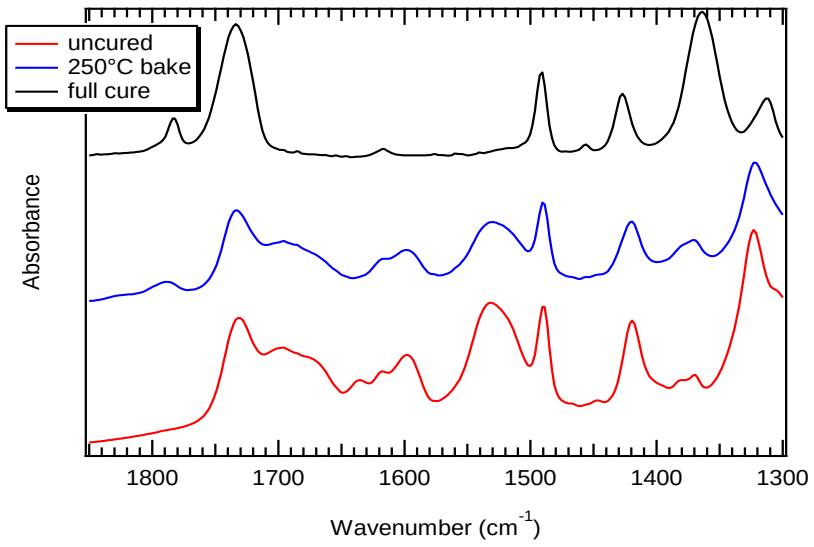

Figure 5.14: IR spectra of 5% $Sc(OTf)_3$ in mPMDA-TFMB-EE during thermal curing

From the Bronsted and Lewis acids tests, it appears that neither are effective catalysts for the imidization of mPMDA-TFMB-EE. In fact, the water-stable transition metal based Lewis acids may actually be damaging the material instead of acting as a curing catalyst. These results are very different then the observed imidization effect from lithium salts, and shows that the imidization process is not due to Lewis acid effects.

MATERIAL PROPERTIES OF CATALYST CURED FILMS

To ensure that the polyimides formed by low temperature curing retained the properties of the standard thermally cured material, the modulus, hardness, and dielectric properties of films cured using DBU BnBr were determined.

Adding the polar DBU BnBr to PI films could adversely affect the dielectric constant, dissipation factor and water absorption, so loadings of 1, 5, and 10 wt% catalyst in mPMDA-TFMB-EE were used determine the extent of curing at 200°C (Figure 5.15). After one hour at 200°C, only the films containing a 10 wt% loading of DBU BnBr were completely cured. In this same period of time, imidization in the catalyst-free film was only about 10%; even a 1 wt% loading resulted in a greater than 50% cure.

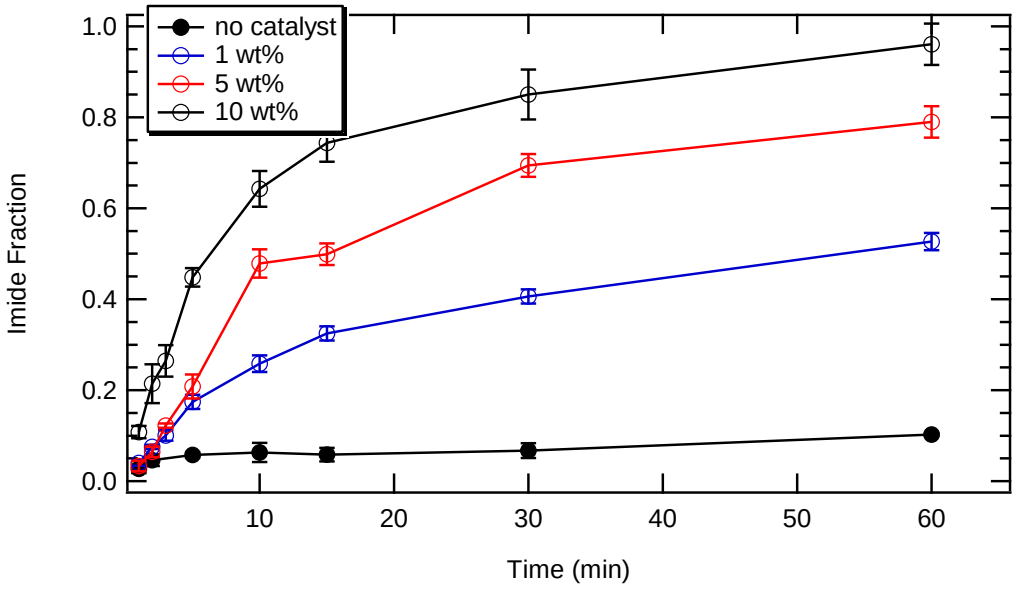

Figure 5.15: Imidization in mPMDA-TFMB-EE films at 200°C as a function of time using various loadings of DBU BnBr

The previous curing studies showed that 5 wt% loading requires temperatures around 220°C for 15 minutes for curing, so we decided that materials properties should be tested at 200, 220, and 350°C for catalyst loadings of 1, 5, and 10 wt% DBU BnBr in mPMDA-TFMB-EE. Unfortunately, our lab is not equipped for mechanical or dielectric testing at present, so Jared Schwartz at the Georgia Institute of Technology performed these measurements. Figure 5.16 shows the modulus and hardness of the film as a function of loading and cure temperature for mPMDA-TFMB-EE cured for 1 hour, as measured by nanoindentation. The modulus of the film does not change significantly with cure temperature, even in the case of the 1 wt% loading where the lower cure temperatures are not sufficient for complete curing. The catalyst appears to slightly increase the modulus with increased loading. The film hardness, however, is a much stronger function of cure temperature (Figure 5.16b). The low temperature catalyst-cured films had almost the same hardness as a film without catalyst fully cured at 350°C.

However, as was the case with modulus, adding catalyst resulted in improved mechanical properties over the standard un-catalyzed high temperature cure.

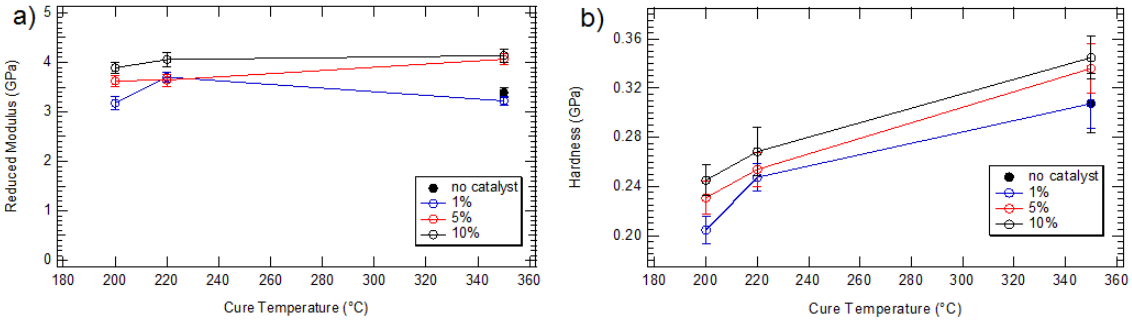

Figure 5.16: Mechanical properties of mPMDA-TFMB-EE cured for 1 hour at various temperatures using various loadings of DBU BnBr catalyst a) reduced modulus b) film hardness

The dielectric properties of the catalyst-cured films were also tested at Georgia Tech (Figure 5.17). These measurements were collected at 200 kHz by the capacitance method (through-plane properties). From the dielectric measurements (Figure 5.17a), the catalyst loading appears to increase the dielectric constant slightly. This was expected due to the ionic character of the catalyst, which should cause a considerable increase in the dielectric constant, even at low frequencies.[144] The most visible difference is in the dielectric constant for the material cured at 200°C using a 1 wt% catalyst loading. At that point the dielectric constant is much larger than the others measured, which is likely due to the lower degree of imidization. The large number of polar, primary amide bonds still present contribute somewhat to increasing the dielectric constant, and the lack of curing also creates problems during aluminum evaporation which also adversely affects the dielectric constant. From Figure 5.17b, it is clear that the ionic catalyst raises the dissipation factor considerably, with the 5 and 10 wt% loadings reaching values of about 0.025. Also noteworthy is that the films cured at 350°C have about the same dielectric

properties regardless of catalyst loading. As the catalyst decomposes around 300°C, the catalyst was largely volatilized during the 350°C cure and the resulting films were essentially catalyst free.

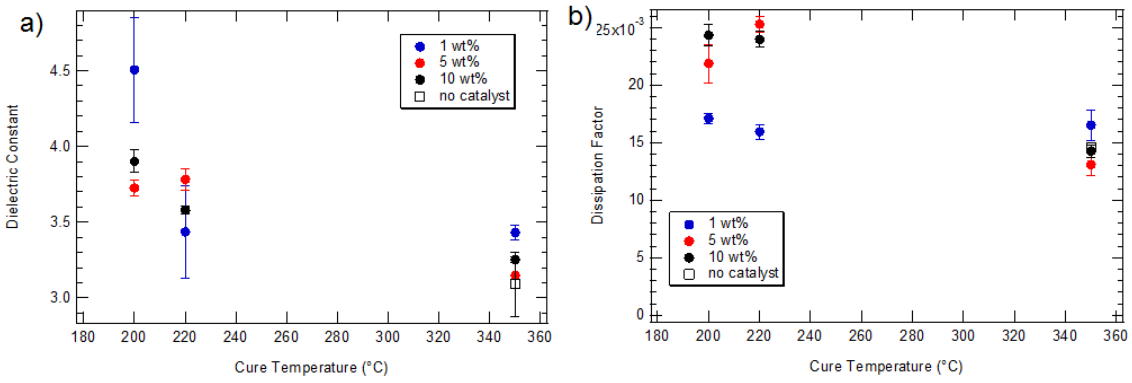

Figure 5.17: Dielectric properties of mPMDA-TFMB-EE cured with DBU BnBr at various temperatures and catalyst loadings at 200 kHz a) Dielectric constant b) Dissipation factor

In summary, the DBU BnBr catalyst adversely affects the dissipation factor and slightly increases the dielectric constant of cured films. However, the modulus of catalyst cured PMDA-TFMB is largely independent of cure temperature, and is actually increased by catalyst loading. Likewise, the film hardness is increased with catalyst loading and is a strong function of cure temperature.

CATALYST CURING OF OTHER POLYIMIDE PRECURSORS

Other PI precursor systems were also tested with the DBU BnBr curing catalyst to ensure the generality of the catalyst. Poly(amic acids), which are much easier to prepare than the amic esters, were tested first using the standard conditions (Figure 5.18a). PAAs begin to imidize at much lower temperatures than either the PAEs or the PIIs, so significant imidization (~50%) occurs at 200°C in 15 minutes. Even a full cure is

achievable at 250°C without the need of catalyst. However, the DBU BnBr is still able to cure the PAA at 200°C, which is not possible in the un-catalyzed film. Figure 5.18b shows the same experiment but instead using the isoimide instead of the amic acid polymer. While PIIs tend to be more soluble than the equivalent PI in polar aprotic solvents, using exclusively rigid dianhydride monomers such as PMDA results in insoluble polymers.[311-312] Attempts to synthesize PMDA-TFMB isomide resulted in formation of an insoluble gel during conversion of the precursor PAA to the PII. So, we substituted 10 mol% of the PMDA with flexible 4,4'-(hexafluoroisopropylidene)diphthalic anhydride (6FDA) to improve the solubility of the otherwise quite rigid PMDA-TFMB isomide polymer. As seen in the figure, the isomide polymer is much more difficult to imidize than the corresponding PAA, only reaching about 40% imidization at 250°C in 15 minutes while the PAA is almost completely cured. Even the addition of DBU BnBr does not completely cure the isoimide, even at 250°C.

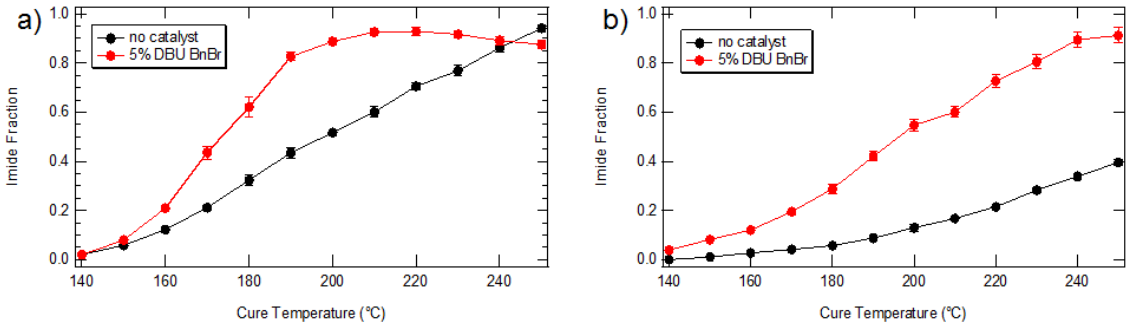

Figure 5.18: Imidization in other PMDA-TFMB precursors using 5 wt% DBU BnBr a) poly(amic acid) b) poly(isoimide)

PIIs are the kinetic product during dehydration of PAAs, and tend to be produced when a dehydrating agent with good leaving group is used.[313-314] Isomides have also been proposed as intermediates in the base-catalyzed imidization of aryl amic esters, and

claimed to imidize more quickly in the presence of amines than the corresponding amic esters.[124] However, no isomide was observed in HPLC studies of model compounds.[124] The isoimide film curing in our study was also more rapid than in the case of the PAE, though the difference at the 250°C cure was only 40% vs. 25% imidization.

We also explored curing the more traditional para PMDA-ODA ethyl ester polymer (pPMDA-ODA-EE) with the DBU BnBr catalyst (Figure 5.19a). The para isomer was used for the study as it had already been prepared for the directly patternable dielectric project. For this polymer, imidization appears to go much more smoothly and results in a higher degree of imidization than in the case of mPMDA-TFME-EE. This is likely due to a combination of both the para linkage as well as the more flexible ODA monomer. The para linked polymer is easier to imidize as it requires less conformational change upon curing than the kinked meta isomer; both the para PAE and the resulting PI are linear. It is also known that residual NMP in the film helps the para isomer cure at lower temperature than the meta isomer.[167, 315] The pPMDA-TFMB-EE polymer unfortunately produced rough and opaque films as discussed in previous chapters, so it was not available as a direct comparison to curing in the meta isomer polymer. The meta PMDA-TFMOB polymer (mPMDA-TFMOB-EE) was also cured using DBU BnBr catalyst (Figure 5.19b). However, the results are considerably different than in the other PAEs. While all the PAEs cured around 200-220°C with the DBU BnBr catalyst, the mPMDA-TFMOB-EE polymer experiences a considerable drop in imidization if the initial curing temperature is higher than 200°C. The other PAEs only show a minor decrease in imidization if baked initially at too high of a temperature while the TFMOB polymer drops to about 70% imidization at 250°C.

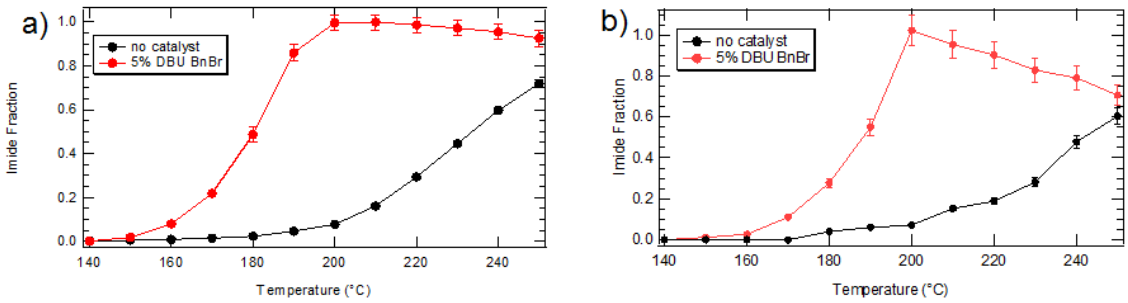

Figure 5.19: Imidization in other PAEs using 5 wt% DBU BnBr. a) pPMDA-ODA-EE b) mPMDA-TFMOB-EE

All of the other polymers studied appear to reach a curing maximum before slowly decreasing, but none to the extent of mPMDA-TFMOB-EE. Interestingly, this decreased imidization trend remains in the TFMOB films initially baked at temperatures above 200°C even after curing at 350°C overnight (Figure 5.20). While the final imidization in films containing no catalyst is unaffected by the initial low temperature bake, no further imidization occurs during the high temperature cure for samples initially baked above 200°C. This is reasonable from a curing perspective, as PIs are often cured in multiple steps[316] and exhibit different properties depending on the cure temperature.[317] Curing at too high of an initial temperature causes a significant loss of solvent from the film very quickly and can lower properties such as glass transition temperature relative to optimally cured films.[316] The glass transition temperature is a proxy for the degree of imidization, so the decreasing imidization at higher temperatures is likely the same phenomenon observed in other papers. However, most other works have focused on the more common and lower curing PAA. The reason we did not observe a lower degree of imidization in the uncatalyzed films may be that an even higher initial curing rate (temperature) is required to freeze the partially cured conformation. In the case of this experiment, the DBU BnBr catalyst increases the reaction rate enough to see this effect. It

is also possible that there is an internal standard issue with the TFMOB polymer and the C-C aromatic peak may not be invariant.

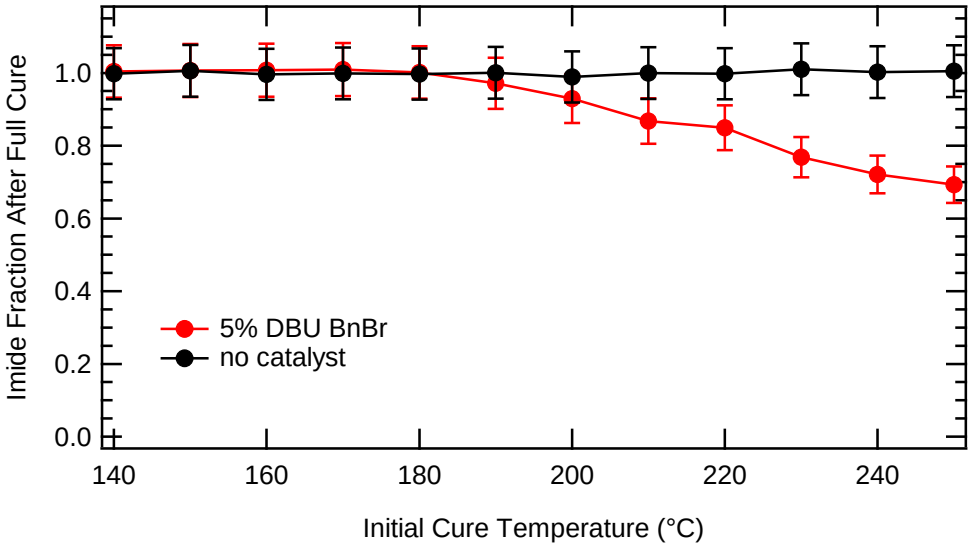

Figure 5.20: Imidization in fully cured mPMDA-TFMOB-EE initially low temperature baked for 15 min at various temperatures.

Finally, the CBDA-TFMB-ME polymer was also cured using a 5 wt% DBU BnBr loading and compared to the mPMDA-TFMB-EE curing (Figure 5.21). Without any catalyst present, both ester polymers exhibit the same lack of imidization, only reaching about 20% imidization after baking at 250°C. However, the DBU BnBr catalyst is effective for curing CBDA-TFMB-ME, unlike the previous attempts with PBGs. The higher temperature required for curing the CBDA ester is also consistent with the kinetic data obtained from amine catalyst CBDA model compound curing. The observed rate constant was much lower, so higher temperatures should be needed to obtain the same degree of curing in 15 minutes. This catalyst does still reduce the curing temperature to under 250°C, so it would allow CBDA-TFMB to be used as a packaging dielectric, though the ability to photo-pattern this material is an issue that still needs to be solved.

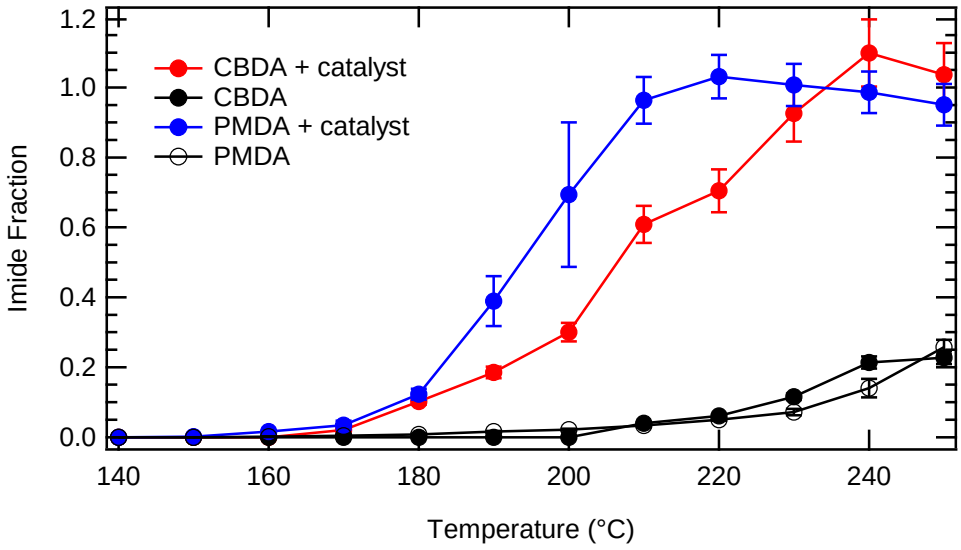

Figure 5.21: Imidization of PMDA-TFMB and CBDA-TFMB ester polymers using 5 wt% DBU BnBr. Films were baked for 15 minutes.

GUANIDINE-BASED SALTS

The conjugated amidine salts (e.g. DBU and DBN salts) as well as BMIM were the best catalysts for imidization and performed better than unconjugated TBA salts. We believed that further conjugation could even further decrease the curing temperature of the resist. To test this, we prepared salts based on 1,5,7-triazabicyclo[4.4.0]dec-5-ene (TBD, Figure 5.22). While TBD is a very strong guanidine base, it cannot be rendered inert by simply reacting with an alkyl halide as was the case for DBU. Doing so only generates a neutral base (and a protonated salt by-product) which instantly gels PAE solutions. TBD must be alkylated twice to form a salt, and the easiest salt to make this way was the dimethyl iodide salt (DMTBD I). Due to stability concerns about the iodide

salt, the tetrafluoroborate salt was also tested. It was prepared easily from the iodide salt using silver tetrafluoroborate in acetonitrile to precipitate insoluble silver iodide.[318]

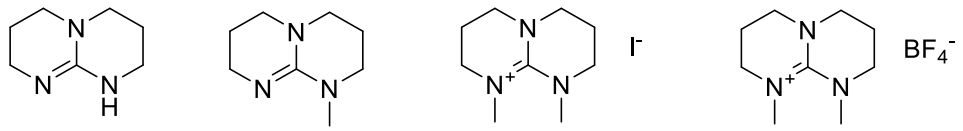

Figure 5.22: TBD and methylated salt derivatives

The effect of 5 wt% loadings of the DMTBD salts is shown in Figure 5.23. While the more stabilized fluoroborate salt appears to perform equally well as DBU BnBr, the iodide salt is by far the best catalyst tested. Complete curing is achievable at 190°C in 15 minutes using this catalyst, whereas almost no imidization occurs in the uncatalyzed control film. Additionally, films containing this catalyst do not begin imidization until 160°C. However, we did experience severe solution stability problems with this catalyst, and unexpectedly these were not due to solution gelation. This instability was first noticed when dissolving the salt in chloroform for NMR. A bright yellow solution formed from the colorless salt. This also occurred when preparing NMP solutions, even in yellow light. The carbonyl to aromatic peak area ratio in IR decreases with initial cure temperature after fully thermally curing the films at 350°C (recall that this is the metric for imidization). Strangely, the ratio was also found to decrease with increasing catalyst loading and the amount of time between preparing the formulation and casting the film. While this would be reasonable in the case of the low temperature cured films, these results are after complete curing, showing that this catalyst can actually decrease imidization if the initial curing temperature or catalyst loading is too high, or if the catalyst is not added to the formulation immediately prior to use.

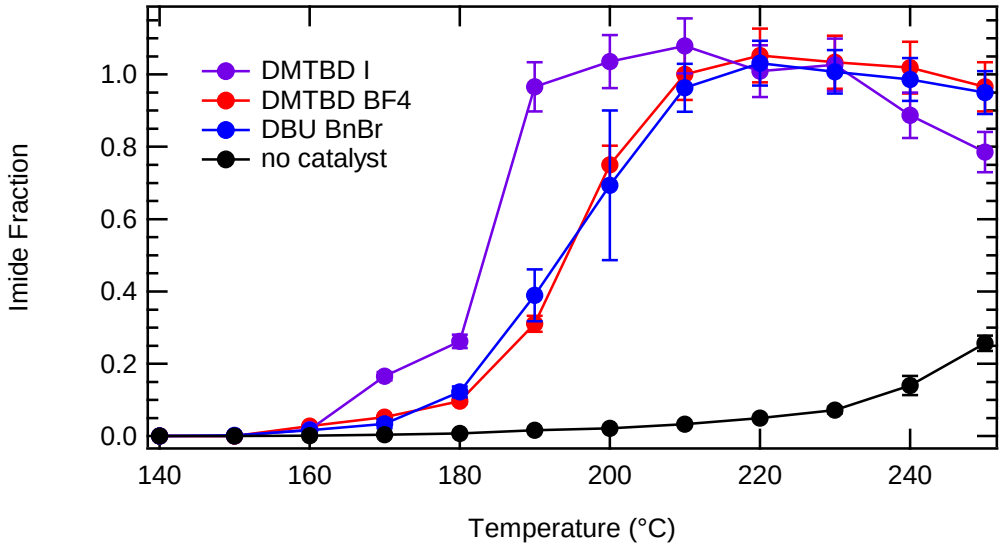

Figure 5.23: Imidization of mPMDA-TFMB-EE using dimethyl TBD salts and DBU BnBr at 5 wt% loadings

CONCLUSIONS

The meta diethyl ester of PMDA-TFMB was exposed to a variety of organic and inorganic salts and then cured at temperatures from 140-250°C. Unexpectedly, it was found that even inorganic salts such as LiCl catalyzed the imidization reaction. However, organic salts performed far better as imidization catalysts and could affect complete curing at temperatures as low as 190°C in 15 minutes. Quaternary ammonium salts were less effective than the more conjugated benzyl DBU, BMIM and DMTBD salts. Additionally, the nucleophility of the anion appears to play a role in the curing process with halide salts being more effective than bis(triflimide), triflate, and tosylate anions.

The mechanical and dielectric properties of films cured with DBU BnBr were studied. It was found that the modulus and hardness of films is actually improved by the addition of catalyst. The dielectric constant and especially the dielectric loss were,

however, negatively affected. This is likely due to the ionic nature of the catalyst as well as it being very hygroscopic.

Finally, other polyimide precursors were cured using DBU BnBr. It was found to be a curing catalyst for PMDA-TFMB PAA and isoimides, as well as PAEs of PMDA-ODA and PMDA-TFMOB. However, there is substantial imidization below 200°C in the case of PAA even without catalyst, and the isoimide still requires a curing temperature of about 250°C with catalyst. PMDA-ODA is cured even more easily than PMDA-TFMB and will completely imidize at 200°C. The PMDA-TFMOB also cures at 200°C, but higher initial curing temperatures result in greatly reduced imidization. Overall, this appears to be a general trend with the more active amidine, guanidine, and imidazole based catalysts, so initial low temperature curing should not be performed at temperatures above about 200°C.

EXPERIMENTAL

General Methods

All solvents and regents were obtained from commercial sources and used as received, unless otherwise specified. DCM and TEA were distilled from CaH_2 while THF and DMF were purified by eluting through an alumina column solvent delivery system under argon. NMP was vacuum distilled from P_2O_5. TFMB was purified by sublimation in vacuum prior to use. Reactions were run in flame-dried glassware and under nitrogen atmosphere, expect where noted. CBDA-TFMB-EE, mPMDA-TFMB-EE, mPMDA-TFMOB-EE and pPMDA-ODA-EE polymers were prepared as described in chapters 3 and 4. ^{1}H and ^{13}C NMR spectra were obtained on a Varian Unity Plus 400 MHz instrument. Solvent proton peaks are used as the internal standard ($CDCl_3$ ^{1}H 7.26 ppm,

^{13}C 77.0 ppm; DMSO-d6 ^{1}H 2.49 ppm, ^{13}C 39.5 ppm; CD_3OD ^{1}H 3.31 ppm, ^{13}49.0 ppm). HRMS (CI) was performed on a VG analytical ZAB2-E instrument and HRMS (ESI) on an Ion Spec FT-ICR instrument. All HRMS is ESI unless otherwise specified. Decomposition temperatures were found using a TA Instruments TGA Q500 at ramp rate of 10°C/min. DSC was performed using a TA Instruments DSC Q100 at 10°C/min.

Degree of Imidization by IR Spectroscopy

Formulations were prepared using a 5 wt% catalyst loading to polymer in NMP at 10 wt% total solids. The solutions were spincoated (1500 rpm) onto double-side polished silicon wafers preheated to 100°C and then baked for 2 minutes at 100°C to obtain films approximately 400 nm thick by ellipsometry (JA Woolam VASE ellipsometer). The wafers were then broken into shards and each shard was heated for 15 minutes at 140, 150,…or 250°C. All the films were then measured on a ThermoSci Nicolet 6700 FT-IR in transmission mode before being fully cured overnight at 350°C in a vacuum oven. No imidization was observed in samples after the post apply bake at 100°C. The degree of imidization was then calculated by:

$$\text{Imidization} = (A_{1783}/ A_{1491})_{\text{sample}} / (A_{1783}/ A_{1491})_{\text{cure}} \quad (5.1)$$

where imidization is the fractional conversion of the ester groups to imides, A_{1783} is the area of the C-O stretch of asymmetric stretch of the imide carbonyl and A_{1491} is the C-C aromatic stretch used as an internal standard in the study. Subscript “sample” after the ratio refers to the polymer baked at each temperature for 15 minutes. “Cure” refers to the samples after complete curing. Error bars were calculated by using the standard deviation

of 3 trials and propagating the error with the standard deviation of 12 fully cured samples for each experiment.

In the case of pPMDA-ODA-EE curing, the C-N peak (1376 cm^{-1}) was used instead of the imide carbonyl peak as there was no overlap with nearby peaks, while the C=C aromatic stretch (1500 cm^{-1}) was still used as the internal standard.

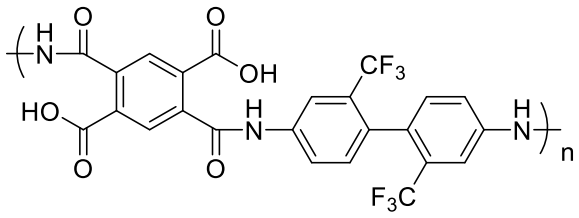

PMDA-TFMB Poly(amic acid)

TFMB (2.94 g, 9.17 mmol) was dissolved in 28 mL NMP in a 100 mL RBF. PMDA (2.00 g, 9.17 mmol) was then added in one portion. The solution immediately turned a dark brown color but after about 30 seconds was yellow. After stirring overnight, the solution was colorless. The 15% PAA solution was then refrigerated and used without further purification.

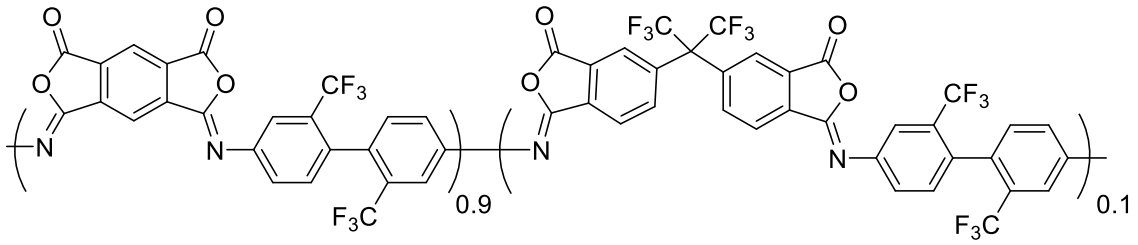

PMDA-TFMB Polyisoimide

Prepared in a similar manner to Seino *et al.*[312] In a 250 mL RBF, TFMB (2.56 g, 8.00 mmol) was dissolved in 20 mL NMP. PMDA (1.57 g, 7.20 mmol) and 6FDA (0.355 g,

0.80 mmol) were then added. The solution quickly became an orange-brown color before fading to a colorless solution. After stirring overnight, phthalic anhydride (0.140 g, 0.95 mmol) was added and the solution stirred for 2 hours. The solution was then diluted with 60 mL NMP and cooled to 0°C. TEA (3.30 mL, 24.0 mmol) was added dropwise, and the solution became quite viscous. Trifluoroacetic anhydride (5.0 mL, 35 mmol) was then added dropwise with vigorous stirring. The solution immediately turned a brilliant yellow color. After stirring for 4 hours, the solution was precipitated into 800 mL of isopropanol, filtered, and dried in vacuum overnight at 80°C to obtain a yellow fibrous solid. (4.34 g, 100%) ^{1}H NMR (400 MHz, DMSO) δ 8.93-7.29 (m)

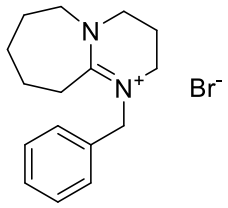

1-benzyl-2,3,4,6,7,8,9,10-octahydropyrimido[1,2-a]azepin-1-ium bromide (DBU BnBr)

In a 250 mL RBF, benzyl bromide was dissolved in 100 mL DCM. The solution was cooled to 0°C and neat DBU was added dropwise. After stirring overnight, the solution was concentrated and the crude product recrystallized from DCM/Et_2O. (6.26g, 98%). Mp 159-162°C. ^{1}H NMR (400 MHz, $CDCl_3$) δ 7.41 – 7.36 (m, 1H), 7.35 – 7.29 (m, 1H), 7.22 – 7.17 (m, 1H), 4.86 (s, 1H), 3.83 – 3.69 (m, 3H), 2.97 – 2.88 (m, 1H), 2.26 – 2.17 (m, 1H), 1.88 – 1.65 (m, 3H). ^{13}C NMR (101 MHz, $CDCl_3$) δ 167.0, 133.9, 129.0, 128.1, 126.1, 56.8, 55.5, 49.4, 47.6, 29.1, 28.1, 25.8, 22.3, 20.0.

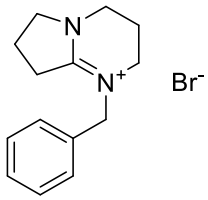

1-benzyl-2,3,4,6,7,8-hexahydropyrrolo[1,2-a]pyrimidin-1-ium bromide (DBN BnBr)

In a 100 mL RBF benzyl bromide (2.75g, 16.1 mmol) was dissolved in 20 mL DCM. The solution was cooled to 0°C and then DBN (2.0g, 16.1 mmol) was added as a neat solid. After addition, the solution was warmed to room temperature and stirred for 6 hours. The solution was then concentrated to obtain an oil. Recrystallization from DCM/THF gave a slightly off-white solid. (4.41g, 93%) ^{1}H NMR (400 MHz, $CDCl_3$) δ 7.29 – 7.23 (m, 2H), 7.23 – 7.18 (m, 1H), 7.18 – 7.14 (m, 2H), 4.59 (s, 2H), 3.80 (t, 2H), 3.47 (t, *J* = 5.9 Hz, 2H), 3.35 (t, 2H), 3.17 (t, *J* = 8.0 Hz, 2H), 2.20 – 2.11 (m, 2H), 2.09 – 2.02 (m, 2H). ^{13}C NMR (101 MHz, $CDCl_3$) δ 165.6, 133.4, 129.3, 128.7, 127.49, 56.8, 54.8, 44.7, 42.77, 31.7, 19.3, 18.4.

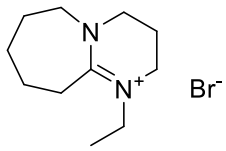

1-ethyl-2,3,4,6,7,8,9,10-octahydropyrrolo[1,2-a]azepin-1-ium bromide (DBU EtBr)

In a 25 mL RBF, ethyl bromide (0.72g, 0.5mL, 6.6 mmol) was dissolved in 5 mL DCM. DBU (1.0g, 6.6 mmol) was added dropwise as a neat liquid. The solution was stirred overnight and the exotherm was much less pronounced than when using BnBr. The solution was concentrated and recrystallized from DCM/THF to obtain translucent white crystals. (1.31g, 76%) ^{1}H NMR (400 MHz, $CDCl_3$) δ 3.60 – 3.55 (m, 2H), 3.49 (ddd, *J* = 14.5, 10.6, 6.5 Hz, 6H), 2.77 (dd, *J* = 7.2, 2.8 Hz, 2H), 2.06 – 1.95 (m, 2H), 1.68 – 1.54

(m, 6H), 1.11 (t, J = 7.3 Hz, 3H). ^{13}C NMR (101 MHz, $CDCl_3$) δ 166.0, 55.1, 49.1, 48.9, 46.4, 28.2, 28.1, 25.8, 22.8, 20.0, 13.7.

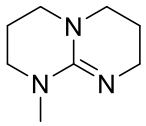

1-methyl-1,3,4,6,7,8-hexahydro-2H-pyrimido[1,2-a]pyrimidine (MTBD)

Dimethyl carbonate (250 mL, 3.0 mol) and TBD (50.0 g, 359 mmol) were added to a 500 mL RBF. The flask was connected to a 3 section Synder distillation column and distillation head with a 2 neck receiving flask. The second neck was connected to a bubbler to prevent air entering the system. The solution was heated to 105°C for 6 hours and then cooled to room temperature overnight. The crude product was then concentrated in vacuum. About 125 mL of heptane and 15 g of celite were added and the solvent was again removed. Additional heptane (175 mL) was added and the resulting slurry filtered through celite under nitrogen. After concentrating, a yellow oil was obtained. The crude product was then distilled (84°C, 0.9 torr) to obtain a colorless, slightly viscous oil (38.6 g, 70%). ^{1}H NMR (400 MHz, benzene) δ 3.60 – 3.56 (m, 2H), 2.93 (s, 3H), 2.73 – 2.65 (m, 4H), 2.58 – 2.53 (m, 2H), 1.67 – 1.60 (m, 2H), 1.53 – 1.46 (m, 2H). ^{13}C NMR (101 MHz, benzene) δ 151.18, 48.84, 48.81, 48.41, 44.87, 37.44, 23.99, 23.57. HRMS $[M+H]^+$ calcd. 154.1339 found 154.1338

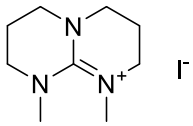

1,9-dimethyl-3,4,6,7,8,9-hexahydro-2H-pyrimido[1,2-a]pyrimidin-1-ium iodide (DMTBD I)

MTBD (1.0 g, 6.5 mmol) was dissolved in 10 mL THF in a 50 mL RBF. Methyl iodide (0.41 mL, 6.5 mmol) was then added in one portion. The solution quickly became cloudy and a white precipitate began to form. After stirring for 1 hour, the reaction was diluted with 20 mL ether and stirred for 5 minutes before the solvent was decanted off. The white solid was washed twice more with 20 mL of ether and the solid dried in vacuum (1.69 g, 88%). mp 258-259°C (decomp) ^{1}H NMR (400 MHz, CD_3OD) δ 3.50 (t, J = 6.3 Hz, 4H), 3.38 (t, J = 5.8 Hz, 4H), 3.08 (s, 6H), 2.13 (dt, J = 12.1, 6.2 Hz, 4H). ^{13}C NMR (101 MHz, CD_3OD) δ 49.32, 49.04, 41.30, 22.21. No other C peaks were observed.

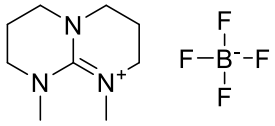

1,9-dimethyl-3,4,6,7,8,9-hexahydro-2H-pyrimido[1,2-a]pyrimidin-1-ium tetrafluoroborate (DMTBD BF_4)

DMTBD I (3.00 g, 10.2 mmol) was dissolved in 9 mL of acetonitrile. In an argon filled glovebox silver tetrafluoroborate (1.98 g, 10.2 mmol) was added to a 100 mL RBF. The sealed flask was removed from the glovebox and placed on a Schlenk line and 21 mL of acetonitrile was added. After the silver tetrafluoroborate had dissolved, the DMTBD I solution was added dropwise at room temperature. A yellow precipitate formed immediately. After stirring for one hour, the solution was filtered through a syringe filter to remove precipitated AgI, concentrated, and recrystallized from DCM/toluene to obtain white needles (1.42 g, 55%). mp 204-208°C (decomp) ^{1}H NMR (400 MHz, $CDCl_3$) δ

3.38 (t, J = 6.3 Hz, 4H), 3.27 – 3.21 (m, 4H), 2.96 (s, 6H), 2.04 (dt, J = 12.2, 6.2 Hz, 4H).

^{13}C NMR (101 MHz, $CDCl_3$) δ 157.91, 48.23, 48.03, 40.72, 20.99.

Chapter 6: More Efficient and Stronger Base Photobase Generators for Photosensitive Polyimides

INTRODUCTION

By now the importance of photoactive compounds (PACs) in the microelectronics industry should be clear to the reader. As discussed in Chapter 1, the use of photoactive compounds is central to the lithographic processes used in the production of computer chips. Typically photoacid generators (PAGs) are used in the industry as they are capable of producing super acids with high quantum efficiency.[26, 54] Radical generating photoinitiators are also utilized in acrylate based crosslinking schemes for negative tone resists, such as commercial PSPIs.[109-110] Photobase generators (PBGs) on the other hand have been more of an academic curiosity. However, as detailed in Chapter 3, the microelectronics industry has been interested in the use of PBGs in photosensitive polyimide formulations as well as for decarboxylating photoresists.[59, 63, 126, 319]

The development of photobase generators has largely come from synthetic organic chemistry. Photosensitive protecting groups (PPGs) have long been required to shield sensitive parts of complex organic molecules from reactions occurring elsewhere in the molecule.[320-322] These groups offer the advantage of being able to be selectively cleaved under mild conditions in the presence of light and provide orthogonal protection to traditional acid/base sensitive protecting groups. Several reviews have been published on PBGs in particular.[61, 323]

The set of requirements for good PBGs closely follows those of photosensitive protecting groups in general. These materials should exhibit the following characteristics:

1) The PBG should absorb in the UV at the desired exposure wavelength. For use in 193 nm photoresists, such as the pitchdivision resists described in Chapter 2, nearly any PBG will meet this requirement. For use in PSPI, this requires that the PBG be significantly red-shifted and have substantial absorbance at i-line (365 nm) or an even longer wavelength.
2) High quantum efficiency (Φ) is desirable. Quantum efficiency is defined as the ratio of the amount of base produced divided by the number of photons absorbed by the PBG. In general, the efficiency is a function of wavelength and tends to be lower for PBGs than PAGs. High quantum efficiency allows for shorter exposures and increased throughput.
3) The PBG should photo-bleach upon exposure. That is, the absorbance of the photoproducts should be lower than the starting PBG. This allows for higher loadings of PBG and for the patterning of the thick films required in packaging dielectrics as the photoproducts do not compete with the unreacted PBG for light.
4) Finally, the PBG should be thermally stable. For pitchdivision resists, temperatures of up to 120°C are required during post exposure bake steps. However, temperatures of at least 140°C are required for PSPI, with even higher thermal stability being desirable.

CARBAMATE PBGS

Typically, PBGs are based on carbamates. These are primary or secondary amines that exist as amides protected by a photosensitive protecting group. Figure 6.1 shows a few representative examples. Upon exposure, the PPG (black) is removed to form a

carbamic acid. These carbamic acids are unstable, especially at post exposure bake temperatures, and release carbon dioxide (blue) to form the free amine (red).

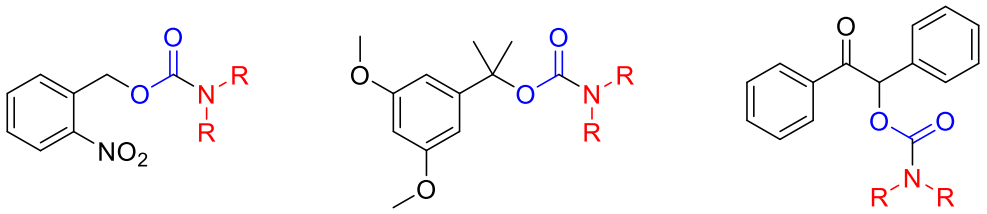

Figure 6.1: Examples of carbamate type PBGs

Of the carbamate class of PBGs, ortho-nitrobenzyl (ONB) carbamates are the most commonly used.[61] The mechanism for base generation upon light exposure is shown in Figure 6.2. In this process an intramolecular redox reaction occurs in which the excited state of the aromatic nitro group abstracts a benzylic proton to form a cyclic intermediate. This intermediate then collapses forming o-nitrosobenzaldehyde, carbon dioxide, and the amine. This protecting group was originally developed by Barltrop *et al.* at Oxford in the 1960s,[321-322] used as a protecting group for amino acids in the 1970s by Patchornik and Woodward,[58] and finally explored as a candidate for PBGs by Cameron and Frechet in the 1990s.[79] As the reaction is intramolecular, it functions in the solid state. The quantum efficiency for standard ONB carbamates was found to be 0.13 at 254 nm, which is reasonably efficient for PBGs.[79] Note, however, that this was performed using IR spectroscopy and calculating quantum efficiency was based on disappearance of starting material and not generation of base. Our results from the pitchdivision base quantification experiments showed that base generation quantum efficiency is often much lower, and values obtained in the Cameron paper are significantly higher than reported literature values for the quantum efficiency.

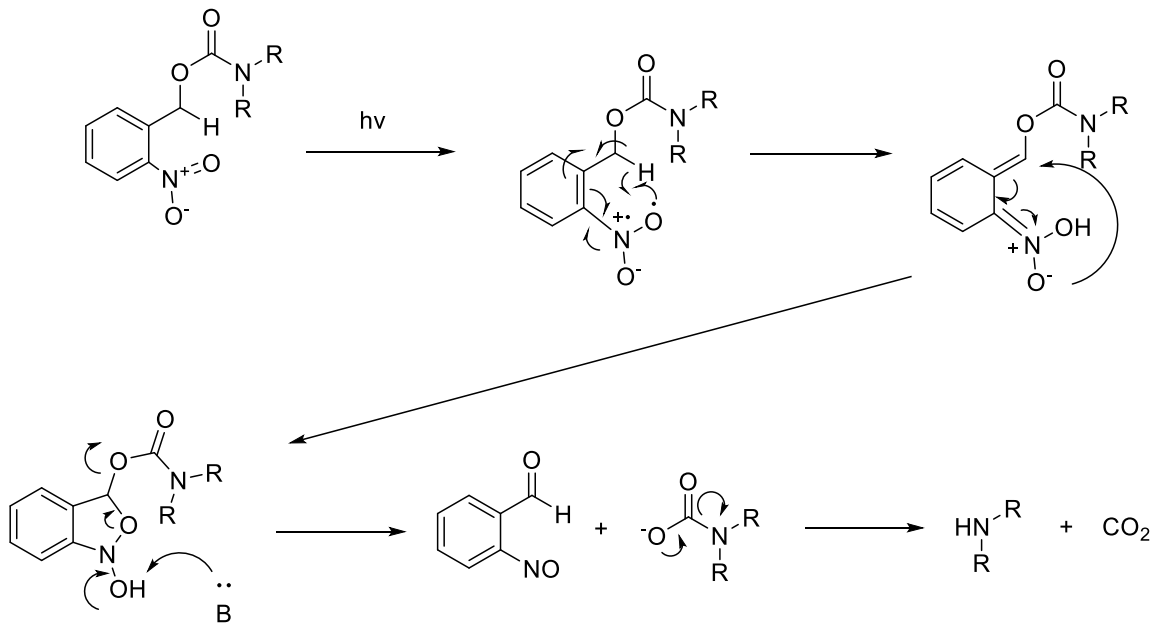

Figure 6.2: Proposed mechanism of the photolysis of o-nitrobenzyl carbamate PBGs[82]

The major drawback of the ONB carbamates is that they only absorb strongly at wavelengths below about 320 nm (Figure 6.3). The ONB group can be modified with electron donating methoxy groups to form the 6-nitroveratryloxycarbonyl (NVOC) chromophore, as discussed in Chapter 3. However, this reduces quantum efficiency significantly (Φ~0.01)[171] and therefore requires large doses for patterning.[276] The synthesis of the stronger base PBG NVOC 2,2,6,6-tetramethylpiperidine (NVOC TMP) was reported by IBM,[324] and we tested it for our PSPI system. However, it actually was less effective than regular piperidine, likely due to the increased steric hindrance. We also tested a mono-methoxy ONB piperidine (MONB piperidine) variation, but found the absorbance at i-line to be insufficient for patterning. The low degree of imidization using the piperidine-based carbamate PBGs in our PSPI system and the ability of low loadings of DBU to completely cure the films at 200°C led us to consider new classes of PBGs that were more efficient and/or generated stronger bases.

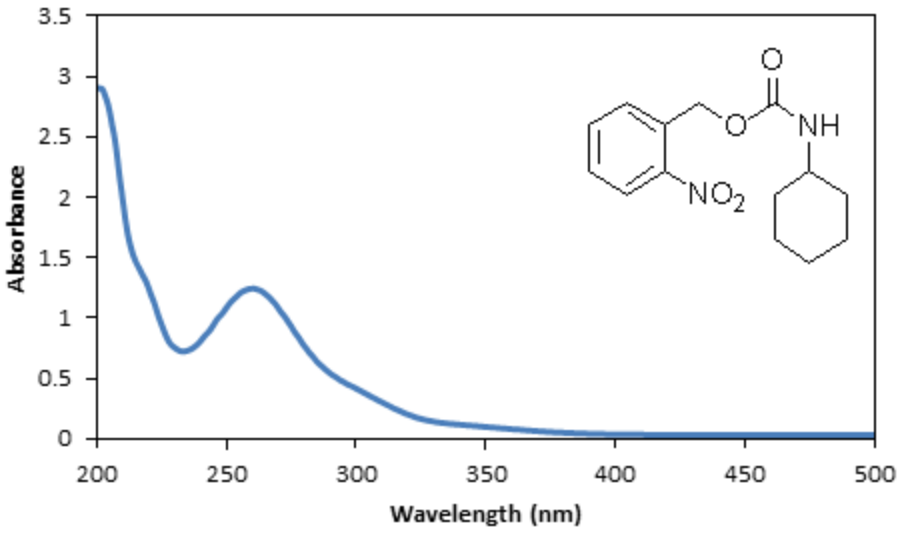

Figure 6.3: UV spectrum of 220 μM ONB cyclohexylcarbamate in acetonitrile

NVOC AMIDINE PBG

Generating tertiary amines or amidine bases present a new challenge when compared to the carbamate based PBGs that generate primary or secondary amines. To create PBGs that produce these bases, three general methods that have been employed. The first is based on photochemical de-alkylation of quaternary salts,[282, 325] the second on decarboxylation of acetate salts[326-327] and the third is conversion of tertiary amines into amidines.[326] The literature also contains a report of using an NVOC protected aminoalkyl lactam that generates DBU upon exposure to cure epoxy resins (NVOC DBU, Figure 6.4).[328] While the dehydration reaction of the aminoalkyl lactam is the commercial route to DBU, this process typically requires an acid catalyst and extended reaction times at high temperature.[329]

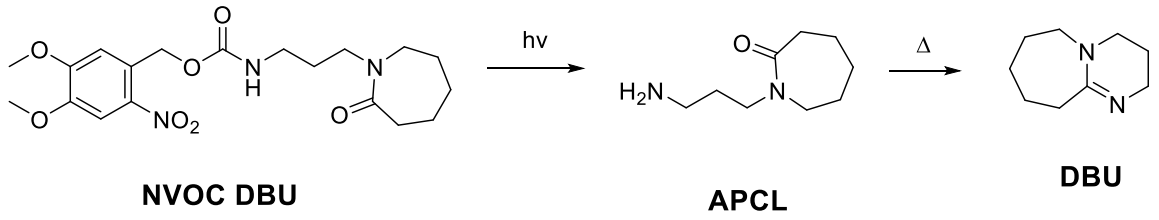

Figure 6.4: Production of DBU from NVOC protected aminoalkyl lactam

However, as this compound is easily prepared, not a salt or an amine, and claimed to generate DBU, it appeared to be a reasonable place to begin in the search for amidine PBGs. Strangely, despite DBU being commercially prepared from the 3-aminopropyl-ε-caprolactam (APCL), the lactam itself is not commercially available. It was synthesized, rather ironically, by first hydrolyzing DBU in a minimal amount of water. The PBG was then prepared by reacting APCL with NVOC chloride in the presence of TEA to absorb the generated acid (Figure 6.5). While the reactions proceeded smoothly, purification of the PBG by flash chromatography proved to be a challenge. NVOC DBU is quite polar and not very soluble in many organic solvents, which resulted in significant streaking on the column, even when using 100% EtOAc as the eluent.

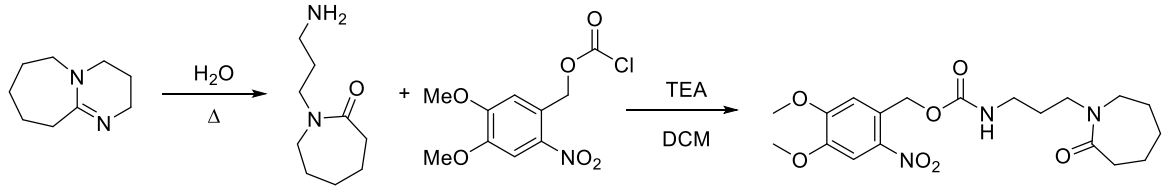

Figure 6.5: Synthesis of NVOC DBU

The NVOC DBU photobase was then tested and compared to NVOC piperidine in its ability to imidize mPMDA-TFMB-EE polymer (Figure 6.6). Both PBGs generate

base, but NVOC DBU is actually less effective than our standard NVOC piperidine photobase. The difference in molecular weight of the PBGs is minimal, so the molar concentration cannot explain the observed difference. It is known that primary amines are slightly worse catalysts then secondary amines for the imidization reaction.[125] From these data, it appears that the primary amine is generated from NVOC DBU, but it does not dehydrate to the much more reactive at these temperatures during a 10 minute PEB. If anything, the gap between the piperidine and DBU PBGs appears to actually grow with increasing temperature. The cyclized DBU is a stronger base and it should diffuse more quickly than the APCL, further suggesting that DBU is not produced on the timescale of minutes. While easy to prepare, NVOC DBU is just not an effective catalyst for the PSPI system.

One other attempt to use a NVOC chromophore focused on modifying the DBN BnBr curing catalyst from Chapter 5 to replace the benzyl group with 3,4 dimethoxy-2-nitrobenzyl (NVDBN Br). While slightly different than the NVOC group due to the lack of a carbonyl spacer, this compound was found to not be a PBG (though it still functioned as a thermal curing catalyst for polyimides). The lack of success in generating amidine bases using the NVOC chromophore lead us to the exploration of other reported amidine PBGs.

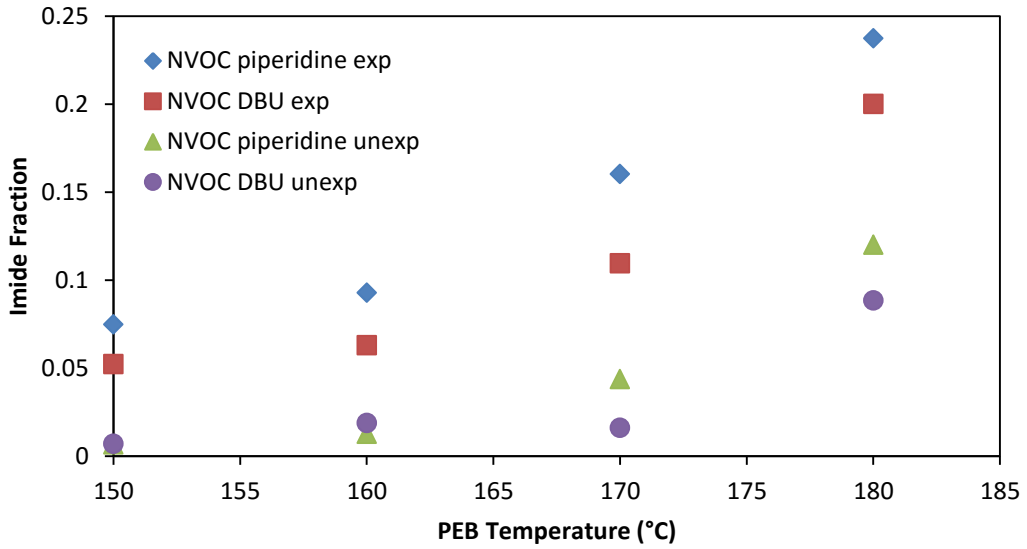

Figure 6.6: Comparison of NVOC piperidine and NVOC DBU on the curing of mPMDA-TFMB-EE. Films were loaded with 5 wt% PBG, exposed to 2 J/cm^2 i-line radiation and baked for 10 minutes at various temperatures

NORRISH TYPE II AMIDINE PBG

Our discovery of the catalytic curing effects of many organic salts on polyimide precursors led us to focus on non-salt precursors to amidines. It is known that the relative effectiveness of amine bases on poly(amic ester) curing increases roughly as 3° < 1 °< 2° << amidine.[124-125] With this knowledge, it seemed possible that significant contrast could be obtained by photochemically converting a tertiary amine into an amidine. Two different routes to this have been reported in patents (Figure 6.7). Both are based on N-alkylated hydrogenated amidines and were developed at Ciba-Geigy (now part of BASF). In the first case, hydrogenated benzyl DBN (Bn-HDBN) derivatives were reported to generate DBN, presumably through an intramolecular redox reaction to give toluene derivatives as the side-product.[326] The other route has been to use phenacyl derivatives

(PA-HBDN) to abstract the proton alpha to the two nitrogen atoms (the 8a position) in a Norrish Type II reaction.[327] Here, only the phenyl derivatives (R = Ph) were explored in detail.

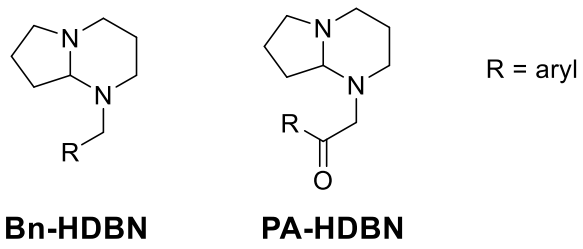

Figure 6.7: Reported tertiary amines that generate DBN upon UV exposure

Bn-HDBN was first tested for thermal stability in the mPMDA-TFMB-EE system (Figure 6.8). The compound is stable to about 100-120°C before degrading and acting as a reasonably effective curing catalyst. This is in agreement with TGA showing the material beginning to degrade around 100°C. Additionally, the poor yield after purification of this compound is assumed to be due to degradation during distillation. A distillation pressure lower than 0.67 torr (87-90°C) is recommend as the material went from a colorless oil to a viscous red gel upon heating. This curing behavior could actually be advantageous as we envisioned that PSPI could be printed by first exposing, baking at low temperature, developing, then heating to about 220°C to affect the full cure.

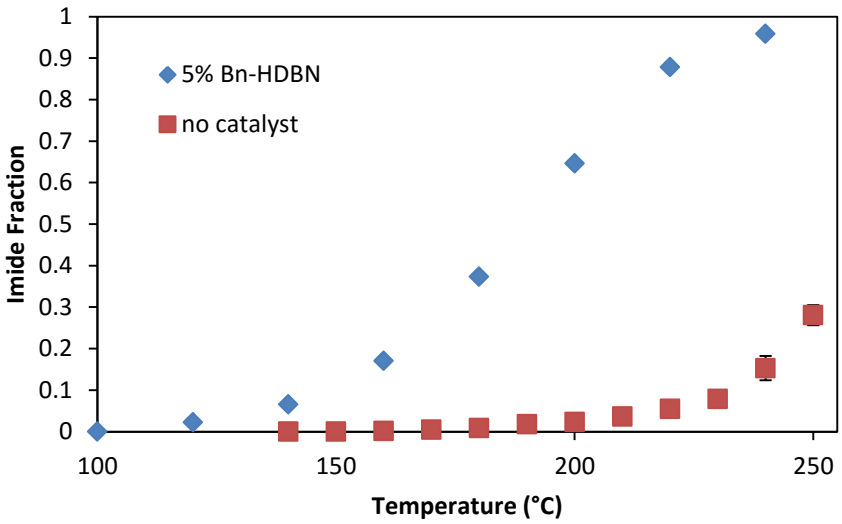

Figure 6.8: Effect of 5 wt% Bn-HBDN on imidization in mPMDA-TFMB-EE. Samples were unexposed and baked 10 minutes at various temperatures

Films of mPMDA-TFMB-EE containing 5 wt% Bn-HDBN and 1.2 equivalents of isopropylthioxanthone (ITX, i-line sensitizer) were exposed to i-line radiation at doses up to 10 J/cm^2 and baked at 120°C. However, no imidization was observed, even at these extremely high doses, so further studies with Bn-HDBN were abandoned.

PA-HDBN was prepared by Dr. Ryan Mesch. This material was designed to undergo a Norrish Type II reaction upon exposure to UV light (Figure 6.9). In this reaction, a γ-hydrogen (a hydrogen atom 3 carbon atoms away from the carbonyl) is abstracted to generate a 1,4 di-radical species.[115] In the desired reaction, the di-radical then fragments into an alkene and an enol.[330] In the case of phenacyl protecting groups, the enol then tautomerizes to acetophenone.

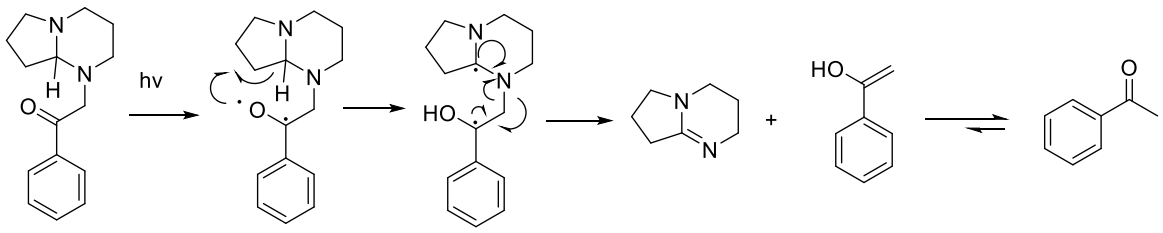

Figure 6.9: Proposed Norrish Type II reaction in PA-HDBN

PA-HDBN was dissolved in acetonitrile in a quartz NMR tube and de-gassed by bubbling nitrogen through the solution. The solution was then exposed to 254 nm radiation in a Rayonet reactor and the progress of the photolysis was monitored by ^{1}H NMR spectroscopy (Figure 6.10). The expected acetophenone product was clearly produced in the reaction. DBN also appeared to be produced based on the appearance of a pair of triplets at 3.2 ppm corresponding to the positions marked red in the figure.

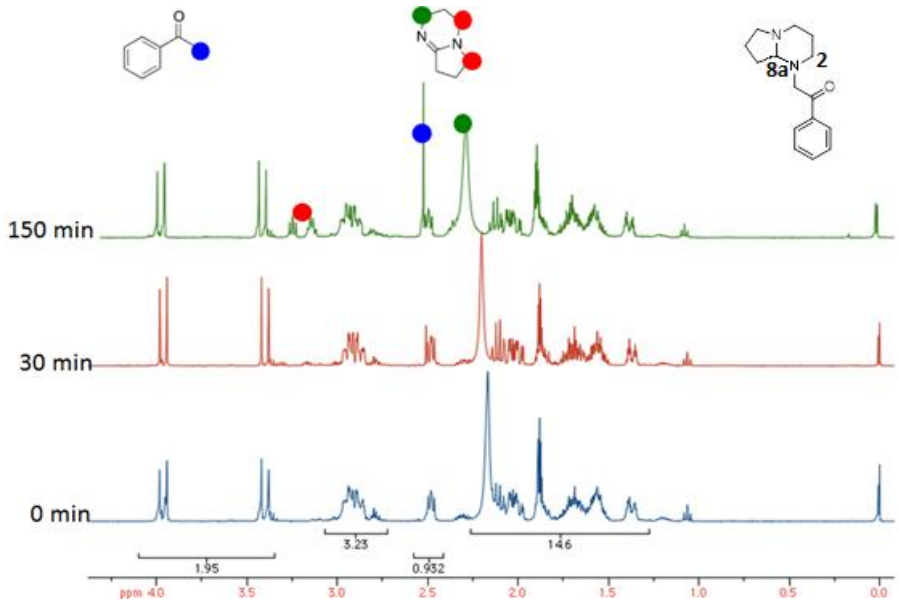

Figure 6.10: NMR spectra of PA-HDBN in acetonitrile after 254 nm exposure

While this result was the goal of this PBG, the PA-HDBN system is a bit more complex than a typical Norrish substrate. There are multiple different γ-hydrogens, there is a nitrogen atom instead of a carbon in the β position, and there is a fused ring system. Of these, we believed that the fused rings and multiple γ-hydrogens could create problems. There are twice as many γ-hydrogens in 2 position as there are in the 8a position (carbon between the nitrogens). The requirement that the carbonyl oxygen must be spatially close to the γ-hydrogen to abstract it means that the carbonyl is more likely to abstract a less sterically hindered hydrogen. Additionally, the fused ring nature of the PBG means that this compound prefers a pseudo trans conformation with the hydrogen and phenacyl groups on opposite sides of the ring at room temperature. In this conformation, the carbonyl group may be too far away to effectively abstract the 8a hydrogen. Taken together, it seems much more likely that hydrogen abstraction should occur at the 2 position to form an imine rather than at the 8a position to form the desired amidine. However, the 1,4 di-radical containing a radical in the 8a position may be significantly more stable than in the 2 position, resulting in the production of DBN in the solution phase. Both phenyl and p-dimethylaminophenyl derivatives of this PBG were explored in the patterning of mPMDA-TFMB-EE films. However, there was no observable difference after baking between exposed and unexposed regions. It appears that this class of PBGs is capable of producing amidine bases in solution as the patent claimed, but unfortunately they are not effective catalysts in the solid phase.

SALT-BASED PBGS

At this point we believed that we had exhausted all of the reported amidine PBGs that did not utilize salts and were still in desperate need of a stronger base PBG, so we

targeted protonated salt PBGs. These PBGs can be thought of as salts formed from the neutralization of an acid and a base. A few examples are shown in Figure 6.11. All of the examples shown generate the guanidine base TBD, which is stronger than amidine bases such as DBU and DBN. However, amine, amidine or even phosphazene bases should be able to be used in theory. In the case of TBD-NP and TBD-XA, these PBGs were prepared simply by mixing solutions of TBD and the free acetic acid derivatives. The salt product then quickly precipitates from solution and can be filtered off to give the pure PBG with no further purification necessary. Both of these PBGs are reported to function in the same manner: upon UV exposure the chromophore dercarboxylates and abstracts a proton from the protonated base, releasing the free base.[284-285, 331]

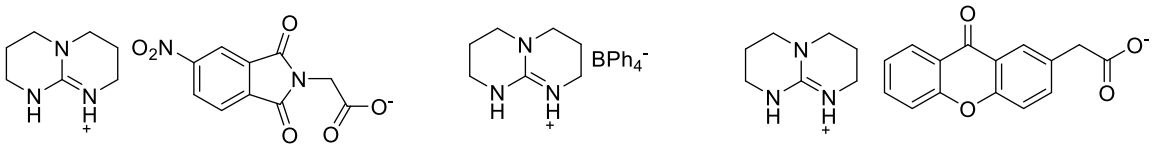

Figure 6.11: Reported PBGs based on protonated salts

Figure 6.12 shows the results of i-line exposure of mPMDA-TFMB-EE containing 5 wt% loadings of TBD-NP and TBD-XA in about 400 nm thick films. Unfortunately, neither appears to generate base photochemically. However, both graphs show that our concerns with using salt-based PBGs were justified; both PBGs caused imidization in the film even without UV exposure at our standard PEB temperature conditions. This was especially true in the case of TBD-NP, where the degree of

imidization in unexposed samples is on par with what we observed in exposed regions using traditional NVOC PBGs in our PSPI system.

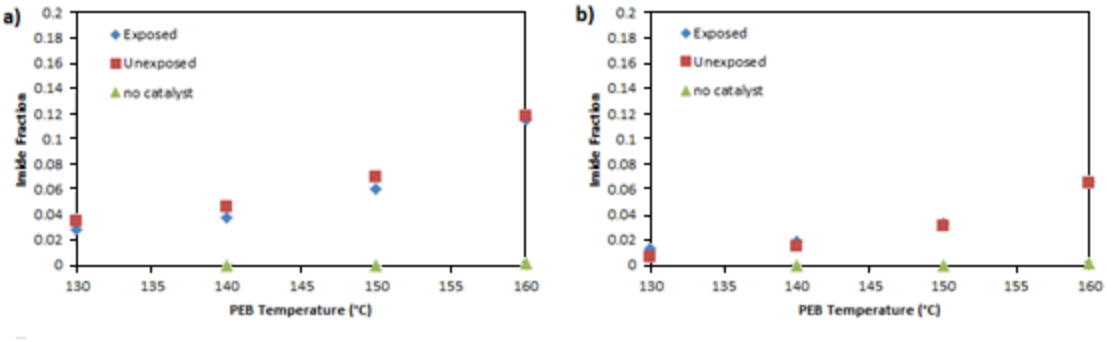

Figure 6.12: Imidization in mPMDA-TFMB-EE using 5 wt% loadings of a) TBD-NP and b) TBD-XA. Samples were exposed to 2 J/cm^2 365 nm radiation then baked for 10 minutes.

TBD-TPB and its derivatives are easy to prepare. TBD was first dissolved in a dilute HCl solution to generate the hydrochloride salt in solution. An aqueous solution of $NaBPh_4$ was then added and the PBG precipitated from solution.[283] The photolysis of the tetraphenylborate anion is well-studied and primarily produces triphenylboron and benzene in the presence of proton sources.[283, 332-333] This means that unlike the cases of the decarboxylating PBGs, the Lewis acidic triphenylboron by-product can complex with the generated base and weaken the effective base strength.

As the tetraphenylborate anion only functions in the deep UV, initial exposures were performed using broadband UV exposures on a Novocure 2100 spot curing system. Thin films (~330 nm thick) of mPMDA-TFMB-EE containing 5 wt% of TBD-TPB were exposed to 330 mJ/cm^2 and baked for 10 minutes (Figure 6.13). Surprisingly, this PBG actually provides a higher degree of imidization than that observed in our best cinnamide PBGs. Additionally, background imidization does not occur until about 130-140°C.

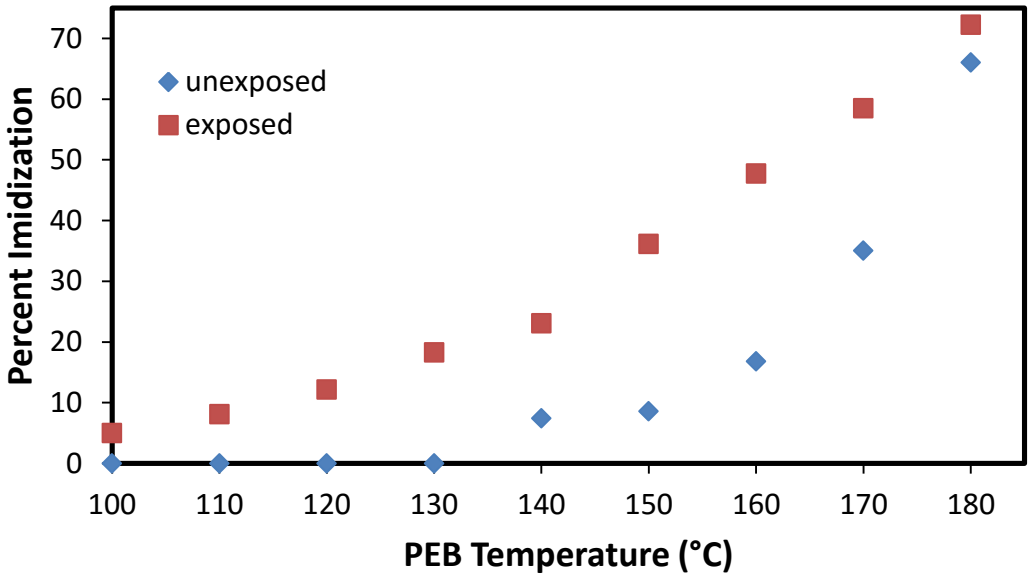

Figure 6.13: Imidization in mPMDA-TFMB-EE using 5 wt% TBD-TPB. Films were exposed to 330 mJ/cm^2 broadband UV and baked for 10 minutes

The major obstacle to implementing TBD-TPB in our system, however, is the non-existent absorbance at i-line.[283] TBD-TPB is not even very absorbent at 254 nm, so no PSPI system using this PBG would be able to print thick films. However, the tetraphenylborate (TPB) anion appears to be structurally similar to the triphenylsulfonium cations in ionic PAGs, so we believed that it may be possible to sensitive TBD-TPB with sensitizers commonly used for ionic PAGs (Figure 6.14). Anthracene and 2-isopropylthioxanthone (ITX) are both i-line sensitizers while 5,12-bis(phenylethynyl)tetracene (DP-tetracene) is a visible light sensitizer. There is even one claim of using ITX to sensitize TBD-TPB,[334] and another using ITX to sensitize tetrabutylammonium tetraphenylborate.[335]

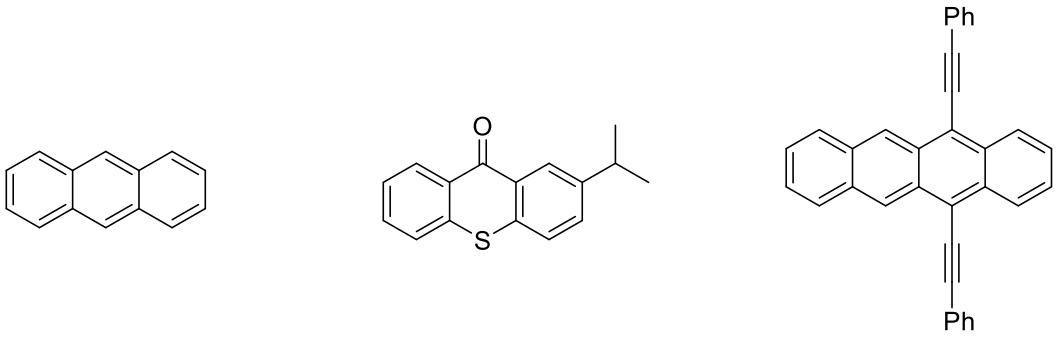

Anthracene **ITX** **DP-tetracene**

Figure 6.14: Typical sensitizers for ionic PAGs

For sensitization experiments, 1.2 equivalents of each sensitizer (to PBG) was added to the standard 5 wt% PBG/ mPMDA-TFMB-EE test polymer. Films were then exposed to variable amounts of narrow band i-line radiation and baked at 140°C for 10 minutes (Figure 6.15). Unexposed films in this study were observed to have ~5% imidization by IR. All three of the sensitizers used in the experiment resulted in significantly imidized films. The DP-tetracene was less effective than either anthracene or ITX, both of which gave similar imidization results. This likely is a result of the triplet energies of these sensitizers decreasing from ITX > anthracene > DP-tetracene.[67] The excited triplet state energy in both ITX and anthracene appears to be sufficiently large that energy transfer to the tetraphenylborate anion is very efficient. It is also possible that DP-tetracene is so conjugated that its molar absorptivity at 365 nm is particularly large. This could cause all of the light to be absorbed at the top of the film, resulting in no imidization at the bottom. Excessive UV exposure would then begin to slowly bleach the sensitizer, allowing light to reach the bottom of the film at high doses. Regardless, both ITX and anthracene were found to be very effective sensitizers for TBD-TPB, resulting in

both higher degrees of imidization at much lower doses than either NVOC or cinnamide PBGs.

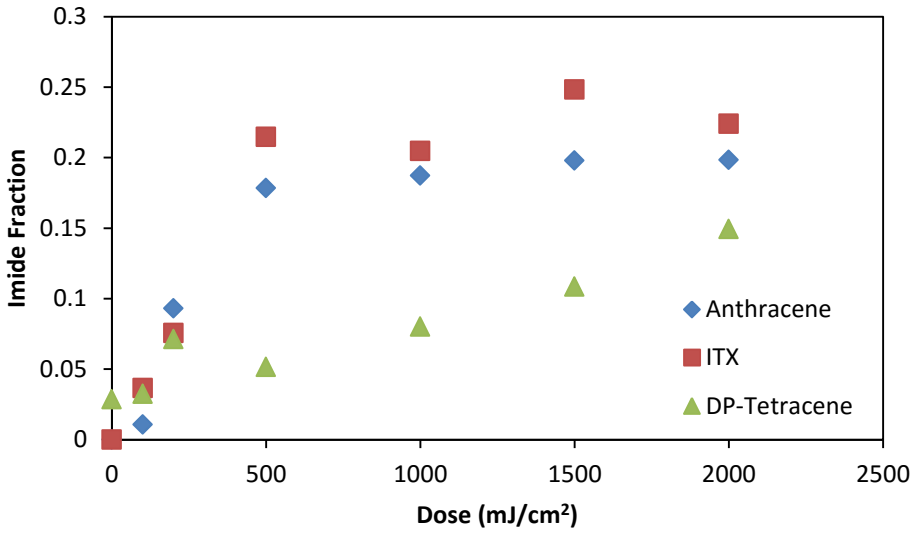

Figure 6.15: Imidization in mPMDA-TFMB-EE using 5 wt% TBD-TPB and 1.2 eq sensitizer. Samples were baked at 140°C for 10 minutes.

As the sensitization results appeared so promising, we decided to explore the effect of bake time and temperature on the system. From Figure 6.13, it is clear that TBD-TPB either begins to act as a catalyst or degrades into a catalyst at temperature above about 140°C. However, base catalyzed imidization is also much more effective at elevated temperatures. Figure 6.16 shows the difference in the degree of imidization between exposed and unexposed regions. It appears that the best contrast is obtained by baking for very short times at higher temperatures, rather than the extended times at low temperatures that we have been using. The simple difference between exposed and unexposed regions may not be the best function to optimize either. There is a degree of imidization where the unexposed regions are no longer soluble in developer, and it does

not matter how much more imidized the exposed region is as nothing will print. At the 170°C bake for 5 minutes, the background imidization is still less than 10%. Development issues should not be an issue in this case and this bake condition is likely the optimal PEB condition.

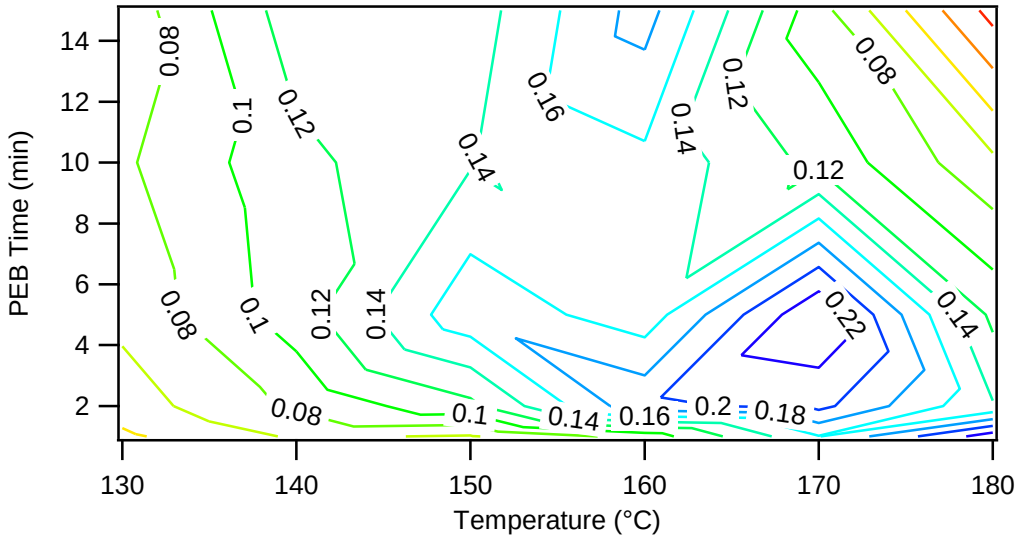

Figure 6.16: Contrast between exposed and unexposed in TBD-TPB/ITX/mPMDA-TFMB-EE system as a function of bake time and temperature. Samples were exposed to 500 mJ/cm^2 i-line radiation.

The sensitized TBD-TPB system is currently the most promising system for patterning mPMDA-TFMB-EE that we have found. We also tested variations on this PBG by using other bases in place of TBD, such as DBN, guanidine, tetramethylguanidine, and proton sponge. However, none of these were as effective as TBD-TBP at imidizing mPMDA-TFMB-EE. Future work will focus on the implementation of this PBG in multiple microns thick films for comparison to NVOC and cinnamide PBG printed line and space patterns.

Finally, there is one other major class of salt-based amidine PBGs: those based on quaternarized amidines. These typically consist of a phenacyl derivative protecting group

attached to the imine nitrogen of the amide along with an aryl borate based anion.[327] The simplest possible example is shown in Figure 6.17. While similar structures without the tetraphenylborate have been synthesized and are reported to not generate base upon UV radiation,[336-337] those incorporating this anion supposedly do. This tetrafluoroborate is reported to generate α-cleavage in the standard Norrish Type I pathway, but no basic species were found.[337] Halide salts generate the protonated amine salts upon exposure.[336] It is unclear from the patent why the tetraphenylborate salts should generate free amines. Nonetheless, we synthesized this compound for testing with the mPMDA-TFMB-EE polymer.

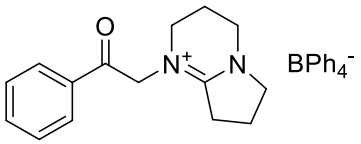

PDBN-TPB

Figure 6.17: Representative example of a quaternarized DBN based PBG

Initial testing of PDBN-TPB was performed in deuterated acetonitrile at an exposure wavelength of 254 nm. The reaction was tracked by ^{1}H-NMR similarly to PA-DBN (Figure 6.18). The color-coding in Figure 6.18 is the same as the PA-DBN exposure in Figure 6.10. Surprisingly from the crude experiment, the same peaks appear as in the PA-DBN exposure. The acetophenone singlet at 2.5 ppm (blue) is clearly visible along with the triplets at 3.2 ppm (red) and broad peak at 2.3 ppm (green) indicating that DBN is present in the solution. Interestingly, the production of base appears to occur much more quickly than in PA-DBN as well.

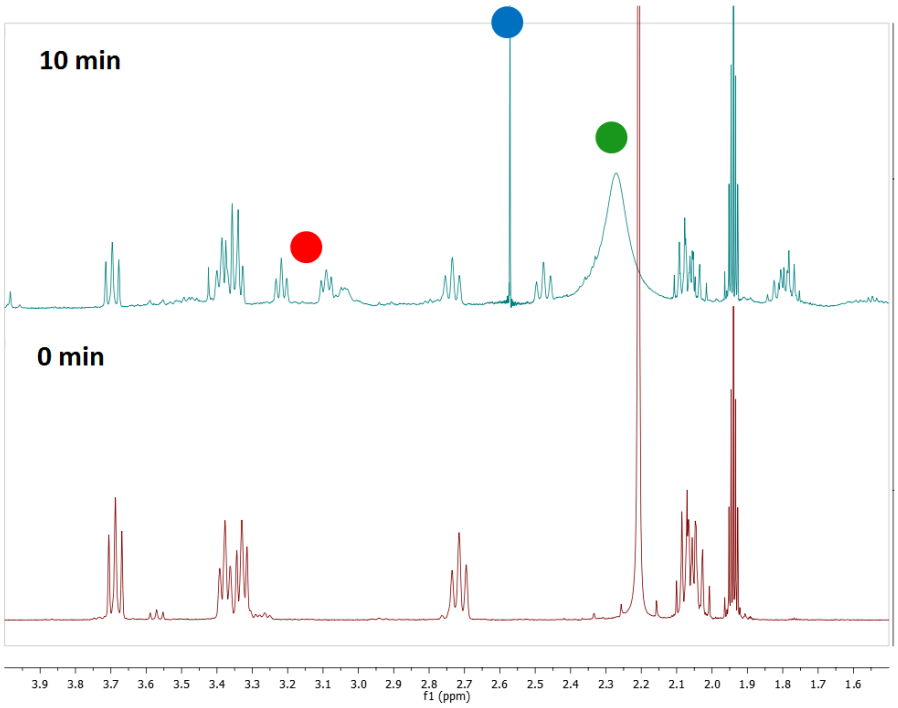

Figure 6.18: NMR spectra of PDBN-TPB before and after 254 nm exposure

PDBN-TPB was then formulated with mPMDA-TFMB-EE as a 10 wt% loading to polymer and cast as films on silicon wafers. The films were exposed to 1 J/cm^2 at 254 nm and then baked for 10 minutes (Figure 6.19). While the loading in this sample was higher than previous PBGs, the degree of imidization is also significantly higher. This PBG also appears to be slightly more thermally stable as background imidization is limited until about 160°C, even at the higher catalyst loading. Unexpectedly, PDBN-TPB appeared to be the most effective catalyst for exposures at 254 nm. However, when we tried to sensitize films containing this PBG with both anthracene and ITX and exposing to i-line radiation, neither had an appreciable effect. Doses up to 10 J/cm^2 were explored, but no noticeable difference in the IR spectra of unexposed and exposed samples was observed. While the PDBN-TPB PBG is very promising, further work is required to find a suitable sensitizer. It may be possible to utilize a more red-shifted chromophore and

eliminate the need for sensitization at all, though this could be synthetically challenging.[325] Even preparing this simple-looking molecule was deceptively challenging; the intermediate bromide salt forms as a nearly white precipitate upon the reaction of DBN with phenacyl bromide in ether/toluene. However, exposing it to moist air during filtering causes the solid to convert into a sticky, bright orange mass instead of an off-white powder. During the next synthesis step the bromide salt was dissolved in water and precipitated as the desired tetraphenylborate salt PBG. If a large chromophore is used to sufficiently red-shift the absorbance, this salt may no longer be soluble in water and further complicate synthesis.

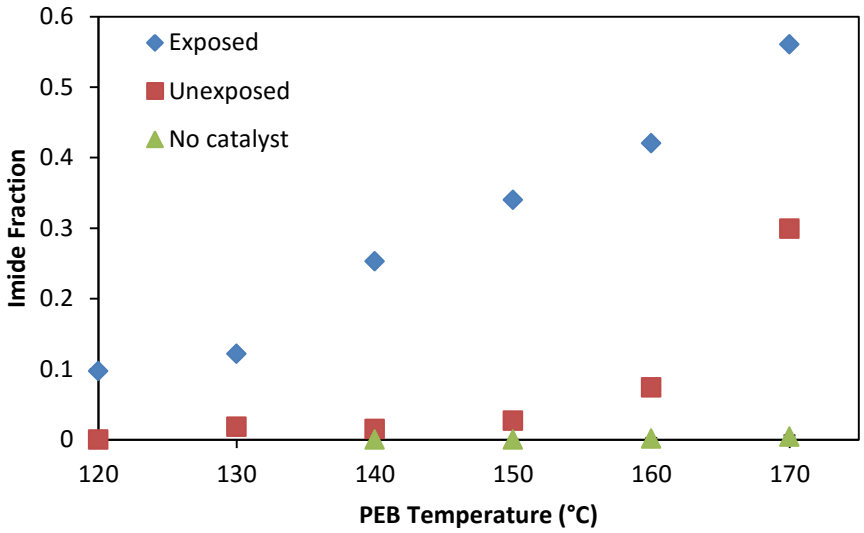

Figure 6.19: Imidization of mPMDA-TMFB-EE using 10 wt% PDBN-TPB. Samples were exposed to 1 J/cm^2 at 254 nm before being baked for 10 minutes.

MORE EFFICIENT PHOTOBASE GENERATORS

During the exploration of new amidine photobase generators for the PSPI system, we also investigated the potential of using more efficient chromophores for patterning. While the NVOC based PBGs were thermally stabile and i-line absorbent, efficiency was very poor (~1%)[170-171] and the photoproducts are more absorbent than the starting PBG. While implementation of the cinnamide class of PBGs was successful (Chapter 3), those materials required acid to generate the catalyst. This could lead to corrosion in the copper metallization and possibly result in electrical failures.

Previous work in our group has focused on modifying known chromophores used in commercial PAGs for use in PBGs.[67-68, 338] These have all been derived from non-ionic PAGs originally developed by Ciba-Geigy (now part of BASF). There has been some precedent for this method, as ONB based PAGs were developed before their corresponding PBGs (Figure 6.20).[79, 339]

Figure 6.20: ONB based PAG (left) and adapted PBG version (right)

BASF produces an i-line non-ionic PAG that has high thermal stability and high sensitivity (Figure 6.21).[340] The UV-Vis spectrum is shown in Figure 6.22. This class of photoactive compounds functions by homolytic cleavage of the N-O bond to generate both an iminyl radical and a carbonate radical. These radicals can then abstract hydrogen atoms, creating imines, and carbamic acids that eventually decarboxylate into amines.

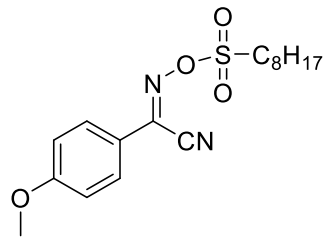

Figure 6.21: CGI 725 non-ionic PAG (BASF)

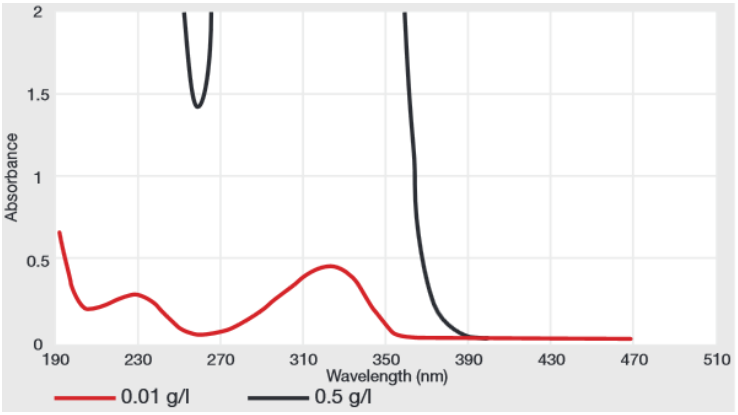

Figure 6.22: CGI 725 absorbance spectrum[340]

We envisioned converting this PAG into a PBG by replacing the sulfonate ester with a carbamate similarly to the ONB example in Figure 6.20. Analogous carbamate oximes have been reported previously.[338, 341-342] The proposed structure is shown in Figure 6.23.

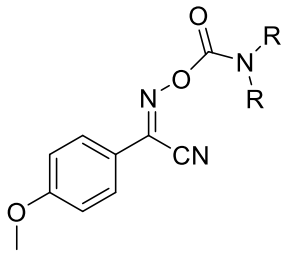

Figure 6.23: Design of PBG adapted from BASF PAG

This PBG is easily prepared in two steps from commercially available starting materials. The precursor oxime is created by the action of butyl nitrite on 4-methoxybenzyl cyanide in strongly basic conditions (Figure 6.24).[343] This reaction is general for compounds containing an acidic hydrogen atom. During the reaction, these compounds are deprotonated and the anion attacks organic nitrites to form oximes. The second step involves a simple nucleophilic acyl substitution on a carbamoyl chloride of choice with the deprotonated oxime.

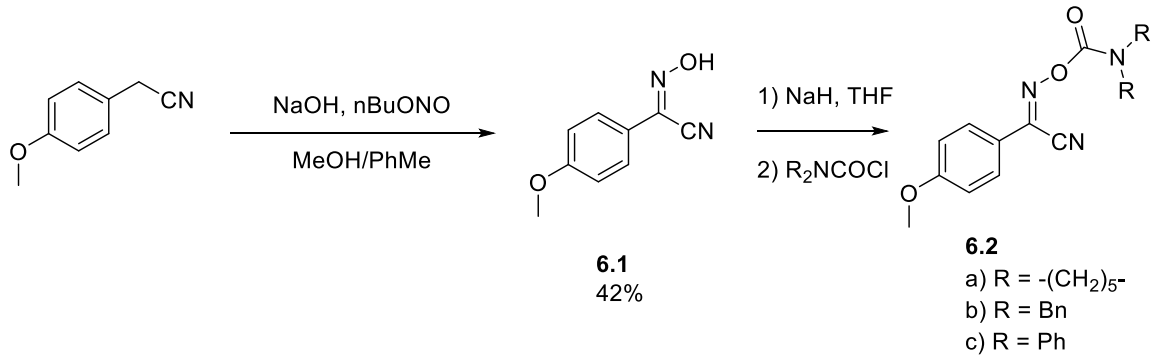

Figure 6.24: Synthesis of benzyl cyanide oxime PBGs

Preliminary exposures were performed on **6.2a** dissolved in deuterated acetonitrile in a Rayonet photo-reactor using 365 nm light (Figure 6.25). After 40 minutes of exposure, the ^{1}H NMR spectrum was acquired. Upon viewing the sample a few hours later, bright orange needles had precipitated from solution. The NMR did not appear to have the characteristic peaks of piperidine present, so 5 μL of piperidine was added and the NMR again was collected to confirm this. From the spectra, it is clear that free piperidine was not generated in appreciable amounts in this processes. These results were at least partially anticipated as fluorenone oxime carbamates are also known to give poor yields of the free amine.[342]

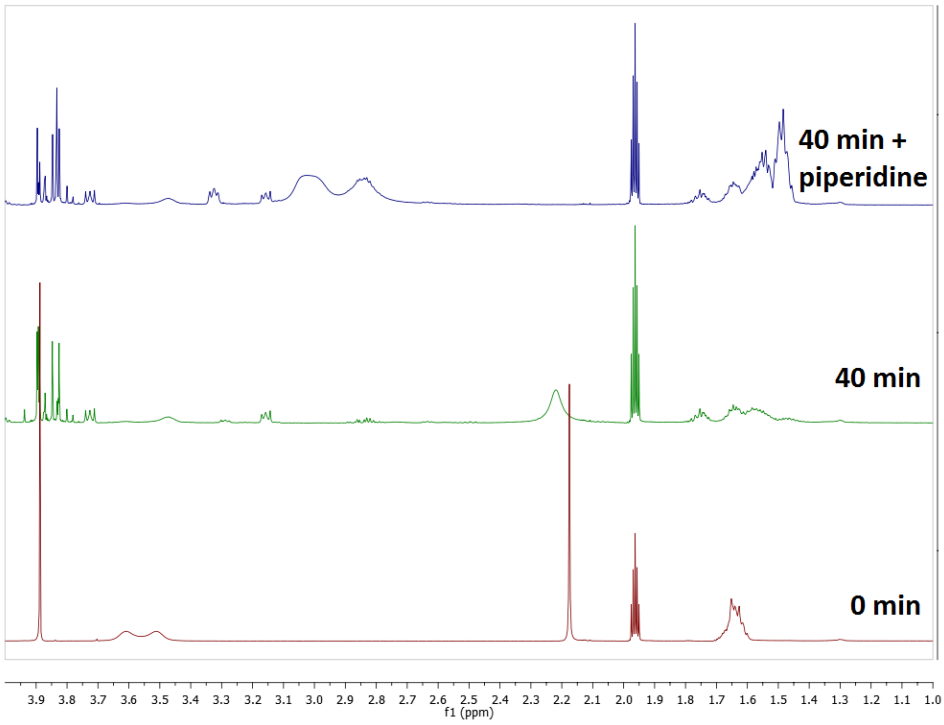

Figure 6.25: NMR spectra of 365 nm exposure of **6.2a** in acetonitrile

While this chromophore may not generate the desired amine upon exposure, the quantum efficiency appeared quite high. When performing TLC on samples during synthesis, the colorless spots would become visible after only a few seconds of exposure from the black light. Additionally, after exposure irradiated solutions were very slightly basic (pH~8), indicating generation of some basic species. To determine the quantum efficiency, PBG **6.2a** was dissolved in acetonitrile at a concentration of 112 μM and exposed to 365 nm radiation in a quartz cuvette. The photolysis was tracked by UV-Vis spectroscopy (Figure 2.26). The absorbance at i-line was found to be much lower than originally expected, and it is actually near an isosbestic point. The general shape changes of the curves with exposure also suggest that the photolysis reaction is quite clean as there are 4 isosbestic points. The increased absorbance in the visible range is likely due to

the formation of azines, formed by the coupling of two iminyl radicals.[342] The consumption of the PBG was plotted as a function of photons absorbed for low conversion (Figure 2.27). Conversion was tracked by monitoring peak changes at 412 nm, the 3 J/cm^2 exposure was assumed to be complete conversion, and only points below 20% conversion were used for the straight line fit for quantum efficiency. The peak at 412 nm was chosen as the absorption maximum remains at 412 nm throughout the exposure. The fit gives a quantum efficiency of 4.9%, which is significantly higher than NVOC. Additionally, it may be possible to improve this by the addition of an additive containing easily abstractable hydrogens in order to discourage radical recombination. Compounds such as cyclohexadiene are good candidates for a hydrogen source, and have been shown to approximately double quantum yields in oxime PBGs.[67]

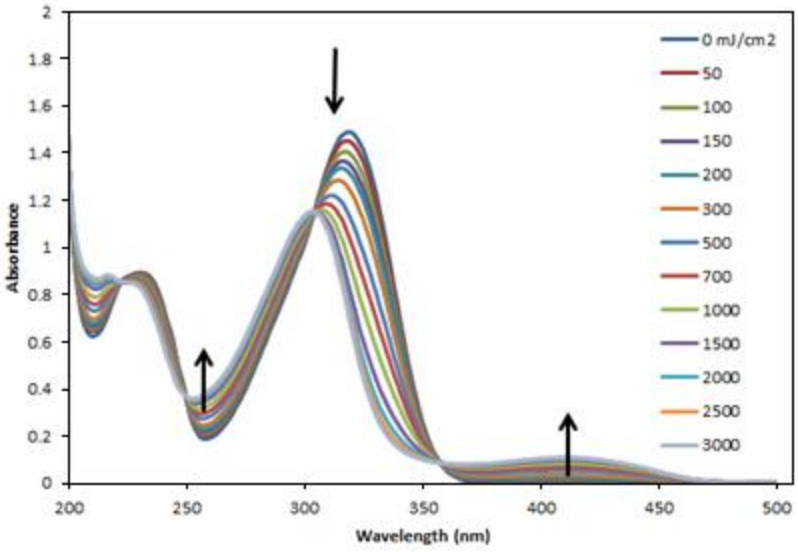

Figure 6.26: Exposure study of 112 μM **6.2a** in acetonitrile at 365 nm

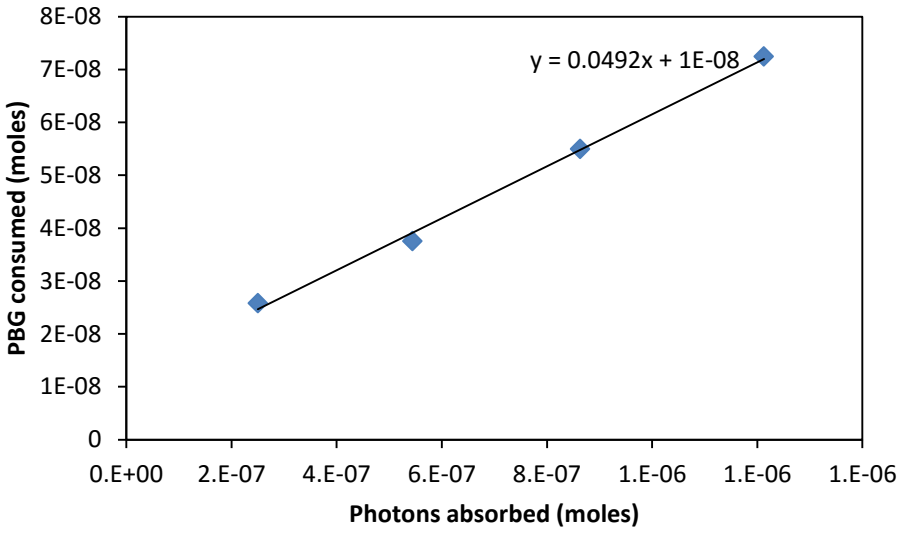

Figure 6.27: PBG **6.2a** consumption as a function of 365 nm photons absorbed

The lack of desired base generation and the low absorbance at i-line of **6.2a** led us to consider other oxime based chromophores. As both anthracene and ITX were effective sensitizers for the tetraphenylborate based amidine PBGs, we targeted incorporation of these chromophores (Figure 6.28). Similar PAG versions using the ITX oxime are reported to have high thermal stabilities and quantum yields around 10%.[344-345] The acetyl anthracene derivative was chosen as it is a red-shifted variation on the acetonapthone oximes previously explored by our group.[67]

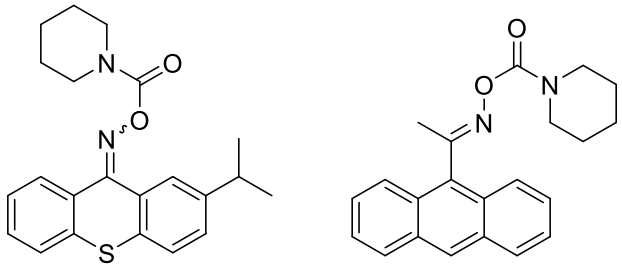

Figure 6.28: Proposed oxime PBGs with increased i-line absorbance

Both oximes were prepared using the more traditional hydroxylamine hydrochloride in pyridine solution route (Figure 6.29). However, this method for making oximes is actually quite poor in the case of de-activated carbonyls, especially xanthones and thioxanthones.[346] Additionally, the use of these two ketones allows for the possibility of two isomers to be formed. In the case of the ITX, a ratio of about 1:1 was observed by ^{1}H NMR. However, the acetyl anthracene oxime **6.3** was obtained as nearly pure E isomer. This is undoubtedly due to the steric hindrance in the Z isomer where the hydroxyl group is repulsed by the anthracene core rather than a much smaller methyl group. The oxime carbamates **6.4** and **6.6** were prepared from their oximes by deprotonation with NaH and reaction with piperidine carbamoyl chloride in THF as for **6.2a**. Both reactions gave the desired oxime carbamate product in excellent yield.

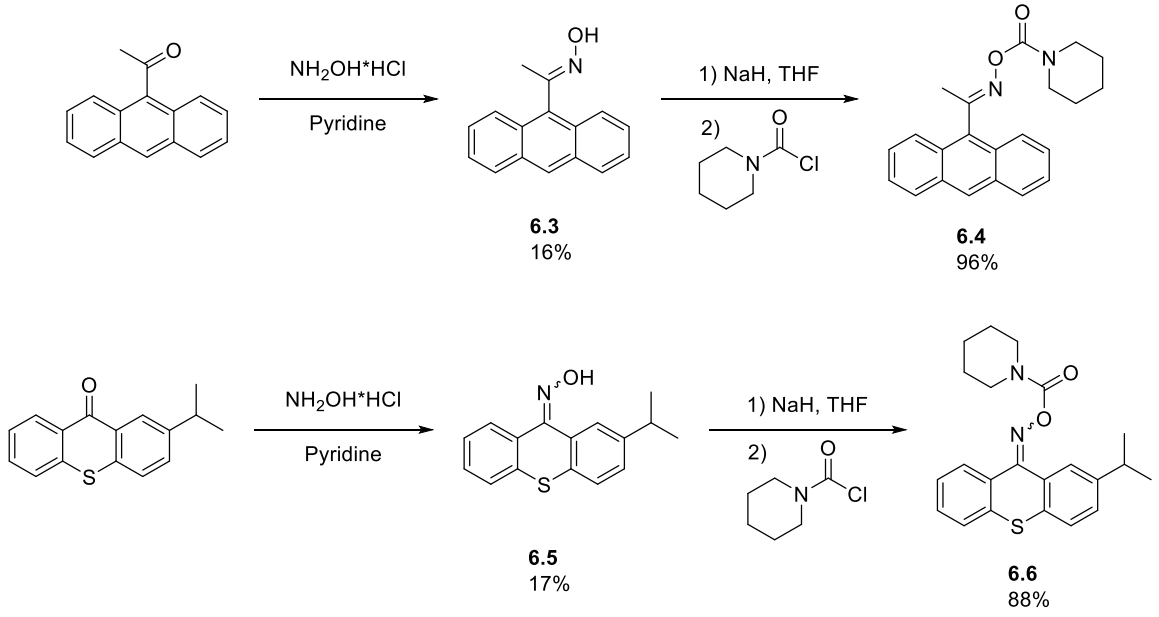

Figure 6.29: Synthesis of anthracene and ITX based oxime PBGs

Both PBGs were then exposed to 365 nm radiation in a quartz cuvette and the reaction was tracked by UV-Vis. Figure 6.30 shows the reaction of **6.6** in acetonitrile at doses up to 10 J/cm^2. The plot of PBG consumed vs photons absorbed is also shown (Figure 6.31). From the UV-Vis spectra, this PBG clearly has a larger extinction coefficient at i-line compared to **6.2a**. Interestingly, the spectrum of **6.6** changes very little upon exposure and increasing absorbance at higher wavelengths appears to be reduced as well. However, the quantum efficiency of this compound is surprisingly poor, at about 1% from the straight line fit of the data below 20% conversion. The poor quantum efficiency reduces the generation rate of radicals, so radical coupling between two imidyl radicals is greatly suppressed. This would lead to lower amounts of azine produced, and could be the cause of the minimal absorbance at higher wavelengths relative to **6.2a**. PBG **6.4** was also exposed to i-line radiation in the same fashion. However, the reaction was not complete even after exposure to 20 J/cm^2 of 365 nm radiation, indicating a quantum efficiency on the order of 0.1% or less.

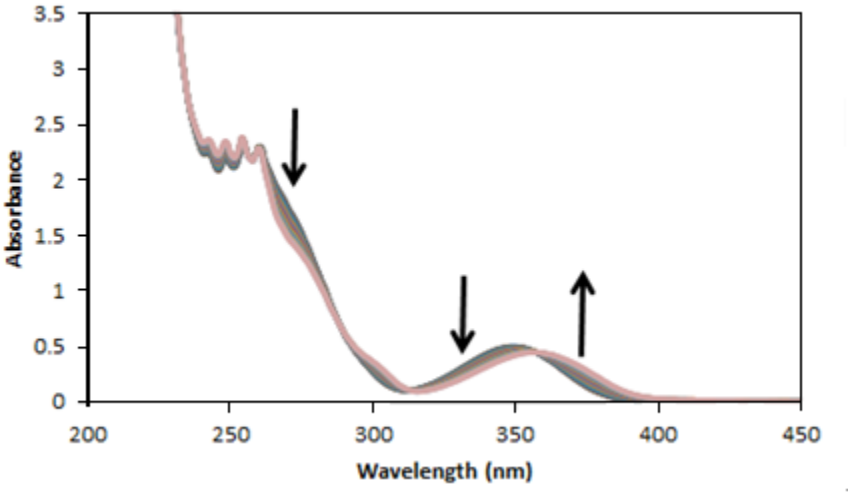

Figure 6.30: UV-Vis spectra of 119 μM **6.6** in acetonitrile exposed to 10 J/cm^2 i-line radiation

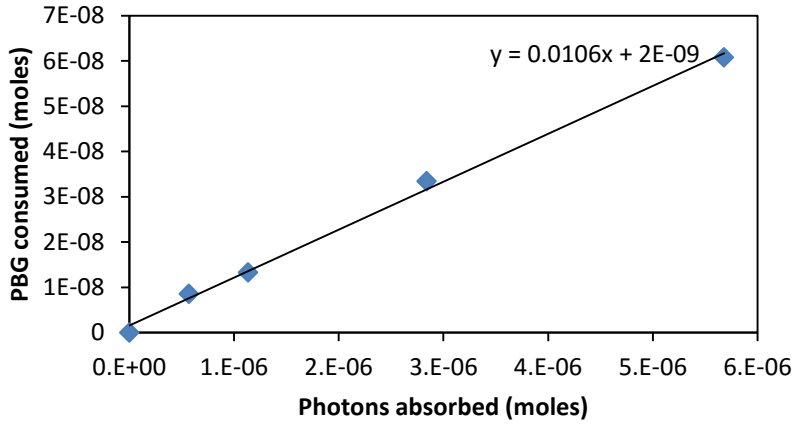

Figure 6.31: PBG **6.6** consumption as a function of photons absorbed for a 365 nm exposure

Unfortunately, neither of the more i-line absorbent oxime PBGs was nearly as efficient as the commercial benzyl cyanide based PBG. Some improvement could likely be made by addition of a hydrogen donating source. However, the general trend of these oxime chromophores is that the sulfonate ester PAGs have much higher quantum efficiencies than the corresponding carbamate PBGs. Even the commercial benzyl cyanide oxime PBG was found to only have a quantum efficiency of 5%, though the desired base was not the major product by NMR.

CONCLUSIONS

Several attempts to use the NVOC chromophore in PBGs to produce stronger bases were made. These strategies involved preparing a tetramethylpiperidine version of the standard NVOC piperidine PBG and an aminoalkyl lactam version that in theory could form an amidine upon exposure and heating. Neither of these ideas, nor others involving NVOC were successful in producing a higher degree of imidization in the

target PSPI system. While both produced a base catalyst, the overall imidization was less than just using the standard NVOC piperidine PBG. This is probably a result of steric effects in the tetramethylpiperidine PBG and insufficient time or bake temperatures in the NVOC DBU PBG.

Several oxime carbamate type PBGs were also prepared in an effort to find a higher quantum efficiency than NVOC. These included a PBG based on a benzyl cyanide oxime chromophore used in commercial non-ionic PAGs, as well as the oximes of ITX and 9-acetylanthracene. In general, the quantum yields were quite poor relative to the reported values for the PAGs versions. Even the benzyl cyanide based oxime used in commercial i-line non-ionic PAGs was only found to have a quantum efficiency of around 5%. However, the 5% quantum yield is a significant improvement over the ~1% in NVOC. This yield only represents the disappearance of starting material, so further work is required to determine the yield of generated base, but preliminary work shows that this PBG could be a vast improvement over standard i-line PBGs.

Finally, a series of amidine and guanidine PBGs were synthesized. Most of these were based on salts of acidic chromophores with the desired base. Benzyl and phenacyl protected reduced DBN PBGs were also prepared. However, neither of these compounds met thermal stability requirements and they were not effective base generators in the solid state. The PBGs that are most effective at imidizing the PSPI system were based on the tetraphenylborate anion. These included TBD-TPB and PDBN-TPB. However, these compounds also work as thermal curing catalysts, like the other salts in Chapter 5. Optimization studies suggest that this dark reaction can be limited and the contrast improved by baking at a higher temperature for a shorter amount of time rather than the standard lower temperature curing for extended periods of time. Further work is still required to optimize these formulations.

EXPERIMENTAL

General Methods

All solvents and reagents were obtained from commercial sources and used as received, unless otherwise specified. The reduced phenacyl DBN PBG (PA-HDBN) was prepared by Dr. Ryan Mesch. DP-tetracene was prepared by Anthony Engler. The mPMDA-TFMB-EE polymer was prepared as described in Chapter 3. Imidization studies were performed by infrared spectroscopy in the manner as described in Chapter 5. DCM, TEA, pyridine, and toluene were distilled from CaH_2 while THF and DMF were purified by eluting through an alumina column solvent delivery system under argon. Reactions were run in flame-dried glassware and under nitrogen atmosphere, expect where noted. ^{1}H and ^{13}C NMR spectra were obtained on a Varian Unity Plus 400 MHz instrument. Solvent proton peaks are used as the internal standard ($CDCl_3$ ^{1}H 7.26 ppm, ^{13}C 77.0 ppm; DMSO-d6 ^{1}H 2.49 ppm, ^{13}C 39.5 ppm). HRMS (CI) was performed on a VG analytical ZAB2-E instrument and HRMS (ESI) on an Ion Spec FT-ICR instrument. All HRMS are ESI unless otherwise noted. Uncorrected melting points were obtained using a Mel-Temp II.

PBG Quantum Efficiency by UV-Vis Spectroscopy

Solutions of the PBG were prepared in HPLC grade acetonitrile (~100 μM) and loaded into quartz cuvettes with a 1 cm path length. These were then placed on a black mat to reduce reflection of un-absorbed photons passing through the solution. The solutions were then exposed to filtered i-line radiation using a Novocure 2100 spot curing system. At regular exposure dose intervals, the UV-Vis spectra were taken using a ThermoSci Evolution 220 UV-Visible spectrometer. The number of photons absorbed at

the exposure wavelength was calculated by multiplying the exposure intensity by the cuvette area and fractional absorption.

Fractional light absorption = 1 - %Transmission(365 nm)/100

%Transmission(365 nm) = 10 ^ [2 – Absorbance(365 nm)]

In general, absorbance changes during the exposure. So the change in photons absorbed between two exposure doses was calculated from the average of the absorbances at those two points. This was then plotted against the amount of PBG consumed, which was found by assuming that 100% conversion was where no further changes in the UV-Vis spectra were observed with increased light exposure. A peak that changed considerably during exposure was chosen and conversion was assumed to be directly proportional to changes in this peak. In the case of **6.2a**, this peak was 412 nm; for **6.6** it was 340 nm.

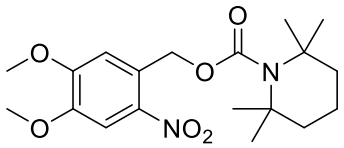

4,5-dimethoxy-2-nitrobenzyl 2,2,6,6-tetramethylpiperidine-1-carboxylate (NVOC TMP)[324]

Phosgene (15% in toluene, 17.8 mL, ~25 mmol) was cooled to -78°C in a 100 mL 3-neck RBF. TMP (7.41 g, 52.5 mmol) was diluted with 10 mL toluene and added dropwise to the phosgene solution, keeping the temperature below -55°C. After addition, the reaction was stirred for 1 hour at -78°C and then warmed to room temperature. The solution was then cooled back to -25°C and then warmed to 10°C to filter off the precipitated solid. The crude orange chloroformate was then returned to the flask and cooled to 0°C.

Nitroveratryl alcohol (5.35 g, 25 mmol), DMAP (0.42 g, 3.75 mmol), TEA (3.5 mL, 25 mmol), and 15 mL dioxane were then added to the flask and the mixture was stirred overnight. The solvent was then removed in vacuum and the crude product partitioned between water and DCM. The organic layer was washed with 1M HCl, water, and brine; dried over Na_2SO_4, filtered, and concentrated. Purification by flash chromatography (3:7 EtOAc:hexanes) followed by recrystallization twice from EtOH gave the product as a slightly yellow solid (2.73 g, 29%). mp 72-74°C. ^{1}H NMR (400 MHz, $CDCl_3$) δ 7.72 (s, 1H), 7.05 (s, 1H), 5.55 (d, J = 0.7 Hz, 2H), 3.95 (d, J = 1.2 Hz, 6H), 1.46 (s, 12H). ^{13}C NMR (101 MHz, $CDCl_3$) δ 156.5, 153.5, 147.8, 139.6, 129.3, 110.0, 108.1, 63.1, 56.5, 56.4, 56.3, 39.4, 29.9, 15.4. HRMS $[M+Na]^+$ calcd. 403.1840 found 403.1847

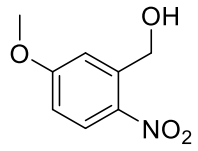

(5-methoxy-2-nitrophenyl)methanol

In a 100 mL RBF with condenser was added 5-methoxy-2-nitrobenzoic acid (5.0 g, 25.4 mmol). BH_3-THF complex (1M in THF, 33 mL, 33 mmol) was added dropwise by syringe. The solution was then heated to reflux for 3 hours and quenched with water. The solution was concentrated and then partitioned between DCM and water. The organic layer was washed with $NaHCO_3$ then brine, dried over Na_2SO_4, filtered and concentrated to obtain a tan solid (76%). ^{1}H NMR (400 MHz, $CDCl_3$) δ 8.18 (d, J = 9.1 Hz, 1H), 7.22 (d, J = 2.8 Hz, 1H), 6.89 (dd, J = 9.1, 2.8 Hz, 1H), 4.99 (s, 2H), 3.92 (s, 3H). ^{13}C NMR (101 MHz, $CDCl_3$) δ 164.4, 140.4, 128.2, 114.4, 113.4, 63.2, 56.1. HRMS $[M+Na]^+$ calcd. 206.0424 found 206.0422

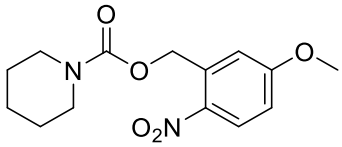

5-methoxy-2-nitrobenzyl piperidine-1-carboxylate (MONB piperidine)

Phosgene (15% in toluene, 11.7 mL, ~16.4 mmol) was cooled to 0°C in a 100 mL RBF. In a separate RBF, (5-methoxy-2-nitrophenyl)methanol (1.0 g, 5.46 mmol) was dissolved in 20 mL THF. The alcohol solution was then added dropwise to the phosgene. Stirring was continued overnight and the phosgene removed under a flowing stream of nitrogen before concentrating the solution. The crude chloroformate ester was then dissolved in 12 mL DCM. Piperidine (1.35 mL, 13.6 mmol) was then added dropwise. After stirring for 3 hours, the solution was partitioned between DCM and 1 N HCl. The organic layer was washed with brine, dried over Na_2SO_4 and concentrated. Purification by flash chromatography (100% DCM) yielded the title compound as a slight yellow, low melting solid (0.61g, 38%) mp 52-53°C. ^{1}H NMR (400 MHz, $CDCl_3$) δ 8.18 (d, J = 9.1 Hz, 1H), 7.01 (d, J = 2.8 Hz, 1H), 6.88 (dd, J = 9.1, 2.8 Hz, 1H), 5.56 (s, 2H), 3.90 (s, 3H), 3.49 (s, 4H), 1.66 – 1.53 (m, 6H). ^{13}C NMR (101 MHz, $CDCl_3$) δ 163.9, 140.4, 137.1, 128.1, 113.75, 112.4, 64.1, 56.0, 45.2, 24.5. HRMS $[M+Na]^+$ calcd. 317.1108 found 317.1112

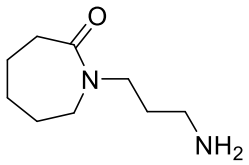

1-(3-aminopropyl)azepan-2-one (APCL)[347]

DBU (5.0 g, 32.8 mmol) was added to a 25 mL RBF with condenser. Water (0.59g , 32.8 mmol) was added and the mixture was heated to 85°C overnight. The crude product was purified by flash chromatography (1:1:8 TEA: MeOH: DCM) to obtain a pale yellow oil.

(2.36 g, 42%). ^{1}H NMR (400 MHz, $CDCl_3$) δ 3.33 (t, *J* = 6.8 Hz, 2H), 3.28 (s, 2H), 3.24 – 3.19 (m, 2H), 2.55 (t, *J* = 6.5 Hz, 2H), 2.42 – 2.38 (m, 2H), 1.64 – 1.48 (m, 8H). ^{13}C NMR (101 MHz, $CDCl_3$) δ 176.0, 49.3, 45.0, 38.6, 37.1, 31.2, 29.8, 28.4, 23.3. HRMS $[M+H]^+$ calcd. 171.4920 found 171.4920

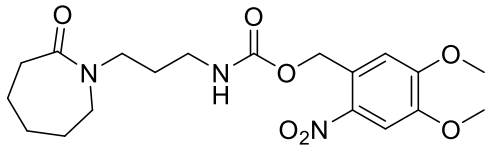

4,5-dimethoxy-2-nitrobenzyl (3-(2-oxoazepan-1-yl)propyl)carbamate (NVOC DBU)

In a 25 mL RBF, NVOC chloroformate (0.809 g, 2.94 mmol) was dissolved in 10 mL DCM. APCL (0.500 g, 2.94 mmol) and TEA (0.41 mL, 2.94 mmol) were then added to the solution. After stirring overnight the reaction was quenched with water, washed with 1N HCl, dried over Na_2SO_4, filtered and concentrated. The crude product was then purified by flash chromatography (EtOAc) to obtain the title compound as a light yellow solid. (0.440 g, 37%) mp 121-122°C. ^{1}H NMR (400 MHz, $CDCl_3$) δ 7.68 (s, 1H), 7.05 (s, 1H), 6.24 (s, 1H), 5.49 (s, 2H), 3.94 (d, *J* = 14.0 Hz, 6H), 3.60 – 3.03 (m, 6H), 2.51 (s, 2H), 1.66 (s, 8H).^{13}C NMR (101 MHz, $CDCl_3$) δ 177.0, 156.1, 153.7, 147.86, 139.5, 129.2, 109.5, 108.1, 63.2, 56.5, 56.5, 49.7, 44.9, 37.4, 37.3, 30.0, 28.6, 27.7, 23.5. HRMS $[M+Na]^+$ calcd. 432.1741 found 432.1758

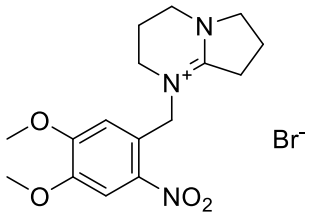

1-(4,5-dimethoxy-2-nitrobenzyl)-2,3,4,6,7,8-hexahydropyrrolo[1,2-a]pyrimidin-1-ium bromide (NVDBN Br)

Nitroveratryl bromide (0.300 g, 1.09 mmol) was dissolved in 5 mL THF in a 25 mL RBF. DBN (0.135 g, 1.09 mmol) was added as a neat liquid. A yellow precipitate formed immediately. After stirring for 10 minutes the precipitate was filtered, washed with ether and dried in vacuum (0.342 g, 79%). ^{1}H NMR (400 MHz, $CDCl_3$) δ 7.67 (s, 1H), 7.46 (s, 1H), 5.15 (s, 2H), 4.11 (s, 3H), 3.95 (s, 3H), 3.85 (t, J = 7.4 Hz, 2H), 3.49 (t, J = 5.9 Hz, 2H), 3.41 (t, J = 7.9 Hz, 2H), 3.34 (t, J = 5.8 Hz, 2H), 2.35 – 2.24 (m, 2H), 2.17 – 2.08 (m, 2H). ^{13}C NMR (101 MHz, $CDCl_3$) δ 166.4, 154.2, 149.4, 140.8, 122.9, 115.6, 108.7, 58.1, 56.6, 54.9, 54.4, 43.7, 42.9, 31.9, 19.2, 18.4.

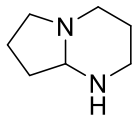

Octahydropyrrolo[1,2-a]pyrimidine (HDBN)[348]

DBN (20.0 g, 161 mmol) was dissolved in 240 mL methyl t-butyl ether in a 500 mL 3-neck RBF. $LiAlH_4$ (6.11 g, 161 mmol) was added in one portion and the solution was heated to refluxed overnight. The reaction was cooled to 0°C and quenched by dropwise addition of 6.1 mL water, then 6.1 mL 15% aq. NaOH, then 18.5 mL of water. The slurry

was then filtered through celite and washed with DCM. The product was then distilled (84°C, 37 torr) to obtain a clear colorless oil (14.05 g, 69%). ^{1}H NMR (400 MHz, $CDCl_3$) δ 3.21 – 3.09 (m, 2H), 3.00 (td, *J* = 8.9, 2.2 Hz, 1H), 2.86 (dd, *J* = 9.3, 6.3 Hz, 1H), 2.66 (ddd, *J* = 13.7, 12.8, 3.5 Hz, 1H), 2.32 – 2.22 (m, 1H), 2.15 (q, *J* = 8.9 Hz, 1H), 2.04 – 1.92 (m, 1H), 1.88 – 1.58 (m, 4H), 1.55 – 1.34 (m, 2H). HRMS $[M+H]^+$ calcd. 127.1230 found 127.1227

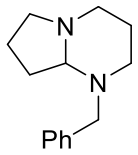

1-benzyloctahydropyrrolo[1,2-a]pyrimidine (Bn-HDBN)[326]

NaOH (2.38 g, 59.4 mmol) and KI (0.66 g, 4.0 mmol) were suspended in 40 mL DCM in a 100 mL RBF. HDBN (5.00 g, 39.6 mmol) was then added and the solution stirred for 10 minutes. Benzyl bromide (4.7 mL, 40 mmol) was then added dropwise over 15 minutes. The solution became warm and cloudy and was then stirred overnight. The reaction was diluted with 25 mL water and the organic layer concentrated. 50 mL of hexanes was then added to precipitate salts. The solution was filtered to obtain a clear viscous oil that was purified by distillation (87-90°C, 0.67 torr) to obtain a clear colorless oil that solidified upon standing (1.69 g, 20%). mp 36-37°C. ^{1}H NMR (400 MHz, $cdcl_3$) δ 7.37 (dd, *J* = 7.8, 1.1 Hz, 2H), 7.32 – 7.26 (m, 2H), 7.25 – 7.19 (m, 1H), 3.93 (d, *J* = 13.2 Hz, 1H), 3.15 – 3.02 (m, 3H), 2.89 – 2.80 (m, 1H), 2.48 – 2.38 (m, 1H), 2.25 (q, *J* = 8.7 Hz, 1H), 2.15 – 1.98 (m, 2H), 1.95 – 1.73 (m, 4H), 1.73 – 1.61 (m, 1H), 1.53 – 1.43 (m,

1H). ^{13}C NMR (101 MHz, cdcl$_3$) δ 139.1, 129.1, 128.2, 126.9, 84.8, 58.6, 52.4, 52.2, 51.3, 29.8, 24.8, 19.6. HRMS $[M+Na]^+$ calcd. 239.1519 found 239.1521

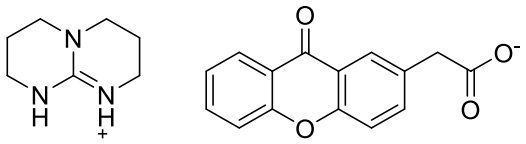

3,4,6,7,8,9-hexahydro-2H-pyrimido[1,2-a]pyrimidin-1-ium 2-(9-oxo-9H-xanthen-2-yl)acetate (TBD-XA)

2-xanthone acetic acid (0.300 g, 1.18 mmol) was dissolved in 15 mL THF in a 100 mL RBF. In a separate flask, TBD (0.164 g, 1.18 mmol) was dissolved in 5 mL THF and passed through a syringe filter to remove insoluble material. The TBD solution was then added dropwise to the acid solution. After 15 minutes the precipitate was filtered and dried to obtain a white powder (0.405 g, 88%) mp 220°C (decomp). ^{1}H NMR (400 MHz, CD_3OD) δ 8.22 (dd, *J* = 8.0, 1.6 Hz, 1H), 8.15 (d, *J* = 2.1 Hz, 1H), 7.84 – 7.74 (m, 2H), 7.56 (d, *J* = 8.4 Hz, 1H), 7.50 (d, *J* = 8.6 Hz, 1H), 7.41 (t, *J* = 7.6 Hz, 1H), 3.61 (s, 2H), 3.29 (t, 4H), 3.22 (t, 4H), 2.01 – 1.88 (m, 4H). ^{13}C NMR (101 MHz, CD_3OD) δ 179.5, 178.6, 157.5, 156.1, 152.4, 138.0, 136.4, 135.8, 127.1, 127.0, 125.1, 122.5, 122.2, 119.2, 118.9, 47.7, 45.5, 39.0, 21.7.

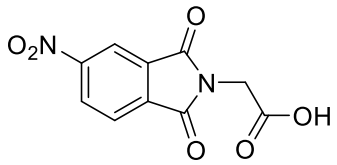

2-(5-nitro-1,3-dioxoisoindolin-2-yl)acetic acid (NP-Gly)[349]

In a 100 mL RBF at 0°C was added 25 mL sulfuric acid and 5 mL nitric acid (68%). N-phthaloylglycine (5.0 g, 24.4 mmol) was added in one portion as a solid powder. After 1

hour the ice bath was removed and the solution allowed to warm to room temperature overnight. The solution was then poured into 150 mL of water to form a yellow precipitate. The precipitate was filtered and recrystallized from water/EtOH to obtain slightly yellow shiny flakes. (3.52 g, 58%) mp 196-197°C ^{1}H NMR (400 MHz, DMSO) δ 8.67 (dd, *J* = 8.2, 2.0 Hz, 1H), 8.57 (dd, *J* = 2.0, 0.5 Hz, 1H), 8.20 (dd, 1H), 4.38 (s, 2H). ^{13}C NMR (101 MHz, DMSO) δ 168.6, 165.7, 165.4, 151.8, 135.9, 132.7, 130.1, 125.1, 118.4, 39.4. HRMS $[M+Na]^{+}$ calcd. 273.0118 found 273.0122

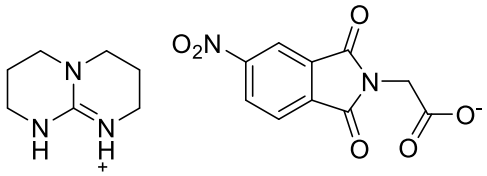

3,4,6,7,8,9-hexahydro-2H-pyrimido[1,2-a]pyrimidin-1-ium 2-(5-nitro-1,3-dioxoisoindolin-2-yl)acetate (TBD-NP)

In a 50 mL RBF, TBD (0.30 g, 2.15 mmol) was dissolved in 10 mL THF. In a separate 25 mL RBF, NP-Gly (0.539 g, 2.15 mmol) was dissolved in 7 mL THF. The acid solution was slowly dripped into the TBD solution. After addition, the solution was stirred for an additional hour and filtered to obtain a slightly yellow powder. (0.681 g, 81%) mp 188°C (decomp) ^{1}H NMR (400 MHz, DMSO) δ 9.66 (s, 1H), 8.63 (dd, *J* = 8.1, 2.0 Hz, 1H), 8.50 (d, *J* = 1.8 Hz, 1H), 8.21 – 8.06 (m, 1H), 3.94 (s, 1H), 3.23 (t, *J* = 5.9 Hz, 2H), 3.10 (t, *J* = 5.7 Hz, 2H), 1.89 – 1.78 (m, 2H). ^{13}C NMR (101 MHz, DMSO) δ 170.4, 166.1, 165.8, 151.5, 151.2, 136.4, 133.2, 129.7, 124.6, 117.9, 46.1, 41.9, 37.2, 20.4

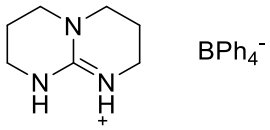

3,4,6,7,8,9-hexahydro-2H-pyrimido[1,2-a]pyrimidin-1-ium tetraphenylborate (TBD-TPB)[283]

TBD (0.387 g, 2.78 mmol) was dissolved in HCl (10% aq., 2.75 mL) in a beaker. $NaBPh_4$ (1.0g , 2.92 mmol) was dissolved in 2.75 mL water in a separate beaker. The tetraphenylborate solution was poured into the acid solution and stired for 15 minutes. The precipitated solid was recrystallized from 4:1 MeOH:$CHCl_3$ to obtain a white microcrystalline solid (0.42 g, 33%) mp 183-184°C. ^{1}H NMR (400 MHz, DMSO) δ 7.40 (br s, 2H), 7.27 – 7.18 (m, 8H), 6.96 (t, *J* = 7.4 Hz, 8H), 6.83 (t, *J* = 7.2 Hz, 4H), 3.17 (t, *J* = 6.0 Hz, 4H), 3.15 – 3.10 (m, 4H), 1.86 – 1.75 (m, 4H). ^{13}C NMR (101 MHz, DMSO) δ 164.1, 163.6, 163.1, 162.6, 150.4, 135.5, 125.35, 125.33, 125.30, 125.27, 121.5, 46.2, 37.6, 20.2.

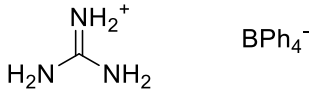

Guanidinium tetraphenylborate

Guanidine hydrochloride (0.279 g, 2.92 mmol) was dissolved in 20 mL water in a beaker. Sodium tetraphenylborate (1.0 g, 2.92 mmol) was dissolved in a separate 20 mL water in another beaker. The tetraphenylborate solution was then poured into the guanidium solution and stir for 15 minutes. The precipitated white solid was then filtered and dried.

(0.967 g, 87%) mp 199-202°C. ^{1}H NMR (400 MHz, DMSO) δ 7.28 – 7.20 (m, 8H), 6.97 (t, *J* = 7.4 Hz, 8H), 6.94 (br s, 6H), 6.87 – 6.80 (m, 4H). ^{13}C NMR (101 MHz, DMSO) δ 164.2, 163.7, 163.2, 162.7, 157.9, 135.6, 125.44, 125.41, 125.39, 125.36, 121.6.

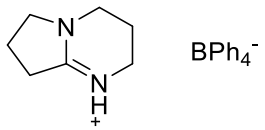

2,3,4,6,7,8-hexahydropyrrolo[1,2-a]pyrimidin-1-ium tetraphenylborate (DBN-TPB)

Prepared similarly to TBD-TPB. (100%) mp 240°C (decomp). ^{1}H NMR (400 MHz, DMSO) δ 9.59 (s, 1H), 7.31 – 7.19 (m, 8H), 6.98 (t, *J* = 7.4 Hz, 8H), 6.84 (t, *J* = 7.2 Hz, 4H), 3.50 – 3.43 (m, 2H), 3.22 (dd, *J* = 10.6, 5.1 Hz, 4H), 2.73 (t, *J* = 8.0 Hz, 2H), 1.93 (dt, *J* = 15.4, 7.6 Hz, 2H), 1.85 – 1.77 (m, 2H). ^{13}C NMR (101 MHz, DMSO) δ 173.6, 173.2, 173.1, 172.6, 172.1, 145.0, 134.84, 134.81, 134.78, 134.76, 131.0, 62.5, 51.3, 47.0, 39.2, 27.7, 27.6.

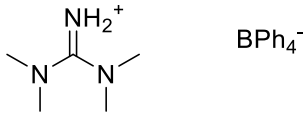

Tetramethylguanidium tetraphenylborate (TMG-TPB)

Prepared as described for TBD-TPB. (90%) mp 224°C (decomp). ^{1}H NMR (400 MHz, DMSO) δ 7.79 (br s, 2H), 7.28 – 7.19 (m, 8H), 6.97 (t, *J* = 7.4 Hz, 8H), 6.83 (t, *J* = 7.2 Hz, 4H), 2.84 (s, 12H). ^{13}C NMR (101 MHz, DMSO) δ 164.1, 163.6, 163.1, 162.7, 160.9, 135.6, 125.37, 125.34, 125.31, 125.29, 121.5, 39.3.

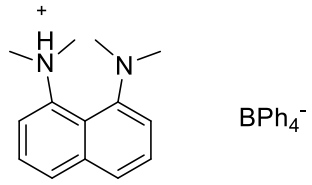

8-(dimethylamino)-N,N-dimethylnaphthalen-1-aminium tetraphenylborate (TMN-TPB)

Prepared as described for TBD-TPB. (86%) mp 189-190°C. ^{1}H NMR (400 MHz, DMSO) δ 8.09 (dd, *J* = 7.7, 7.0 Hz, 4H), 7.74 (t, *J* = 7.9 Hz, 2H), 7.20-7.15 (m, 8H), 6.92 (t, *J* = 7.4 Hz, 8H), 6.79 (t, *J* = 7.2 Hz, 4H), 3.12 (d, *J* = 2.5 Hz, 12H). ^{13}C NMR (101 MHz, DMSO) δ 144.6, 135.5, 128.9, 126.9, 125.34, 125.32, 125.29, 125.26, 121.8, 121.5, 45.8.

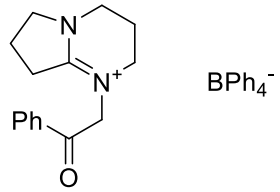

1-(2-oxo-2-phenylethyl)-2,3,4,6,7,8-hexahydropyrrolo[1,2-a]pyrimidin-1-ium tetraphenylborate (PDBN-TBD)

DBN (1.00 g, 8.05 mmol) was dissolved in 10 mL Et_2O. The solution was passed through a 0.2 μm syringe filter to remove the small amount of precipitate formed. Phenacyl bromide (1.60 g, 8.05 mmol) was dissolved in 10 mL toluene. The DBN solution was then added dropwise and a slightly orange precipitate began to form immediately. After 30 minutes the extremely hygroscopic bromide salt was filtered and washed with large amounts of ether, avoiding exposure to air as much as possible. The wet solid was dried in vacuum to obtain the bromide salt as a light orange solid (1.85 g, 71%).

The crude bromide salt (0.50 g, 1.55 mmol) was then dissolved in 10 mL of water and filtered through a syringe filter to give a clear, pale yellow solution. $NaBPh_4$ (0.529 g, 1.55 mmol) was dissolved in a separate 5 mL of water and poured into the bromide salt solution. A white precipitate formed immediately. After stirring 5 minutes, the precipitate was filtered and washed with water repeatedly, then dried in vacuum to give a white powder. (0.86 g, 98%) mp 193°C (decomp). ^{1}H NMR (400 MHz, DMSO) δ 8.05 – 7.97 (m, 2H), 7.77 – 7.69 (m, 1H), 7.65 – 7.56 (m, 2H), 7.25 – 7.19 (m, 8H), 6.96 (t, *J* = 7.4 Hz, 8H), 6.82 (t, *J* = 7.2 Hz, 4H), 5.21 (s, 2H), 3.66 (t, *J* = 7.4 Hz, 2H), 3.40 – 3.34 (m, 4H), 2.81 (t, *J* = 7.9 Hz, 2H), 2.04 – 1.92 (m, 4H). ^{13}C NMR (101 MHz, DMSO) δ 193.1, 165.5, 164.1, 163.6, 163.1, 162.62, 135.5, 134.3, 134.1, 128.9, 128.2, 125.36, 125.34, 125.31, 125.28, 121.5, 58.6, 54.1, 46.0, 42.0, 30.0, 18.7, 17.6.

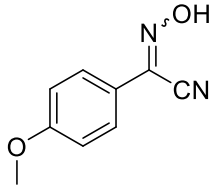

N-hydroxy-4-methoxybenzimidoyl cyanide[343] (6.1)

NaOH (2.72 g, 68.0 mmol) was crushed in a mortar and pestle. The powder NaOH was then suspended in 25 mL toluene and 5 mL MeOH in a 100 mL RBF with an addition funnel. The solution was heated to 40°C and 4-methoxybenzyl cyanide (5.00 g, 34.0 mmol) was then added to the solution. N-butyl nitrite (3.86 g, 37.4 mmol) was added to the addition funnel and added dropwise to the solution over 45 minutes. After complete addition, stirring was continued for an additional 2 hours at 40°C and at room

temperature overnight. The reaction was quenched with 20 mL of water and the layers separated. The organic layer was extracted with 20 mL of 1N NaOH and the combined aqueous layers were acidified to pH 2. The aqueous layer was then extracted with ether (3 x 50 mL), dried over Na_2SO_4, filtered and concentrated. Recrystallization from toluene gave a pale yellow solid as a single isomer (2.49 g, 42%). mp 74-76°C. ^{1}H NMR (400 MHz, $CDCl_3$) δ 7.76 – 7.68 (m, 2H), 6.97 – 6.93 (m, 2H), 3.86 (s, 3H). ^{13}C NMR (101 MHz, $CDCl_3$) δ 162.1, 133.5, 128.0, 121.8, 114.7, 109.6, 55.7. HRMS $[M+H]^+$ calcd. 177.0659 found 177.0655

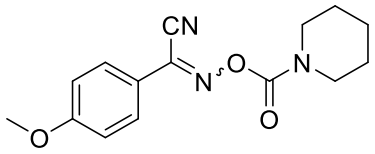

4-methoxy-N-((piperidine-1-carbonyl)oxy)benzimidoyl cyanide (6.2a)

6.1 (0.500 g, 2.83 mmol), piperidinecarbonyl chloride (0.628 g, 4.25 mmol), and TEA (0.60 mL, 4.25 mmol) were dissolved in 30 mL DMF in a 100 mL RBF. The solution was stirred overnight then the solvent evaporated in vacuo. The crude product was then poured into water, filtered, and washed with water to obtain the crude product as a light brown solid (800 mg, 98%). Analytical samples were prepared by recrystallization from heptane to obtain a fluffy white solid. mp 85-86°C. ^{1}H NMR (400 MHz, $CDCl_3$) δ 7.94 – 7.85 (m, 2H), 7.01 – 6.93 (m, 2H), 3.87 (d, J = 7.2 Hz, 3H), 3.58 (br d, J = 25.5 Hz, 4H), 1.65 (br s, 6H). ^{13}C NMR (101 MHz, $CDCl_3$) δ 163.2, 151.8, 136.66, 129.8, 120.6, 114.7, 109.4, 55.7, 45.8, 45.5, 25.9, 25.6, 24.3. HRMS $[M+Na]^+$ calcd. 310.1162 found 310.1170

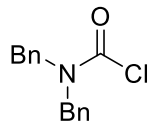

Dibenzylcarbamic chloride[350]

Triphosgene (3.44 g, 11.6 mmol) was dissolved in 100 mL DCM in a 500 mL RBF at 0°C. Tribenzylamine (10.0 g, 34.8 mmol) was dissolved in 40 mL DCM in a separate flask and added to the triphosgene solution by syringe to form a cloudy white solution. After the addition was complete, the solution warmed to room temperature overnight. The crude carbamoyl chloride was then purified by flash chromatography (3:97 EtOAc:hex) to obtain a slightly cloudy, colorless oil (6.09 g, 67%). ^{1}H NMR (400 MHz, $CDCl_3$) δ 7.47 – 7.31 (m, 6H), 7.30 – 7.25 (m, 4H), 4.65 (s, 2H), 4.54 (s, 2H). ^{13}C NMR (101 MHz, $CDCl_3$) δ 150.5, 135.4, 135.2, 129.1, 129.0, 128.5, 128.3, 128.22, 127.4, 53.1, 51.4. HRMS $[M+H]^+$ calcd. 260.0837 found 260.0842

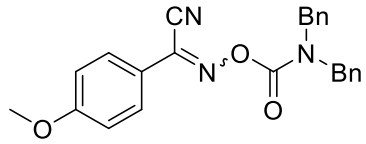

N-((dibenzylcarbamoyl)oxy)-4-methoxybenzimidoyl cyanide (6.2b)

6.1 (0.352 g, 2.0 mmol) was dissolved in 10 mL THF in a 25 mL RBF. NaH (60% in mineral oil, 0.084 g, 2.0 mmol) was then added and the solution bubbled vigorously. After 10 minutes a white precipitate formed. Dibenzylcarbamic chloride (0.519 g, 2.0 mmol) was then added dropwise and the solution became clearer. After stirring overnight, the solvent was removed and the crude product purified by flash chromatography

(EtOAc/hex) to obtain a white solid (0.677 g, 85%). mp 100-102°C. ^{1}H NMR (400 MHz, $CDCl_3$) δ 7.96 – 7.89 (m, 2H), 7.40 – 7.29 (m, 10H), 7.03 – 6.94 (m, 2H), 4.58 (d, J = 5.4 Hz, 4H), 3.88 (s, 3H). ^{13}C NMR (101 MHz, $CDCl_3$) δ 163.4, 153.4, 137.4, 129.4, 128.9, 128.6, 128.1, 128.0, 120.5, 114.8, 109.3, 55.7, 50.4, 49.2. HRMS $[M+Na]^+$ calcd. 422.1475 found 422.1482

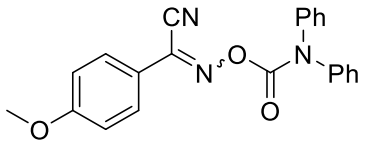

N-((diphenylcarbamoyl)oxy)-4-methoxybenzimidoyl cyanide (6.2c)

Prepared similarly to **6.2b** using diphenylcarbamoyl chloride (0.431 g, 58%). mp 136-138°C. ^{1}H NMR (400 MHz, $CDCl_3$) δ 7.89 – 7.82 (m, 2H), 7.47 – 7.35 (m, 8H), 7.34 – 7.26 (m, 2H), 6.99 – 6.91 (m, 2H), 3.86 (s, 3H). ^{13}C NMR (101 MHz, $CDCl_3$) δ 163.4, 151.3, 138.0, 129.4, 129.4, 127.2, 126.8, 120.4, 114.8, 108.7, 55.7. No other signals were observed. HRMS $[M+Na]^+$ calcd. 394.1162 found 394.1170

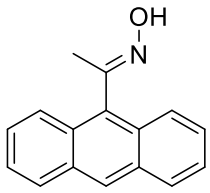

(E)-1-(anthracen-9-yl)ethan-1-one oxime (6.3)

9-Acetylanthracene (2.00 g, 9.08 mmol), hydroxylamine hydrochloride (2.21 g, 31.8 mmol), pyridine (6 mL, 75.4 mmol), and 25 mL EtOH were added to a 100 mL RBF with condenser. The mixture was heated to reflux for 24 hours. The solution was then poured

into 200 mL water and extracted with DCM, dried over Na_2SO_4, filtered, and concentrated. The crude product was then purified by flash chromatography (100% hexanes to 2:3 EtOAc:hexanes) to give a yellow solid as one isomer (0.350 g, 16%). ^{1}H NMR (400 MHz, DMSO) δ 11.46 (s, 1H), 8.64 (s, 1H), 8.17 – 8.08 (m, 2H), 7.91 (ddd, *J* = 7.3, 5.4, 3.2 Hz, 2H), 7.61 – 7.49 (m, 4H), 2.34 (s, 3H). ^{13}C NMR (101 MHz, DMSO) δ 153.4, 132.7, 130.9, 128.9, 128.6, 127.1, 126.3, 125.5, 125.2, 17.4. HRMS $[M+H]^+$ calcd. 236.1070 found 236.1072

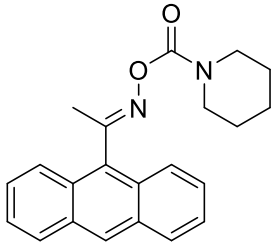

(E)-1-(anthracen-9-yl)ethan-1-one O-piperidine-1-carbonyl oxime (6.4)

6.3 (0.273 g, 1.16 mmol) was dissolved in 5 mL THF. NaH (60% in mineral oil, 0.050 g, 1.22 mmol) was then added in one portion. The solution bubbled vigourously and turns yellow-orange. After 5 minutes piperidinecarbonyl chloride (0.180 g, 1.22 mmol) was added dropwise. The solution color quickly faded and the solution became cloudy. After 15 minutes the reaction mixture was concentrated and the crude material purified by flash chromatography (100% hexanes to 2:3 EtOAc:hexanes) to obtain a white crystalline solid (0.385 g, 96%). mp 157-158°C. ^{1}H NMR (400 MHz, $CDCl_3$) δ 8.49 (s, 1H), 8.04 – 7.97 (m, 4H), 7.54 – 7.44 (m, 4H), 3.63 (br s, 4H), 2.55 (s, 3H), 1.69 (br s, 6H). ^{13}C NMR (101 MHz, $CDCl_3$) δ 162.9, 153.8, 131.3, 130.2, 129.4, 128.7, 128.4, 126.6, 125.4, 125.3, 45.4, 24.5, 19.6. HRMS $[M+Na]^+$ calcd. 369.1573 found 369.1581

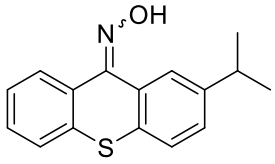

2-isopropyl-9H-thioxanthen-9-one oxime (6.5)

2-isopropylthioxanthone (2.00 g, 7.86 mmol) was added to a 50 mL RBF with condenser. Hydroxylamine hydrochloride (1.64 g, 23.6 mmol) and pyridine (25 mL) were then added and the mixture refluxed for 24 hours. The solution was then poured into 200 mL water and extracted with DCM, dried over Na_2SO_4, filtered, and concentrated. The crude product was then purified by flash chromatography (1:9 to 8:2 DCM:hexanes) to give an off white solid (0.356 g, 17%). ^{1}H NMR (400 MHz, $CDCl_3$) mixture of 2 isomers in 1:1 ratio δ 8.43 – 8.39 (m, 1H), 8.30 (d, *J* = 1.9 Hz, 1H), 7.84 (dd, *J* = 7.6, 1.5 Hz, 1H), 7.73 (d, *J* = 1.9 Hz, 1H), 7.53 – 7.48 (m, 1H), 7.45 – 7.41 (m, 2H), 7.39 – 7.29 (m, 5H), 7.26 (d, *J* = 1.3 Hz, 1H), 7.24 (d, *J* = 1.9 Hz, 1H), 3.02 – 2.90 (m, 2H), 1.28 (d, *J* = 2.0 Hz, 6H), 1.27 (d, *J* = 2.0 Hz, 6H). ^{13}C NMR (101 MHz, $CDCl_3$) δ 149.29, 149.27, 147.9, 146.4, 134.5, 133.1, 132.2, 131.5, 131.5, 131.3, 131.2, 131.0, 129.8, 129.5, 129.5, 128.8, 128.1, 127.5, 126.7, 126.6, 126.5, 126.0, 125.8, 125.7, 125.4, 124.5, 34.1, 34.0, 24.1, 24.1. HRMS (CI) calcd. 269.0874 found 269.0876

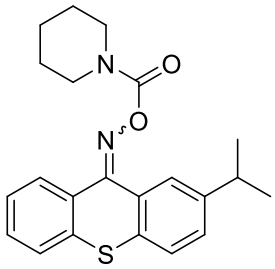

2-isopropyl-9H-thioxanthen-9-one O-piperidine-1-carbonyl oxime (6.6)

2-isopropythioxanthone oxime (0.500 g, 1.86 mmol) was dissolved in 15 mL THF in a 50 mL RBF. NaH (60% in mineral oil, 0.078 g, 1.86 mmol) was then added in one portion. The solution was stirred for 5 minutes then piperidinecarbonyl chloride (0.274 g, 1.86 mmol) was added. The solution was stirred for 10 minutes, becoming cloudy. The solution was concentrated in vacuum and then the crude product was purified by flash chromatography (100% hexanes to 2:3 EtOAc:hexanes). The title compound was recovered as a white fluffy solid (0.624 g, 88%). 1:1 mixture of isomers. ^{1}H NMR (400 MHz, $CDCl_3$) δ 8.11 – 8.05 (m, 2H), 7.95 (dd, *J* = 12.1, 2.0 Hz, 2H), 7.56 – 7.52 (m, 1H), 7.48 (d, *J* = 8.2 Hz, 1H), 7.45 – 7.41 (m, 1H), 7.40 – 7.30 (m, 5H), 7.28 (dd, *J* = 8.2, 2.0 Hz, 2H), 3.50 (s, 8H), 3.04 – 2.88 (m, 2H), 1.67 – 1.50 (m, 12H), 1.27 (d, *J* = 3.0 Hz, 6H), 1.25 (d, *J* = 3.0 Hz, 6H). ^{13}C NMR (101 MHz, $CDCl_3$) δ 153.83, 153.81, 153.79, 153.5, 148.1, 146.4, 135.3, 133.2, 132.1, 130.8, 130.2, 130.0, 129.9, 129.8, 129.4, 128.7, 128.5, 128.0, 127.8, 126.98, 126.96, 126.87, 126.0, 125.9, 125.8, 125.6, 125.5, 125.2, 77.5, 77.2, 76.8, 45.5, 45.4, 34.3, 34.0, 24.5, 24.4, 24.1, 24.0. HRMS (CI) $[M+H]^+$ calcd. 381.1631 found 381.1643

Appendix

Raw data of HPLC counts obtained for photolysis of ONBM-An and ONB2M-An in acetonitrile at 254 nm. Exposures were performed in quartz NMR tubes in a Rayonet photochemical reactor using 2 254 nm bulbs.

1 stage ONBM-An exposure

	Aniline Counts at 230 nm (μV*s)			1 Stage Counts at 275 nm (μV*s)		
Exp Time (min)	Trial 1	Trial 2	Trial 3	Trial 1	Trial 2	Trial 3
0	0	0	0	23262966		
1	2339644	2204596	2275984	21315322	21278975	21974564
2	4331947	4159394	3634579	20772196	20583047	21449454
3	5154733	5490105	5989669	19294429	19177716	20163437
5	10484095	10546242	8074466	14977074	16184609	13329296
10	19996807	18553454	20309676	13120039	11301033	11739458
20	29495912	27031363	27500587	7564690	6366347	6291655
30	31301880	30116787	30582732	4464779	3316110	3348130
40	31752926	32678015	31713766	2088719	1738106	1974777

2 stage ONB2M-An exposure

	Aniline Counts at 230 nm (μV*s)			1 Stage Counts at 275 nm (μV*s)		
Exp Time (min)	Trial 1	Trial 2	Trial 3	Trial 1	Trial 2	Trial 3
0	0	0	0	0	0	0
1	178909	139724	172775	703949	646460	768680
2	375256	426791	673770	1185496	1256519	1423218
3	660626	651499	819363	1713103	1648521	1757044
5	2023465	2242406	2343502	2912949	2718457	2607060
10	5965497	6269290	5982081	3567654	3401800	3111206
20	10755479	10263576	10389431	2696821	2568811	2537142
30	13534019	13218486	13050830	1897586	1622112	1713872
40	16320980	14652542	13581619	1436261	1128732	1176476

	2 Stage Counts at 275 nm (μV*s)		
Exp Time (min)	Trial 1	Trial 2	Trial 3
0	17948263		
1	16264508	17394156	17340630
2	15607226	15820548	16347424
3	14830318	14882745	14950142
5	13510690	11821525	11739629
10	9122811	8302123	7686464
20	3614909	2883310	3026454
30	1636824	1247972	1285681
40	700630	680463	678536

Calibration

Species	Counts/ (mg/mL)
Aniline (230 nm)	6080000
ONBM-An (275 nm)	3070000
ONB2M-An (275 nm)	5670000

Glossary

3FAPAB	4-amino-2-(trifluoromethyl)phenyl 4-aminobenzoate
6FAPAB	4-amino-2,6-bis(trifluoromethyl)phenyl 4-aminobenzoate
6FDA	4,4'-(Hexafluoroisopropylidene)diphthalic anhydride
ACN	Acetonitrile
AcOH	Acetic acid
APAB	4-aminophenyl 4-aminobenzoate
APCL	1-(3-aminopropyl)azepan-2-one
BnBr	Benzyl bromide
Bn-HDBN	1-benzyloctahydropyrrolo[1,2-a]pyrimidine
BPDA	4,4'-Biphthalic dianhydride
CAR	Chemically amplified resists
CBDA	Cyclobutane-1,2,3,4-tetracarboxylic dianhydride
CTC	Charge transfer complex
CTE	Coefficient of thermal expansion
DBN	1,5-Diazabicyclo[4.3.0]non-5-ene
DBN BnBr	1-benzyl-2,3,4,6,7,8-hexahydropyrrolo[1,2-a]pyrimidin-1-ium bromide
DBOP	Diphenyl (2-thioxobenzo[d]oxazol-3(2H)-yl)phosphonate
DBU	1,8-Diazabicyclo[5.4.0]undec-7-ene
DBU BnBr	1-benzyl-2,3,4,6,7,8,9,10-octahydropyrimido[1,2-a]azepin-1-ium bromide
DBU EtBr	1-ethyl-2,3,4,6,7,8,9,10-octahydropyrrolo[1,2-a]azepin-1-ium bromide
DCM	Dichloromethane
DF	Dissipation factor

DM-CBDA	(1R, 2R, 3S, 4S)-2,4-bis(methoxycarbonyl)cyclobutane-1,3-dicarboxylic acid
DMAP	4-dimethylaminopyridine
DMF	Dimethylformamide
DMSO	Dimethylsulfoxide
DMTBD BF_4	1,9-dimethyl-3,4,6,7,8,9-hexahydro-2H-pyrimido[1,2-a]pyrimidin-1-ium tetrafluoroborate
DMTBD I	1,9-dimethyl-3,4,6,7,8,9-hexahydro-2H-pyrimido[1,2-a]pyrimidin-1-ium iodide
DNQ	Diazonapthoquinone
DSC	Differential scanning calorimetry
DUV	Deep ultraviolet
ε_r	Dielectric constant
E_0	Positive threshold
EDC	1-ethyl-3-(3-dimethylaminopropyl)carbodiimide
E_n	Negative threshold
EtOAc	Ethyl acetate
EUV	Extreme ultraviolet
FPI	Fluorinated polyimide
GC(MS)	Gas chromatography (mass spectrometry)
HPLC	High pressure liquid chromatography
HRMS	High resolution mass spectrometry
IR	Infrared
ITX	2-isopropylthioxanthone
L/S	Line/space

LER	Line edge roughness
LWR	Line width roughness
MONB piperidine	5-methoxy-2-nitrobenzyl piperidine-1-carboxylate
mPMDA-TFMB-EE	Meta poly(amic ethyl ester) of PMDA and TFMB
MTBD	1-methyl-1,3,4,6,7,8-hexahydro-2H-pyrimido[1,2-a]pyrimidine
n	Index of refraction
NMP	N-methyl-2-pyrrolidone
NMR	Nuclear magnetic resonance
NVOC DBU	4,5-dimethoxy-2-nitrobenzyl (3-(2-oxoazepan-1-yl)propyl)carbamate
NVOC piperidine	4,5-dimethoxy-2-nitrobenzyl piperidine-1-carboxylate
NVOC TMP	4,5-dimethoxy-2-nitrobenzyl 2,2,6,6-tetramethylpiperidine-1-carboxylate
ODA	4,4'-oxydianiline
ONB	2-nitrobenzyl
OTf	Triflate
OTs	Tosylate
PAA	Poly(amic acid)
PAB	Post apply bake
PAC	Photoactive compound
PAE	Poly(amic ester)
PAG	Photoacid generator
PBG	Photobase generator
PDBN-TBD	1-(2-oxo-2-phenylethyl)-2,3,4,6,7,8-hexahydropyrrolo[1,2-a]pyrimidin-1-ium tetraphenylborate
PEB	Post exposure bake

PI	Polyimide
PII	Polyisoimide
PMDA	Pyromellitic dianhydride
PPBT	3,3'-(phenylphosphoryl)bis(benzo[d]thiazol-2(3H)-one)
PPD	Para-phenylenediamine
PPG	Photosensitive protecting group
PSPI	Photosensitive polyimide
SADP	Self-aligned double patterning
SEM	Scanning electron microscope
SPDR	Split post dielectric resonance
TBAB	Tetrabutylammonium bromide
TBAF	Tetrabutylammonium fluoride
TBD-NP	3,4,6,7,8,9-hexahydro-2H-pyrimido[1,2-a]pyrimidin-1-ium 2-(5-nitro-1,3-dioxoisoindolin-2-yl)acetate
TBD-TPB	3,4,6,7,8,9-hexahydro-2H-pyrimido[1,2-a]pyrimidin-1-ium tetraphenylborate
TBD-XA	3,4,6,7,8,9-hexahydro-2H-pyrimido[1,2-a]pyrimidin-1-ium 2-(9-oxo-9H-xanthen-2-yl)acetate
t-BOC	Tert-butyl carbonate
TCA	Trichloroacetic acid
tCHDA	Trans-1,4-cyclohexanediamine
TEA	Triethylamine
TFA	Trifluoroacetic acid
TFMB	2,2'-bis(trifluoromethyl)benzidine
TFMOB	2,2'-bis(trifluoromethoxy)benzidine

T_g	Glass transition temperature
TGA	Thermogravimetric analysis
THF	Tetrahydrofuran
TLC	Thin layer chromatography
TMAH	Tetramethylammonium hydroxide
UV	Ultraviolet

References

1. Moye, W. T. ENIAC: The Army-Sponsored Revolution. http://ftp.arl.mil/~mike/comphist/96summary/index.html.
2. Fritz, W. B., ENIAC-a problem solver. *IEEE Annals of the History of Computing* **1994,** *16* (1), 25-45.
3. Harlow, F. H.; Metropolis, N., Computing and Computers Weapons Simulation Leads to the Computer Era. *Los Alamos Science* **1983**.
4. ENIAC. http://encyclopedia2.thefreedictionary.com/ENIAC.
5. Dalakov, G. History of Computers: ENIAC. http://history-computer.com/ModernComputer/Electronic/ENIAC.html.
6. Weik, M. H. The ENIAC Story. http://ftp.arl.mil/mike/comphist/eniac-story.html.
7. Bardeen, J.; Brattain, W. H., The Transistor, A Semi-Conductor Triode. *Phys. Rev.* **1948,** *74* (2), 230-231.
8. Brattain, W. H.; Bardeen, J., Nature of the Forward Current in Germanium Point Contacts. *Phys. Rev.* **1948,** *74* (2), 231-232.
9. Shockley, W.; Pearson, G. L., Modulation of Conductance of Thin Films of Semi-Conductors by Surface Charges. *Phys. Rev.* **1948,** *74* (2), 232-233.
10. 1st-Transistor. https://commons.wikimedia.org/wiki/File:1st-Transistor.jpg.
11. Kilby, J. Jack Kilbly describes how he developed the world's first integrated circuits. http://www.ti.com/corp/docs/company/history/timeline/semicon/1950/docs/58kilby-ic-interview.htm.
12. Hoerni, J. A. In *Planar silicon diodes and transistors*, Electron Devices Meeting, 1960 Internationa, 1960; 1960; pp 50-50.
13. Norman, R.; Last, J.; Haas, I. In *Solid-state micrologic elements*, Solid-State Circuits Conference. Digest of Technical Papers. 1960 IEEE International, 10-12 Feb. 1960; 1960; pp 82-83.
14. Moore, G. E., Cramming More Components Onto Integrated Circuits. *Proc. IEEE* **1998,** *86* (1), 82-85.
15. Moore, G. E., Progress in digital integrated electronics. *Electron Devices Meeting, 1975 International* **1975,** *21*, 11-13.
16. Transistor Count and Moore's Law-2011. https://commons.wikimedia.org/wiki/File:Transistor_Count_and_Moore's_Law_-_2011.svg.
17. Mack, C., *Fundamental Principles of Optical Lithography*. Wiley: 2011; p 534.
18. French, R. H.; Tran, H. V., Immersion Lithography: Photomask and Wafer-Level Materials. *Annual Review of Materials Research* **2009,** *39* (1), 93-126.
19. Minsk, L. M.; Van Deusen, W. P.; Robertson, M., Photosensitization of polymeric cinnamic acid esters. Google Patents: 1952.

20. Van, D. W. P.; M, M. L.; M, R. E., Photosensitization of polymeric cinnamic acid esters. Google Patents: 1954.
21. Willson, C. G., Organic Resist Materials — Theory and Chemistry. In *Introduction to Microlithography*, AMERICAN CHEMICAL SOCIETY: 1983; Vol. 219, pp 87-159.
22. Thompson, L. F.; Willson, C. G.; Bowden, M. J., *Introduction to Microlithography (ACS Professional Reference Book)*. 2 ed.; American Chemical Society: 1994; p 540.
23. Pacansky, J.; Lyerla, J. R., Photochemical Decomposition Mechanisms for AZ-Type Photoresists. *IBM J. Res. Dev.* **1979,** *23* (1), 42-55.
24. Thompson, L. F.; Willson, C. G.; Bowden, M. J., *Introduction to Microlithography*. AMERICAN CHEMICAL SOCIETY: 1983; Vol. 219, p 380.
25. Willson, C.; Ito, H.; Fréchet, J.; Tessier, T.; Houlihan, F., Approaches to the Design of Radiation-Sensitive Polymeric Imaging Systems with Improved Sensitivity and Resolution. *J. Electrochem. Soc.* **1986,** *133*, 181.
26. Crivello, J. V.; Lam, J. H. W., Diaryliodonium Salts. A New Class of Photoinitiators for Cationic Polymerization. *Macromolecules* **1977,** *10* (6), 1307-1315.
27. MacDonald, S. A.; Hinsberg, W. D.; Wendt, H. R.; Clecak, N. J.; Willson, C. G.; Snyder, C. D., Airborne contamination of a chemically amplified resist. 1. Identification of problem. *Chem. Mater.* **1993,** *5* (3), 348-356.
28. Jain, K.; Willson, C. G.; Lin, B. J., Ultrafast deep UV Lithography with excimer lasers. *IEEE Electron Device Letters* **1982,** *3* (3), 53-55.
29. Kunz, R. R.; Palmateer, S. C.; Forte, A. R.; Allen, R. D.; Wallraff, G. M.; Diperto, R. A.; Hofer, D. C., *Limits to etch resistance for 193-nm single-layer resists*. Society of Photo-Optical Instrumentation Engineers: Bellingham, WA, ETATS-UNIS, 1996; Vol. 2724, p 12.
30. Bates, A. K.; Rothschild, M.; Bloomstein, T. M.; Fedynyshyn, T. H.; Kunz, R. R.; Liberman, V.; Switkes, M., Review of technology for 157-nm lithography. *IBM J. Res. Dev.* **2001,** *45* (5), 605-614.
31. Strahan, J. Advanced Organic Materials for Lithographic Applications. Doctoral Thesis, University of Texas at Austin, 2010.
32. Jacobsson, M. MATERIALS DEVELOPMENT FOR STEP AND FLASH IMPRINT LITHOGRAPHY. Doctoral Thesis, University of Texas at Austin, 2011.
33. Bates, C. M. Advanced Materials for Block Copolymer Lithography. University of Texas at Austin, 2013
34. Berro, A. J.; Gu, X.; OConnor, N.; Jockusch, S.; Nagai, T.; Ogata, T.; Zimmerman, P.; Rice, B. J.; Adolph, E.; Byargeon, T.; Gonzalez, J.; Turro, N. J.; Willson, C. G., Optical threshold layer and intermediate state two-photon PAG approaches to double exposure lithography. *Proc SPIE, Advances in Resist Materials and Processing Technology XXVI* **2009,** (7273), 72731B.
35. Koay, C.-S.; Holmes, S.; Petrillo, K.; Colburn, M.; Burns, S.; Dunn, S.; Cantone, J.; Hetzer, D.; Kawakami, S.; van Dommelen, Y.; Jiang, A.; Many, M.; Routh, R.; Huli, L.; Martinick, B.; Rodgers, M.; Tomizawa, H.; Kini, S., Evaluation of double-patterning

techniques for advanced logic nodes. *Proc SPIE, Optical Microlithography XXIII* **2010,** *7640*, 764009.
36. Bencher, C.; Chen, Y.; Dai, H.; Montgomery, W.; Huli, L., 22nm half-pitch patterning by CVD spacer self alignment double patterning (SADP). **2008**, 69244E-69244E-7.
37. Asano, M., Sub-100 nm Lithography with KrF Exposure Using Multiple Development Method. *Jpn. J. Appl. Phys.* **1999,** *38* (12S), 6999.
38. Bencher, C.; Smith, J.; Miao, L.; Cai, C.; Chen, Y.; Cheng, J. Y.; Sanders, D. P.; Tjio, M.; Truong, H. D.; Holmes, S.; Hinsberg, W. D., Self-assembly patterning for sub-15nm half-pitch: a transition from lab to fab. *Proc. SPIE, Alternative Lithographic Technologies III* **2011,** *7970*, 79700F.
39. Jeng, S.-P.; Havemann, R. H.; Chang, M.-C., Process Integration and Manufacturasility Issues for High Performance Multilevel Interconnect. *MRS Online Proceedings Library Archive* **1994,** *337*, 25 (7 pages).
40. Volksen, W.; Miller, R. D.; Dubois, G., Low Dielectric Constant Materials. *Chem. Rev.* **2010,** *110* (1), 56-110.
41. Morgen, M.; Ryan, E. T.; Zhao, J.-H.; Hu, C.; and, T. C.; Ho, P. S., Low Dielectric Constant Materials for ULSI Interconnects. *Annu. Rev. Mater. Sci.* **2000,** *30* (1), 645-680.
42. Gu, X. Design and Development of Material-based Resolution Enhancement Techniques for Optical Lithography. Doctoral Thesis, University of Texas at Austin, 2011.
43. Mesch, R. Catalysis and Materials Development for Photolithography. Doctoral Thesis, The University of Texas at Austin, 2014.
44. ASML confident of 2016 EUV goals. http://optics.org/news/7/1/21.
45. Clarke, P. EUV litho keeps progressing, keeps slipping. http://www.eetimes.com/document.asp?doc_id=1256589.
46. Hakey, M. C.; Holmes, S. J.; Horak, D. V.; Katnani, A. D.; Patel, N. M.; Rabidoux, P. A. Frequency doubling hybrid photoresist having negative and positive tone components and method of preparing the same. US 6114082, 2000.
47. Roeschert, H.; Dammel, R. R.; Eckes, C.; Kamiya, K.; Meier, W.; Przybilla, K. J.; Spiess, W.; Pawlowski, G. In *DN 21, DN 41: negative-tone photoresists for deep-UV lithography*, Proc SPIE, 1992; pp 157-171.
48. Fedynyshyn, T. H. Multi-tone resist compositions. US8110339 B2, Mar, 2012.
49. Fonseca, C.; Somervell, M.; Scheer, S.; Kuwahara, Y.; Nafus, K.; Gronheid, R.; Tarutani, S.; Enomoto, Y. In *Advances in dual-tone development for pitch frequency doubling*, Proc. SPIE, 2010; pp 76400E-76400E-12.
50. Fonseca, C. A.; Somervell, M.; Scheer, S.; Printz, W. P. Dual tone development with a photo-activated acid enhancement component in lithographic applications. US8574810 B2, 2013.
51. Hori, Y.; Watanabe, R.; Tsunoda, R.; Mori, T.; Shimizu, H.; Yamazaki, A., Development of Materials-based Pitch Split Process *J. Photopolym. Sci. Technol.* **2016,** *29* (1), 55-58.

52. Gu, X.; Bates, C. M.; Cho, Y.; Kawakami, T.; Nagai, T.; Ogata, T.; Sundaresan, A. K.; Turro, N. J.; Bristol, R.; Zimmerman, P.; Willson, C. G., Photobase generator assisted pitch division. *Proc SPIE, Advances in Resist Materials and Processing Technology XXVII* **2010,** *7639*, 763906.
53. Tsiartas, P.; Schmid, G.; Johnson, H.; Stewart, M.; Willson, C., Quantifying acid generation efficiency for photoresist applications. *Journal of Vacuum Science & Technology B: Microelectronics and Nanometer Structures* **2005,** *23*, 224.
54. Tsiartas, P. C.; Schmid, G. M.; Johnson, H. F.; Stewart, M. D.; Willson, C. G., Quantifying acid generation efficiency for photoresist applications. *Journal of Vacuum Science & Technology B* **2005,** *23* (1), 224-228.
55. Gu, X.; Bates, C.; Cho, Y.; Costner, E.; Marzuka, F.; Nagai, T.; Ogata, T.; Shi, C.; Sundaresan, A. K.; Turro, N. J., A New Materials-based Pitch Division Technique. *J. Photopolym. Sci. Technol.* **2009,** *22* (6), 773-781.
56. Zhang, H.; Du, Y.; Wong, M. D. F.; Topaloglu, R. O., Characterization and decomposition of self-aligned quadruple patterning friendly layout. *Proc SPIE, Optical Microlithography XXV* **2012,** *8326*, 83260F1.
57. Nakayama, K.; Kodama, C.; Kotani, T.; Nojima, S.; Mimotogi, S.; Miyamoto, S., Self-aligned double and quadruple patterning layout principle. *Proc SPIE, Design for Manufacturability through Design-Process Integration VI* **2012,** *8327*, 83270V1.
58. Patchornik, A.; Amit, B.; Woodward, R. B., Photosensitive protecting groups. *J. Am. Chem. Soc.* **1970,** *92* (21), 6333-6335.
59. Mckean, D. R.; Wallraff, G. M.; Volksen, W.; Hacker, N. P.; Sanchez, M. I.; Labadie, J. W., Base-Catalyzed Photosenstive Polyimide. *ACS Symp. Ser.* **1994,** *537*, 417-427.
60. McKean, D. R.; Wallraff, G. M.; Volksen, W.; Hacker, N. P.; Sanchez, M. I.; Labadie, J. W., Base-catalyzed photosensitive polyimide. *Proc SPIE, Advances in Resist Technology and Processing X* **1993,** *1925*, 192507.
61. Suyama, K.; Shirai, M., Photobase generators: Recent progress and application trend in polymer systems. *Prog. Polym. Sci.* **2009,** *34* (2), 194-209.
62. Leung, M.-k.; Frechet, J. M. J.; Cameron, J. F.; Willson, C. G., Design and Synthesis of Photoactive Polymer Systems Based on Amine-Catalyzed Intramolecular Imidization of Polymer Side Chains. *Macromolecules* **1995,** *28* (13), 4693-4700.
63. Frechet, J. M. J.; Leung, M.-k.; Urankar, E. J.; Willson, C. G.; Cameron, J. F.; MacDonald, S. A.; Niesert, C. P., Photogenerated Base in Resist and Imaging Materials: Design of Functional Polymers Susceptible to Base Catalyzed Decarboxylation. *Chem. Mater.* **1997,** *9* (12), 2887-2893.
64. Endo, M.; Tani, Y.; Sasago, M.; Nomura, N., o-Nitrobenzyl Ester Based Deep UV Resist for KrF Excimer Laser Lithography. *Polym. J.* **1989,** *21* (8), 603-607.
65. Nishikubo, T.; Takehara, E.; Kameyama, A., Photogeneration of polyfunctional amines and novel thermal curing reactions of epoxy resin and polyurethane oligomer using these amines. *J. Polym. Sci., Part A: Polym. Chem.* **1993,** *31* (12), 3013-3020.
66. Holtzman, B. Photogeneration of amines. Masters Thesis, University of Texas at Austin, 1999.

67. Heath, W. H. Design, Synthesis, and Evaluation of Materials for Microelectronics Applications. Doctoral Thesis, University of Texas at Austin, 2006.
68. Bell, W. K. Photocrosslinkable Nonlinear Optical Polymers and Directly Patternable Polyimide Dielectrics. Doctoral Thesis, University of Texas at Austin, 2014.
69. Postnikov, S. Transport Properties of Photogenerated Acid and Silylating Agent in Polymer Films. Doctoral Thesis, University of Texas at Austin, Austin, 1999.
70. Cho, Y.; Gu, X.; Hagiwara, Y.; Kawakami, T.; Ogata, T.; Rawlings, B.; Li, Y.; Sundaresan, A. K.; Turro, N. J.; Bristol, R.; Blackwell, J. M.; Willson, C. G., Polymer-bound photobase generators and photoacid generators for pitch division lithography. *Proc. SPIE, Advances in Resist Materials and Processing Technology XXVIII* **2011,** *7972*, 797221.
71. Tkachenko, N. V., Appendix C. Two photon absorption. In *Optical Spectroscopy: Methods and Instrumentations*, Elsevier: 2006; p 293.
72. Pirrung, M. C.; Pieper, W. H.; Kaliappan, K. P.; Dhananjeyan, M. R., Combinatorial discovery of two-photon photoremovable protecting groups. *Proc. Natl. Acad. Sci. U.S.A.* **2003,** *100* (22), 12548-12553.
73. Bristol, R.; Shykind, D.; Kim, S.; Borodovsky, Y.; Schwartz, E.; Turner, C.; Masson, G.; Min, K.; Esswein, K.; Blackwell, J. M.; Suetin, N., Double-exposure materials for pitch division with 193nm lithography: requirements, results. *Proc SPIE, Advances in Resist Materials and Processing Technology XXVI* **2009,** *7273*, 727307.
74. Shykind, D.; Bristol, R.; Roberts, J.; Blackwell, J.; Borodovsky, Y., Reaction kinetics of non-reciprocal photo-base generator (NRPBG) patterning. *Proc SPIE, Advances in Resist Materials and Processing Technology XXVII* **2010,** *7639*, 76391Y.
75. Poonawala, A.; Borodovsky, Y.; Milanfar, P., ILT for double exposure lithography with conventional and novel materials. *Proc. SPIE, Optical Microlithography XX* **2007,** *6520*, 65202Q.
76. Lee, S.; Byers, J.; Jen, K.; Zimmerman, P.; Rice, B.; Turro, N. J.; Willson, C. G., An analysis of double exposure lithography options. In *Optical Microlithography*, Levinson, H. J.; Dusa, M., Eds. International Society for Optics and Photonics: 2008; Vol. 6924, pp 69242A-69242A-12.
77. Hagiwara, Y.; Mesch, R. A.; Kawakami, T.; Okazaki, M.; Jockusch, S.; Li, Y.; Turro, N. J.; Grant Willson, C., Design and synthesis of a photoaromatization-based two-stage photobase generator for pitch division lithography. *J. Org. Chem.* **2013,** *78* (5), 1730-1734.
78. Turro, N. J.; Li, Y.; Jockusch, S.; Hagiwara, Y.; Okazaki, M.; Mesch, R. A.; Schuster, D. I.; Willson, C. G., Study of a two-stage photobase generator for photolithography in microelectronics. *J. Org. Chem.* **2013,** *78* (5), 1735-1741.
79. Cameron, J. F.; Frechet, J. M. J., Photogeneration of organic bases from o-nitrobenzyl-derived carbamates. *J. Am. Chem. Soc.* **1991,** *113* (11), 4303-4313.
80. Pelliccioli, A. P.; Wirz, J., Photoremovable protecting groups: reaction mechanisms and applications. *Photochem. Photobiol. Sci.* **2002,** *1* (7), 441-458.

81. Arán, V. J.; Díez-Barra, E.; de la Hoz, A.; Sánchez-Verdú, P., Selective synthesis of 2-substituted indazolin-3-ones without N-1 protection. *Heterocycles* **1997,** *45* (1), 129-136.
82. Kurth, M. J.; Olmstead, M. M.; Haddadin, M. J., Claimed 2,1-benzisoxazoles are indazalones. *J. Org. Chem.* **2005,** *70* (3), 1060-1062.
83. Wagner, P. J.; Hammond, G. S., Mechanism of Type II Photoelimination. *J. Am. Chem. Soc.* **1965,** *87* (17), 4009-4011.
84. Hinsberg, W.; Houle, F. A.; Hoffnagle, J.; Sanchez, M.; Wallraff, G.; Morrison, M.; Frank, S., Deep-ultraviolet interferometric lithography as a tool for assessment of chemically amplified photoresist performance. *J. Vac. Sci. Technol. B* **1998,** *16* (6), 3689-3694.
85. Rivera, J., Worldwide Semiconductor Assembly and Test Services Market Grew 2.3 Percent in 2013, According to Final Results by Gartner. 2014.
86. DSI Introduces Solderable Coatings and Face Metallization Optical Coatings.
87. Intel Unveils New Product Plans for High-Performance Computing. http://www.intel.com/pressroom/archive/releases/2010/20100531comp.htm.
88. Myslewski, R. Happy 40th birthday, Intel 4004! http://www.theregister.co.uk/2011/11/15/the_first_forty_years_of_intel_microprocessors/.
89. Brown, T. Device Packages. http://ecee.colorado.edu/~ecen4610/wiki/index.php/Device_Packages.
90. Kang, S.-M.; Leblebici, Y., *CMOS Digital Integrated Circuits* 3ed.; McGraw-Hill: 2002.
91. Pecht, M., *Integrated Circuit, Hybrid, and Multichip Module Package Design Guidelines: A Focus on Reliability*. Wiley: 1994.
92. Blackshear, E. D.; Cases, M.; Klink, E.; Engle, S. R.; Malfatt, R. S.; Araujo, D. N. d.; Oggioni, S.; LaCroix, L. D.; Wakil, J. A.; Pham, N. H.; Hougham, G. G.; Russell, D. J., The evolution of build-up package technology and its design challenges. *IBM J. Res. Dev.* **2005,** *49* (4.5), 641-661.
93. Wheeler, R. EPROM Microchip SuperMacro. https://commons.wikimedia.org/wiki/File:EPROM_Microchip_SuperMacro.jpg.
94. McSherry, L. AMD Phenom X4 9750 https://commons.wikimedia.org/wiki/File:AMD_Phenom_X4_9750_%28Underside%29.JPG.
95. Intel Land Grid Array (LGA) Socket and Package Technology. http://www.intel.com/content/dam/www/public/us/en/documents/guides/lga-socket-and-package-technology-training-guide.pdf.
96. Srinivasan, R., Etching polymer films with ultraviolet laser pulses of long (10–400 μs) duration. *J. Appl. Phys.* **1992,** *72* (4), 1651-1653.
97. Antesberger, T. Laser Drilling for Electrical Interconnection in Advanced Flexible Electronics Applications. http://people.ccmr.cornell.edu/~cober/MSE5420/page2/files/LaserProcessing.pdf.

98. *Polyimides: Fundamentals and Applications*. Marcel Dekker: New York, NY, 1996.
99. Makino, D., *ACS Symp. Ser.* **1994,** *537*, 380-402.
100. Odian, G., *Principles of Polymerization*. 4th ed.; John Wiley & Sons: 2007; p 840.
101. Hasegawa, M.; Horiuchi, M.; Kumakura, K.; Koyama, J., Colorless polyimides with low coefficient of thermal expansion derived from alkyl-substituted cyclobutanetetracarboxylic dianhydrides. *Polym. Int.* **2014,** *63* (3), 486-500.
102. Fukukawa, K.-i.; Ueda, M., Recent Progress of Photosensitive Polyimides. *Polym. J* **2008,** *40* (4), 281-296.
103. Negi, Y. S.; Damkale, S. R.; Ansari, S., PHOTOSENSITIVE POLYIMIDES. *Journal of Macromolecular Science, Part C* **2001,** *41* (1-2), 119-138.
104. Nakayama, T.; Mochizuki, A.; Ueda, M., New positive-type photosensitive polyimide: poly(hydroxyimide) with diazonaphthoquinone. *React. Funct. Polym.* **1996,** *30* (1–3), 109-115.
105. Seino, H.; Mochizuki, A.; Haba, O.; Ueda, M., A positive-working photosensitive alkaline-developable polyimide with a highly dimensional stability and low dielectric constant based on poly(amic acid) as a polyimide precursor and diazonaphthoquinone as a photosensitive compound. *J. Polym. Sci., Part A: Polym. Chem.* **1998,** *36* (13), 2261-2267.
106. Mochizuki, A.; Teranishi, T.; Ueda, M.; Matsushita, K., Positive-working alkaline-developable photosensitive polyimide precursor based on polyisoimide using diazonaphthoquinone as a dissolution inhibitor. *Polymer* **1995,** *36* (11), 2153-2158.
107. Hsu, S. L.-C.; Lee, P.-I.; King, J.-S.; Jeng, J.-L., Novel positive-working aqueous-base developable photosensitive polyimide precursors based on diazonaphthoquinone-capped polyamic esters. *J. Appl. Polym. Sci.* **2003,** *90* (8), 2293-2300.
108. Shin, G. J.; Jung, J. C.; Chi, J. H.; Oh, T. H.; Kim, J. B., Synthesis and micropatterning properties of a novel base-soluble, positive-working, photosensitive polyimide having an o-nitrobenzyl ether group. *J. Polym. Sci., Part A: Polym. Chem.* **2007,** *45* (5), 776-788.
109. Rubner, R.; Ahne, H.; Kuhn, E.; Kolodziej, G., PHOTO-POLYMER - DIRECT WAY TO POLYIMIDE PATTERNS. *Photographic Science and Engineering* **1979,** *23* (5), 303-309.
110. Yoda, N.; Hiramoto, H., New Photosensitive High Temperature Polymers for Electronic Applications. *Journal of Macromolecular Science: Part A - Chemistry* **1984,** *21* (13-14), 1641-1663.
111. Flack, W. W.; Flores, G. E.; Christensen, L. D.; Newman, G. In *Investigation of the properties of photosensitive polyimide films*, 1996; pp 169-185.
112. Ree, M.; Nunes, T. L.; Chen, K. J. R., Structure and properties of a photosensitive polyimide: Effect of photosensitive group. *J. Polym. Sci., Part B: Polym. Phys.* **1995,** *33* (3), 453-465.

113. Lin, A. A.; Sastri, V. R.; Tesoro, G.; Reiser, A.; Eachus, R., On the crosslinking mechanism of benzophenone-containing polyimides. *Macromolecules* **1988,** *21* (4), 1165-1169.
114. Rohde, O.; Smolka, P.; Falcigno, P. A.; Pfeifer, J., *Photopolymers, Principles-Processes and Materials*. Society of Plastics Engineers, Inc.: Ellenville, NY, 1991.
115. Turro, N. J.; Scaiano, J. C.; Ramamurthy, V., *Modern molecular photochemistry of organic molecules*. University Science Books: Sausalito, Calif., 2010; p xxxiii, 1084 p.
116. Omote, T.; Koseki, K. i.; Yamaoka, T., Fluorine-containing photoreactive polyimide. 6. Synthesis and properties of a novel photoreactive polyimide based on photo-induced acidolysis and the kinetics for its acidolysis. *Macromolecules* **1990,** *23* (22), 4788-4795.
117. Naitoh, K.; Ishii, K.; Yamaoka, T.; Omote, T., Photosensitive Polyimide Protected by Tetra-Hydropyranyl Group Based on Chemical Amplification. *J. Photopolym. Sci. Technol.* **1992,** *5* (2), 339-342.
118. Kim, S. H.; Cotts, P. M., Light scattering and size exclusion chromatography of semi-flexible polyimide precursors. *J. Polym. Sci., Part B: Polym. Phys.* **1991,** *29* (1), 109-117.
119. Volksen, W.; Yoon, D. Y.; Hedrick, J. L.; Hofer, D., Chemistry and Characterization Of Polyimides Derived from Poly(Amic Alkyl Esters). *MRS Online Proceedings Library* **1991,** *227*, 23-34.
120. Miwa, T.; Numata, S., A mechanism describing polyamic acid solution viscosity change on storage at high temperature. *Polymer* **1989,** *30* (5), 893-896.
121. Tong, Y.; Liu, T.; Veeramani, S.; Chung, T.-S., Bulk Viscosity and Its Unstable Behavior upon Storage in Polyimide Precursor Solutions. *Industrial & Engineering Chemistry Research* **2002,** *41* (17), 4266-4272.
122. Tomikawa, M.; Yoshida, S.; Okamoto, N., Novel Partial Esterification Reaction in Poly(amic acid) and Its Application for Positive-Tone Photosensitive Polyimide Precursor. *Polym. J* **2009,** *41* (8), 604-608.
123. Bell, V. L.; Jewell, R. A., Synthesis and properties of polyimidazopyrrolones. *Journal of Polymer Science Part A-1: Polymer Chemistry* **1967,** *5* (12), 3043-3060.
124. Volksen, W.; Pascal, T.; Labadie, J. W.; Sanchez, M. I., Base-Catalyzed Cyclization of ortho-Aromatic Amide Alkyl Esters. In *Polymers for Microelectronics*, American Chemical Society: 1993; Vol. 537, pp 403-416.
125. Leung, M.-k.; Frechet, J. M. J., Amine catalyzed intramolecular imidization of alkyl and aryl phthalamates. Kinetics and mechanism in deuteriated chloroform. *Journal of the Chemical Society, Perkin Transactions 2* **1993,** (12), 2329-2335.
126. Fréchet, J. M. J.; Cameron, J. F.; Chung, C. M.; Haque, S. A.; Willson, C. G., Photogenerated base as catalyst for imidization reactions. *Polym. Bull.* **1993,** *30* (4), 369-375.
127. Fukukawa, K.-i.; Shibasaki, Y.; Ueda, M., Direct patterning of poly(amic acid) and low-temperature imidization using a photo-base generator. *Polym. Adv. Technol.* **2006,** *17* (2), 131-136.

128. Mizoguchi, K.; Shibasaki, Y.; Ueda, M., Development of Negative-type Photosensitive Semi-alicyclic Polyimide using a Photobase Generator. *J. Photopolym. Sci. Technol.* **2007,** *20* (2), 181-186.
129. Ogura, T.; Mizoguchi, K.; Ueda, M., Development of Negative-type Photosensitive Polyimide, Based on Poly(amic acid)s, Photo Base Generator and Thermal Base Generator. *J. Photopolym. Sci. Technol.* **2008,** *21* (1), 125-130.
130. Fukuda, S.; Katayama, M.; Sakayori, K., Photosensitive Polyimide using a Highly Sensitive Photobase Generator. *J. Photopolym. Sci. Technol.* **2009,** *22* (3), 391-392.
131. Ogura, T.; Higashihara, T.; Ueda, M., Low-CTE photosensitive polyimide based on semialicyclic poly(amic acid) and photobase generator. *J. Polym. Sci., Part A: Polym. Chem.* **2010,** *48* (6), 1317-1323.
132. Fukuda, S.; Amagai, K.; Kanke, S.; Sakayori, K., Photosensitive Polyimide using a Highly Sensitive Photobase Generator (2). *J. Photopolym. Sci. Technol.* **2011,** *24* (3), 267-268.
133. Sunohara, M.; Tokunaga, T.; Kurihara, T.; Higashi, M. In *Silicon interposer with TSVs (Through Silicon Vias) and fine multilayer wiring*, Electronic Components and Technology Conference, 2008. ECTC 2008. 58th, 27-30 May 2008; 2008; pp 847-852.
134. Feiring, A. E.; Auman, B. C.; Wonchoba, E. R., Synthesis and properties of fluorinated polyimides from novel 2,2'-bis(fluoroalkoxy)benzidines. *Macromolecules* **1993,** *26* (11), 2779-2784.
135. Auman, B. C., Fluorinated, Low Thermal Expansion Coefficient Polyimides For Interlayer Dielectric Application: Thermal Stability, Refractive Index And High Temperature Modulus Measurements. *MRS Online Proceedings Library Archive* **1995,** *381*, 19-29.
136. Liou, H.-C.; Ho, P. S.; Stierman, R., Thickness dependence of the anisotropy in thermal expansion of PMDA-ODA and BPDA-PDA thin films. *Thin Solid Films* **1999,** *339* (1–2), 68-73.
137. DuPont Kapton® Polyimide Film. http://www.dupont.com/content/dam/dupont/products-and-services/membranes-and-films/polyimde-films/documents/DEC-Kapton-summary-of-properties.pdf.
138. PI-2600 Series - Low Stress Applications. http://www.hdmicrosystems.com/HDMicroSystems/en_US/products/non_photodefineable/2600_dry_etch.html.
139. ITRS Package Substrates: Cost Performance. http://www.itrs.net/Links/2012ITRS/2012Tables/AssemblyPkg_2012Tables.xlsx.
140. Kotov, B. V.; Gordina, T. A.; Voishchev, V. S.; Kolninov, O. V.; Pravednikov, A. N., Aromatic polyimides as charge transfer complexes. *Polymer Science U.S.S.R.* **1977,** *19* (3), 711-716.
141. Dine-Hart, R. A.; Wright, W. W., A study of some properties of aromatic imides. *Die Makromolekulare Chemie* **1971,** *143* (1), 189-206.
142. Tang, C. W., Two-layer organic photovoltaic cell. *Appl. Phys. Lett.* **1986,** *48* (2), 183-185.

143. Tasios, N.; Grigoriadis, C.; Hansen, M. R.; Wonneberger, H.; Li, C.; Spiess, H. W.; Müllen, K.; Floudas, G., Self-Assembly, Dynamics, and Phase Transformation Kinetics of Donor−Acceptor Substituted Perylene Derivatives. *J. Am. Chem. Soc.* **2010,** *132* (21), 7478-7487.
144. Maex, K.; Baklanov, M. R.; Shamiryan, D.; lacopi, F.; Brongersma, S. H.; Yanovitskaya, Z. S., Low dielectric constant materials for microelectronics. *J. Appl. Phys.* **2003,** *93* (11), 8793-8841.
145. Korshak, V. V.; Vinogradova, S. V.; Vygodskii, Y. S., Cardo Polymers. *Journal of Macromolecular Science, Part C* **1974,** *11* (1), 45-142.
146. Simpson, J. O.; St.Clair, A. K., Fundamental insight on developing low dielectric constant polyimides. *Thin Solid Films* **1997,** *308–309*, 480-485.
147. Nabeshima, S.; Morikawa, A., Synthesis and properties of polyimides having a hexaphenylbenzene unit. *High Perform. Polym.* **2015,** *27* (6), 772-781.
148. Hougham, G.; Tesoro, G.; Shaw, J., Synthesis and Properties of Highly Fluorinated Polyimides. *Macromolecules* **1994,** *27* (13), 3642-3649.
149. Miller, K. J.; Hollinger, H. B.; Grebowicz, J.; Wunderlich, B., On the conformations of poly(p-xylylene) and its mesophase transitions. *Macromolecules* **1990,** *23* (16), 3855-3859.
150. Pine, S. H., *Organic Chemistry*. 5th ed. ed.; McGraw-Hill: New York, 1987.
151. Brown, W. H.; Foote, C. S.; Iverson, B. L., *Organic Chemistry*. 4th ed. ed.; Thomson Brooks/Cole: Mason, OH, 2007.
152. Ying-Hung, S.; Stark, E.; Yongfu, L.; Stokich, T.; Ober, K.; Achen, A.; Scheck, D.; Kisting, S.; Hetzner, J.; Baranek, K.; Curphy, J.; Thurston, S.; Beach, E.; Folkenroth, J.; Richardson, T.; Rozeveld, S. In *Aqueous-Base-Developable Benzocyclobutene (BCB)-Based Material Curable in Air*, Proceedings Electronic Components and Technology, 2005. ECTC '05., May 31 2005-June 3 2005; 2005; pp 1228-1233.
153. DOW CYCLOTENE 3000 Series Advanced Electronics Resins. http://msdssearch.dow.com/PublishedLiteratureDOWCOM/dh_08b4/0901b803808b4ed7.pdf?filepath=cyclotene/pdfs/noreg/888-00006.pdf&fromPage=GetDoc.
154. DOW CYCLOTENE 4000 Series Advanced Electronic Resins. http://www.dow.com/cyclotene/docs/cyclotene_4000_immersion_dev.pdf.
155. HD-8820 Aqueous Positive Polyimide. http://hdmicrosystems.com/HDMicroSystems/en_US/pdf/HD-8820_ProcessGuide.pdf.
156. HD-4100 Series. http://www.hdmicrosystems.com/HDMicroSystems/en_US/pdf/HD-4100_ProcessGuide.pdf.
157. everythingRF Dielectric Constant, Strength, and Loss Tangent. http://www.rfcafe.com/references/electrical/dielectric-constants-strengths.htm.
158. Kaatze, U., Complex permittivity of water as a function of frequency and temperature. *Journal of Chemical & Engineering Data* **1989,** *34* (4), 371-374.
159. Maier, G., Low dielectric constant polymers for microelectronics. *Prog. Polym. Sci.* **2001,** *26* (1), 3-65.

160. Coefficients of Linear Thermal Expansion. http://www.engineeringtoolbox.com/linear-expansion-coefficients-d_95.html.
161. Soliman, H. M.; Waheed, A. F., Effect of Differential Thermal Expansion Coefficient on Stresses Generated in Coating. *J. Mater. Sci. Technol.* **1999,** *15* (5), 457-462.
162. Lau, J.; Danksher, W.; Vianco, P. In *Acceleration models, constitutive equations, and reliability of lead-free solders and joints*, Electronic Components and Technology Conference, 2003. Proceedings. 53rd, May 27-30, 2003; 2003; pp 229-236.
163. Cheang, P.; Christensen, L.; Reynaga, C. In *Optimization of Photosensitive Polyimide Process for Cost Effective Packaging*, Surface Mount Technology Seminar, 1996.
164. Volksen, W., personal communication. 2013.
165. Neuber, C.; Giesa, R.; Schmidt, H.-W., Synthesis and Properties of Lyotropic para-Linked Aromatic Poly(amic ethyl ester)s. *Macromol. Chem. Phys.* **2002,** *203* (3), 598-604.
166. Becker, K. H.; Schmidt, H. W., Para-linked aromatic poly(amic ethyl esters): precursors to rodlike aromatic polyimides. 1. Synthesis and imidization study. *Macromolecules* **1992,** *25* (25), 6784-6790.
167. Stoffel, N. C.; Chandra, S.; Kramer, E. J.; Volksen, W.; Russell, T. P., Forward recoil spectrometry study of the diffusion of PMDA/ODA-based poly(amic ethyl esters). *Polymer* **1997,** *38* (20), 5073-5078.
168. Dill, F. H., Optical Lithography. *IEEE Trans. Electron Devices* **1975,** *75*, 440.
169. Mack, C. Lithography: Photoresist ABCs. http://lithoguru.com/scientist/CHE323/course.html.
170. Wood, J. S.; Koszelak, M.; Liu, J.; Lawrence, D. S., A Caged Protein Kinase Inhibitor. *J. Am. Chem. Soc.* **1998,** *120* (28), 7145-7146.
171. Buhr, F.; Kohl-Landgraf, J.; tom Dieck, S.; Hanus, C.; Chatterjee, D.; Hegelein, A.; Schuman, E. M.; Wachtveitl, J.; Schwalbe, H., Design of Photocaged Puromycin for Nascent Polypeptide Release and Spatiotemporal Monitoring of Translation. *Angew. Chem. Int. Ed.* **2015,** *54* (12), 3717-3721.
172. Prolith. http://www.kla-tencor.com/Lithography-Software/chip-prolith.html.
173. Wang, B.; Zheng, A., A photo-sensitive protecting group for amines based on coumarin chemistry. *Chemical & pharmaceutical bulletin* **1997,** *45* (4), 715-718.
174. Hershfield, R.; Schmir, G. L., Lactonization of ring-substituted coumarinic acids. Structural effects on the partitioning of tetrahedral intermediates in esterification. *J. Am. Chem. Soc.* **1973,** *95* (22), 7359-7369.
175. Amagai, K.; Sakayori, K.; Fukuda, T.; Katayama, A. Photobase generators, negative photosensitive polyimide compostions, method for relief pattern formation, and articles prepared therefrom. 2012.
176. Merriman, B. T.; Craig, J. D.; Nader, A. E.; Goff, D. L.; Pottiger, M. T.; Lautenberger, W. J. In *New low coefficient of thermal expansion polyimide for inorganic substrates*, Electronic Components Conference, 1989. Proceedings., 39th, 22-24 May 1989; 1989; pp 155-159.

177. Russell, T. P.; Gugger, H.; Swalen, J. D., In-plane orientation of polyimide. *Journal of Polymer Science: Polymer Physics Edition* **1983,** *21* (9), 1745-1756.
178. Takahashi, N.; Yoon, D. Y.; Parrish, W., Molecular order in condensed states of semiflexible poly(amic acid) and polyimide. *Macromolecules* **1984,** *17* (12), 2583-2588.
179. Boese, D.; Lee, H.; Yoon, D. Y.; Swalen, J. D.; Rabolt, J. F., Chain orientation and anisotropies in optical and dielectric properties in thin films of stiff polyimides. *J. Polym. Sci., Part B: Polym. Phys.* **1992,** *30* (12), 1321-1327.
180. Numata, S.; Kinjo, N.; Makino, D., Chemical structures and properties of low thermal expansion coefficient polyimides. *Polymer Engineering & Science* **1988,** *28* (14), 906-911.
181. Saraf, R. F.; Tong, H.-M.; Poon, T. W.; Silverman, B. D.; Ho, P. S.; Rossi, A. R., Thickness–direction thermal-expansion measurements. *J. Appl. Polym. Sci.* **1992,** *46* (8), 1329-1337.
182. Chen, S. T.; Wagner, H. H., Out-of-plane thermal expansion coefficient of biphenyldianhydride-phenylenediamine polyimide film. *J. Electron. Mater.* **1993,** *22* (7), 797-799.
183. Mary, T. A.; Evans, J. S. O.; Vogt, T.; Sleight, A. W., Negative Thermal Expansion from 0.3 to 1050 Kelvin in ZrW2O8. *Science* **1996,** *272* (5258), 90-92.
184. Sleight, A. W., Isotropic Negative Thermal Expansion. *Annu. Rev. Mater. Sci.* **1998,** *28* (1), 29-43.
185. Yang, J.; Yang, Y.; Liu, Q.; Xu, G.; Cheng, X., Preparation of Negative Thermal Expansion ZrW2O8 Powders and Its Application in Polyimide/ZrW2O8 Composites. *Journal of Materials Science & Technology* **2010,** *26* (7), 665-668.
186. Sullivan, L. M.; Lukehart, C. M., Zirconium Tungstate (ZrW2O8)/Polyimide Nanocomposites Exhibiting Reduced Coefficient of Thermal Expansion. *Chem. Mater.* **2005,** *17* (8), 2136-2141.
187. Yamashina, N.; Isobe, T.; Ando, S., Low Thermal Expansion Composites Prepared from Polyimide and ZrW_2O_8 Particles with Negative Thermal Expansion. *J. Photopolym. Sci. Technol.* **2012,** *25* (3), 385-388.
188. Evans, J. S. O.; Mary, T. A.; Vogt, T.; Subramanian, M. A.; Sleight, A. W., Negative Thermal Expansion in ZrW2O8 and HfW2O8. *Chem. Mater.* **1996,** *8* (12), 2809-2823.
189. Zhi, C.; Bando, Y.; Terao, T.; Tang, C.; Kuwahara, H.; Golberg, D., Towards Thermoconductive, Electrically Insulating Polymeric Composites with Boron Nitride Nanotubes as Fillers. *Adv. Funct. Mater.* **2009,** *19* (12), 1857-1862.
190. Terao, T.; Bando, Y.; Mitome, M.; Zhi, C.; Tang, C.; Golberg, D., Thermal Conductivity Improvement of Polymer Films by Catechin-Modified Boron Nitride Nanotubes. *The Journal of Physical Chemistry C* **2009,** *113* (31), 13605-13609.
191. Terao, T.; Zhi, C.; Bando, Y.; Mitome, M.; Tang, C.; Golberg, D., Alignment of Boron Nitride Nanotubes in Polymeric Composite Films for Thermal Conductivity Improvement. *The Journal of Physical Chemistry C* **2010,** *114* (10), 4340-4344.
192. Agilent Split Post Dielectric Resonators for Dielectric Measurements of Substrates. http://cp.literature.agilent.com/litweb/pdf/5989-5384EN.pdf.

193. Krupka, J.; Geyer, R. G.; Baker-Jarvis, J.; Ceremuga, J. In *Measurements of the complex permittivity of microwave circuit board substrates using split dielectric resonator and reentrant cavity techniques*, Dielectric Materials, Measurements and Applications, Seventh International Conference on (Conf. Publ. No. 430), IET: 1996; pp 21-24.
194. Krupka, J.; Gregory, A. P.; Rochard, O. C.; Clarke, R. N.; Riddle, B.; Baker-Jarvis, J., Uncertainty of complex permittivity measurements by split-post dielectric resonator technique. *J. Eur. Ceram. Soc.* **2001,** *21* (15), 2673-2676.
195. Alajarín, M.; Molina, P.; Vidal, A.; Tovar, F., Intramolecular [2 + 2] cycloaddition of ketenimines with imines. Synthesis and chemical behaviour of azeto[2,1-b]quinazolines. *Tetrahedron* **1997,** *53* (39), 13449-13472.
196. Mueller, B. K.; Schwartz, J. M.; Sutlief, A. E.; Bell, W. K.; Hayes, C. O.; Elce, E.; Grant Willson, C.; Kohl, P. A., Chemically Amplified, Positive Tone, Polynorbornene Dielectric for Microelectronics Packaging. *ECS Journal of Solid State Science and Technology* **2015,** *4* (1), N3001-N3007.
197. Houlihan, F. M.; Bachman, B. J.; Wilkins, C. W.; Pryde, C. A., Synthesis and characterization of the tert-butyl ester of the oxydianiline/pyromellitic dianhydride polyamic acid. *Macromolecules* **1989,** *22* (12), 4477-4483.
198. Houlihan, F. M.; Bachman, B. J.; Wilkins, C. W.; Pryde, C. A., Synthesis and Characterization of the t-Butyl Ester of the Oxydianiline—Pyromellitic Dianhydride Polyamic Acid. In *Polymeric Materials for Electronics Packaging and Interconnection*, American Chemical Society: 1989; Vol. 407, pp 101-113.
199. Ueda, M.; Mori, H., Synthesis of polyamic acid di-tert-butyl esters by direct polycondensation of di-tert-butyl esters of tetracarboxylic acids with diamines using diphenyl (2,3-dihydro-2-thioxo-3-benzoxazolyl)phosphonate. *Makromol. Chem.* **1993,** *194* (2), 511-21.
200. Jin, M. Y.; Lee, J. B.; Choi, K.-Y.; Kim, S. T.; Shin, D. M., Thermolytic acidolysis of polyamic ester containing t-butyl unit. *Korea Polym. J.* **1999,** *7* (1), 11-17.
201. Ueda, M.; Mochizuki, A.; Hiratsuka, I.; Oikawa, H., 3,3'-(Phenylphosphinylidene)bis[2(3H)-benzoxazolone] and 3,3'-(Phenylphosphinylidene)bis[2(H)-benzothiazolone]. New Activating Agents. *Bull. Chem. Soc. Jpn.* **1985,** *58* (11), 3291-3297.
202. Ueda, M.; Kameyama, A.; Hashimoto, K., Diphenyl (2,3-dihydro-2-thioxo-3-benzoxazolyl)phosphonate: a new, reactive activating agent for the synthesis of amides and polyamides. *Macromolecules* **1988,** *21* (1), 19-24.
203. Ueda, M.; Kameyama, A.; Ikeda, C., Synthesis of Polyamides by Direct Polycondensation with Diphenyl 2,3-Dihydro-2-oxo-3-benzothiazolyl Phosphate as a New Activating Agent. *Polym. J.* **1987,** *19* (6), 673-679.
204. Okada, Y. Polyimide precursors and photosensitive resin compositions therewith. JP2002356554A, 2002.
205. Cheng, H.; Chang, Y.; Zhang, L.; Luo, J.; Tu, Z.; Lu, X.; Zhang, Q.; Lu, J.; Ren, X.; Ding, K., Identification and Optimization of New Dual Inhibitors of B-Raf and

Epidermal Growth Factor Receptor Kinases for Overcoming Resistance against Vemurafenib. *J. Med. Chem.* **2014,** *57* (6), 2692-2703.
206. Yagupol'skii, L. M.; Il'chenko, A. Y.; Kondratenko, N. V., The Electronic Nature of Fluorine-containing Substituents. *Russian Chemical Reviews* **1974,** *43* (1), 32.
207. Sheppard, W. A., α-Fluorinated Ethers. I. Aryl Fluoroalkyl Ethers1. *The Journal of Organic Chemistry* **1964,** *29* (1), 1-11.
208. Pellerin, J.; Fox, R.; Ho, H.-M., Low Dielectric Constant Fluorinated Polyimides for Interlayer Dielectric Applications. *MRS Online Proceedings Library Archive* **1997,** *476*, 113 (7 pages).
209. Matsuura, T.; Ishizawa, M.; Hasuda, Y.; Nishi, S., Polyimides derived from 2,2'-bis(trifluoromethyl)-4,4'-diaminobiphenyl. 2. Synthesis and characterization of polyimides prepared from fluorinated benzenetetracarboxylic dianhydrides. *Macromolecules* **1992,** *25* (13), 3540-3545.
210. Huang, W.; Gao, L.; Zhang, X.; Xu, J.; Ding, M., Chromatographic separation and 13C NMR characterization of aromatic diester-diacids isomers. *Macromol. Chem. Phys.* **1996,** *197* (4), 1473-1484.
211. Huang, W.; Li, Y.; Xu, J.; Ding, M., Synthesis and miscibility studies of rodlike/ flexible polyimide molecular composites via para-para linked aromatic poly(amic ester) precursors. *Polymer* **1997,** *38* (16), 4261-4265.
212. Yang, A. C.; Brown, H. R., Solvent Induced Crack-Like Defects in Adhered Polyimide Films. *MRS Online Proceedings Library Archive* **1986,** *72*, 217 (6 pages).
213. Hasegawa, M.; Horie, K., Photophysics, photochemistry, and optical properties of polyimides. *Prog. Polym. Sci.* **2001,** *26* (2), 259-335.
214. Suzuki, H.; Abe, T.; Takaishi, K.; Narita, M.; Hamada, F., The synthesis and X-ray structure of 1,2,3,4-cyclobutane tetracarboxylic dianhydride and the preparation of a new type of polyimide showing excellent transparency and heat resistance. *J. Polym. Sci., Part A: Polym. Chem.* **2000,** *38* (1), 108-116.
215. Volksen, W.; Cha, H. J.; Sanchez, M. I.; Yoon, D. Y., Polyimides derived from nonaromatic monomers: synthesis, characterization and potential applications. *React. Funct. Polym.* **1996,** *30* (1–3), 61-69.
216. Matsumoto, T., Nonaromatic Polyimides Derived from Cycloaliphatic Monomers. *Macromolecules* **1999,** *32* (15), 4933-4939.
217. Seino, H.; Sasaki, T.; Mochizuki, A.; Ueda, M., Synthesis of Fully Aliphatic Polyimides. *High Perform. Polym.* **1999,** *11* (3), 255-262.
218. Li, J.; Kato, J.; Kudo, K.; Shiraishi, S., Synthesis and properties of novel soluble polyimides having an unsymmetric spiro tricyclic dianhydride unit. *Macromol. Chem. Phys.* **2000,** *201* (17), 2289-2297.
219. Mathews, A. S.; Kim, I.; Ha, C.-S., Synthesis, characterization, and properties of fully aliphatic polyimides and their derivatives for microelectronics and optoelectronics applications. *Macromolecular Research* **2013,** *15* (2), 114-128.
220. Hasegawa, M.; Kasamatsu, K.; Koseki, K., Colorless poly(ester imide)s derived from hydrogenated trimellitic anhydride. *Eur. Polym. J.* **2012,** *48* (3), 483-498.

221. Hasegawa, M.; Hirano, D.; Fujii, M.; Haga, M.; Takezawa, E.; Yamaguchi, S.; Ishikawa, A.; Kagayama, T., Solution-processable colorless polyimides derived from hydrogenated pyromellitic dianhydride with controlled steric structure. *J. Polym. Sci., Part A: Polym. Chem.* **2013,** *51* (3), 575-592.
222. Hasegawa, M.; Fujii, M.; Ishii, J.; Yamaguchi, S.; Takezawa, E.; Kagayama, T.; Ishikawa, A., Colorless polyimides derived from 1S,2S,4R,5R-cyclohexanetetracarboxylic dianhydride, self-orientation behavior during solution casting, and their optoelectronic applications. *Polymer* **2014,** *55* (18), 4693-4708.
223. Hasegawa, M.; Horiuchi, M.; Wada, Y., Polyimides Containing Trans-1,4-cyclohexane Unit (II). Low-K and Low-CTE Semi- and Wholly Cycloaliphatic Polyimides. *High Perform. Polym.* **2007,** *19* (2), 175-193.
224. Itamura, S.; Yamada, M.; Tamura, S.; Matsumoto, T.; Kurosaki, T., Soluble polyimides with polyalicyclic structure. 1. Polyimides from bicyclo[2.2.2]oct-7-ene-2-exo,3-exo,5-exo,6-exo-tetracarboxylic 2,3:5,6-dianhydrides. *Macromolecules* **1993,** *26* (14), 3490-3493.
225. Moore, J. A.; Dasheff, A. N., An intrinsically photosensitive polyimide. *Chem. Mater.* **1989,** *1* (1), 163-166.
226. Nawata, H.; Ohtsuka, Y.; Ohrai, Y.; Sewahata, K.; Nihira, T.; Suzuki, H.; Fukuro, H., Synthesis of novel alicyclic polyimides and their application as liquid crystal alignment layers. In *Polyimides and other high temperature polymers: synthesis, characterization and applications*, Mittal, K. L., Ed. VSP: Boston, 1999; Vol. 1, pp 217-223.
227. High performance flexible films for photovoltaic substrates. http://www.dupont.com/content/dam/dupont/products-and-services/solar-photovoltaic-materials/solar-photovoltaic-materials-landing/documents/dec-Kapton-for-PV.pdf.
228. Chou, W.-Y.; Kuo, C.-W.; Chang, C.-W.; Yeh, B.-L.; Chang, M.-H., Tuning surface properties in photosensitive polyimide. Material design for high performance organic thin-film transistors. *J. Mater. Chem.* **2010,** *20* (26), 5474-5480.
229. Hasegawa, M.; Miura, H.; Haga, N.; Hayakawa, A.; Saito, K., Preparation and Properties of High Molecular Weight Polyamic Ester Having a Cyclobutane Moiety in the Main Chain. *High Perform. Polym.* **1998,** *10* (1), 11-21.
230. Furusato, Y.; Saito, M. Liquid crystal display element with characteristics such as short response time and high voltage holding ratio. WO2016002252A1, 2016.
231. Sakumoto, N.; Nagao, M.; Noguchi, Y. Polyimide precursor compositions containing polyamic alkyl esters with good adhesion and storage stability and high imidization ratio. WO2010114103A1, 2010.
232. Sakumoto, N.; Kondo, M.; Tokunaga, K.; Nagao, M.; Kita, H. Tetracarboxylic acid derivatives, processes for producing same, and liquid-crystal alignment material. WO2010092989A1, 2010.
233. Sakumoto, N.; Iinuma, Y.; Nagao, M.; Noguchi, Y. Liquid crystal alignment agent containing polyamic acid ester, and liquid crystal alignment film. WO2011115118A1, 2011.

234. Hori, T.; Sakumoto, N. Method for manufacturing liquid crystal alignment film, liquid crystal alignment film, and liquid crystal display element. WO2013039168A1, 2013.
235. Hori, T.; Iinuma, Y.; Noguchi, Y.; Sakumoto, N. Liquid crystal aligning agent, liquid crystal alignment film and liquid crystal display element. WO2014157143A1, 2014.
236. Mandai, A.; Noguchi, Y. Polyimide-based liquid crystal aligning agent, and liquid crystal display element using same. WO2015072554A1, 2015.
237. Mandai, A.; Hori, T.; Noguchi, Y. Liquid crystal aligning agent and liquid crystal alignment film using same. WO2015012316A1, 2015.
238. Ripin, D. H.; Evans, D. A., Evans pKa Table. 11/4/05 ed.; 2005.
239. St.Clair, A. K.; St.Clair, T. L.; Selmp, W. S.; Ezzell, K. S. *Optically Transparent/Colorless Polyimides*; NASA TM-87650; NASA: Hampton, VA, 1985.
240. Hasegawa, M.; Koseki, K., Poly(ester imide)s Possessing Low Coef-cient of Thermal Expansion and Low Water Absorption. *High Perform. Polym.* **2006,** *18* (5), 697-717.
241. Hasegawa, M.; Tsujimura, Y.; Koseki, K.; Miyazaki, T., Poly(ester imide)s Possessing Low CTE and Low Water Absorption (II). Effect of Substituents. *Polym. J* **2007,** *40* (1), 56-67.
242. Hasegawa, M.; Sakamoto, Y.; Tanaka, Y.; Kobayashi, Y., Poly(ester imide)s possessing low coefficients of thermal expansion (CTE) and low water absorption (III). Use of bis(4-aminophenyl)terephthalate and effect of substituents. *Eur. Polym. J.* **2010,** *46* (7), 1510-1524.
243. Hehre, W. J.; Ditchfield, R.; Pople, J. A., Self—Consistent Molecular Orbital Methods. XII. Further Extensions of Gaussian—Type Basis Sets for Use in Molecular Orbital Studies of Organic Molecules. *The Journal of Chemical Physics* **1972,** *56* (5), 2257-2261.
244. Becke, A. D., Density-functional thermochemistry. III. The role of exact exchange. *The Journal of Chemical Physics* **1993,** *98* (7), 5648-5652.
245. Stephens, P. J.; Devlin, F. J.; Chabalowski, C. F.; Frisch, M. J., Ab Initio Calculation of Vibrational Absorption and Circular Dichroism Spectra Using Density Functional Force Fields. *The Journal of Physical Chemistry* **1994,** *98* (45), 11623-11627.
246. Kruse, H.; Goerigk, L.; Grimme, S., Why the Standard B3LYP/6-31G* Model Chemistry Should Not Be Used in DFT Calculations of Molecular Thermochemistry: Understanding and Correcting the Problem. *The Journal of Organic Chemistry* **2012,** *77* (23), 10824-10834.
247. Guillevic, M.-A.; Light, M. E.; Coles, S. J.; Gelbrich, T.; Hursthouse, M. B.; Bruce, D. W., Synthesis of dinuclear complexes of rhenium(I) as potential metallomesogens. *J. Chem. Soc., Dalton Trans.* **2000,** (9), 1437-1445.
248. Peglow, T.; Cherkaoui, Z. M.; Moia, F. Polymerizable dichromophoric dichroic azo dyes. 2005.

249. Kang, S.; Min, H.-J.; Kang, M.-S.; Jung, M.-G.; Kim, S., Discovery of novel 2-hydroxydiarylamide derivatives as TMPRSS4 inhibitors. *Bioorg. Med. Chem. Lett.* **2013,** *23* (6), 1748-1751.
250. Yang, H.; Wang, L.; Shao, R.; Clark, N. A.; Ortega, J.; Etxebarria, J.; Albouy, P.-A.; Walba, D. M.; Keller, P., Novel liquid-crystalline mesogens and main-chain chiral smectic thiol-ene polymers based on trifluoromethylphenyl moieties. *J. Mater. Chem.* **2009,** *19* (39), 7208-7215.
251. Imamura, S.; Oguro, Y., Fused heterocyclic derivatives and use thereof. Google Patents: 2007.
252. Jacobs, R. L., Synthesis of nitrotrifluoromethylphenols and related compounds from nitrotrifluoromethylchlorobenzenes. *The Journal of Organic Chemistry* **1971,** *36* (1), 242-243.
253. Tseng, C. P.; Hsieh, P. W.; Chang, Y. W., Composition of 5-nitrobenzoate derivatives as anti-metastatic agent that inhibits tumor cell-induced platelet aggregation. Google Patents: 2014.
254. Ackermann, J.; Aebi, J.; Binggeli, A.; Grether, U.; Hirth, G.; Kuhn, B.; Maerki, H. P.; Meyer, M.; Mohr, P.; Wright, M., Aniline derivatives, their manufacture and use as pharmaceuticals. Google Patents: 2004.
255. Kuze, K.; Miwa, S., Wholly aromatic polyamides. I. The relation between physical properties and chemical structures of wholly aromatic copolymers. *Kogyo Kagaku Zasshi* **1968,** *71* (3), 443-9.
256. Bellamy, F. D.; Ou, K., Selective reduction of aromatic nitro compounds with stannous chloride in non acidic and non aqueous medium. *Tetrahedron Lett.* **1984,** *25* (8), 839-842.
257. Corcoran, J. P. T.; Kalindjian, S. B.; Borthwick, A. D.; Adams, D. R.; Brown, J. T.; Taddei, D. M. A.; Shiers, J. J., Therapeutic Aryl-Amido-Aryl Compounds and Their Use. Google Patents: 2012.
258. Kim, S. D.; Kim, S. Y.; Chung, I. S., Soluble and transparent polyimides from unsymmetrical diamine containing two trifluoromethyl groups. *J. Polym. Sci., Part A: Polym. Chem.* **2013,** *51* (20), 4413-4422.
259. Makosza, M.; Sienkiewicz, K., Hydroxylation of nitroarenes with alkylhydroperoxide anions via vicarious nucleophilic substitution of hydrogen. *The Journal of Organic Chemistry* **1990,** *55* (17), 4979-4981.
260. Makosza, M.; Sienkiewicz, K., Hydroxylation of Nitroarenes with Alkyl Hydroperoxide Anions via Vicarious Nucleophilic Substitution of Hydrogen. *The Journal of Organic Chemistry* **1998,** *63* (13), 4199-4208.
261. Girouard, R. Mark5 Reflow Oven. http://hellerindustries.com/reflow-1826.php.
262. Jones, R. J.; Cassey, H. N. Low temperature curing polyimides. US3926913A, 1975.
263. Jones, R. J.; Green, H. E.; Quinlivan, S. C. Low temperature curable compliant bismaleimide compositions. US4179551A, 1979.
264. Serafini, T. T.; Delvigs, P. Low temperature crosslinking polyimides. US161253A0, 1980.

265. Delvigs, P. *Low-curing-temperature PMR polyimides*; 0499-9320; Natl. Aeronaut. Space Adm.: 1982; p 11 pp.
266. Delvigs, P., Lower-curing-temperature PMR polyimides. *Polym. Compos.* **1983,** *4* (3), 150-3.
267. Waters, J. F.; Sukenik, C. N.; Kennedy, V. O.; Livneh, M.; Youngs, W. J.; Sutter, J. K.; Meador, M. A. B.; Burke, L. A.; Ahn, M. K., Lower temperature curing thermoset polyimides utilizing a substituted norbornene endcap. *Macromolecules* **1992,** *25* (15), 3868-3873.
268. Wilson, D., PMR-15 processing, properties and problems—a review. *British Polymer Journal* **1988,** *20* (5), 405-416.
269. Hubbard, R. L.; Fathi, Z.; Ahmad, I.; Matsutani, H.; Hattori, T. In *Low temperature curing of polyimide wafer coatings*, Electronics Manufacturing Technology Symposium, 2004. IEEE/CPMT/SEMI 29th International, July 14-16, 2004; 2004; pp 149-151.
270. Matsutani, H.; Hattori, T.; Ohe, M.; Ueno, T.; Hubbard, R. L.; Fathi, Z., Low Temperature Curing of Polyimide Precursors by Variable Frequency Microwave. *J. Photopolym. Sci. Technol.* **2005,** *18* (2), 327-332.
271. Hubbard, R. L., Curing Dielectric Layers for Microelectronics with Microwaves: Chemistry, Mechanisms, and Applications. *ECS Transactions* **2007,** *6* (3), 737-753.
272. Sung, T.; Bidstrup Allen, S. A.; Kohl, P. A., Low temperature rapid curing of polymer dielectrics on metalized organic laminates by variable frequency microwave processing. *J. Microelectron. Electron. Packag.* **2005,** *2* (2), 142-154.
273. Oba, M., Effect of curing accelerators on thermal imidization of polyamic acids at low temperature. *J. Polym. Sci., Part A: Polym. Chem.* **1996,** *34* (4), 651-658.
274. Kim, S. W.; Shin, S. J.; Oh, D. H.; Kim, K. J., Low temperature curable polyimide resin and method of preparing the same. Google Patents: 2012.
275. Kreuz, J. A.; Endrey, A. L.; Gay, F. P.; Sroog, C. E., Studies of thermal cyclizations of polyamic acids and tertiary amine salts. *Journal of Polymer Science Part A-1: Polymer Chemistry* **1966,** *4* (10), 2607-2616.
276. Mochizuki, A.; Teranishi, T.; Ueda, M., Novel Photosensitive Polyimide Precursor Based on Polyisoimide Using an Amine Photogenerator. *Macromolecules* **1995,** *28* (1), 365-369.
277. Fukukawa, K.-i.; Ogura, T.; Shibasaki, Y.; Ueda, M., Thermo-base Generator for Low Temperature Solid-phase Imidation of Poly(amic acid). *Chem. Lett.* **2005,** *34* (10), 1372-1373.
278. Fukukawa, K.-i.; Shibasaki, Y.; Ueda, M., Efficient Catalyst for Low Temperature Solid-Phase Imidization of Poly(amic acid). *Chem. Lett.* **2004,** *33* (9), 1156-1157.
279. Ahn, T.; Choi, Y.; Jung, H. M.; Yi, M., Fully aromatic polyimide gate insulators with low temperature processability for pentacene organic thin-film transistors. *Org. Electron.* **2009,** *10* (1), 12-17.
280. Ishikawa, T., *Superbases for organic synthesis: guanidines, amidines and phosphazenes and related organocatalysts*. Wiley: Wiltshire, United Kingdom, 2009.

281. Suyama, K.; Araki, H.; Shirai, M., Quaternary Ammonium Salt as DBU-Generating Photobase Generator. *J. Photopolym. Sci. Technol.* **2006,** *19* (1), 81-84.
282. Tachi, H.; Yamamoto, T.; Shirai, M.; Tsunooka, M., Photochemical reactions of quaternary ammonium dithiocarbamates as photobase generators and their use in the photoinitiated thermal crosslinking of poly(glycidyl methacrylate). *J. Polym. Sci., Part A: Polym. Chem.* **2001,** *39* (9), 1329-1341.
283. Sun, X.; Gao, J. P.; Wang, Z. Y., Bicyclic Guanidinium Tetraphenylborate: A Photobase Generator and A Photocatalyst for Living Anionic Ring-Opening Polymerization and Cross-Linking of Polymeric Materials Containing Ester and Hydroxy Groups. *J. Am. Chem. Soc.* **2008,** *130* (26), 8130-8131.
284. Arimitsu, K.; Endo, R., Application to Photoreactive Materials of Photochemical Generation of Superbases with High Efficiency Based on Photodecarboxylation Reactions. *Chem. Mater.* **2013,** *25* (22), 4461-4463.
285. Arimitsu, K.; Fukuda, K.; Sakai, N., Photochemical generation of superbases from carboxylates consisting of phthalimidoacetic acid derivatives and superbases. *Chem. Lett.* **2014,** *43* (6), 831-833.
286. Shiraishi, A.; Kimura, H., Photobase generator. Google Patents: 2011.
287. Atsushi, S. Heat Base Generator. JP2014097930, 2014.
288. Ouk, S.; Thiébaud, S.; Borredon, E.; Le Gars, P., High performance method for O-methylation of phenol with dimethyl carbonate. *Applied Catalysis A: General* **2003,** *241* (1–2), 227-233.
289. Benzyl bromide. http://www.sigmaaldrich.com/catalog/product/aldrich/b17905.
290. Sanda, F.; Kaizuka, T.; Sudo, A.; Endo, T., A Novel Thermally Latent Anionic Initiator. Polymerization of Epoxide with Hydroxylamide Based on Thermal Dissociation. *Macromolecules* **2003,** *36* (4), 967-968.
291. Shirai, M.; Suyama, H. Amine precursors, their resin compositions, amine formation, and curing of epoxy resins therewith. JP2008280279A, 2008.
292. Katayama, A.; Sakayori, K. Base generators, photosensitive resin compositions and pattern-forming materials containing them, method for forming relief patterns therefrom, and articles therewith. JP2013204019A, 2013.
293. Taylor, J. E.; Jones, M. D.; Williams, J. M. J.; Bull, S. D., Friedel−Crafts Acylation of Pyrroles and Indoles using 1,5-Diazabicyclo[4.3.0]non-5-ene (DBN) as a Nucleophilic Catalyst. *Org. Lett.* **2010,** *12* (24), 5740-5743.
294. Taylor, J. E.; Jones, M. D.; Williams, J. M. J.; Bull, S. D., N-Acyl DBN Tetraphenylborate Salts as N-Acylating Agents. *The Journal of Organic Chemistry* **2012,** *77* (6), 2808-2818.
295. Taylor, J. E.; Williams, J. M. J.; Bull, S. D., N-Acyl 1,5-diazabicyclo[4.3.0]non-5-ene (DBN) tetraphenylborate salts as O-acylating agents. *Tetrahedron Lett.* **2012,** *53* (32), 4074-4076.
296. Carafa, M.; Mesto, E.; Quaranta, E., DBU-Promoted Nucleophilic Activation of Carbonic Acid Diesters. *Eur. J. Org. Chem.* **2011,** *2011* (13), 2458-2465.

297. Mesto, E.; Quaranta, E., Hydrogen-bonded and [pi]-interaction assembly in two 8-alkoxycarbonyl-1,8-diazabicyclo[5.4.0]undec-7-enium chloride salts. *Acta Crystallographica Section C* **2013,** *69* (4), 444-447.
298. Krossing, I.; Raabe, I., Noncoordinating Anions—Fact or Fiction? A Survey of Likely Candidates. *Angew. Chem. Int. Ed.* **2004,** *43* (16), 2066-2090.
299. Elsinger, F.; Schreiber, J.; Eschenmoser, A., Notiz über die Selektivität der Spaltung von Carbonsäuremethylestern mit Lithiumjodid. *Helv. Chim. Acta* **1960,** *43* (1), 113-118.
300. Magnus, P.; Gallagher, T., Studies on the synthesis of the antitumour agent CC-1065. Synthesis of the cyclopropapyrroloindole portion. *J. Chem. Soc., Chem. Commun.* **1984,** (6), 389-390.
301. Mc Murry, J., Ester Cleavages via SN2-Type Dealkylation. In *Organic Reactions*, John Wiley & Sons, Inc.: 2004.
302. Al-Azzawi, A. M.; Abd Al-Razzak, M. S., Synthesis, characterization and antibacterial screening of new Schiff bases linked to phthalimide. *Int. J. Res. Pharm. Chem.* **2013,** *3* (3), 682-690.
303. Kütt, A.; Rodima, T.; Saame, J.; Raamat, E.; Mäemets, V.; Kaljurand, I.; Koppel, I. A.; Garlyauskayte, R. Y.; Yagupolskii, Y. L.; Yagupolskii, L. M.; Bernhardt, E.; Willner, H.; Leito, I., Equilibrium Acidities of Superacids. *The Journal of Organic Chemistry* **2011,** *76* (2), 391-395.
304. Parr, R. G.; Pearson, R. G., Absolute hardness: companion parameter to absolute electronegativity. *J. Am. Chem. Soc.* **1983,** *105* (26), 7512-7516.
305. p-Toluenesulfonic Acid. http://www.worldofchemicals.com/chemicals/chemical-properties/p-toluenesulfonic-acid.html.
306. Luche, J.-L.; Rodriguez-Hahn, L.; Crabbe, P., Reduction of natural enones in the presence of cerium trichloride. *J. Chem. Soc., Chem. Commun.* **1978,** (14), 601-602.
307. Mine, N.; Fujiwara, Y.; Taniguchi, H., Trichlorolanthanoid(LnCl3)-Catalyzed Friedel-Crafts Alkylation Reactions. *Chem. Lett.* **1986,** *15* (3), 357-360.
308. Wamser, C. A., Equilibria in the System Boron Trifluoride—Water at 25°. *J. Am. Chem. Soc.* **1951,** *73* (1), 409-416.
309. Kobayashi, S., Scandium Triflate in Organic Synthesis. *Eur. J. Org. Chem.* **1999,** *1999* (1), 15-27.
310. Likhar, P.; Kumar, M.; Bandyopadhyay, A., Ytterbium Trifluoromethanesulfonate Yb (OTf)~ 3: An Efficient, Reusable Catalyst for Highly Selective Formation of beta-Alkoxy Alcohols via Ring-Opening of 1, 2-Epoxides with Alcohols. *Synlett* **2001**, 836-838.
311. Seino, H.; Haba, O.; Mochizuki, A.; Yoshioka, M.; Ueda, M., Preparation and Properties of Polyisoimides as a Highly Dimensionally Stable Polyimide Precursor with Low Dielectric Constant. *High Perform. Polym.* **1997,** *9* (3), 333-344.
312. Seino, H.; Haba, O.; Ueda, M.; Mochizuki, A., Photosensitive polyimide-precursor based on polyisoimide: dimensionally stable polyimide with a low dielectric constant. *Polymer* **1999,** *40* (3), 551-558.

313. Sauers, C. K.; Gould, C. L.; Ioannou, E. S., Reactions of N-arylphthalamic acids with acetic anhydride. *J. Am. Chem. Soc.* **1972,** *94* (23), 8156-8163.
314. Mochizuki, A.; Teranishi, T.; Ueda, M., Preparation and Properties of Polyisoimide as a Polyimide-Precursor. *Polym. J.* **1994,** *26* (3), 315-323.
315. Stoffel, N. C.; Kramer, E. J.; Volksen, W.; Russell, T. P., Solvent and isomer effects on the imidization of pyromellitic dianhydride-oxydianiline-based poly(amic ethyl ester)s. *Polymer* **1993,** *34* (21), 4524-4530.
316. Ning, W.; Li, H.; Zhu, C.; Luo, L.; Chen, D.; Duan, Z., The effects of cure temperature history on the stability of polyimide films. *Journal of Semiconductors* **2013,** *34* (6).
317. Jou, J. H.; Huang, P. T., Effect of thermal curing on the structures and properties of aromatic polyimide films. *Macromolecules* **1991,** *24* (13), 3796-3803.
318. King, J. A.; Phelps, P. D., Hexasubstituted guanidinium salts and ultracapacitors employing them as electrolytes. Google Patents: 1998.
319. Cameron, J. F.; Frechet, J. M. J., Base catalysis in imaging materials. 1. Design and synthesis of novel light-sensitive urethanes as photoprecursors of amines. *J. Org. Chem.* **1990,** *55* (23), 5919-5922.
320. Sheehan, J. C.; Wilson, R. M.; Oxford, A. W., Photolysis of methoxy-substituted benzoin esters. Photosensitive protecting group for carboxylic acids. *J. Am. Chem. Soc.* **1971,** *93* (26), 7222-7228.
321. Barltrop, J. A.; Schofield, P., Organic photochemistry. Part II. Some photosensitive protecting groups. *Journal of the Chemical Society (Resumed)* **1965,** (0), 4758-4765.
322. Barltrop, J. A.; Plant, P. J.; Schofield, P., Photosensitive protective groups. *Chemical Communications (London)* **1966,** (22), 822-823.
323. Shirai, M.; Tsunooka, M., Photoacid and photobase generators: chemistry and applications to polymeric materials. *Prog. Polym. Sci.* **1996,** *21* (1), 1-45.
324. Martina, S.; MacDonald, S. A.; Enkelmann, V., Photosensitive Tetramethylpiperidine Urethanes: Synthesis and Characterization. *The Journal of Organic Chemistry* **1994,** *59* (12), 3281-3283.
325. Takuya, I.; Atsushi, S. Photobase generator. JP2014/005755, 2015.
326. Baudin, G.; Dietliker, K.; Jung, T. Photoactivable nitrogen bases, their manufacture and use in photo-polymerization or crosslinking. WO2003033500A1, 2003.
327. Hall-Goulle, V.; Turner, S. C.; Cunningham, A. F. Photoactivatable nitrogen-containing bases based on α-ammonium ketones, iminium ketones or amidinium ketones and aryl borates, and compositions using photoactivatable catalysts. US6551761B1, 2003.
328. Takashima, Y.; Mukai, T. N-(2-nitrophenylalkoxycarbonyaminoalkyl)acetamide or N-(2-nitrophenylalkoxycarbonyaminoalkyl)lactam photobase generators, curable resin compositions containing them, and method for manufacture of cured products of the compositions. JP2011116869A, 2011.
329. Ma, Z. Process for preparation of 1,8-diazabicyclo[5.4.0]-7-undecene. CN1546492A, 2004.

330. IUPAC, *Compendium of Chemical Terminology*. 2 ed.; Blackwell Scientific Publications: Oxford, 1997.
331. Blake, J. A.; Gagnon, E.; Lukeman, M.; Scaiano, J. C., Photodecarboxylation of Xanthone Acetic Acids: C−C Bond Heterolysis from the Singlet Excited State. *Org. Lett.* **2006,** *8* (6), 1057-1060.
332. Williams, J. L. R.; Doty, J. C.; Grisdale, P. J.; Searle, R.; Regan, T. H.; Happ, G. P.; Maier, D. P., Boron photochemistry. I. Irradiation of sodium tetraarylborates in aqueous solution. *J. Am. Chem. Soc.* **1967,** *89* (20), 5153-5157.
333. Wilkey, J. D.; Schuster, G. B., Irradiation of tetraphenylborate does not generate a borene anion. *The Journal of Organic Chemistry* **1987,** *52* (11), 2117-2122.
334. Chatani, S.; Gong, T.; Earle, B. A.; Podgórski, M.; Bowman, C. N., Visible-Light Initiated Thiol-Michael Addition Photopolymerization Reactions. *ACS Macro Letters* **2014,** *3* (4), 315-318.
335. Shin, J.; Matsushima, H.; Comer, C. M.; Bowman, C. N.; Hoyle, C. E., Thiol−Isocyanate−Ene Ternary Networks by Sequential and Simultaneous Thiol Click Reactions. *Chem. Mater.* **2010,** *22* (8), 2616-2625.
336. Laird, T.; Williams, H., Photolysis of phenacyl-sulphonium and -ammonium salts. *Journal of the Chemical Society C: Organic* **1971,** (0), 1863-1869.
337. Ko, M.; Sato, T.; Otsu, T., Photopolymerization of vinyl monomers with quaternary ammonium salts. *Journal of Polymer Science: Polymer Chemistry Edition* **1974,** *12* (12), 2943-2951.
338. Hayes, C. O.; Bell, W. K.; Cassidy, B. R.; Willson, C. G., Synthesis and Characterization of a Two Stage, Nonlinear Photobase Generator. *The Journal of Organic Chemistry* **2015,** *80* (15), 7530-7535.
339. Houlihan, F. M.; Shugard, A.; Gooden, R.; Reichmanis, E., Nitrobenzyl ester chemistry for polymer processes involving chemical amplification. *Macromolecules* **1988,** *21* (7), 2001-2006.
340. Photoacid Generator Selection Guide for the electronics industry and energy curable coatings. http://product-finder.basf.com/group/corporate/product-finder/en/literature-document:/Brand+Irgacure-Brochure--Photoacid+Generator+Selection+Guide-English.pdf.
341. Bucher, G.; Scaiano, J. C.; Sinta, R.; Barclay, G.; Cameron, J., Laser Flash Photolysis of Carbamates Derived from 9-Fluorenone Oxime. *J. Am. Chem. Soc.* **1995,** *117* (13), 3848-3855.
342. Chae, K. H., Thermal curing reaction of poly(glycidyl methacrylate) using photogenerated amines from oxime-urethane derivatives. *Macromol. Rapid Commun.* **1998,** *19* (1), 1-4.
343. Dietliker, K.; Kunz, M.; Yamato, H.; De Leo, C. Alkysulfonyloximes for high-resolution i-line photoresists of high sensitivity. WO9810335A1, 1998.
344. Shirai, M.; Okamura, H., i-Line sensitive photoacid generators for UV curing. *Prog. Org. Coat.* **2009,** *64* (2–3), 175-181.

345. Okamura, H.; Sakai, K.; Tsunooka, M.; Shirai, M.; Fujiki, T.; Kawasaki, S.; Yamada, M., I-Line Sensitive Photoacid Generators and Their Use for Photocrosslinking of Polysilane/diepoxyfluorene Blend. *J. Photopolym. Sci. Technol.* **2003,** *16* (1), 87-90.
346. Nagarajan, K.; Kulkarni, C. L.; Venkateswarlu, A., Condensed heterotricycles. Beckmann rearrangement of xanthone and thioxanthone oximes as a route to dibenz[b,f][1,4]-oxazepines and thiazepines. *Indian J. Chem.* **1974,** *12* (3), 247-51.
347. Gonçalves, R. S.; Abdelnur, P. V.; Santos, V. G.; Simas, R. C.; Eberlin, M. N.; Magalhães, A.; Pérez González, E. R., Synthesis of potentially bioactive PABA-related N-(aminoalkyl)lactamic amino acids and esters via selective SNAr reactions. *Amino Acids* **2011,** *40* (1), 197-204.
348. Dietliker, K.; Misteli, K.; Studer, K.; Jung, T.; Engelbrecht, L. A. Photoactivable nitrogen bases as photoinduced cross-linking catalysts. WO2008119688A1, 2008.
349. Li, J., Synthesis, Characterization and Antibacterial Activity of N-(N-Acetic Acid-yl-Phthalimide-5-yl) Maleamic Acid Dihydrate. *J. Chem. Crystallogr.* **2010,** *40* (5), 428-431.
350. Jorand-Lebrun, C.; Valognes, D.; Halazy, S., Use of Triphosgene for Direct Preparation of Carbamoyl Chlorides from Tertiary Benzylamines. *Synth. Commun.* **1998,** *28* (7), 1189-1195.